Effective Field Theory for Baryon Masses

Xiulei Ren

NNT : 2015SACLS156

THESE DE DOCTORAT
de
BEIHANG UNIVERSITY
et de
L'UNIVERSITE PARIS-SACLAY
préparée à l'Université Paris-Sud

ÉCOLE DOCTORALE N°576
Particules, Hadrons, Énergie, Noyau, Instrumentation, Imagerie, Cosmos et Simulation (PHENIICS)
GRADUATE SCHOOL of PHYSICS

Spécialité de doctorat: Physique Hadronique

Par

M. XiuLei REN

Effective Field Theory for Baryon Masses

Thèse présentée et soutenue à Beijing, Chine, le 10/12/2015:

Composition du Jury :

M. B.-S. Zou, Directeur de Recherche, ITP-CAS, Président du Jury
M. U. van Kolck, Directeur de Recherche, CNRS, Directeur de thèse
M. J. Meng, Professeur, Peking & Beihang University, CoDirecteur de thèse
M. L.-S. Geng, Professeur, Beihang University, Co-encadrant de thèse
Mme C. Alexandrou, Professeur, University of Cyprus, Rapporteurse
M. M. Schindler, Professeur, University of South Carolina, Rapporteur
M. L.-H. Zhu, Professeur, Beihang University, Examinateur
M. J. Carbonell, Directeur de Recherche, CNRS, Examinateur

To My Dear and Loving Parents and Maternal Grandma

Copyright Clarify

Abstract

Mass is one of the most fundamental properties of matter. Understanding its origin has long been a central topic in physics. According to modern particle and nuclear physics, the key to this issue is to understand the origin of nucleon (lowest-lying baryon) masses from the nonperturbative strong interaction. With the development of computing technologies, lattice Quantum Chromodynamics simulations provide great opportunities to understand the origin of mass from first principles. However, due to the limit of computational resources, lattice baryon masses have to be extrapolated to the physical point. Chiral perturbation theory, as an effective field theory of low-energy QCD, provides a model independent method to understand nonperturbative strong interactions and to guide the lattice multiple extrapolations. Therefore, we present the interplay between lattice QCD and chiral perturbation theory to systematically study the baryon masses.

In the SU(3) sector, we study the lowest-lying octet baryon masses in covariant baryon chiral perturbation theory with the extended-on-mass-shell scheme up to next-to-next-to-next-to-leading order. In order to consider lattice artifacts from finite lattice box sizes, finite-volume corrections to lattice baryon masses are estimated. By constructing chiral perturbation theory for Wilson fermions, we also obtain the discretization effects of finite lattice spacings. We perform a systematic study of all the latest $n_f = 2+1$ lattice data with chiral extrapolation ($m_q \to m_q^{\text{phys.}}$), finite-volume corrections ($V \to \infty$), and continuum extrapolation ($a \to 0$). We find that finite-volume corrections are important to describe the present lattice baryon masses. On the other hand, the discretization effects of lattice simulations up to $\mathcal{O}(a^2)$ are of the order 1% when $a \sim 0.1$ fm and can be safely ignored. Furthermore, we find that the lattice data from different collaborations are consistent with each other, though their setups are quite different.

Using the chiral formulas of octet baryon masses, we accurately predict the octet baryon sigma terms via the Feynman-Hellmann theorem by analyzing the latest high-statistics lattice QCD data. Three key factors — lattice scale setting effects, chiral expansion truncations and strong-interaction isospin-breaking effects — are taken into account for the first time. In particular, the predicted pion- and strangeness-nucleon sigma terms, $\sigma_{\pi N} = 55(1)(4)$ MeV and $\sigma_{sN} = 27(27)(4)$ MeV, are consistent with the most latest lattice results of nucleon sigma terms.

With the success in the study of octet baryon masses, we also present a systematic analysis of the lowest-lying decuplet baryon masses in covariant baryon chiral perturbation theory by simultaneously fitting $n_f = 2+1$ lattice data. A good description for both the lattice and the experimental decuplet baryon masses is achieved. The convergence of covariant baryon chiral perturbation theory in the SU(3) sector is discussed. Furthermore, the pion- and strangeness-sigma terms for decuplet baryons are predicted by the Feynman-Hellmann theorem.

In addition, understanding the excitation spectrum of hadrons is still a challenge, especially the first positive-parity nucleon resonance, the Roper(1440). The baryon spectrum shows a very unusual pattern that the Roper state is lower than the negative-parity state $N(1535)$. Most lattice studies suggest that the Roper mass exhibits much larger chiral-log effects than that of the nucleon. Therefore, we calculate the Roper mass in chiral perturbation theory by explicitly including the nucleon/Delta contributions. The mixed contributions between nucleon and Roper to the baryon masses are taken into account for the first time. A first analysis of lattice Roper masses is presented.

Keywords: effective field theory, chiral Lagrangians, lattice QCD, baryon masses, sigma terms

Résumé

La masse est une des propriétés les plus fondamentales de la matière. Comprendre son origine a longtemps été un sujet central en physique. D'après la physique nucléaire et la physique des particules modernes, la clef de ce problème réside dans la compréhension de l' origine de la masse du nucléon (baryon de masse la plus petite) à partir de l' interaction forte. Avec le développement des technologies informatiques, la chromodynamique quantique sur réseau offre la possibilité de comprendre l' origine de la masse à partir des premiers principes. Cependant, dû aux ressources de calcul limitées, les masses obtenues à partir des calculs sur réseau doivent être extrapolées jusqu'au point physique. La théorie chirale des perturbations en tant que théorie effective des champs de QCD à basse énergie est une méthode indépendante de modèle permettant de comprendre l' interaction forte dans la région non perturbative et de guider les diverses extrapolations nécessaires pour passer du résultat lattice au résultat physique. Le but de cette thèse est donc d'utiliser la complémentarité entre QCD sur réseau et théorie chirale des perturbations afin d'étudier de façon systématique les masses des baryons.

Nous étudions les masses de l'octet baryonique le plus léger dans le cadre de la théorie chirale covariante des perturbations pour les baryons. Nous utilisons la méthode "extended on mass shell" jusqu'à l'ordre trois fois sous dominant. Afin d'étudier les artefacts des calculs sur réseau dûs à la taille finie de la boîte nous calculons les effets de volume fini. Adaptant la théorie chirale des perturbations à des fermions de Wilson nous obtenons aussi les effets de discrétisation dû au pas a fini du réseau. Nous étudions de façon systématique toutes les données réseau en tenant compte à la fois de l' extrapolation au continu ($a \to 0$), des corrections de volume finie ($V \to \infty$) et de l'extrapolation chirale ($m_\pi \to m_\pi^{\rm phys}$ où m_π est la masse du pion). Nous démontrons l'importance des corrections de volume fini dans la description des masses des baryons sur réseau. Par contre les effets de discrétisation sont de l'ordre de 1% jusqu'à l'ordre a^2 et peuvent donc être ignorés sans problème. De plus nous trouvons que toutes les données sur réseau prises en compte sont consistentes entre elles malgré des différences notables dans les procédures adoptées.

Utilisant les formules chirales des masses des baryons nous prédisons de façon précise leurs termes sigma via le théorème de Feynman-Hellmann en analysant les données sur réseau les plus récentes dont la statistique est élevée. Les effets dûs au pas du réseau, à la troncation de la série de perturbation chirale et à la violation d'isospin de l'interaction forte sont pris en compte pour la première fois. En particulier le terme sigma pion nucléon $\sigma_{\pi N} = 55(1)(4)$ MeV et le "strangeness sigma term" $\sigma_{sN} = 27(27)(4)$ MeV sont en accord avec les résultats réseau les plus récents.

Au vue des succès rencontrés lors de l'étude des masses de l'octet baryonique nous avons aussi fait une analyse systématique des masses du décuplet baryonique le plus léger dans la théorie chirale covariante des perturbations pour les baryons en fittant de façon simultanée les données réseau $n_f = 2 + 1$. Une bonne description à la fois des données réseau et des masses expérimentales est obtenue. La convergence de la série de perturbations dans le secteur SU(3) est discutée. De plus les termes sigma sont prédits à l'aide du théorème de Feynman-Hellmann.

Enfin comprendre le spectre d'excitation des hadrons est encore un challenge. En particulier le spectre des baryons a une structure très inhabituelle, la résonance Roper (1440) de parité positive étant plus légère que l'état de parité négative N(1535). La plupart des études sur réseau suggère que les effets des log chiraux sont plus importants pour la masse de la résonance Roper que pour celle des nucléons. Nous avons donc calculé la masse de cette résonance en théorie chirale des perturbations en tenant en compte de façon explicite des contributions du nucléon et du Δ. Les contributions venant du mélange entre le nucléon et la résonance Roper sont étudiées pour la première fois. Une première analyse de la masse de cette particule est présentée.

Mots cls: thorie effective des champs, Lagrangiens chiraux, QCD sur rseau, masses des baryons, termes sigma

Contents

List of Tables

List of Figures

CHAPTER 1

Introduction

Mass, as an essential property of matter, was firstly introduced by Issac Newton in his book *The Mathematical Principles of Natural Philosophy* in 1687 [1]. According to the different methods to measure the mass, there are two definitions of mass: inertial and gravitational mass. Inertial mass, which can be measured by the use of Newton's second law $F = ma$, denotes the inertia of an object. Gravitational mass, which can be measured by Newton's law of gravity $F = GMm/r^2$ (F is the force between the masses M and m, G is the gravitational constant, and r is the distance between the centers of the masses), represents the response of one object to the gravitational force. With the requirement of Einstein's equivalence principle [2], gravitational mass is identical to inertial mass. Up to now, all experimental researches, e.g. the famous Eötvös experiment [3], also show that inertial mass and gravitational mass are equivalent.

Mass has been introduced in many physical theories as a fundamental quantity. However, understanding the origin of mass is still a hot topic in the exploration of our ordinary matter world [1]. In the 1960s, with the famous Higgs boson proposed, the masses of fundamental particles (such as quarks, leptons, gauge bosons) can be produced by the Brout-Englert-Higgs mechanism [4–6]. This mechanism was confirmed in 2012, when the Higgs particle was observed by the ATLAS [7] and the CMS [8] experiments at CERN's Large Hadron Collider. Following the discovery, Peter Higgs and François Englert were awarded the Nobel Prize in Physics in 2013 for their extraordinary work in theory. However, the Brout-Englert-Higgs mechanism does not tell the whole story. When one explores the production mechanism of mass of ordinary matter, one finds that the Higgs mechanism can only provide about 1%. Where is the majority of contributions coming from?

1.1 Origin of mass

In order to understand the origin of mass, let us first examine the hierarchy of ordinary matter. Ordinary matter is made up of atoms and molecules (an electrically neutral group of two or more atoms). Because the binding energies of atoms/molecules introduced by van der Waals' interaction and chemical bond are much weaker compared to atomic masses, the study of the origin of mass can be attributed to the understanding of atomic mass. As illustrated in Fig. 1.1, an atom is composed of one or more electrons [9] and a nucleus [10], which is a bound system of protons or/and neutrons [11]. According to the Standard Model of particle physics, the proton and the neutron are comprised by u, u, d and u, d, d three quarks [12, 13], respectively. These fundamental particles within the atom interact with each other via

[1]The ordinary matter is always called baryonic matter, which is not only the everything you see (e.g. the sun, rivers, mountains, mobile devices, food etc.), but also the nonvisible matter composed of baryons.

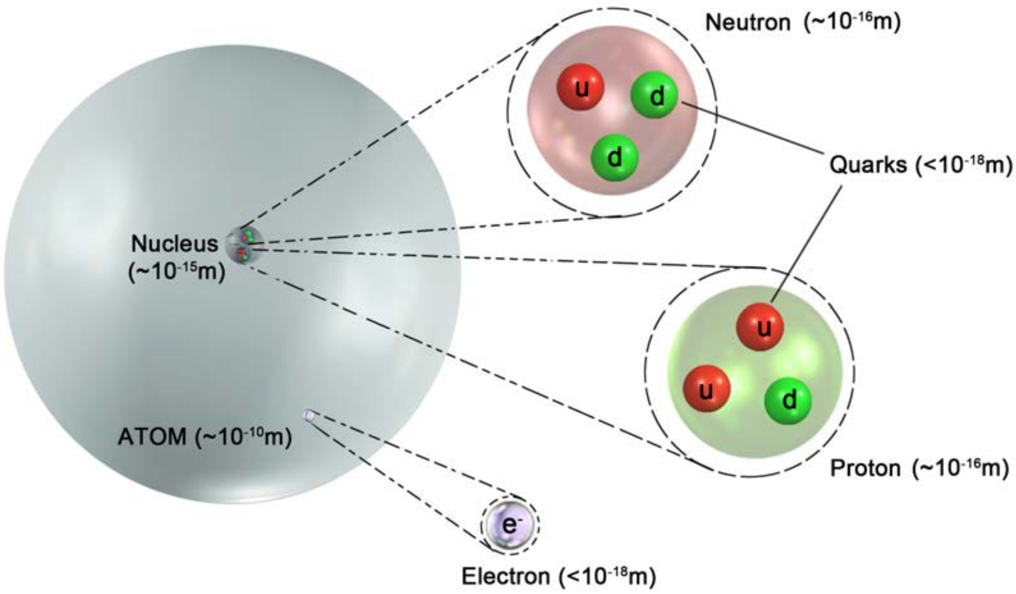

Figure 1.1: Structure within the atom.

four fundamental interactions: gravitational interaction, electromagnetic interaction, strong interaction, and weak interaction.

However, on the scale of atomic matter, the gravitational force can be neglected due to the weak interaction strength. The weak interaction can also be ignored, since it is responsible for the nuclear decay processes and irrelevant to the formation of bound systems. As a long-range force, the electromagnetic force plays an important role in binding electrons and nucleus to form an atom. And, the strong interaction, the strongest force of the four, is responsible for binding u, d quarks to form nucleons and binding nucleons to form a nucleus.

All in all, the mass of ordinary matter can be the sum of the masses of particles within the atom (shown in Fig. 1.1) and the energy of electromagnetic and strong interactions (according to Einstein's mass-energy relation $E = mc^2$ [14], with the light speed $c = 1$ in natural units).

At the hadronic level, the picture is quite intuitive that the mass of an atom equals to the masses of electrons and nucleus minus the binding energies between electrons and nucleus. The electron mass is $m_e = 511$ keV, which is about 1/1836 of nucleon mass ($M_N = 939$ MeV), and the mass loss induced by binding is extremely small (at electron volt (eV) level). Therefore, the mass of an atom is mainly from the nucleus mass. Because protons and neutrons are bound into a nucleus with the residual strong interaction, the mass of nucleus equals to the sum of masses of nucleons minus the binding energy. The average nuclear binding energy is about 8 MeV per nucleon, which only accounts for less than 1% of nucleon mass, therefore, the mass loss is negligible comparing to the total nuclear mass. Consequently, we find that the masses of nucleons provide the vast majority of atomic mass. In order to make this point clearly, we take iron-56 (^{56}Fe), one of the most tightly bound nuclei (binding energy is about 8.8 MeV per nucleon), for example. It contains 26 electrons, 26 protons, and 30 neutrons. The atomic mass of ^{56}Fe is 55.935 u ($\sim$ 52103.1 MeV) in unified atomic mass units. The masses of electrons, $26 \times 0.511 = 13.286$ MeV, only account about 0.025% of total mass of ^{56}Fe. The major contributions are the nucleus mass of ^{56}Fe, $56 \times 939 - 56 \times 8.8 = 52091.2$ MeV, where

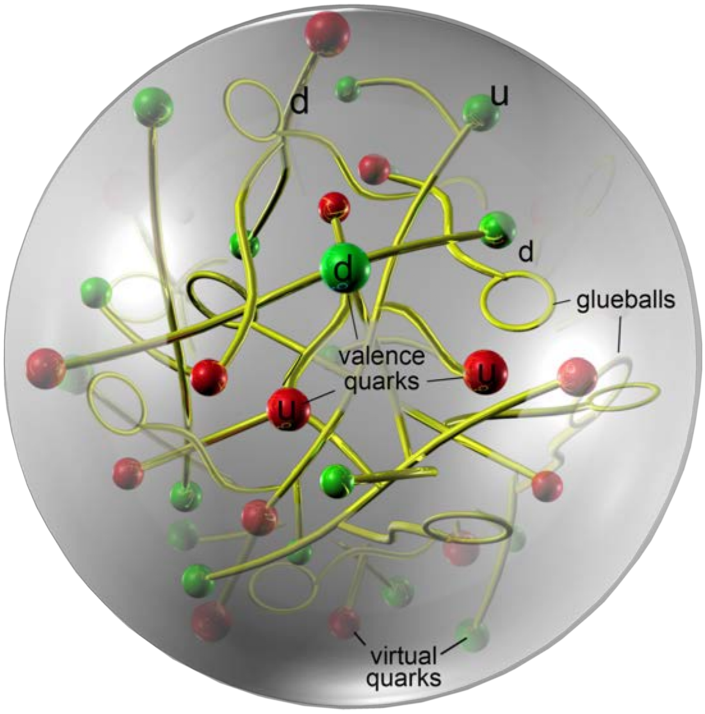

Figure 1.2: The composition of proton.

the binding energy accounts about 0.95%. Therefore, the masses of nucleons provide 99% of the atomic mass of iron-56.

As mentioned above, the nucleon is made up of three quarks, which are bound together by strong interactions. But the physical picture becomes more complicated than the nucleus, since the sum of quark masses is about 10 MeV ($m_u = 2.3^{+0.7}_{-0.5}$ MeV, $m_d = 4.8^{+0.5}_{-0.3}$ MeV at a renormalization scale $\mu \approx 2$ GeV [15]), which accounts for about 1% of nucleon mass. The other 99% contributions are the mass-energy from strong interaction. In order to clearly understand this phenomena, in Fig. 1.2, we present a more realistic picture of the composition of proton. We can see that the proton not only contains three valence quarks, but also includes tremendous sea quarks (quark and anti-quark pairs) and gluons, which provide most of proton mass. Therefore, almost 98% of the mass of atomic matter could be from the strong interaction. It would be of fundamental interest to understand the strong interaction to produce the nucleon masses.

1.2 Baryon masses from QCD

Quantum Chromodynamics (QCD), as an important component of the Standard Model of particle physics, is the part of the theory describing the strong interaction. The basic degrees of freedom are quarks and gluons. In principle, QCD could provide a reasonable explanation of the 98% of atomic mass. However, being a non-Abelian gauge theory, QCD possesses two peculiar properties: asymptotic freedom and confinement. As illustrated in Fig. 1.3, quarks

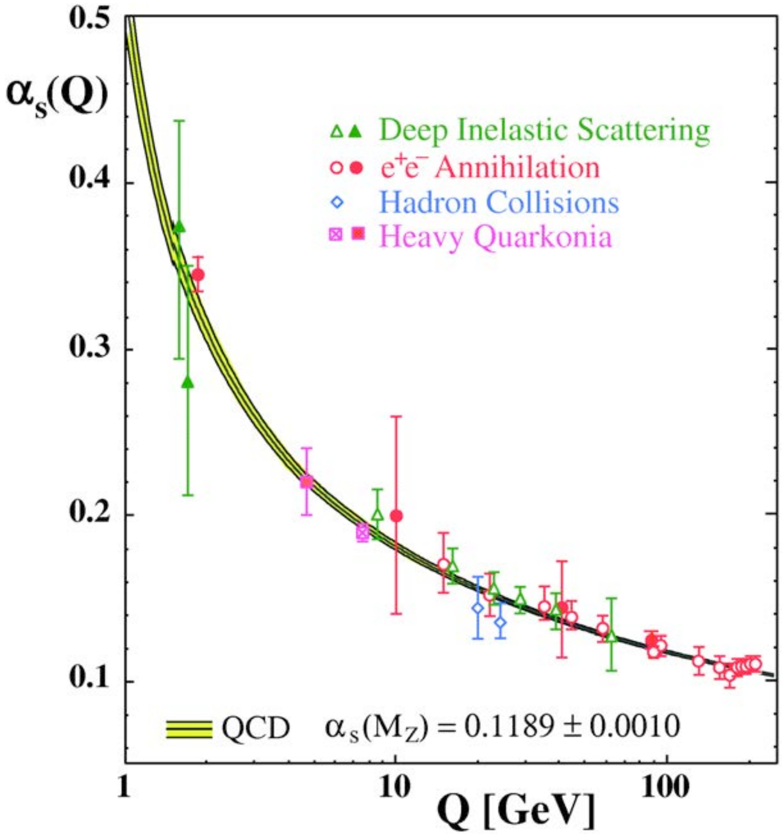

Figure 1.3: Running coupling constant $\alpha_s(Q)$ as a function of the respective energy scale Q. The figure is taken from Ref. [16].

and gluons interact very weakly at high energy, allowing perturbative expansion in powers of the running coupling constant α_s. On the other hand, due to confinement, α_s takes large value at low energies, and QCD becomes nonperturbative. In order to tackle this problem, lattice quantum chromodynamics (LQCD), effective field theories, and phenomenological quark models are developed. Because the former two methods are usually deemed as the theory of QCD, we would like to focus on their studies of nucleon (baryon) masses to understand the origin of atomic mass.

Lattice quantum chromodynamics simulation is a numerical method for solving QCD in the non perturbative regime with the QCD action directly discretized in a finite space-time hypercube. The corresponding lattice QCD gauge theory was firstly formulated by Wilson in 1974 [17]. The quark fields are located on lattice sites and the gluon fields are defined as the links to connect adjacent two sites. With the development of computational ability and advances of numerical algorithms, lattice QCD has undergone three developing stages: the "quenched" approximation [18, 19] in 1990s, the "partial-quenched" approximation [20, 21] in 2000s, and the fully dynamical simulations nowadays (around 2010). Therefore, lattice simulations provide a powerful framework for a quantitative analysis of the baryon masses from the nonperturbative strong interaction.

Recently, several LQCD collaborations have performed studies of lowest-lying octet and decuplet masses [22–29], especially the BMW Collaboration [22], which presented a significant explanation of the origin of mass from first principles. However, due to the limited computing resources, most lattice simulations have to employ larger than physical light-quark masses [2], finite lattice volumes and lattice spacings. In order to extract the observables at the physical point, one has to perform multiple extrapolations of lattice baryon masses to the physical point with physical quark masses ($m_q \to m_q^{\text{phys.}}$), to infinite space-time ($L \to \infty$), and to the continuum ($a \to 0$). For many observables, these extrapolations have led to uncertainties comparable to or even larger than the inherent statistical uncertainties.

On the theoretical side, chiral perturbation theory (ChPT), proposed by Weinberg [32] in 1978, is an effective field theory for low-energy QCD. The quintessence of ChPT is the effective Lagrangian technique with an expansion in powers of external momenta and light quark masses, which is constrained by chiral symmetry and its breaking pattern. After the further generalization by Gasser and Leutwyler [33, 34], ChPT became a very popular method in studies of nonperturbative strong interaction physics [32–46]. At present, it has been successfully applied to the meson sector (including static properties of mesons, the meson-meson interactions, semileptonic decays, etc.) and the baryon sector (including static properties of baryons, baryon-baryon interactions and other related processes). In ChPT, there exist unknown low-energy constants (LECs) in the effective Lagrangians. But, once the values of LECs are determined, ChPT can provide a model independent tool to explore the low-energy QCD.

Therefore, the combination between lattice QCD and chiral perturbation theory is a powerful strategy to study the nonperturbative strong interaction, and it can provide a trustworthy interpretation of the majority of baryon masses from the strong interaction to further answer the origin of mass.

Gratifyingly, chiral perturbative theory provides a model independent framework to study the light-quark mass dependence, lattice volume effects and discretization effects of LQCD results. In the last decades, baryon chiral perturbation theory (BChPT) has been applied to study the ground state octet and decuplet baryon masses [47–68] with different renormalization methods. Because the baryon masses do not vanish in the chiral limit, Weinberg power-counting is violated in BChPT if one is not careful. In order to restore chiral power counting, there are mainly three renormalization schemes, the so-called Heavy-Baryon (HB) ChPT [69], the infrared (IR) BChPT [70] and the extended-on-mass-shell (EOMS) [71, 72] BChPT. In addition to these dimensional renormalization schemes (MS and its derivatives), to speed up the convergence of BChPT, other renormalization/regularization schemes are also proposed, e.g., the cutoff scheme [73], the finite range regulator (FRR) method [58, 74, 75], and the partial summation approach [59]. Although the baryon masses have been systematically studied, most calculations are up to next-to-next-to-leading order (NNLO). If one wants to perform a higher order (e.g. next-to-next-to-next-to-leading order, N^{3}LO) calculation, the number of LECs is too large to be determined by the experimental results of baryon masses. Fortunately, as above mentioned lattice baryon masses, such a study of N^{3}LO expansion baryon masses becomes available by fitting the lattice data. This study also provides a good opportunity to study the convergence properties of SU(3) BChPT. Up to NNLO, it is found that HBChPT converges not well [76]. And, the situation is much better in FRR and EOMS BChPT in the analysis of PACS-CS and LHPC lattice data [56, 58]. Furthermore, as a covariant method, the EOMS

[2] We also notice that few lattice simulations with physical light-quark masses have become available (see, e.g., Refs. [30, 31]) lately, which (will) largely reduce the systematic uncertainties related to chiral extrapolations to the physical light-quark masses.

approach not only satisfies all fundamental symmetries and analyticity constraints, but also converges relatively fast. Therefore, in this work we would like to apply EOMS BChPT to perform the chiral extrapolation of baryon masses up to next-to-next-to-next-to-leading order. In order to apply this chiral formulas of baryon masses to analyze lattice data, one has to consider the artifacts from finite volumes and lattice spacings.

Because the commonly employed lattice box size L is about $3 \sim 5$ fm, finite-volume effects cannot be neglected or included in statistical errors. In Refs. [77, 78], Gasser and Leutwyler suggested that one could use ChPT to evaluate finite-volume corrections [3]. In the past decades, most studies have employed either HB ChPT or IR BChPT and focused on the two flavor sector (see, e.g., Refs. [80, 81]). Recently, two studies in the three-flavor sector have been performed with HB ChPT [29] and EOMS BChPT [57] up to NNLO. It was pointed out that both HB ChPT and EOMS BChPT can describe the NPLQCD data well with different values of baryon octet and decuplet couplings [57]. However, it should be noted that the EOMS BChPT extrapolation to the physical point is in better agreement with data than HB's with the LECs determined from LQCD data.

In order to apply ChPT to study LQCD results, in principle, one should first take the continuum limit, since ChPT describes continuum QCD and is not valid for nonzero lattice spacing. In the last decades, studies of the discretization effects of LQCD have made great progress with Symanzik's effective field theory [82–85]. At present, there are three versions of discretized BChPT for Wilson fermions (WChPT), for staggered fermions (SChPT), and for twisted mass fermions (tmChPT), respectively. The discretization effects on the ground-state meson/baryon properties, such as masses, decay constants, electromagnetic form factors, etc., have been extensively studied in Wilson HBChPT [86–94]. Furthermore, similar studies have also been performed in SChPT [95–102] and tmChPT [103–109]. However, the corresponding studies are still missing in the framework of EOMS BChPT. It is interesting to note that recently several attempts have been made to determine the unknown LECs of WChPT [110–114].

Furthermore, in SU(3) BChPT one should also be careful about the contributions of the decuplet resonances since the average mass gap between the baryon octet and the baryon decuplet $\delta = m_D - m_0 \sim 0.3$ GeV is similar to the pion mass and well bellow those of the kaon and eta mesons, M_K, M_η. In Ref. [47], HBChPT was enlarged to include the decuplet and applied to calculate the octet baryon masses up to $\mathcal{O}(p^3)$. It was shown in Ref. [48] that the effects of the virtual decuplet on the octet baryon masses start out at $\mathcal{O}(p^4)$ in the same framework. For the spin-dependent quantities, the virtual decuplet contributions are found to be important in HBChPT, such as magnetic moments [115] and axial vector form factors [116, 117]. In EOMS BChPT, the effects of the virtual decuplet are found to be negligible for the magnetic moments of the octet baryons if the "consistent" coupling scheme for the octet-decuplet-pseudoscalar coupling is adopted [118]. On the other hand, up to NNLO, the virtual decuplet contributions seem to play an important role in describing the NPLQCD volume-dependent data [57] and in the determination of the baryon sigma terms [119]. Therefore, it is necessary to study the effects of the virtual decuplet on the light-quark mass and on the volume dependence of the LQCD data at N^{3}LO.

[3] The finite-volume corrections of scattering process can be studied by using the Lüscher formula [79] and its resummed version.

To sum up, in this work, we would like to use EOMS BChPT to study octet and decuplet baryon masses up to next-to-next-to-next-to-leading order. By constructing the chiral effective field theory to take the lattice artifacts from finite-lattice volumes and lattice spacings into account self-consistently, we could perform a trustworthy analysis of the lattice baryon masses. With the obtained LECs, we could explore the convergent property of EOMS BChPT at different chiral orders and predict the baryon sigma terms to interpret the composition of baryon masses. We also can apply this strategy to study the baryon masses of excitation states by including the excitation resonances in chiral perturbation theory.

1.3 Outline of the dissertation

In Chapter 2, the basic ideas and fundamental knowledge of lattice QCD are briefly introduced. We take the lowest-lying octet baryons for example and review the recent lattice baryon masses in detail. As the theoretical basis, in Chapter 3, chiral perturbation theory is elaborated by including the essence of effective field theory, chiral symmetry of low-energy QCD and its spontaneous and explicit breaking pattern. Applying Weinberg's theorem, the general form of chiral effective Lagrangians is constructed for the meson and baryon sectors. We also discuss the three renormalization schemes to deal with the power-counting breaking terms appearing in the calculation of baryon chiral perturbation theory. Next, we present the application of ChPT to the study of lattice baryon masses in chapters 4-7. Firstly, in Chapter 4, we perform a systematic study of lowest-lying octet baryon masses in covariant baryon chiral perturbation theory with the extended-on-mass-shell scheme up to next-to-next-to-next-to-leading order. The corresponding meson-meson and meson-baryon chiral Lagrangians are given. After calculating Feynman diagrams, we obtain the chiral corrections to octet baryon self-energies and the finite-volume corrections at $\mathcal{O}(p^4)$. By constructing Wilson BChPT in the SU(3) sector, we obtain the discretization effects for finite lattice spacing. In Chapter 5, we utilize the theoretical expressions of octet baryon masses in a discretized finite-volume hypercube and perform a systematic study of all the published lattice QCD data by including chiral extrapolation of octet baryon masses, finite-volume effects, and finite-lattice spacing discretization effects. In addition, the virtual decuplet effects on the chiral extrapolation and finite-volume effects are systematically explored. In Chapter 6, we predict the octet baryon sigma terms, $\sigma_{\pi B}$ and σ_{sB}, via the Feynman-Hellmann theorem by analyzing the latest high-statistics lattice QCD data. Three key factors in determining sigma terms are clarified for the first time, including effects of lattice scale setting, systematic uncertainties originating from chiral expansion truncations, and constraint of strong-interaction isospin breaking effects. As a natural extension, in Chapter 7, we present an analysis of lowest-lying decuplet baryon masses up to next-to-next-to-next-to-leading order in EOMS BChPT. In order to determine the unknown low-energy constants, we perform a simultaneous fit of lattice data from the PACS-CS, QCDSF-UKQCD, and HSC collaborations, with finite-volume corrections included self-consistently. The pion- and strangeness-sigma terms of the decuplet baryons are also predicted. With the development of computer techniques, the baryon masses of excitation states are becoming available in lattice simulations, especially for the Roper. In Chapter 8, the nucleon, Delta and Roper masses and widths are systematically studied in an extension of chiral perturbation theory that includes the Delta-nucleon and Roper-nucleon mass differences as low-energy scales. The contributions due to the mixing between nucleon and Roper are taken into account explicitly. The virtual Roper effects on the nucleon and Delta masses are evaluated up to next-to-next-to-leading order, as well as the effects of the nucleon and Delta in the Roper mass and width. Finally, a brief summary and perspectives are given in Chapter 9. Furthermore, in Appendix A, we tabulate the latest $n_f = 2+1$ lattice results of lowest-lying octet baryon masses. In Appendices B and C, the utilized Feynman rules and the method of loop integrals are presented, respectively. In Appendix D, the strong isospin-breaking effects on octet baryon masses are calculated.

Chapter 2

Lattice Quantum Chromodynamics

Lattice Quantum Chromodynamics, as a numerical method to deal with nonperturbative low-energy QCD from first principles, was proposed by Wilson [17] in the 1980s. LQCD has the same input parameters as QCD: the running coupling constant α_s and the quark masses. There are three steps to carry out a nonperturbative lattice simulation. First, in order to deal with the renormalization problem of QCD, one should introduce an ultraviolet regulator into the discretized theory in terms of the finite space-time grid. Second, using the path integral and the Monte Carlo numerical method, the Green's functions of lattice QCD can be evaluated. Third, one should perform multiple extrapolations (chiral extrapolation, finite-volume corrections and continuum extrapolation) to obtain the observables of interest in continuum space-time. In this chapter, we present the basic ideas and fundamental knowledge of lattice QCD. Taking lattice octet baryon masses as an example, we briefly introduce the extraction method, the adopted lattice actions, volumes and spacings. And, recent LQCD studies of Roper mass are summarized. For more details and the recent developments of LQCD, we refer to the recent excellent reviews [120–129].

2.1 Fundamentals of lattice QCD

In this section, we overview the basic and key techniques in lattice QCD simulation. Because the transition matrix elements can be evaluated by using the Feynman path integral approach, we first discuss the technique of path integrals in LQCD.

In continuum QCD, the expectation value of one chronological operator $\hat{O}[\psi,\bar{\psi},A_\mu]$ can be expressed in terms of a path integral in Euclidean space and time [1]

$$\langle\mathcal{O}\rangle = \frac{1}{\mathcal{Z}}\int\mathcal{D}\psi\mathcal{D}\bar{\psi}\int\mathcal{D}A_\mu\hat{O}[\psi,\bar{\psi},A_\mu]e^{-(\bar{\psi}M\psi+S_G)}, \tag{2.1}$$

where ψ and $\bar{\psi}$ are quark and anti-quark fields, and A_μ is gauge field. The M is $M = \not{D} + m$ with the gauge covariant derivative $D_\mu = \partial_\mu + igA_\mu$ and quark mass m. The gluon gauge action is $S_G = \frac{1}{4}G_{\mu\nu}G^{\mu\nu}$ with the gluon field strength $G_{\mu\nu} = \partial_\mu A_\nu - \partial_\nu A_\mu - ig[A_\mu, A_\nu]$, where g is the SU(3) structure constant. $A_\mu = A_\mu^a T_a$ with the eight gluon fields A_μ^a and T_a being the SU(3) generators in the **3** representation. The partition function $\mathcal{Z}$ in Euclidean space-time is [130, 131]

$$\mathcal{Z} = \int\mathcal{D}\psi\mathcal{D}\bar{\psi}\int\mathcal{D}A_\mu e^{-(\bar{\psi}M\psi+S_G)}. \tag{2.2}$$

After performing the integration over fermion fields analytically and using its Gaussian structure,

$$\int\mathcal{D}\psi\mathcal{D}\bar{\psi}e^{-\bar{\psi}M\psi} \propto \det(M), \tag{2.3}$$

[1] We want to mention that the expectation values $\langle\hat{O}\rangle$ in the path integral approach correspond to time-ordered correlation functions.

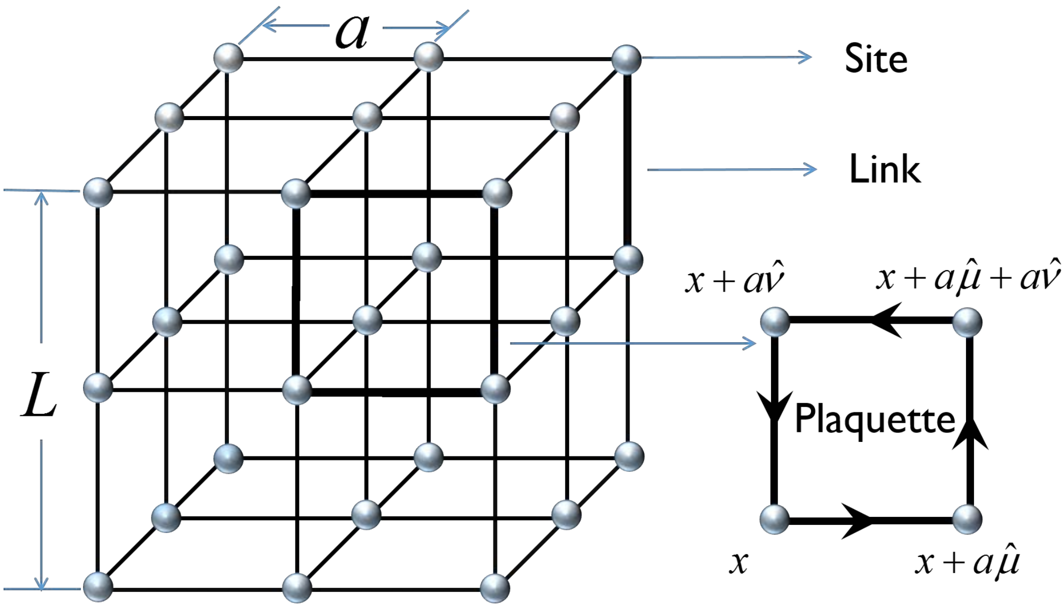

Figure 2.1: The fundamental ingredients of lattice QCD simulations in three dimensions: lattice site, gauge link, plaquette (the smallest loop).

we can express the expectation value as

$$\langle \mathcal{O} \rangle = \frac{1}{\mathcal{Z}} \int \mathcal{D}A_\mu \det(M) \hat{O}[M^{-1}, A_\mu] e^{\int d^4x(-\frac{1}{4}G_{\mu\nu}G^{\mu\nu})}, \tag{2.4}$$

with

$$\mathcal{Z} = \int \mathcal{D}A_\mu \det(M) e^{\int d^4x(-\frac{1}{4}G_{\mu\nu}G^{\mu\nu})}. \tag{2.5}$$

Therefore, the expectation value of $\hat{O}[\psi, \bar{\psi}, A_\mu]$ and the partition function are integrals over only the background gluon gauge configurations with the quark contribution encoded in the non-local term $\det(M)$.

In order to evaluate the path integral [Eq. (2.1)] in lattice QCD, one can discretize a finite Euclidean space-time with length L into a number of unit cells with the lattice spacing a, as illustrated in Fig. 2.1 for three dimensions. Here we only focus on the common isotropic case in which the lattice spacings in all directions are equal. The corresponding temporal/spatial coordinates of lattice sites are

$$x_\mu = n_\mu a, \quad \text{with} \quad n_\mu = 0, \cdots, N_\mu - 1, \tag{2.6}$$

where the a and N_μ are the lattice spacing and the number of lattice sites in the direction μ, respectively. The lattice size in the direction μ is $L_\mu = aN_\mu$. In the studies of the properties of hadronic ground states, the number of lattices in temporal dimension (N_t) is always $3 \sim 5$ times larger than the one in the spacial dimension (N_s).

In the discretized space-time, the quark field ($\Psi(x)$) is located in the lattice site,

$$\psi \to \Psi(x) = (u(x), d(x), s(x), \dots)^T, \tag{2.7}$$

with three light quark fields $u(x), d(x), s(x)$, and the gluon gauge field $(U_\mu(x,y))$ is defined as the link connecting the two adjacent sites,

$$A_\mu \to U_\mu(x,y) = P\exp(-\int_x^y A_\mu(x')dx'). \tag{2.8}$$

In terms of discretized fields, the expectation value of operator $\langle \mathcal{O} \rangle$ can be written as

$$\langle \mathcal{O} \rangle = \frac{1}{\mathcal{Z}} \int \mathcal{D}\Psi\mathcal{D}\bar{\Psi} \int \mathcal{D}U_\mu \; O[\Psi, \bar{\Psi}, U_\mu] \; e^{-(\bar{\Psi}M(U)\Psi + S_G[U])}, \tag{2.9}$$

in the discretized space-time, with the quark operator $M(U)$ and the gluon gauge action $S_G(U)$, which depend on the gauge field U. In principle, we can perform the integration over the quark fields, and obtain

$$\langle \mathcal{O}(q, \bar{q}, U) \rangle = \frac{1}{\mathcal{Z}} \int \mathcal{D}U_\mu(x) \mathrm{det} M(U) O[M^{-1}(U), U_\mu] \; e^{-S_G(U)}. \tag{2.10}$$

Because there are 4 gauge links for each lattice site, and every gauge link is described by an SU(3) matrix with 8 parameters, the number of integration variables in Eq. (2.10) is huge: $N_s^3 \times N_t \times 4 \times 8$. Therefore, direct numerical integration is impractical and one has to use Monte-Carlo techniques to generate all the sets of U on all links. The cost of lattice QCD is roughly expressed as [132] [2]

$$\text{Cost} \propto \left(\frac{L}{a}\right)^4 \frac{1}{a} \frac{1}{M_\pi^2 a}, \tag{2.11}$$

where the first factor is the number of lattice sites ($N_s^3 N_t$), and the second and third factors are due to "critical-slowing-down" of the algorithms used for the simulation. Here, we want to mention that, at the annual conference of lattice QCD 2001, a practical formula was given by Ukawa [133] with the standard Hybrid-Monte-Carlo (HMC) algorithm employed the CP-PACS and JLQCD collaborations. In 2006, an updated formula of lattice cost was presented using the domain decomposition ideas (DD) with HMC algorithm [134]. The number of N_{op} of floating-point can be expressed as

$$N_{\text{op}} = k \left(\frac{20 \text{ MeV}}{\bar{m}}\right) \left(\frac{L}{3 \text{ fm}}\right)^5 \left(\frac{0.1 \text{ fm}}{a}\right)^6 \text{ Tflops} \times \text{year}, \tag{2.12}$$

where $\bar{m}$ is the running sea-quark mass in the $\overline{\text{MS}}$ scheme at renormalization scale $\mu = 2$ GeV and $k \simeq 0.05$ when one employs the $\mathcal{O}(a)$-improved action. In order to guarantee precision and statistical quality, the lattice spacing a is usually taken about 0.1 fm, and the lattice box size is $L = 3 \sim 5$ fm.

In the last century, under the limitation of computer resources, the "quenched" approximation was employed in the lattice simulations [18, 19], wherein quark fields are treated as non-dynamical "frozen" variables. It corresponds to taking $\det(M) =$ constant and neglecting quark loop effects. After that, the so called "partially quenched" approximation [20, 21], where the determinant $\det(M) = \det(\not{D}(U) + m_{\text{sea}})$ and the quark propagator $= (\not{D} + m_{\text{val}})^{-1}$ with $m_{\text{sea}} \neq m_{\text{val}}$, was proposed. In this case, the quark loop contributions are partially taken into account. Nowadays, with the development of computing power and numerical algorithms, full-dynamical lattice simulations have become feasible. The international activity has

[2]

begun to share the lattice QCD configurations, such as the International Lattice Data Grid (ILDG) [http://plone.jldg.org/]. From this website, one can find several large collections of ensembles of configurations.

When one discretizes the equation of motion for fermions, the fermion doubling problem appears, which is manifested through the existence of extra poles in the Dirac propagator on the lattice. These poles do not disappear even in the continuum limit $a \to 0$. In order to explicitly show this problem, we write out the Dirac propagator in momentum space

$$D(p) = \frac{i(1/a)\sum_{\mu}\gamma_\mu \sin(ap_\mu) + m}{[(1/a)\sum_{\mu}\sin(ap_\mu)]^2 + m^2}. \tag{2.13}$$

In addition to the physical pole at $p^2 = -m^2$, there are also 15 additional poles located at the edges of the Brillouin zone. This is because of the chiral anomaly [135] [3], which exists in the continuum theory, while it is absent in lattice QCD [136].

In practical lattice calculations, one has to fix the fermion doubling problem by employing different types of fermion actions, such as staggered fermions [137–139], Wilson fermions [140], twisted mass fermions [141, 142], and chiral symmetric fermions [143–146] (e.g. domain wall fermions, overlap fermions).

2.2 Extracting baryon masses

In this section, we present the techniques to extract physical observables, especially baryon masses. Hadron matrix elements can be calculated using two- or three-point correlation functions. In order to extract the baryon masses, we take the two-point correlation function for example:

$$\langle 0|\mathcal{O}_f(\boldsymbol{x}, t)\mathcal{O}_i^\dagger(\boldsymbol{0}, 0)|0\rangle, \tag{2.14}$$

with the "source" operator $\mathcal{O}_i$ and the "sink" operator $\mathcal{O}_f$, representing the amplitude for creating a state with the quantum numbers of $\mathcal{O}_i$ at space-time point $(\boldsymbol{0}, 0)$, annihilated by $\mathcal{O}_f$ at $(\boldsymbol{x}, t)$. For the specific octet baryon state $|B\rangle$, the two operators should have non-zero overlaps with $|B\rangle$ ($\langle 0|\mathcal{O}_{i,f}|B\rangle \neq 0$).

One can perform Fourier-transforms in the spatial directions for Eq. (2.14)

$$C_{if}(\boldsymbol{p}, t) = \sum_{\boldsymbol{x}} \langle 0|\mathcal{O}_f(\boldsymbol{x}, t)\mathcal{O}_i^\dagger(\boldsymbol{0}, 0)|0\rangle e^{-i\boldsymbol{p}\cdot\boldsymbol{x}}. \tag{2.15}$$

Inserting a complete set of energy eigenstates, the correlation function becomes

$$C_{if}(\boldsymbol{p}, t) = \sum_n \frac{1}{2E_n(\boldsymbol{p})} \langle 0|\mathcal{O}_f|n\rangle\langle n|\mathcal{O}_i^\dagger|0\rangle e^{-E_n(\boldsymbol{p})t}, \tag{2.16}$$

where the energy $E_n(\boldsymbol{p})$ is the nth-eigenvalue of H, and the factor $1/2E_n(\boldsymbol{p})$ is due to the relativistic normalization. If the octet baryon state $|B\rangle$ happens to be the lowest energy state, the correlation function can become

$$C_{if}(t) \xrightarrow{t\to\infty} \frac{1}{2E_0(\boldsymbol{p})} \langle 0|\mathcal{O}_f|B\rangle\langle B|\mathcal{O}_i^\dagger|0\rangle e^{-E_0(\boldsymbol{p})t}, \tag{2.17}$$

[3] Frequently, a symmetry of a classical theory is also a symmetry of the quantum theory based on the same Lagrangian. When it is not, the symmetry is said to be anomalous.

since all other states die at the large enough t. Therefore, the octet baryon mass $m_B = E_0$ can be extracted with the product of matrix elements $\langle 0|\mathcal{O}_f|B\rangle\langle B|\mathcal{O}_i^\dagger|0\rangle$.

In principle, the expression of the correlator $C_{if}(\boldsymbol{p}, t)$ can also be used to obtain the energies of the excited hadron states, which have the same quantum numbers as the operators $\mathcal{O}_{i,f}$, by fitting the correlation function to a sum of exponentials. However, it is complicated to extract excited state masses from these exponents as the correlation functions decay quickly. The standard method is the variational method to determine the excited state hadron spectrum [147, 148]. This method has been widely applied in the study of the hadron spectrum. Recently, a new method called Athens Model Independent Analysis Scheme (AMIAS) was proposed in Ref. [149] and applied to study the excited state of nucleon [150].

The physical quantities computed from lattice QCD always depend on the lattice unit (unknown lattice spacing a). Therefore, one has to use the scale-setting method, which is to choose a well-known quantity at the physical point to determine the lattice spacing a, to obtain the lattice results with the physical unit. We want to mention that a suitable physical quantity demands the following conditions: it is easily calculated in lattice QCD with small statistical errors, and it should have a weak dependence on the quark masses (for a recent review, see Ref. [151]). Commonly, there are two main scale setting methods: the mass-independent (phenomenological) scales and the mass-dependent (theoretical) scales. For the former, one assumes that the lattice spacing is independent of the bare quark masses at a fixed bare coupling. Then, the lattice spacing a, which is the same for all lattice ensembles, can be determined by using the physical quantities, such as the Ω mass or the pseudoscalar meson decay constants f_π, f_K at the physical point. For the mass-dependent scales, the lattice spacing varies with different bare quark masses. The lattice spacing a can be determined by using a physical quantity, which is assumed to be independent with the quark masses, such as the Sommer scales r_0, r_1 from the static quark potential $V(r)$ [152],

$$r^2 \frac{dV(r)}{dr}\bigg|_{r=r_0} = 1.65, \quad r^2 \frac{dV(r)}{dr}\bigg|_{r=r_1} = 1.0, \tag{2.18}$$

and the scales t_0, w_0 from the gradient current [153, 154],

$$\mathscr{E}(t)|_{t=t_0} = 0.3, \quad t\frac{d\mathscr{E}(t)}{dt}\bigg|_{t=w_0^2} = 0.3, \tag{2.19}$$

with $\mathscr{E}(t) = t^2\langle E(t)\rangle$, where $\langle E(t)\rangle$ being the expectation value of the continuum-like action density $G_{\mu\nu}(t)G^{\mu\nu}(t)/4$.

2.3 Lattice data of baryon masses

In the past decades, with the increase of computing power and the continuous improvement of numerical algorithms, lattice QCD has been shown to be extremely successful in studying the nonperturbative regime of QCD. There are many applications to low-energy hadronic physics, e.g. the hadronic spectrum (especially the ground state hadron masses) [128, 155], the structure of hadrons [156], the mechanism of quark confinement and chiral symmetry breaking [157], the equilibrium properties of QCD at finite temperature and finite chemical potential [158], etc. Besides that, lattice simulations can vary the input parameters, especially the quark masses,

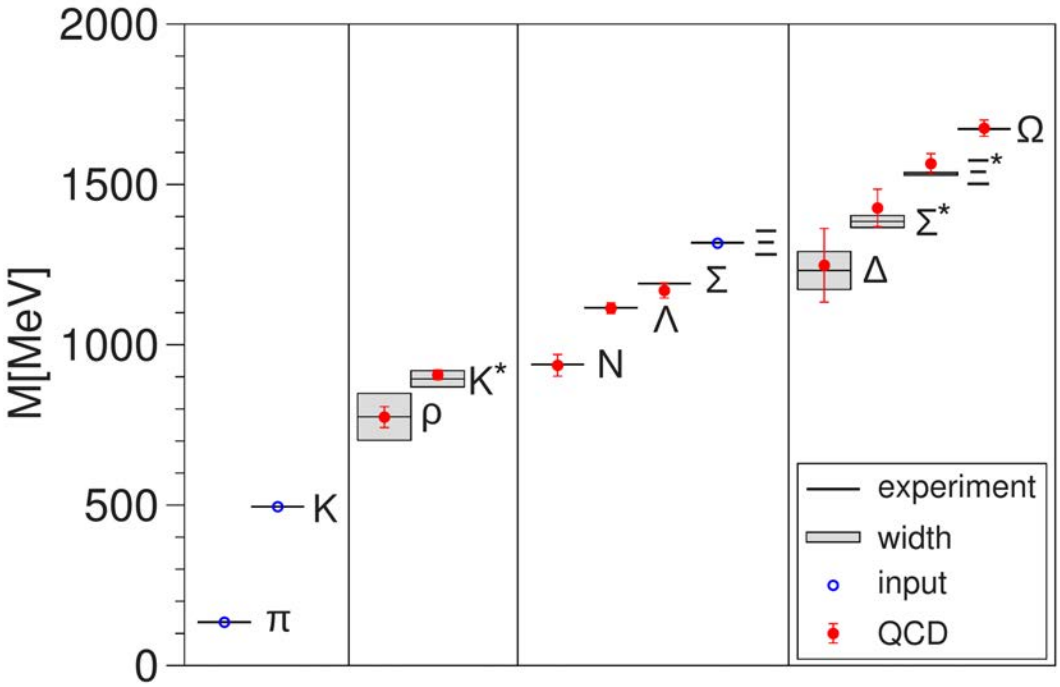

Figure 2.2: Extrapolation results for the light hadron spectrum from the BMW Collaboration. Horizontal lines and bands are experimental values and the LQCD results are denoted as solid circles. The figure is taken from Ref. [22].

to predict the dependence of observables on the running coupling constant α_s [159]. Here we would like to present the recent studies of baryon masses from lattice simulations. The latest developments of lattice QCD in the study of low-energy particle physics are reviewed in Ref. [129].

Recently, the lowest-lying baryon masses, composed of up, down and strange quarks, has been simulated by various LQCD collaborations [22–29, 160]. Here we want to mention that, as the first systematic and accurate study of proton and nucleon masses and other light hadrons (including the ground state of pseudoscalar octet meson, vector nonet meson, octet baryon and decuplet baryon masses), the BMW Collaboration provided an accurate interpretation of the origin of mass from first principles [22]. In the BMW calculations, the lightest pion mass is $M_\pi \approx 190$ MeV, very close to its physical value $M_\pi^{\text{phys.}} = 139$ MeV, which guarantees a valid chiral extrapolation to the physical region. Three different values of lattice spacing $a = 0.125$, 0.085, and 0.065 fm are employed to take into account lattice discretization effects and to perform the continuum extrapolation of lattice data. Several lattice box size L are considered, to include finite-volume corrections. The effects of the heavier c, b, and t quarks are included in the coupling constant and light quark masses. With the above considerations, the extrapolation results of light hadron spectrum are very close to the corresponding experimental data (Fig. 2.2). Furthermore, in Fig. 2.3, they present the chiral extrapolation of the nucleon lattice data with three different lattice spacings. We can see that the extrapolation result for the nucleon mass is 953(29)(19) MeV, which is almost the same as the experimental value $m_N^{\text{phys.}} = 939(1)$ MeV [15]. More recently, the ETMC Collaboration have studied the lowest-lying baryon

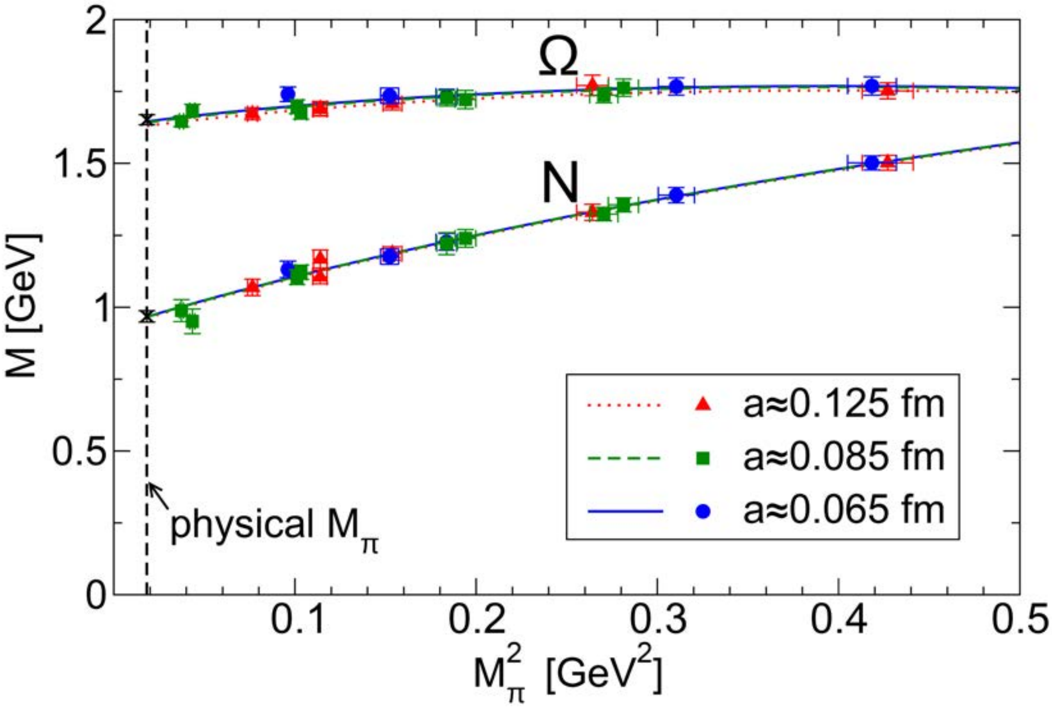

Figure 2.3: The extrapolation of the nucleon and omega masses as function of the pion mass M_π^2 for all three values of the lattice spacing. The figure is taken from Ref. [22].

masses with $n_f = 2+1+1$ twisted mass fermions [160], where a strange and a charm quark masses fixed to approximately their physical values. The pseudoscalar masses in the range of 210 MeV to 430 MeV with three different lattice spacings $a = 0.0936(13),\ 0.0823(10),\ 0.0646(7)$ fm.

During the same period, several lattice QCD collaborations have also performed $n_f = 2+1$ simulations of light hadron spectrum [23–29]. In Table 2.1, we tabulate the quark/gluon gauge actions and lattice spacings which are utilized in the BMW [22], PACS-CS [23], LHPC [25], HSC [26], QCDSF-UKQCD [28], NPLQCD [29], and ETMC [160] simulations. From Table 2.1, we can see that most lattice simulations employ a lattice spacing $a \approx 0.1$ fm and the $\mathcal{O}(a)$-improved action. On the other hand, although all these five collaborations adopt different fermion and gauge actions, all of them are believed to lead to the same continuum theory – QCD. Therefore, it is crucial to clarify whether all these simulation results of octet baryon masses are consistent with each other [161]. It should be mentioned that, in this work, we would like to limit our studies in the SU(3) sector to analyze the lattice baryon masses from $n_f = 2+1$ simulations. Therefore, the ETMC results and the unpublicable BMW results are not studied.

As has been stated in introduction, lattice calculations are performed with larger than physical light quark masses and finite volumes. In Fig. 2.4, we show the lattice simulation points of the PACS-CS, LHPC, HSC, QCDSF-UKQCD and NPLQCD collaborations in the $(2M_K^2 - M_\pi^2)$ $-M_\pi^2$ plane and in the L–M_π^2 plane. There is only one point for the NPLQCD simulation at $M_\pi = 389$ MeV on the left panel, because the main purpose of the NPLQCD collaboration was to study finite-volume effects on the baryon masses. The large range of light

Table 2.1: The quark/gluon gauge action, and lattice spacings which are employed in the BMW, PACS-CS, LHPC, HSC, QCDSF-UKQCD, NPLQCD, and ETMC simulations.

lattice coll.	quark action	gluon action	lattice spacing a [fm]
BMW	clover-improved Wilson	Symanzik-improved	~ 0.125, ~ 0.085 ~ 0.065
PACS-CS	$\mathcal{O}(a)$-improved Wilson	Iwasaki	0.0907(13)
LHPC	asqtad sea/ domain wall valence	Symanzik-improved	0.12406(248)
HSC	anisotropic clover	Symanzik-improved	$a_t = 0.03506(23)$ $a_s = 0.1227(8)$
QCDSF-UKQCD	$\mathcal{O}(a)$-improved Wilson	Symanzik-improved	0.0795(3)
NPLQCD	anisotropic clover	Symanzik-improved	$a_t = 0.03506(23)$ $a_s = 0.1227(8)$
ETMC	twisted mass Wilson	Iwasaki improved	0.0936(13), 0.0823(10) 0.0646(7)

pion masses provides the opportunity to explore the applicability of ChPT for extrapolation of baryon masses. Although the light u/d quark masses adopted are always larger than their physical counterpart, the strange quark masses vary from collaboration to collaboration: those of the PACS-CS and LHPC collaborations are larger than the physical one; those of the HSC and NPLQCD groups are a bit smaller, whereas those of the QCDSF-UKQCD collaboration are all lighter than the physical one. In the L–M_π^2 plane, it is seen that the PACS-CS and LHPC simulations adopt a single value of lattice volume; the HSC and QCDSF-UKQCD simulations use two different lattice volumes and the NPLQCD simulations are performed with four different lattice volumes in order to study the finite-volume effects on the octet baryon masses. Many of the simulations are still performed with $M_\phi L$ from 3 to 5 and with M_ϕ larger than 300 MeV. As a result, finite-volume corrections (FVCs) may not be negligible (see, e.g., Ref. [57]).

In Appendix A, we tabulate the octet baryon masses of the PACS-CS, the LHPC, the HSC, the QCDSF-UKQCD and the NPLQCD collaborations. The numbers are given in physical units using either the lattice scale specified in the original publications [23, 25, 26, 29] or the method of ratios such as QCDSF-UKQCD [28].

Nowadays, the lowest-lying hadron spectrum is now well understood with controllable lattice artifacts [128]. But, for the light quark hadrons, there are many excited states whose physical properties are poorly understood. In particular, the first even-parity excited state of the nucleon, $J^P = (1/2)^+$ Roper resonance $N(1440)$ or $P_{11}(1440)$, has been very interesting since its discovery [162]. In the quark model, the Roper, as an S-wave excitation, is lighter than the first odd-parity excited state $N(1530)$ or $S_{11}(1530)$, a P-wave excitation. This abnormal phenomenology stimulates a large number of studies to explain its structure with a possible exotic nature. Recently, several LQCD collaborations [150, 163–167] have performed studies of the low-lying excitation spectrum of nucleon (octet baryons) with a special attention to the

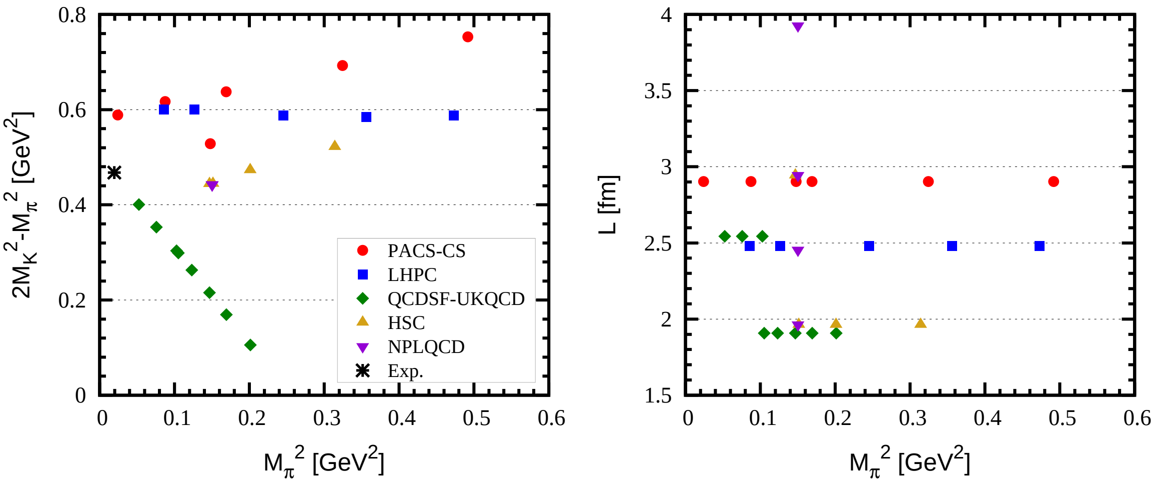

Figure 2.4: Landscape of LQCD simulations of the ground-state octet baryon masses data form the PACS-CS, LHPC, QCDSF-UKQCD, HSC, and NPLQCD collaborations in the $2M_K^2 - M_\pi^2$ vs. M_π^2 plane (left panel) and in the L vs. M_π^2 plane (right panel). The star denotes the physical point with the physical light- and strange-quark masses. The figure is taken from Ref. [64].

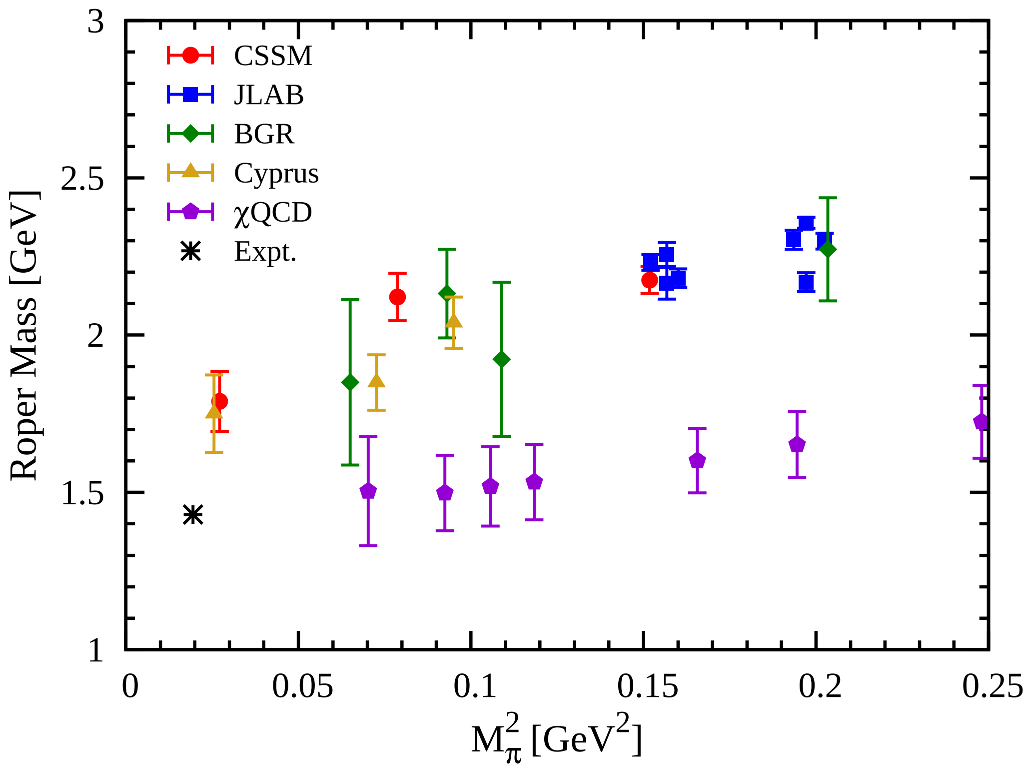

Figure 2.5: Roper mass from the CSSM, JLab, BGR, Cyprus, and χQCD collaborations.

mass of Roper resonance. In Fig. 2.5, lattice Roper masses from the CSSM [163], JLab [164], BGR [165], Cyprus [150, 166], and χQCD [167] collaborations are illustrated. We can see that lattice Roper masses exhibit much larger chiral-log effects than that of the nucleon, except the χQCD simulation adopting the Sequential Empirical Bayesian method with the overlap fermion [167]. The Roper mass from χQCD shows almost the same pion mass dependence as the nucleon. Furthermore, most lattice data of Roper mass correspond to an unstable Roper particle for $M_\pi < 500$ MeV. Therefore, LQCD calculation of Roper mass should need more efforts to clarify this large discrepancy.

Chapter 3

Chiral Perturbation Theory

In this chapter, we discuss the theoretical framework of the present dissertation. Chiral perturbation theory (ChPT), as an effective field theory of low-energy QCD, was firstly proposed by Weinberg [32] in 1979. Since its proposal, it has been widely applied in the study of low-energy hadronic physics. Firstly, we give a general introduction about the basic ideas of effective field theory. Following that, we turn to the low-energy region of QCD and discuss chiral symmetry and its breaking pattern. We introduce the construction principles of chiral effective Lagrangians in the mesonic sector and extend chiral perturbation theory to the one-baryon sector with three different renormalization schemes. In this chapter, we cannot cover all the details of ChPT and we suggest the interested readers to refer to several excellent reviews [36–46].

3.1 Effective field theory

Effective Field Theory (EFT) is a powerful theoretical tool to describe low-energy physics. Nowadays, the EFT technique has become popular in particle and nuclear physics. The basic idea of EFT is that the low energy dynamics does not depend on the details of the high energy dynamics, which can be integrated out. In order to construct an EFT to describe low-energy physics, one has to ensure a characteristic heavy scale Λ (called "hard energy scale") to separate low and high energy regions, and make an expansion in powers of Q/Λ with $Q \ll \Lambda$, where Q is the soft momentum scale of the energy region of interest. When the relevant degrees of freedom (light fields) are determined, the general possible effective Lagrangian can be written down according to a theorem, proposed in Weinberg's original work [32]:

> "If one writes down the most general possible Lagrangian, including all terms consistent with assumed symmetry principles, and then calculates matrix elements with this Lagrangian to any given order of perturbation theory, the result will simply be the most general possible S-matrix consistent with analyticity, perturbative unitary, cluster decomposition, and the assumed symmetry principles."

The general form of effective Lagrangians can be expressed as

$$\mathcal{L}_{\text{eff.}} = \sum_i c_i \mathcal{O}_i, \tag{3.1}$$

where the operators $\mathcal{O}_i$ are constructed with the light fields, and the couplings c_i are called low-energy constants (LECs) and contain the information about heavy degrees of freedom which are integrated out in the EFT. In principle, the values of c_i can be computed from a more fundamental high energy theory. If the fundamental theory is weakly coupled (e.g. QED), one can explicitly obtain the values of c_i, but if the theory is strongly coupled (e.g. QCD), one usually treats the c_i as free parameters, which can be fixed by the relevant experimental and the lattice data. Usually, we can organize the operators by using naïve dimensional analysis (NDA) [168]. First, the canonical dimensions of the light fields can be determined by using the kinetic terms in the free Lagrangian. Thus, one can easily obtain the dimension of the operators $\mathcal{O}_i$, denoted as d_i. In the four dimensional space-time, the estimated magnitudes of all the corresponding LECs should be $c_i \sim (4\pi)^{N-2}/\Lambda^{d_i-4}$.

According to the dimensions of operators, we can distinguish three types of operators with different behaviours:

- Relevant operators with $d < 4$: These operators become more relevant at low energy with large values of the coefficients $c_i \sim \Lambda^{4-d_i}$. The number of possible relevant operators is small, such as unit operator ($d = 0$), boson mass terms ($d = 2$) and fermion mass terms ($d = 3$).
- Marginal operators with $d = 4$: These operators, lying between relevancy and irrelevancy, are equally important at all energy scales. There are some well-known examples: ϕ^4 term in scalar field theory, a Yukawa interaction $\bar{\psi}\psi\phi$, and QED/QCD interactions.
- Irrelevant operators with $d > 4$: Their contributions are small at low energies with the values of couplings $\sim 1/\Lambda^{d-4}$, which can suppress the contributions from these operators. But they cannot be ignored because they usually contain information about the high energy physics.

The operators mentioned above can be systematically organized based on their contributions in an EFT. This principle of organization is the so called "power counting". As mentioned in Ref. [40], for the weakly-coupled cases, the power counting is just a dimensional expansion, as we discussed above. This kind of EFT is the decoupling effective field theory. We can write the corresponding effective Lagrangian in a general form

$$\mathcal{L}_{\text{eff.}} = \mathcal{L}_{\leq 4} + \mathcal{L}_5 + \mathcal{L}_6 + \cdots \,, \tag{3.2}$$

where $\mathcal{L}_{\leq 4}$ contains all terms with dimension $d \leq 4$, $\mathcal{L}_5$ contains the terms with dimension 5, and so on. Generally speaking, the first term $\mathcal{L}_{\leq 4}$, which only contains the relevant and marginal operators, can be renormalizable. If the irrelevant operators are included (such as $\mathcal{L}_5$, $\mathcal{L}_6$, $\cdots$), the EFT becomes renormalizable order by order. The corrections from the $d > 4$ parts are suppressed by $(E/\Lambda)^{d-4}$. There are several decoupling EFTs: QED, the Fermi theory of weak interaction, and the Standard Model. But for the un-decoupling EFT [40], the situation will be very different when one has to tackle the strongly-coupled theories with spontaneous symmetry breaking down. The fundamental degrees of freedom are replaced by the light pseudo-Goldstone bosons at low energies. There are two examples of non-decoupling EFTs, the Standard Model without Higgs bosons and chiral perturbation theory. In the next section, we will give the details of chiral perturbation theory.

Generally, there are infinite terms in the effective Lagrangian. However, at a specific expansion order, EFT is described by a number of finite terms in the Lagrangian with several coupling constants. Once the effective Lagrangian is written out at a given order, the EFT can provide a powerful prediction ability for many different processes. Besides, there must exist a range of applicability for an EFT, which usually depends on the characteristic energy scale Λ.

At some high energy region, one has to find another high energy theory, which could lead to the corresponding EFT. In this section, we only give a brief overview of EFT, the interested readers can find more details in the reviews [169–176].

3.2 Chiral perturbation theory

In this section, we begin to introduce a powerful EFT for the study of nonperturbative strong interactions. As mentioned above, this EFT should have the same symmetries as QCD and in particular chiral symmetry. That is why this EFT is named as Chiral Perturbation Theory. We discuss how to construct chiral perturbation theory from low-energy QCD, mainly focusing on the meson sector. Chiral perturbation theory in its modern form was introduced by Weinberg [32], and Gasser and Leutwyler [33]. The basic idea of ChPT is an two-fold expansion in small momentum and small quark masses.

3.2.1 Chiral symmetry and its breaking

In the Standard Model, there are six different quark flavors with three "light" quarks (u, d, s) and three "heavy" quarks (c, b, t), compared with the splitting energy scale $\Lambda_\chi \sim 1$ GeV [1] (In the following, this energy scale is denoted as the chiral symmetry breaking scale). Because we mainly talk about the low-energy region in the following, we will focus on the three-flavor QCD. The corresponding Lagrangian can be expressed as

$$\mathcal{L}_{\mathrm{QCD}} = \sum_{f=u,d,s} (\bar{q}_f i\not{D} q_f - m_f \bar{q}_f q_f) - \frac{1}{4} G_{\mu\nu,a} G_a^{\mu\nu}. \tag{3.3}$$

In order to better present the approximate chiral symmetry, we would like to rewrite the QCD Lagrangian as

$$\mathcal{L}_{\mathrm{QCD}} = \mathcal{L}^0_{\mathrm{QCD}} + \mathcal{L}_M, \tag{3.4}$$

with

$$\mathcal{L}^0_{\mathrm{QCD}} = \sum_{f=u,d,s} \bar{q}_f i\not{D} q_f - \frac{1}{4} G_{\mu\nu,a} G_a^{\mu\nu}, \quad \mathcal{L}_M = \bar{q}\mathcal{M}q, \tag{3.5}$$

where the three light quark masses are collected in a diagonal matrix $\mathcal{M} = \mathrm{diag}(m_u,\ m_d,\ m_s)$.

Firstly, we introduce two projection operators $P_{L,R}$ with the chirality operator γ_5,

$$P_L = \frac{1}{2}(1-\gamma_5), \quad P_{\mathrm{R}} = \frac{1}{2}(1+\gamma_5). \tag{3.6}$$

Thus, the quark spinor field q_f can be decomposed into left- and right-handed components, $q_{f,L}$ and $q_{f,R}$, respectively,

$$q_f = \frac{1}{2}(1-\gamma_5) q_f + \frac{1}{2}(1+\gamma_5) q_f = P_L q_f + P_R q_f \equiv q_{f,L} + q_{f,R}. \tag{3.7}$$

In terms of this decomposition, one can re-express the Lagrangian $\mathcal{L}^0_{\mathrm{QCD}}$ as

$$\mathcal{L}^0_{\mathrm{QCD}} = \sum_{f=u,d,s} \bar{q}_{f,L} i\not{D} q_{f,L} + \bar{q}_{f,R} i\not{D} q_{f,R} - \frac{1}{4} G_{\mu\nu,a} G_a^{\mu\nu}, \tag{3.8}$$

[1] Λ_χ is associated with the mass of rho meson, $m_\rho = 770$ MeV, and the chiral symmetry breaking scale $4\pi f_\pi \sim 1170$ MeV.

with the total separation between left- and right-handed quark fields. The above Lagrangian has a classical global $U(3)_L \times U(3)_R$ symmetry. According to group theory, the $U(3)_L \times U(3)_R$ can be expressed as

$$U(3)_L \times U(3)_R \equiv SU(3)_L \times SU(3)_R \times U(1)_V \times U(1)_A, \tag{3.9}$$

where the vectorial symmetry $U(1)_V$ is the conservation of baryon number, but the axial symmetry $U(1)_A$ is broken by instanton effects ($U(1)_A$ anomaly) [177]. Because the baryon number is invariant in the strong interaction, the Lagrangian $\mathcal{L}^0_{\rm QCD}$ is actually invariant under the remaining $SU(3)_L \times SU(3)_R$ transformation,

$$q_{f,L} \to e^{i\frac{\lambda^a}{2}\alpha^a_L} q_{f,L}, \quad q_{f,R} \to e^{i\frac{\lambda^a}{2}\alpha^a_R} q_{f,R}, \tag{3.10}$$

with the Gell-Mann $SU(3)$ matrices λ^a $(a = 1, \ldots, 8)$.

By using Nöther's theorem [178–180], one can establish the connections between continuous symmetries and conserved quantities. For the chiral symmetry group $SU(3)_L \times SU(3)_R$, there are $2(n_f^2 - 1) = 16$ (with $n_f = 3$) Nöther currents divided into left- and right-handed conserved currents,

$$J^{\mu,a}_L = \bar{q}_{\rm L}\gamma^\mu \frac{\lambda^a}{2} q_{\rm L}, \quad J^{\mu,a}_R = \bar{q}_{\rm R}\gamma^\mu \frac{\lambda^a}{2} q_{\rm R}, \tag{3.11}$$

with $\partial_\mu J^{\mu,a}_{L/R} = 0$. Usually, one can use linear combinations of the above chiral currents to obtain the vector and axial-vector currents

$$\begin{aligned} V^{\mu,a} &= J^{\mu,a}_R + J^{\mu,a}_L = \bar{q}\gamma^\mu \frac{\lambda^a}{2} q, \\ A^{\mu,a} &= J^{\mu,a}_R - J^{\mu,a}_L = \bar{q}\gamma^\mu \gamma_5 \frac{\lambda^a}{2} q. \end{aligned} \tag{3.12}$$

The corresponding conserved Nöther charges are

$$\begin{aligned} Q^a_V &= \int d^3x q^\dagger(x) \frac{\lambda^a}{2} q(x), \quad \text{with} \quad \frac{dQ^a_V}{dt} = 0, \\ Q^a_A &= \int d^3x q^\dagger(x) \gamma_5 \frac{\lambda^a}{2} q(x), \quad \text{with} \quad \frac{dQ^a_A}{dt} = 0. \end{aligned} \tag{3.13}$$

Before we go on to discuss chiral symmetry breaking, we want to mention that there are two realizations of chiral symmetry [2]. One is the Wigner-Weyl mode, which is the linear representation, with the trivial (empty) vacuum ($Q^a_V|0\rangle = Q^a_A|0\rangle = 0$). Another is the Nambu-Goldstone mode, which is the non-linear realization, with a non-trivial vacuum ($Q^a_V|0\rangle = 0$, $Q^a_A|0\rangle \neq 0$).

Up to now, the discussion about chiral symmetry is based on the chiral limit with three zero light-quark masses. But, in fact, chiral symmetry is not quite exact in QCD. Recalling the full QCD Lagrangian at low-energies [Eq. (3.4)], the mass part is

$$\mathcal{L}_M = -\bar{q}\mathcal{M}q = -(\bar{q}_R\mathcal{M}q_L + \bar{q}_L\mathcal{M}q_R). \tag{3.14}$$

We can see that left- and right-handed quark fields are mixed by the quark-mass matrix. Therefore, chiral symmetry is explicitly broken by the non-zero quark masses.

[2] Generally, a classical symmetry is realized in quantum field theory in two different ways depending on how the vacuum responds to a symmetry transformation.

Due to the small masses of u, d, and s quarks, QCD possesses an approximate chiral symmetry and this symmetry should be approximately presented in the hadronic spectrum. That means there should exist (almost) degenerate parity doublets [3] under Wigner's realization mode of chiral symmetry. In experiment, one can find two observed bands with different parity, but they are not degenerate. Furthermore, the masses of lowest-lying pseudoscalar mesons (π, K, η) are very small in comparison with other hadronic states. Therefore, in order to explain these two observations, we can deduce that chiral symmetry is conserved in the QCD Lagrangian but it is spontaneously broken by the vacuum state. In the Nambu-Goldstone realization mode, the global chiral symmetry $SU(3)_L \times SU(3)_R$ is spontaneously broken to the vectorial subgroup $SU(3)_V = SU(3)_{L+R}$,

$$SU(3)_L \times SU(3)_R \xrightarrow{\text{SSB}} SU(3)_V, \tag{3.15}$$

where $SU(3)_V$ is the symmetry group of vacuum. According to Goldstone's theorem [181], in this process, an octet of pseudoscalar massless Goldstone bosons should be produced due to the eight broken generators of chiral symmetry group. If we denote $G = SU(3)_L \times SU(3)_R$ and $H = SU(3)_V$, the Goldstone boson manifold is the coset space G/H which is isomorphic to $SU(3)$. Furthermore, when considering that the light quark masses are not zero but small, we can easily find the candidates for the eight Goldstone bosons in the hadronic spectrum. There are three pions, $\pi^{0,\pm}$, four kaons, $K^{\pm,0}, \bar{K}^0$, and the eta, η. Therefore, we can explain the above two experimental phenomena by using Goldstone's theorem.

3.2.2 Lowest order chiral effective Lagrangian

In the preceding section, we identified the relevant degrees of freedom, the pseudoscalar mesons π, K, η, at low-energy region. Therefore, the chiral perturbation theory can be constructed by applying Weinberg's theorem. The corresponding effective Lagrangian should demand all the symmetries of QCD, such as Lorentz invariant, $SU(3)_C$ gauge invariance, charge conjugation (C), parity (P), and time reversal (T) symmetries, and chiral symmetry. Because chiral symmetry is spontaneously broken, one cannot directly write down the effective Lagrangian from the nonperturbative QCD Lagrangian due to the replacement of quarks and gluons with Goldstone bosons. In the 1970s, the standard method to construct effective field theory for a spontaneously broken symmetry was formulated by Callan, Coleman, Wess, and Zumino [182, 183].

Usually, the Goldstone boson fields (π, K, η) are collected in a unitary matrix field $U(\phi)$

$$U(\phi) = \exp\left(i\frac{\phi}{F_\phi}\right), \tag{3.16}$$

$$\phi = \sum_{a=1}^{8} \phi_a \lambda_a = \sqrt{2}\begin{pmatrix} \frac{1}{\sqrt{2}}\pi^0 + \frac{1}{\sqrt{6}}\eta & \pi^+ & K^+ \\ \pi^- & -\frac{1}{\sqrt{2}}\pi^0 + \frac{1}{\sqrt{6}}\eta & K^0 \\ K^- & \bar{K}^0 & -\frac{2}{\sqrt{6}}\eta \end{pmatrix}, \tag{3.17}$$

with the meson decay constant F_ϕ and the law of transformation for $U(\phi)$

$$U(\phi) \to g_R U(\phi) g_L^\dagger, \quad U^\dagger(\phi) \to g_L U^\dagger(\phi) g_R^\dagger, \tag{3.18}$$

[3]For a given spin and parity hadronic state, there would be another state with the same spin but the opposite parity.

where g_L and g_R are $SU(3)_L$ and $SU(3)_R$ transformations, respectively. On the other hand, a more basic matrix field $u(\phi)$ is the square root of $U(\phi)$ with the chiral transformation

$$u(\phi) \to g_R u(\phi) h(g,\phi)^{-1}, \tag{3.19}$$

with the unbroken transformation $h(g,\phi) \in SU(3)_V$.

In the following, we could construct the general effective Lagrangians in terms of $U(\phi)$ or $u(\phi)$. As a first step, we want to discuss how to obtain the lowest order chiral Lagrangian corresponding to the QCD Lagrangian $\mathcal{L}^0_{\text{QCD}}$ in the chiral limit.

Since the Goldstone bosons are pseudoscalar, in order to guarantee parity invariance, the effective Lagrangian should contain an even number of meson fields. More precisely, one U should accompany $U^\dagger$ due to the parity transformation $\phi \xrightarrow{\text{parity}} -\phi/U \xrightarrow{\text{parity}} U^\dagger$. The most general invariant term can be the product of terms with the form,

$$\langle UU^\dagger \cdot UU^\dagger \cdot ...\rangle, \tag{3.20}$$

where $\langle ...\rangle$ denotes the trace of flavor space. At lowest order, due to $UU^\dagger = I$, in order to obtain a non-trivial interaction, the derivative of U is required. With the limitation of Lorentz invariance, one has to introduce even numbers of derivative on the meson fields. The only possible term of lowest order is $\langle \partial_\mu U \partial^\mu U^\dagger\rangle$. We will investigate whether this term is invariant or not under the chiral transition. The elements of $\langle \partial_\mu U \partial^\mu U^\dagger\rangle$ have the following transformation properties,

$$\partial_\mu U \to g_R \partial_\mu U g_L^\dagger, \qquad \partial_\mu U^\dagger \to g_L \partial_\mu U^\dagger g_R^\dagger. \tag{3.21}$$

It is easy to see that

$$\langle \partial_\mu U \partial^\mu U^\dagger\rangle \to \langle g_R \partial_\mu U g_L^\dagger g_L \partial^\mu U^\dagger g_R^\dagger\rangle = \langle g_R^\dagger g_R \partial^\mu U \partial^\mu U^\dagger\rangle = \langle \partial_\mu U \partial^\mu U^\dagger\rangle. \tag{3.22}$$

Finally, we obtain the lowest order chiral effective Lagrangian

$$\mathcal{L}^{(2)}_\phi = \frac{F_\phi^2}{4}\langle \partial_\mu U \partial^\mu U^\dagger\rangle, \tag{3.23}$$

where the superscript 2 denotes two derivatives. The coefficient $F_\phi^2/4$ is to ensure the kinetic terms having the traditional form with $\frac{1}{2}\partial_\mu\phi_a\partial^\mu\phi_a$. This can be clearly shown when one performs the expansion of U

$$U = 1 + \frac{i\phi}{F_\phi} + \cdots, \quad U^\dagger = 1 - \frac{i\phi}{F_\phi} + \cdots, \tag{3.24}$$

$$\partial_\mu U = \frac{i}{F_\phi}\partial_\mu\phi + \cdots, \quad \partial_\mu U^\dagger = -\frac{i}{F_\phi}\partial_\mu\phi + \cdots, \tag{3.25}$$

as the effective Lagrangian becomes

$$\mathcal{L}^{(2)}_\phi = \frac{1}{2}\langle \partial_\mu\phi\partial^\mu\phi\rangle + \frac{1}{12F_\phi^2}\langle(\phi\partial_\mu\phi)(\phi\partial_\mu\phi)\rangle + \mathcal{O}\left(\frac{\phi^6}{F_\phi^4}\right). \tag{3.26}$$

Here we want to mention that the Lagrangian $\mathcal{L}^{(2)}_\phi$ trivially satisfies $U(1)_V$ invariance with baryon number zero.

As mentioned in the preceding section, chiral symmetry is explicitly broken by the non-zero quark masses. When constructing the effective Lagrangian, one has to incorporate the consequences of mixing left- and right-handed fields. According to the discussion in Ref. [184], if the quark mass matrix transformed as

$$\mathcal{M} \to g_R \mathcal{M} g_L^\dagger, \tag{3.27}$$

the mass term $\mathcal{L}_M$ would be invariant under the chiral transformation. We can construct the lowest order term in the effective Lagrangian with $\mathcal{M}$ using the same arguments as before. There is one term $\langle \mathcal{M}U^\dagger + U\mathcal{M}\rangle$ which is Lorentz invariant, and parity and chiral symmetric. Therefore, the lowest order Lagrangian can be written as

$$\mathcal{L}_{\text{SB}} = \frac{F_\phi^2 B_0^2}{2}\langle \mathcal{M}U^\dagger + U\mathcal{M}\rangle, \tag{3.28}$$

where the subscript (SB) denotes the chiral symmetry explicitly breaking in QCD. The constant $B_0 = -\langle 0|\bar{q}q|0\rangle / F_\phi^2$ relates to the quark condensate and cannot fixed by symmetry requirements alone.

After expanding U and $U^\dagger$ in powers of ϕ, we obtain

$$\mathcal{L}_{\text{SB}} = -B_0\langle \mathcal{M}\phi^2\rangle + \frac{B_0}{6F_\phi^2}\langle \mathcal{M}\phi^4\rangle + O\left(\frac{\phi^6}{F_\phi^4}\right). \tag{3.29}$$

The first term provides the relationships between the masses of Goldstone bosons and the quark masses with exact isospin symmetry [4] ($m_u = m_d \equiv m_l$),

$$\begin{aligned} M_\pi^2 &= 2B_0 m_l, \\ M_K^2 &= B_0(m_l + m_s), \\ M_\eta^2 &= \frac{2}{3}B_0(m_l + 2m_s), \end{aligned} \tag{3.30}$$

and gives the Gell-Mann-Okubo relation [185–187]

$$4M_K^2 = M_\pi^2 + 3M_\eta^2, \tag{3.31}$$

which is not dependent on B_0. Furthermore, the second term of Eq. (3.29) gives higher order corrections to the masses of pseudoscalar mesons. In Appendix D, we also calculate the strong isospin-splitting effects on the meson masses.

Combining Eq. (3.23) and Eq. (3.28), the lowest order chiral Lagrangian is

$$\mathcal{L}_\phi^{(2)} = \frac{F_\phi^2}{4}\left[\langle \partial_\mu U \partial^\mu U^\dagger\rangle + 2B_0^2\langle \mathcal{M}U^\dagger + U\mathcal{M}\rangle\right]. \tag{3.32}$$

3.2.3 General chiral effective Lagrangians

The general form of the chiral Lagrangian for the mesonic sector is

$$\mathcal{L}_\phi^{\text{eff}} = \sum_n \mathcal{L}_\phi^{(2n)}[U, U^\dagger, \partial_\mu U, \partial_\mu U^\dagger, \mathcal{M}], \quad n = 1,\ 2,\ \cdots, \tag{3.33}$$

[4] The up and down quarks have very small masses ($m_u \sim m_d \sim$ few MeV) compared to Λ_{QCD}.

with the even order only. The superscripts $2n$ refer to the power of the momentum and quark mass expansion. As discussed in the above subsection, the index 2 denotes two derivatives terms or a single quark mass term. The higher order Lagrangians, e.g. $\mathcal{L}_\phi^{(4)}$, $\mathcal{L}_\phi^{(6)}$, contains more complicated terms. The expression of $\mathcal{L}_\phi^{(4)}$ is given in Eq. (4.2) of Chapter 4. The chiral Lagrangians are organized in a momentum expansion based on the chiral counting rules

$$U, U^\dagger \sim O(p^0), \quad \partial_\mu U, \partial_\mu U^\dagger \sim O(p^1), \quad \mathcal{M} \sim O(p^2), \tag{3.34}$$

with the small momentum p. This can be easy to understand with the derivative generating four momentum, $\partial_\mu \sim p_\mu$, and the on-shell condition $\mathcal{M} \propto M_\phi^2 = p^2$.

The above discussion is at the ordinary QCD level. When one wants to study the interactions with external fields at the low energies, a more general QCD Lagrangian is

$$\mathcal{L}_{\rm QCD}^{\rm External} = \mathcal{L}_{\rm QCD}^0 + \sum_{f=u,d,s} \bar{q}_f \gamma^\mu (v_\mu + \gamma_5 a_\mu) q_f - \sum_{f=u,d,s} \bar{q}_f (s - i\gamma_5 \psi_p) q_f, \tag{3.35}$$

where the external vector v_μ, axial-vector a_μ, scalar s, and pseudoscalar ψ_p fields are Hermitian 3×3 matrices in flavor space. In this situation, the effective field theory becomes more powerful and can be used to study the electromagnetic interactions and semileptonic weak interactions.

Applying Weinberg's theorem, the extended QCD Lagrangian, $\mathcal{L}_{\rm QCD}^{\rm External}$, can be mapped into the most general effective Lagrangian

$$\mathcal{L}_{\rm QCD}^{\rm External}[\bar{q}_f, q_f, G_{\mu\nu}, v_\mu, a_\mu, s, \psi_p] \to \mathcal{L}_\phi^{\rm eff}[U, \partial_\mu U, v_\mu, a_\mu, s, \psi_p], \tag{3.36}$$

which has been given in Ref. [34]. The chiral counting rules for the new induced terms are

$$v_\mu, a_\mu \sim O(p^1), \quad s, \psi_p \sim O(p^2). \tag{3.37}$$

Additionally, let us re-examine the lowest order of chiral Lagrangian which naturally includes the external field interactions,

$$\mathcal{L}_\phi^{(2)} = \frac{F_\phi}{4} \langle D_\mu U^\dagger D^\mu U + U^\dagger \chi + \chi^\dagger U \rangle, \tag{3.38}$$

where v_μ, a_μ can only appear through the covariant derivatives

$$D_\mu U = \partial_\mu U - i r_\mu U + i U l_\mu, \tag{3.39}$$

with $l_\mu = v_\mu - a_\mu$, $r_\mu = v_\mu + a_\mu$. The scalar field s and the pseudoscalar field ψ_p are encoded in

$$\chi = 2B_0(s + i\psi_p). \tag{3.40}$$

If taking the external field l_μ and r_μ as

$$l_\mu = r_\mu = -eQ\mathcal{A}_\mu, \tag{3.41}$$

with the external electromagnetic field $\mathcal{A}_\mu$ and $Q = {\rm diag}(2/3, -1/3, -1/3)$, or,

$$l_\mu = -\frac{g}{\sqrt{2}}(W_\mu^+ T_+ + {\rm H.c.}), \quad r_\mu = 0, \tag{3.42}$$

with the gauge coupling g, the massive charged weak bosons $W_\mu^\pm = (W_{1\mu} \mp i W_{2\mu})/\sqrt{2}$, and

$$T_+ = \begin{pmatrix} 0 & V_{ud} & V_{us} \\ 0 & 0 & 0 \\ 0 & 0 & 0 \end{pmatrix}, \tag{3.43}$$

one can study the electromagnetic interaction of Goldstone bosons or the semileptonic decay.

3.2.4 Weinberg's power counting

In principle, the chiral effective Lagrangian contains an infinite number of terms with an infinite number of parameters. One has to find a systematic method to collect the important contributions at a specific chiral order. This concept is called "power counting". Under the rule of power counting, we also can test the convergence of the chiral expansion by increasing chiral order.

It was shown that, in the meson sector, there is one-to-one correspondence between chiral orders and loop diagrams [33]. The general form of an amplitude $\mathcal{A}$ for a given Feynman diagram is

$$\mathcal{A} \propto \int (d^4p)^L \frac{1}{(p^2)^{N_M}} \prod_d p^{dN_d} \equiv p^{n_{\mathrm{ChPT}}}, \tag{3.44}$$

where L is the number of meson loops, N_M is the number of internal lines (meson propagators), N_d is the number of vertices with dimension d obtained from chiral Lagrangian $\mathcal{L}_\phi^{(d)}$. In a mass-independent subtraction scheme, the only dimensional parameters are the momentum p and the pion mass. The chiral dimension n_{ChPT} can be written as

$$n_{\mathrm{ChPT}} = 4L - 2N_M + \sum_d dN_d. \tag{3.45}$$

The chiral Lagrangian starts at leading order $d \geq 2$, therefore, the chiral dimension should be $n_{\mathrm{ChPT}} \geq 2$.

3.3 Chiral perturbation theory in baryon sector

3.3.1 Meson-baryon effective Lagrangians

As an effective field theory of low-energy QCD, chiral perturbation theory can also be applied to study baryon systems. The difference between the meson sector and the baryon sector is that the baryon mass is not zero at the chiral limit. We take the lowest-lying octet baryon as an example to construct the general effective Lagrangian.

The octet baryon fields can be collected in a traceless 3×3 matrix B,

$$B = \sum_{a=1}^{8} \frac{B_a \lambda_a}{\sqrt{2}} = \begin{pmatrix} \frac{1}{\sqrt{2}}\Sigma^0 + \frac{1}{\sqrt{6}}\Lambda & \Sigma^+ & p \\ \Sigma^- & -\frac{1}{\sqrt{2}}\Sigma^0 + \frac{1}{\sqrt{6}}\Lambda & n \\ \Xi^- & \Xi^0 & -\frac{2}{\sqrt{6}}\Lambda \end{pmatrix}. \tag{3.46}$$

Under the chiral symmetry $SU(3)_L \times SU(3)_R$, the baryon field B transforms as any matter field,

$$B \to B' = KBK^\dagger, \tag{3.47}$$

with $K(U, g_L, g_R)$ the compensator field [40] representing an element of the conserved subgroup $SU(3)_V$. For convenience, we introduce two definitions, the so-called chiral connection Γ_μ,

$$\Gamma_\mu = \frac{1}{2}\left[u^\dagger(\partial_\mu - ir_\mu)u + u(\partial_\mu - il_\mu)u^\dagger\right], \tag{3.48}$$

and the axial current u_μ,

$$u_\mu = i\left[u^\dagger(\partial_\mu - ir_\mu)u - u(\partial_\mu - il_\mu)u^\dagger\right]. \tag{3.49}$$

They transform as

$$\Gamma_\mu \to K\Gamma_\mu K^\dagger - (\partial_\mu K)K^\dagger, \quad u_\mu \to K u_\mu K^\dagger. \tag{3.50}$$

The covariant derivative of the baryon field is defined as

$$D_\mu B = \partial_\mu B + [\Gamma_\mu,\ B], \tag{3.51}$$

with the transformation law

$$D_\mu B \to K(D_\mu B)K^\dagger. \tag{3.52}$$

As given in Ref. [188], the chiral counting scheme of the building blocks is

$$\begin{aligned} &B, \bar{B} = \mathcal{O}(p^0), \quad D_\mu B = \mathcal{O}(p^0), \quad (i\not{D} - m_0)B = \mathcal{O}(p^1), \\ &1, \gamma_\mu, \gamma_5\gamma_\mu, \sigma_{\mu\nu} = \mathcal{O}(p^0), \quad \gamma_5 = \mathcal{O}(p). \end{aligned} \tag{3.53}$$

This counting rule can be understood from bilinears $\bar{B}\Gamma B$ with the plane waves solutions of the free Dirac equation. The details can be seen in the page 154 of Ref. [46]. With the contraction between Dirac matrices and derivatives of baryon field, the most general Lagrangians can be expressed as

$$\mathcal{L}^{\rm eff}_{\phi B} = \mathcal{L}^{(1)}_{\phi B} + \mathcal{L}^{(2)}_{\phi B} + \mathcal{L}^{(3)}_{\phi B} + \mathcal{L}^{(4)}_{\phi B} + \cdots, \tag{3.54}$$

with the gradual increase of chiral order. The lowest order of meson-baryon effective Lagrangian $\mathcal{L}^{(1)}_{\phi B}$ can be expressed as

$$\mathcal{L}^{(1)}_{\phi \rm B} = \langle \bar{B}(i\not{D} - m_0)B\rangle + \frac{D}{2}\langle \bar{B}\gamma^\mu\gamma_5\{u_\mu, B\}\rangle + \frac{F}{2}\langle \bar{B}\gamma^\mu\gamma_5[u_\mu, B]\rangle, \tag{3.55}$$

where m_0 denotes the baryon mass in the chiral limit, and the constants D and F are the axial-vector coupling constants, which can be determined from the baryon semi-leptonic decays.

After including baryons in the ChPT, the chiral order of a specific diagram with L loops is calculated as

$$n_{\rm ChPT} = 4L - 2N_M - N_B + \sum_d dV_d, \tag{3.56}$$

where N_B is the number of internal baryon propagators. However, because the baryon mass does not vanish in the chiral limit and its value is close to the chiral symmetry breaking scale Λ_χ, Weinberg's power counting is naively violated in the baryon chiral perturbation theory [5]. This problem was first pointed out by Gasser, Sainio, and Svarc [35] in the 1990s. In order to illustrate the power-counting breaking (PCB) terms that appear in the loop calculations, we take a scalar loop integral with one pion and one nucleon propagators for example,

$$H(p^2, d) = -i\int \frac{d^dq}{(2\pi)^d}\frac{1}{q^2 - m_\pi^2 + i\varepsilon}\frac{1}{(p-q)^2 - m_0^2 + i\varepsilon}. \tag{3.57}$$

By using the dimensional regularization scheme and limiting $d \to 4$, one obtains

$$H = -\frac{1}{16\pi^2}\left(-2 + \log\frac{m_0^2}{\mu^2} + \frac{m_\pi^2}{m_0^2}\log\frac{m_\pi}{m_0} + \frac{2m_\pi}{m_0}\sqrt{1 - \frac{m_\pi^2}{4m_0^2}}\arccos\frac{m_\pi}{2m_0}\right). \tag{3.58}$$

[5] It is easy to see from the derivative of baryon field, $i\partial^\mu B = p^\mu_B B = [(m_B, \vec{0}) + (E_B - m_B, \vec{p}_B)]B$, where the first term is the baryon mass in the chiral limit and cannot be thought as "small quantity".

According to the chiral order of Eq. (3.56), this Feynman diagram with one scalar loop is $\mathcal{O}(p^1)$, therefore, the first two terms

$$-\frac{1}{16\pi^2}\left(-2+\log\frac{m_0^2}{\mu^2}\right), \tag{3.59}$$

are the power-counting breaking terms and should be removed from the loop contributions (equivalent to be absorbed by counter terms).

In order to systematically restore the PC, the so-called Heavy-Baryon (HB) ChPT was first proposed by Jenkins and Manohar [69], considering baryons as heavy static sources. Later, covariant BChPT implementing a consistent PC with different renormalization methods have been developed, such as the infrared (IR) [70] and the extended-on-mass-shell (EOMS) [71, 72] renormalization schemes. In the following subsections, we will briefly summarize the essential features of HB ChPT, IR BChPT and EOMS BChPT.

In addition to the afore-mentioned dimensional renormalization schemes (MS and its derivatives), other renormalization/regularization schemes have been proposed, such as the cutoff scheme [73], the finite range regulator (FRR) method [74, 75], and the partial summation approach [59] etc., to speed up the convergence of BChPT.

3.3.2 Heavy baryon approach

Drawing on the experience of heavy quark physics and of QED applied to atomic and molecular physics, the basic idea of heavy baryon scheme [69] is to take the baryon as heavy (nearly on-shell) and divide the baryon momentum into a large piece and a small residual piece,

$$p_\mu = m_0 v_\mu + k_\mu, \tag{3.60}$$

where v_μ is the baryon velocity with $v^2 = 1$ and $v_0 \geq 1$, and k_μ denotes the soft residual momentum with $k_\mu \cdot v \ll m_0,\ \Lambda_\chi$ (at rest frame with $v_\mu = (1,0,0,0)$). Therefore, in the heavy baryon scheme, one can perform a two-fold expansion in terms of

$$\frac{k}{\Lambda_\chi}, \quad \frac{k}{m_0}. \tag{3.61}$$

According to the decomposition of baryon momentum, the baryon field can also be separated into light and heavy components

$$B(x) = e^{im_0 v\cdot x}\left[\mathcal{B}_v(x) + \mathcal{H}_v(x)\right], \tag{3.62}$$

with light $\mathcal{B}_v$ and heavy $\mathcal{H}_v$ fields

$$\mathcal{B}_v(x) \equiv e^{im_0 v\cdot x} P_{v+} B(x), \quad \mathcal{H}_v(x) \equiv e^{im_0 v\cdot x} P_{v-} B(x). \tag{3.63}$$

Here, the projection operators $P_{v\pm}$ are defined as

$$P_{v\pm} \equiv \frac{1 \pm \not{v}}{2}, \tag{3.64}$$

with the properties of

$$P_{v+} + P_{v-} = 1, \quad P_{v\pm}^2 = P_{v\pm}, \quad P_{v\pm}P_{v\mp} = 0. \tag{3.65}$$

It should be mentioned that the light field $\mathcal{B}_v(x)$ is usually called heavy baryon field and $\partial_\mu \mathcal{B}_v(x)$ produces a small residual momentum k_μ. From the leading order covariant effective Lagrangian [Eq. (3.55)], one can perform the path integral and integrate out the heavy component $\mathcal{H}_v(x)$ to obtain the corresponding heavy baryon effective Lagrangians in terms of heavy baryon fields $\mathcal{B}_v(x)$ with definite velocity v_μ,

$$\hat{\mathcal{L}}_{\phi B}^{(1)} = \langle \bar{\mathcal{B}}_v iv \cdot D\mathcal{B}_v \rangle - D\langle \bar{\mathcal{B}}_v S^\mu \langle \{u_\mu, \mathcal{B}_v\} \rangle\} - F\langle \bar{\mathcal{B}}_v S^\mu [u_\mu, \mathcal{B}_v] \rangle, \tag{3.66}$$

where $\hat{}$ indicates the heavy-baryon formalism. The derivative on the heavy baryon field is defined as the same in Eq. (3.51) with the replacement of $B \to \mathcal{B}_v$. The covariant spin-operator $S_\mu = \frac{i}{2}\gamma_5 \sigma_{\mu\nu} v^\nu$ is the spin matrix with

$$S \cdot v = 0, \quad S^2 = \frac{1-d}{4}, \quad \{S_\mu, S_\nu\} = \frac{1}{2}(v_\mu v_\nu - g_{\mu\nu}), \quad [S_\mu, S_\nu] = i\varepsilon_{\mu\nu\alpha\beta} v^\alpha S^\beta, \tag{3.67}$$

in d space-time dimensions. It should be noted that the leading order Lagrangian $\hat{\mathcal{L}}_{\phi B}$ [Eq. (3.66)] does not have the baryon mass m_0 terms. The baryon mass is shuffled from the propagators to the vertices. Therefore, heavy baryon ChPT has the same power counting as Weinberg's power counting for mesons with the chiral counting order of building blocks

$$\mathcal{B}_v, \bar{\mathcal{B}}_v \sim \mathcal{O}(p^0), \quad v_\mu, S_\mu, \sim \mathcal{O}(p^0) \quad D_\mu \mathcal{B}_v, u_\mu \sim O(p^1). \tag{3.68}$$

The propagator of heavy baryon, derived from $\hat{\mathcal{L}}_{\phi B}^{(1)}$, can be written as

$$G_v(k) = \frac{P_{v+}}{v \cdot k + i\varepsilon}. \tag{3.69}$$

In order to better understand the HB method, let us reconsider the integral of a scalar loop diagram with one meson and one baryon propagator, which can be expressed as

$$\begin{aligned} H_{\mathrm{HB}} &= -i \int \frac{d^d q}{(2\pi)^d} \frac{1}{(q^2 - m_\pi^2 + i\varepsilon)} \frac{1}{v \cdot (k-q) + i\varepsilon} \\ &= -\frac{1}{16\pi^2} \frac{\pi m_\pi}{2m_0}, \end{aligned} \tag{3.70}$$

in the limit $d \to 4$. We can see that the HB result is clearly of order $\mathcal{O}(p^1)$ as required from the counting rules.

HBChPT has been successfully applied to study low-energy physical phenomena, particularly in two-flavor sector [38]. However, in order to ensure HBChPT is reparameterization invariant or Lorentz invariant at a specific order, one has to take into account the $1/m_0$ correction Lagrangians [189]. Therefore, the heavy baryon effective Lagrangians have more terms than the covariant counterparts at the same chiral order [190]. One also found that the convergence of HBChPT is not fast enough in the calculation of some physical quantities, such as electroweak form factors [191] and electromagnetic form factors [192] of nucleon.

3.3.3 Infrared regularization

In order to avoid the shortcomings of HBChPT, one has to find a regularization method to combine the proper power counting of the HB approach and proper analyticity. As a first attempt, Tang and Ellis [193, 194] pointed out that the loop integral can be divided into soft-and hard-momentum parts. The hard-momentum terms are always polynomials and can be totally absorbed into the LECs. However, this division relies on specific loop integrals which cannot be always valid. Becher and Leutwyler [70] proposed a systematic method to extract the soft- and hard-momentum parts, which is known as Infrared Regularization (IR) of baryon chiral perturbation theory.

To illustrate the main idea of IR BChPT, we would like to also take one scalar loop integral [Eq. (3.57)] for example. It is clear that the infrared singularity appears in the region of integration of $m_\pi \to 0$. Because the nucleon momentum is close to the mass shell $(m_0^2 - p^2) \sim O(p)$, the infrared singularity is of the order $\mathcal{O}(p^{d-3})$. On the other hand, the so called hard-momentum parts with large momenta are just the ordinary Taylor expansion of momentum and can be totally absorbed into the LECs.

Following the discussion of Ref. [70], in order to isolate the infrared parts, one can introduce two dimensionless variables,

$$\alpha = \frac{m_\pi}{m_0}, \quad \Omega = \frac{p^2 - m_0^2 - m_\pi^2}{2m_\pi m_0}, \tag{3.71}$$

which count as $\mathcal{O}(p)$ and $\mathcal{O}(p^0)$, respectively. After using the standard Feynman parametrization and performing the momentum shift $k \to k + pz$, the scalar loop becomes

$$H(p^2, d) = -i \int_0^1 dz \int \frac{d^dq}{(2\pi)^d} \frac{dz}{[q^2 - \mathcal{M}(z)]^2}, \tag{3.72}$$

with

$$\mathcal{M}(z) = m_0[z^2 - 2\alpha\Omega z(1-z) + \alpha^2(1-z)^2]. \tag{3.73}$$

Performing the integration over k, we can get

$$H(p^2, d) = \kappa(d) \int_0^1 dz[\mathcal{M}(z) - i\varepsilon]^{\frac{d}{2}-2} = \kappa(d) \int_0^1 dz \left(\frac{1}{\mathcal{M}(z) - i\varepsilon}\right)^{\frac{4-d}{2}}, \tag{3.74}$$

with $\kappa(d) = \Gamma(2 - d/2)/(4\pi)^{d/2}$. Therefore, the infrared singularity originates where $\mathcal{M}(z)$ goes to zero as $m_\pi \to 0$ at the small values of z. In order to isolate the divergent part, we perform a change of variable $z = \alpha x$, then

$$H(p^2, d) = \kappa(d) \int_0^{\frac{1}{\alpha}} dx\alpha[\mathcal{M}(\alpha x) - i\varepsilon]^{\frac{d}{2}-2}. \tag{3.75}$$

With $m_\pi \to 0$, the upper limit of integral $x = 1/\alpha \to \infty$, therefore, the integral I, which contains the same infrared singularity, can be expressed as

$$I \equiv \kappa(d)\alpha^{d-3} \int_0^\infty [D(x) - i\varepsilon]^{\frac{d}{2}-2} dx, \tag{3.76}$$

where

$$D(x) = 1 - 2\Omega x + x^2 + 2\alpha x(\Omega x - 1) + \alpha^2 x^2. \tag{3.77}$$

In order to satisfy the relation of $H = I - R$, the regular part of H is defined as

$$R \equiv \kappa(d) \int_1^\infty dz[\mathcal{M}(z) - i\varepsilon]^{\frac{d}{2}-2}. \tag{3.78}$$

For arbitrary values of d, the explicit expressions for H, I, and R involve hypergeometric functions. The chiral expansion of I has the form

$$I = \mathcal{O}(p^{d-3}) + \mathcal{O}(p^{d-2}) + \mathcal{O}(p^{d-1}) + \cdots , \tag{3.79}$$

while for any value of d the corresponding expansion of R is

$$R = \mathcal{O}(p^0) + \mathcal{O}(p^1) + \mathcal{O}(p^2) + \cdots . \tag{3.80}$$

This expansion form can be easily understood at the threshold region, $p^2 = (m_\pi + m_0)^2$. The infrared part reads

$$\begin{aligned} I_{\text{thr.}} &= \kappa(d)\alpha^{d-3} \int_0^\infty dx \left\{[(1+\alpha)x - 1]^2 - i\varepsilon\right\}^{\frac{d}{2}-2} \\ &= \kappa(d)\alpha^{d-3} \frac{1}{(d-3)(1+\alpha)} \frac{1}{(n-3)(1+\alpha)} \\ &= \frac{\Gamma(2-\frac{d}{2})}{(4\pi)^{\frac{d}{2}}(d-3)} \frac{m_\pi^{d-3}}{m_0 + m_\pi}, \end{aligned} \tag{3.81}$$

while the regular part is

$$R_{\text{thr.}} = \frac{\Gamma(2-\frac{d}{2})}{(4\pi)^{\frac{d}{2}}(d-3)} \frac{m_0^{d-3}}{m_0 + m_\pi}. \tag{3.82}$$

Furthermore, according to the definitions of I [Eq. (3.76)]and R [Eq. (3.78)], we can explicitly compute the loop diagrams taking the limit of $d \to 4$,

$$I = -\frac{1}{16\pi^2} \left\{ \left[-\frac{m_\pi}{2m_0} + \frac{m_\pi}{m_0} \log \frac{m_\pi}{m_0} \frac{2m_\pi}{m_0} + \sqrt{1 - \frac{m_\pi^2}{4m_0^2}} \arccos\left(-\frac{m_\pi}{2m_0}\right) \right] \right\}, \tag{3.83}$$

$$\begin{aligned} R &= \frac{1}{16\pi^2} \left\{ -2 + \log \frac{m_0^2}{\mu^2} + \frac{m_\pi^2}{m_0^2} - \frac{2m_\pi}{m_0} \sqrt{1 - \frac{m_\pi^2}{4m_0^2}} \arccos\left(1 - \frac{m_\pi^2}{2m_0^2}\right) \right\}, \\ &= \frac{1}{16\pi^2} \left(-2 + \log \frac{m_0^2}{\mu^2} - \frac{m_\pi^2}{m_0^2} + \frac{m_\pi^4}{6m_0^4} + \cdots \right). \end{aligned} \tag{3.84}$$

From the general expansion form of I and R, one can conclude that the infrared part I contains non-integer powers of momenta and quark masses, while the regular part R is the ordinary Taylor expansion in momenta and quark masses. Therefore, the regular part R can be totally absorbed by the LECs appearing in the chiral effective Lagrangian, and the power counting scheme is valid with the replacement of the general integral H by the corresponding infrared part I. Besides, the infrared part contains the full $1/m_0$ correction terms, which represents the infinite sum of the kinetic energy corrections to the baryon propagator. Therefore, one has to carefully choose a proper regularization scale μ to absorb the divergences from $1/m_0$ higher order corrections. This problem has been stressed in Ref. [70].

Comparison with Eq. (3.57) and Eq. (3.83), the function $\arccos(m_\pi/2m_0)$ appearing in the $\overline{\text{MS}}$ calculation becomes $\arccos(-m_\pi/2m_0)$ in IR scheme. This transformation has large effects on the light-quark mass evolution of some physical observables, e.g. the nucleon/baryon magnetic moments [195, 196]. Furthermore, the analyticity of the infrared method is also broken at a scale of twice the baryon mass, although this large scale should not effect the low-energy expansions. At present, there are several studies to reformulate the IRBChPT [197, 198] to overcome these drawbacks.

3.3.4 Extended-on-mass-shell scheme

The extended-on-mass-shell (EOMS) scheme, which also deals with the power-counting breaking problem, was originally proposed by Gegelia *et al.* [71] and has been applied to study the nucleon mass in detail in Ref. [72]. As mentioned in the above subsection, the regular part R is considered as the power-counting breaking terms and totally removed in infrared chiral perturbation theory. However, one also found that R can contain power counting allowed terms, which are not necessarily absorbed by the counter terms. Therefore, Gegelia *et al.* [71] tried to separate the exact power-counting breaking terms from the loop integral and proposed the extended-on-mass-shell (EOMS) scheme [6]. More precisely, the basic idea of the EOMS method is to absorb the PCB terms by performing finite subtractions from the results of loop integration with the $\widetilde{\mathrm{MS}}$ regularization scheme. Results must satisfy the power-counting rules.

The key technical point for the EOMS scheme is to extract the power-counting breaking terms from the results of loop integration. In order to illustrate this point clearly, as presented in Ref. [42], we would like to consider the scalar loop H in the chiral limit,

$$H(p^2, d, m_\pi = 0) = -i \int \frac{d^d q}{(2\pi)^d} \frac{1}{q^2 + i\varepsilon} \frac{1}{(p-q)^2 - m_0^2 + i\varepsilon}. \tag{3.85}$$

After introducing a small dimensionless quantity

$$\Delta = \frac{p^2 - m_0^2}{m_0^2}, \tag{3.86}$$

which counts as $\mathcal{O}(q)$ due to the baryon mass closing to the mass shell, the integral H can be written as

$$H(p^2, d, m_\pi = 0) = \kappa(d) m_0^{d-4} \int_0^1 dz [C(z,\Delta)]^{\frac{d}{2}-2}, \tag{3.87}$$

with $C(z,\Delta) = z^2 - \Delta z(1-z) - i\varepsilon$. Using the identity

$$\int_0^1 dz [C(z,\Delta)]^{\frac{d}{2}-2} = (-\Delta)^{\frac{d}{2}-2} \int_0^1 dz\, z^{\frac{d}{2}-2} \left(1 - \frac{1+\Delta}{\Delta} z\right)^{\frac{d}{2}-2}, \tag{3.88}$$

and the hypergeometric function F

$$F(a,b;c;z) = \frac{\Gamma(c)}{\Gamma(b)\Gamma(c-b)} \int_0^1 dt\, t^{b-1}(1-t)^{c-b-1}(1-tz)^{-a}, \mathrm{Re}(c) > \mathrm{Re}(b) > 0, \tag{3.89}$$

one can obtain the loop function

$$H(p^2, d, m_\pi = 0) = \kappa(d) m_0^{d-4} \frac{\Gamma\left(\frac{d}{2}-1\right)}{\Gamma\left(\frac{d}{2}\right)} (-\Delta)^{\frac{d}{2}-2} F\left(2 - \frac{d}{2}, \frac{d}{2}; \frac{d}{2}; \frac{1+\Delta}{\Delta}\right), \tag{3.90}$$

with $a = 2 - d/2$, $b = d/2 - 1$, $c = d/2$, and $z = (1+\Delta)/\Delta$. Applying the properties of F,

$$F(a,b;c;z) = (1-z)^{-a} F\left(a, c-b; c; \frac{z}{z-1}\right), \tag{3.91}$$

$$F(a,b;c;z) = F(b,a;c;z), \tag{3.92}$$

[6] Since the substraction point is $p^2 = m_0^2$, the renormalization condition is denoted "extended on-mass-shell" scheme in analogy with the on-mass-shell renormalization scheme in renormalizable theories.

the loop function becomes as

$$\begin{aligned}
H(p^2, d, m_\pi = 0) &= \kappa(d) m_0^{d-4} \frac{\Gamma\left(\frac{d}{2}-1\right)}{\Gamma\left(\frac{d}{2}\right)} F\left(1, 2-\frac{d}{2}; \frac{d}{2}; \frac{p^2}{m_0^2}\right) \\
&= \frac{m_0^{d-4}}{(4\pi)^{\frac{d}{2}}} \left[\frac{\Gamma\left(2-\frac{d}{2}\right)}{d-3} F\left(1, 2-\frac{d}{2}; 4-d; -\Delta\right)\right. \\
&\quad \left. + (-\Delta)^{d-3}\Gamma\left(\frac{d}{2}-1\right)\Gamma(3-d) F\left(\frac{d}{2}-1, d-2; n-2; -\Delta\right)\right] \\
&\equiv F(d,\Delta) + \Delta^{d-3} G(d,\Delta), \qquad (3.93)
\end{aligned}$$

where $F(d,\Delta)$ and $G(d,\Delta)$ are proportional to hypergeometric functions.

We can expand the hypergeometric function F for $|z| < 1$,

$$F(a, b; c; z) = 1 + \frac{ab}{c} z + \frac{a(a+1)b(b+1)}{c(c+1)} \frac{z^2}{2} + \cdots, \qquad (3.94)$$

and find

$$\begin{aligned}
F(d,\Delta) &= \mathcal{O}(p^0) + \mathcal{O}(p^1) + \mathcal{O}(p^2) + \cdots, \qquad (3.95) \\
G(d,\Delta) &= \mathcal{O}(p^{d-3}) + \mathcal{O}(p^{d-2}) + \mathcal{O}(p^{d-1}) + \cdots. \qquad (3.96)
\end{aligned}$$

Therefore, the PCB terms are contained in the first term of loop function and should be subtracted. Generally, there are two approaches to systematically obtain the PCB terms. First, one can calculate a Feynman diagram using the $\overline{\text{MS}}$ scheme to obtain analytical results, and pick out the subtracting PCB terms by using the chiral counting order for the building blocks. This method is obvious when the loop integral has a simple Lorentz structure and can easily generate explicit expressions for the analytic terms. For example, one can calculate the one-loop chiral corrections to the nucleon self-energy. But, in most cases the loop integrals are rather difficult to perform explicitly, therefore, one has to find another method to determine the subtraction terms for these cases.

In the second alternative, one can first expand the integrand in terms of the small quantities, e.g. m_π, p, or $1/m_0$ to identify the relevant terms of the final PCB terms with the naive chiral counting analysis, and then perform the integration to obtain the corresponding PCB terms. Here, we want to mention that, since the PCB terms are always finite and analytic, this method should always work.

After using the EOMS scheme, the one scalar loop integral Eq. (3.57) becomes

$$H_{\text{EOMS}} = -\frac{1}{16\pi^2}\left(\frac{m_\pi^2}{m_0^2}\log\frac{m_\pi}{m_0} + \frac{2m_\pi}{m_0}\sqrt{1-\frac{m_\pi^2}{4m_0^2}}\arccos\frac{m_\pi}{2m_0}\right). \qquad (3.97)$$

We can see that H_{EOMS} is the same as Eq. (3.57) except for the power-counting breaking terms.

Finally, we would like to summarize the differences among the $\overline{\text{MS}}$, HB, IR and EOMS renormalization schemes. As an important feature of ChPT, the HB, IR, and EOMS methods satisfy the power-counting rule. More precisely, comparing with the Eqs. (3.70),(3.83), and (3.97), we can find that the results of HB scheme only contain terms of the specified chiral order, while the other two methods also have a series of higher order terms (recoil corrections). In addition, one can obtain the HB results by expanding the IR results in powers of $1/m_0$

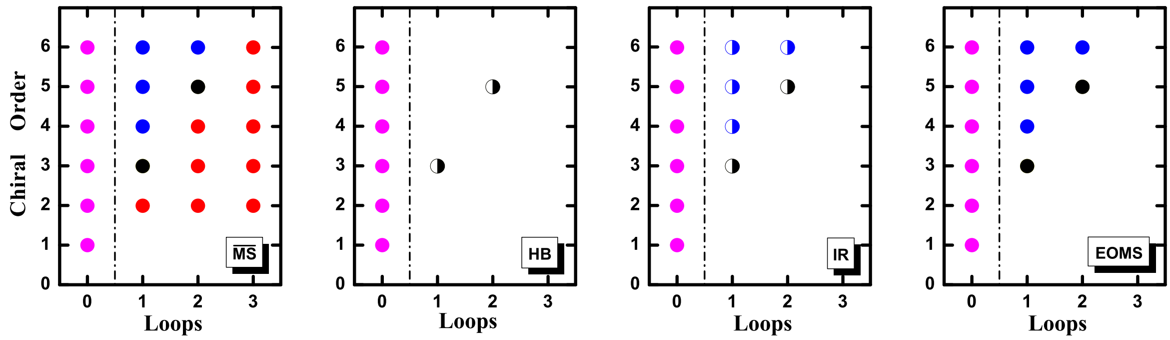

Figure 3.1: Power counting scheme of BChPT with $\overline{\mathrm{MS}}$, HB, IR, and EOMS renormalization schemes. Pink-filled points denote the contact terms. Red-filled circle are the PCB terms. Black and blue circles indicate the strict PC terms and the higher order corrections, respectively. Half- and full-filled circles denote the analytical terms which have the different analyticity (The details can be seen in text). The figure is taken from Ref. [199].

up to specific orders. Both HBChPT and IR BChPT spoil the analytical structure of loop amplitudes, the EOMS scheme has the same analyticity as the $\overline{\mathrm{MS}}$. These two features are clearly illustrated in Fig. 3.1 for the case of the pion-nucleon scattering.

Chapter 4

Octet Baryon Masses in ChPT

In this chapter, we perform the chiral expansion of octet baryon masses in covariant baryon chiral perturbation theory with the extend-on-mass-shell scheme up to next-to-next-to-next-to-leading order. The virtual decuplet baryon contributions are explicitly included. In order to take into account lattice QCD artifacts, finite-volume corrections are carefully examined in the same framework. Furthermore, finite lattice spacing discretization effects are calculated by constructing covariant baryon chiral perturbation theory for Wilson fermions.

4.1 Chiral expansion of octet baryon self-energies

In the past decades, the ground-state octet baryon masses have been studied extensively [47–56, 58–63]. It is found that SU(3) HBChPT converges rather slowly [76] in several versions of BChPT. Most calculations are performed only up to NNLO because of the many unknown LECs at N^{3}LO except those of Refs. [50, 51, 53, 61–63]. Regarding chiral extrapolations, Young and Thomas [58] obtained very good results using the FRR scheme, which induced a form factor in HBChPT to decrease the loop contributions, up to NNLO by fitting the LHPC [25] and PACS-CS [23] lattice data. In Ref. [56], we applied the NNLO EOMS-BChPT to analyze the same lattice data and found that the EOMS-BChPT can provide a better description of lattice data and is more suitable for chiral extrapolation purposes than HBChPT and NLO BChPT. Recently, using a partial summation scheme up to N^{3}LO, Semke and Lutz [61, 63, 200, 201] found that the BMW [22], HSC [26], PACS-CS [23], LHPC [25], QCDSF-UKQCD [28], and ETMC [160] lattice results can be well described.

On the other hand, up to now, a simultaneous description of all the $n_f = 2 + 1$ lattice data with finite-volume effects taken into account self-consistently is still missing. [1] Such a study is necessary for exploring the convergence properties of the SU(3) BChPT by numerically evaluating the contributions of different orders. And, it is also helpful to test the consistency between different lattice simulations. Furthermore, it also provides a good opportunity to determine/constrain the many unknown LECs of BChPT at N^{3}LO.

4.1.1 Chiral effective Lagrangians

In this subsection, we collect the relevant chiral Lagrangians for the calculation of octet baryon masses in the u, d, s three-flavor sector up to N^{3}LO. Firstly, we would like to present the meson-baryon effective Lagrangians without including decuplet baryon interactions. After that, the related decuplet baryon Lagrangians are discussed.

[1] In Ref. [63], Semke and Lutz showed that their partial summation approach can reproduce the results of the HSC and QCDSF-UKQCD collaborations by fitting the BMW, PACS-CS and LHPC data.

Chiral effective Lagrangians without decuplet

The Lagrangians can be written as the sum of a mesonic part and a meson-baryon part:

$$\mathcal{L}_{\rm eff} = \mathcal{L}_{\phi}^{(2)} + \mathcal{L}_{\phi}^{(4)} + \mathcal{L}_{\phi B}^{(1)} + \mathcal{L}_{\phi B}^{(2)} + \mathcal{L}_{\phi B}^{(3)} + \mathcal{L}_{\phi B}^{(4)}, \tag{4.1}$$

where superscript (i) denotes the corresponding chiral order $\mathcal{O}(p^i)$, $\phi = (\pi,\ K,\ \eta)$ represents the pseudoscalar Nambu-Goldstone boson fields, and $B = (N,\ \Lambda,\ \Sigma,\ \Xi)$ lowest-lying octet baryons.

Pseudoscalar meson Lagrangians

The lowest order meson Lagrangian has been given in Eq. (3.38) of Chapter 3, and the corresponding notations can be found in there.

The most general meson Lagrangian at $\mathcal{O}(q^4)$ allowed by symmetries has the following form [34]:

$$\begin{aligned}
\mathcal{L}_{\phi}^{(4)} &= L_1[\langle D_\mu U(D^\mu U)^\dagger\rangle]^2 + L_2\langle D_\mu U(D_\nu U)^\dagger\rangle\langle D^\mu U(D^\nu U)^\dagger\rangle \\
&+L_3\langle D_\mu U(D^\mu U)^\dagger D_\nu D(D^\nu U)^\dagger\rangle + L_4\langle D_\mu U(D^\mu U)^\dagger\rangle\langle \chi U^\dagger + U\chi^\dagger\rangle \\
&+L_5\langle D_\mu U(D^\mu U)^\dagger(\chi U^\dagger + U\chi^\dagger)\rangle + L_6[\langle \chi U^\dagger + U\chi^\dagger\rangle]^2 \\
&+L_7[\langle \chi U^\dagger - U\chi^\dagger\rangle]^2 + L_8\langle U\chi^\dagger U\chi^\dagger + \chi U^\dagger\chi U^\dagger\rangle \\
&-iL_9\langle f_{\mu\nu}^R D^\mu U(D^\nu U)^\dagger + f_{\mu\nu}^L(D^\mu U)^\dagger D^\nu U\rangle + L_{10}\langle U f_{\mu\nu}^L U^\dagger f_R^{\mu\nu}\rangle \\
&+H_1\langle f_{\mu\nu}^R f_R^{\mu\nu} + f_{\mu\nu}^L f_L^{\mu\nu}\rangle + H_2\langle\chi\chi^\dagger\rangle,
\end{aligned} \tag{4.2}$$

where the field-strength tensors are defined as $f_R^{\mu\nu} = \partial^\mu r^\nu - \partial^\nu r^\mu - i[r^\mu, r^\nu]$ and $f_L^{\mu\nu} = \partial^\mu l^\nu - \partial^\nu l^\mu - i[l^\mu, l^\nu]$ with $r_\mu = v_\mu + a_\mu$, $l_\mu = v_\mu - a_\mu$ with v_μ and a_μ the external vector and axial currents. The LECs $L_{1,\cdots,10}$ and $H_{1,2}$ are scale-dependent and absorb the infinities generated by the one-loop graphs.

Pseudoscalar meson-octet baryon Lagrangians

The effective pseudoscalar meson-octet baryon Lagrangians contain terms of odd and even chiral orders,

$$\mathcal{L}_{\phi B}^{\rm eff} = \mathcal{L}_{\phi B}^{(1)} + \mathcal{L}_{\phi B}^{(2)} + \mathcal{L}_{\phi B}^{(3)} + \mathcal{L}_{\phi B}^{(4)}. \tag{4.3}$$

The lowest order meson-baryon Lagrangian has been presented in Eq. (3.55) of Chapter 3.

The meson-baryon Lagrangian at order $\mathcal{O}(p^2)$ can be written as

$$\mathcal{L}_{\phi B}^{(2)} = \mathcal{L}_{\phi B}^{(2,\ \rm sb)} + \mathcal{L}_{\phi B}^{(2)\prime}. \tag{4.4}$$

This separation is motivated by the fact that the first part appears in tree and loop graphs, whereas the latter only contributes to masses via loops. The explicit chiral symmetry breaking part reads as

$$\mathcal{L}_{\phi B}^{(2,\rm sb)} = b_0\langle\chi_+\rangle\langle\bar{B}B\rangle + b_D\langle\bar{B}\{\chi_+, B\}\rangle + b_F\langle\bar{B}[\chi_+, B]\rangle, \tag{4.5}$$

where b_0, b_D, and b_F are LECs, and $\chi_+ = u^\dagger\chi u^\dagger + u\chi^\dagger u$. For the latter part, we take the same form as in Ref. [202]:

$$\mathcal{L}_{\phi B}^{(2)\prime} = b_1\langle\bar{B}[u_\mu, [u^\mu, B]]\rangle + b_2\langle\bar{B}\{u_\mu, \{u^\mu, B\}\}\rangle$$

$$
\begin{aligned}
&+b_3\langle\bar{B}\{u_\mu,[u^\mu,B]\}\rangle+b_4\langle\bar{B}B\rangle\langle u^\mu u_\mu\rangle\\
&+ib_5\left(\langle\bar{B}[u^\mu,[u^\nu,\gamma_\mu D_\nu B]]\rangle-\langle\bar{B}\overleftarrow{D}_\nu[u^\nu,[u^\mu,\gamma_\mu B]]\right)\\
&+ib_6\left(\langle\bar{B}[u^\mu,\{u^\nu,\gamma_\mu D_\nu B\}]\rangle-\langle\bar{B}\overleftarrow{D}_\nu\{u^\nu,[u^\mu,\gamma_\mu B]\}\right)\\
&+ib_7\left(\langle\bar{B}\{u^\mu,\{u^\nu,\gamma_\mu D_\nu B\}\}\rangle-\langle\bar{B}\overleftarrow{D}_\nu\{u^\nu,\{u^\mu,\gamma_\mu B\}\}\rangle\right)\\
&+ib_8\left(\langle\bar{B}\gamma_\mu D_\nu B\rangle-\langle\bar{B}\overleftarrow{D}_\nu\gamma_\mu B\rangle\right)\langle u^\mu u^\nu\rangle+\cdots,
\end{aligned}
\tag{4.6}
$$

where $b_{1,\cdots,4}$ have dimension mass^{-1} and $b_{5,\cdots,8}$ have dimension mass^{-2}. If one works for a set of fixed quark masses (e.g., Ref. [54]), all terms with one or two covariant derivatives can be absorbed in the structures proportional to $b_{1,\cdots,4}$. However, for our purposes, we need to retain all the terms because they lead to different quark mass dependencies.

The contributions from the third chiral order Lagrangian are at least $\mathcal{O}(p^5)$, which beyond the accuracy of our studies. The fourth-order effective Lagrangian relevant to our study is [50]:

$$
\begin{aligned}
\mathcal{L}_{\phi B}^{(4)} \;=\;& d_1\langle\bar{B}[\chi_+,[\chi_+,B]]\rangle+d_2\langle\bar{B}[\chi_+,\{\chi_+,B\}]\rangle\\
&+d_3\langle\bar{B}\{\chi_+,\{\chi_+,B\}\}\rangle+d_4\langle\bar{B}\chi_+\rangle\langle\chi_+B\rangle\\
&+d_5\langle\bar{B}[\chi_+,B]\rangle\langle\chi_+\rangle+d_7\langle\bar{B}B\rangle\langle\chi_+\rangle^2\\
&+d_8\langle\bar{B}B\rangle\langle\chi_+^2\rangle.
\end{aligned}
\tag{4.7}
$$

Chiral effective Lagrangians with decuplet

The baryon decuplet consists of a SU(3)-flavor multiplet of spin-3/2 resonances. Usually, the spin-3/2 particle can be described by the *Rarita-Schwinger* (RS) field [203], ψ_μ. The corresponding free Lagrangian is

$$
\mathcal{L}_{\rm RS}^{\rm free}=\bar{\psi}_\mu(i\gamma^{\mu\nu\alpha}\partial_\alpha-M\gamma^{\mu\nu})\psi_\nu, \tag{4.8}
$$

with the mass M and the totally antisymmetric gamma matrix products $\gamma^{\mu\nu}=\frac{1}{2}[\gamma^\mu,\gamma^\nu]$, $\gamma^{\mu\nu\alpha}=\frac{1}{2}\{\gamma^{\mu\nu},\gamma^\alpha\}=-i\varepsilon^{\mu\nu\alpha\beta}\gamma_\beta\gamma_5$ (using the convention $\varepsilon_{0123}=-\varepsilon^{0123}=+1$). After, one can obtain the Euler-Lagrange field equations

$$
\begin{aligned}
(i\partial\!\!\!/-M)\psi_\mu &= 0, &(4.9)\\
\partial^\mu\psi_\mu &= 0, &(4.10)\\
\gamma^\mu\psi_\mu &= 0. &(4.11)
\end{aligned}
$$

Due to the last two constraints, it is clearly that the 16 components of vector-spinor field are reduced to 4 independent components which is the physical number of spin degrees of freedom of the massive spin-3/2 particle.

For the interacting case, because the physical and unphysical components may couple in a nontrivial way, the situation becomes more complicated. The most general form of an interaction among a spin-3/2 particle, a nucleon (Ψ) and a (pseudo-)scalar boson (ϕ) is given by [204],

$$
\mathcal{L}_{\rm Int}=g\bar{\psi}_\mu\left[g^{\mu\nu}-(z+\frac{1}{2})\gamma^\mu\gamma^\nu\right]\Psi\partial_\nu\phi+{\rm H.c.}, \tag{4.12}
$$

where g denotes the coupling constant and z is the off-shell parameter. This is the so-called inconsistent coupling and may often involve the unphysical spin-1/2 components. On the other hand, the "consistent" spin-3/2 couplings, proposed by Pascalutsa [205, 206], satisfy the gauge invariant ($\psi_\mu \to \phi_\mu + \partial_\mu \varepsilon$, with a spinor field ε) and remove the spin-1/2 background,

$$\mathcal{L}_{\mathrm{Int}}^{\mathrm{GI}} = g\varepsilon^{\mu\nu\alpha\beta}(\partial_\mu \bar{\psi}_\nu)\gamma_5\gamma_\alpha \Psi \partial_\beta \phi + \mathrm{H.c.}. \tag{4.13}$$

Following, we would like to employ this method to include the decuplet baryon in the chiral effective Lagrangians.

For the decuplet baryon, T_μ^{abc}, the physical fields are assigned to the tensor as $T^{111} = \Delta^{++}$, $T^{112} = \Delta^+/\sqrt{3}$, $T^{122} = \Delta^0/\sqrt{3}$, $T^{222} = \Delta^-$, $T^{113} = \Sigma^{*+}/\sqrt{3}$, $T^{123} = \Sigma^{*0}/\sqrt{6}$, $T^{223} = \Sigma^{*-}/\sqrt{3}$, $T^{133} = \Xi^{*0}/\sqrt{3}$, $T^{233} = \Xi^{*-}/\sqrt{3}$, and $T^{333} = \Omega^-$. The covariant free Lagrangian for decuplet baryons is

$$\mathcal{L}_D = \bar{T}_\mu^{abc}\left(i\gamma^{\mu\nu\alpha}D_\alpha - m_D\gamma^{\mu\nu}\right)T_\nu^{abc}, \tag{4.14}$$

where m_D is the decuplet-baryon mass in the chiral limit and the derivative of the decuplet baryon fields is defined as

$$D_\nu T_\mu^{abc} = \partial_\nu T_\mu^{abc} + (\Gamma_\nu, T_\mu)^{abc}, \tag{4.15}$$

with the definition $(X, T_\mu)^{abc} \equiv (X)_d^a T_\mu^{dbc} + (X)_d^b T_\mu^{adc} + (X)_d^c T_\mu^{abd}$. In the previous and following Lagrangians, we always apply the Einstein notation to sum over any repeated SU(3)-index, and $(X)_b^a$ denotes the element of row a and column b of the matrix representation of X.

The $\mathcal{O}(p^2)$ Lagrangian for decuplet baryons is:

$$\mathcal{L}_{\phi D}^{(2)} = \frac{t_0}{2}\bar{T}_\mu^{abc} g^{\mu\nu} T_\nu^{abc}\langle\chi_+\rangle + \frac{t_D}{2}\bar{T}_\mu^{abc} g^{\mu\nu}(\chi_+, T_\nu)^{abc}, \tag{4.16}$$

where the parameters t_0, t_D are two unknown LECs.

At $\mathcal{O}(p^3)$, the chiral effective Lagrangian, describing the interaction of octet and decuplet baryons with pseudoscalar mesons, can be written as [118]

$$\mathcal{L}_{\phi BD}^{(1)} = \frac{i\mathcal{C}}{m_D F_\phi}\varepsilon^{abc}(\partial_\alpha \bar{T}_\mu^{ade})\gamma^{\alpha\mu\nu} B_c^e \partial_\nu \phi_b^d + \mathrm{H.c.}, \tag{4.17}$$

where the coefficient $\mathcal{C}$ denotes the ϕBT "consistent" coupling.

4.1.2 Octet baryon self-energies up to N^{3}LO

Baryon self-energy up to N^{3}LO

The physical baryon mass is defined at the pole, $\not{p} = m_B$, in the two-point function of the baryon field $\psi_B(x)$

$$S_0(x) = -i\langle 0|T[\psi_B(x)\bar{\psi}_B(0)]|0\rangle = \frac{1}{\not{p} - m_0 - \Sigma(\not{p})}, \tag{4.18}$$

where $\Sigma(\not{p})$ corresponds to the baryon self-energy,

$$m_B - m_0 - \Sigma(\not{p} = m_B) = 0, \quad \Rightarrow \quad m_B = m_0 + \Sigma(\not{p} = m_B). \tag{4.19}$$

The leading contribution to the self-energy, $\Sigma_a = m_B^{(2)}$, is of order $\mathcal{O}(p^2)$ [Fig. 4.1(a)]. The self-energy $\Sigma_b = m_B^{(3)}$ of the one-loop diagram [Fig. 4.1(b)] is of order $\mathcal{O}(p^3)$. One tree diagram contribution from $\mathcal{L}_{\phi B}^{(4)}$ [Fig. 4.1(c)] and two loop diagrams [Figs. 4.1(d,e)] are of order $\mathcal{O}(p^4)$,

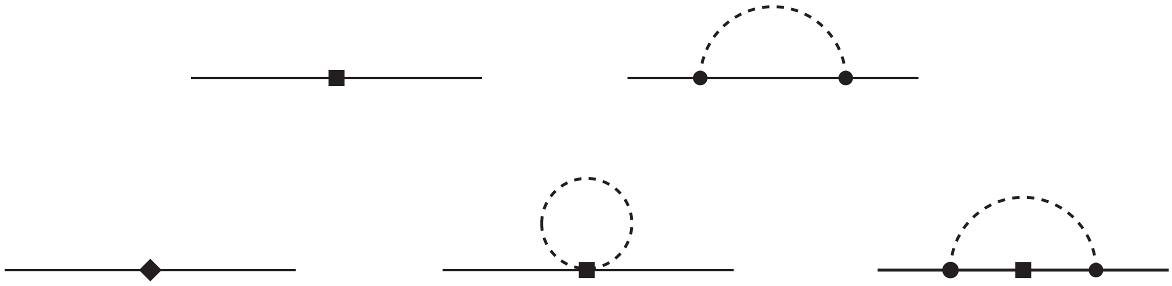

Figure 4.1: Feynman diagrams contributing to the octet-baryon masses up to $\mathcal{O}(p^4)$ in the EOMS-BChPT. The solid lines correspond to octet-baryons and dashed lines refer to Goldstone bosons. The black boxes (diamonds) indicate second (fourth) order couplings. The solid dot indicates an insertion from the dimension one meson-baryon Lagrangians. Wave function renormalization diagrams are not explicitly shown but included in the calculation.

$m_B^{(4)} = \Sigma_c + \Sigma_d + \Sigma_e$. We remark that due to parity conservation, there are no first order contributions. The baryon mass up to fourth order in chiral expansion can be expressed as

$$m_B = m_0 + m_B^{(2)} + m_B^{(3)} + m_B^{(4)}. \tag{4.20}$$

The tree diagrams [Fig. 4.1(a,c)] can be calculated straightforwardly. The corresponding results are shown below. The three one-loop diagrams [Figs. 4.1(b,d,e)] yield, generically,

$$G_b = i \int \frac{d^4k}{(2\pi)^4}\, \not{k}\gamma_5 \frac{1}{\not{p} - \not{k} - m_0 + i\varepsilon} \not{k}\gamma_5 \frac{1}{k^2 - M_\phi^2 + i\varepsilon}, \tag{4.21}$$

$$G_d = i \int \frac{d^4k}{(2\pi)^4}\, \{1,\ k_\mu k^\mu,\ k_\mu k_\nu p^\mu \gamma^\nu\} \frac{1}{k^2 - M_\phi^2 + i\varepsilon}, \tag{4.22}$$

$$G_e = i\, m_B^{(2)} \int \frac{d^4k}{(2\pi)^4}\, \not{k}\gamma_5 \left(\frac{1}{\not{p} - \not{k} - m_0 + i\varepsilon}\right)^2 \not{k}\gamma_5 \frac{1}{k^2 - M_\phi^2 + i\varepsilon}, \tag{4.23}$$

where M_ϕ represents the mass of a Nambu-Goldstone boson. These loop integrations can be calculated in the standard way as given in Appendix C. The above loop functions contain PCB terms and therefore additional steps need to be taken to conserve a proper chiral power-counting scheme. As we have demonstrated before, the EOMS scheme has shown a relatively better convergence property than HB or IR approaches. Therefore, we would like to employ the EOMS scheme to subtract the PCB terms. After calculating all the Feynman diagrams shown in Fig. 4.1, we obtain the chiral expansion of octet baryon masses up to N^{3}LO.

At $\mathcal{O}(p^2)$, the tree level contribution provides the leading order (LO) SU(3)-breaking corrections to the chiral limit octet baryon mass

$$m_B^{(2)} = \sum_{\phi=\pi,\ K} \xi_{B,\phi}^{(a)} M_\phi^2, \tag{4.24}$$

where the coefficients $\xi_{B,\phi}^{(a)}$ are listed in Table 4.1.

Table 4.1: Coefficients of the NLO contribution to the self-energy of octet baryons [Eq. (4.24)].

	N	Λ	Σ	Ξ
$\xi^{(a)}_{B,\pi}$	$-(2b_0+4b_F)$	$\frac{-2}{3}(3b_0-2b_D)$	$-(2b_0+4b_D)$	$-(2b_0-4b_F)$
$\xi^{(a)}_{B,K}$	$-(4b_0+4b_D-4b_F)$	$\frac{-2}{3}(6b_0+8b_D)$	$-4b_0$	$-(4b_0+4b_D+4b_F)$

Table 4.2: Coefficients of the NNLO contribution to the self-energy of octet baryons [Eq. (4.25)].

	N	Λ	Σ	Ξ
$\xi^{(b)}_{B,\pi}$	$\frac{3}{2}(D+F)^2$	$2D^2$	$\frac{2}{3}(D^2+6F^2)$	$\frac{3}{2}(D-F)^2$
$\xi^{(b)}_{B,K}$	$\frac{1}{3}(5D^2-6DF+9F^2)$	$\frac{2}{3}(D^2+9F^2)$	$2(D^2+F^2)$	$\frac{1}{3}(5D^2+6DF+9F^2)$
$\xi^{(b)}_{B,\eta}$	$\frac{1}{6}(D-3F)^2$	$\frac{2}{3}D^2$	$\frac{2}{3}D^2$	$\frac{1}{6}(D+3F)^2$

At $\mathcal{O}(p^3)$ diagram Fig. 4.1(b) gives the NLO SU(3)-breaking corrections to octet baryon masses

$$m_B^{(3)} = \frac{1}{(4\pi F_\phi)^2} \sum_{\phi=\pi,\ K,\ \eta} \xi^{(b)}_{B,\phi} H_B^{(b)}(M_\phi), \tag{4.25}$$

where the coefficients $\xi^{(b)}_{B,\phi}$ are given in Table 4.2, and the corresponding loop functions $H_B^{(b)}(M_\phi)$ is

$$\begin{aligned} H_B^{(b)}(M_\phi) \;&=\; -\frac{2M_\phi^3}{m_0}\left[\sqrt{4m_0^2-M_\phi^2}\arctan\left(\frac{M_\phi}{\sqrt{4m_0^2-M_\phi^2}}\right)\right. \\ &\left. +\sqrt{4m_0^2-M_\phi^2}\arctan\left(\frac{2m_0^2-M_\phi^2}{M_\phi\sqrt{4m_0^2-M_\phi^2}}\right)+M_\phi\log\frac{M_\phi}{m_0}\right]. \end{aligned} \tag{4.26}$$

The NNLO SU(3)-breaking corrections to the octet baryon masses are

$$\begin{aligned} m_B^{(4)} \;&=\; \xi^{(c)}_{B,\pi}M_\pi^4 + \xi^{(c)}_{B,K}M_K^4 + \xi^{(c)}_{B,\pi K}M_\pi^2 M_K^2 \\ &+\frac{1}{(4\pi F_\phi)^2}\sum_{\phi=\pi,\ K,\ \eta}\left[\xi^{(d,1)}_{B,\phi}H_B^{(d,1)}(M_\phi)+\xi^{(d,2)}_{B,\phi}H_B^{(d,2)}(M_\phi)+\xi^{(d,3)}_{B,\phi}H_B^{(d,3)}(M_\phi)\right] \\ &+\frac{1}{(4\pi F_\phi)^2}\sum_{\substack{\phi=\pi,\ K,\ \eta \\ B'=N,\ \Lambda,\ \Sigma,\ \Xi}} \xi^{(e)}_{BB',\phi}\cdot H^{(e)}_{B,B'}(M_\phi). \end{aligned} \tag{4.27}$$

The first three terms of Eq. (4.27) are the tree contributions of diagram Fig. 4.1(c), and the corresponding coefficients $\xi^{(c)}_{B,\pi}$, $\xi^{(c)}_{B,K}$, $\xi^{(c)}_{B,\pi K}$ can be found in Table 4.3. The next term is the contribution from the tadpole diagram Fig. 4.1(d) and the Clebsch-Gordan coefficients are listed in Table 4.4. The last term is from the one-loop diagram of Fig. 4.1(e), together with the wave function renormalization diagrams not shown, and $\xi^{(e)}_{BB',\phi}$ can be found in Table 4.5. After using the EOMS scheme to remove the PCB terms, the loop functions are written as:

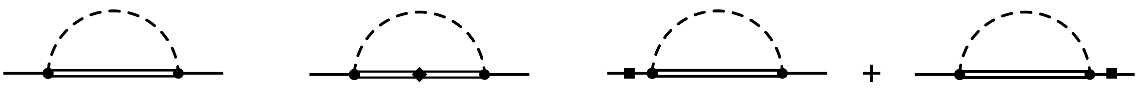

Figure 4.2: Feynman diagrams contributing to the octet baryon masses with the intermediate decuplet resonances. The solid lines correspond to octet baryons, the double lines to decuplet baryons, and the dashed lines denote pseudoscalar mesons. Black dots indicate an insertion from the dimension one chiral Lagrangian [Eq. (4.17)], and black boxes (diamonds) indicate $\mathcal{O}(p^2)$ mass insertions.

$$H_B^{(d,1)}(M_\phi) = M_\phi^2\left[1+\ln\left(\frac{\mu^2}{M_\phi^2}\right)\right], \tag{4.28}$$

$$H_B^{(d,2)}(M_\phi) = M_\phi^4\left[1+\ln\left(\frac{\mu^2}{M_\phi^2}\right)\right], \tag{4.29}$$

$$H_B^{(d,3)}(M_\phi) = m_0\left\{\frac{M_\phi^4}{4}\left[1+\ln\left(\frac{\mu^2}{M_\phi^2}\right)\right]+\frac{1}{8}M_\phi^4\right\}, \tag{4.30}$$

$$\begin{aligned} H_{B,B'}^{(e)}(M_\phi) = {} & \frac{2M_\phi^3}{m_0^2\sqrt{4m_0^2-M_\phi^2}}\left[6m_0^2(m_B^{(2)}-m_{B'}^{(2)})-M_\phi^2(2m_B^{(2)}-m_{B'}^{(2)})\right]\arccos\frac{M_\phi}{2m_0} \\ & -M_\phi^2\left[3(m_B^{(2)}-m_{B'}^{(2)})+\frac{3m_0^2(m_B^{(2)}-m_{B'}^{(2)})-M_\phi^2(2m_B^{(2)}-m_{B'}^{(2)})}{m_0^2}\ln\frac{M_\phi^2}{m_0^2}\right. \\ & \left.+(m_B^{(2)}+m_{B'}^{(2)})\ln\frac{m_0^2}{\mu^2}\right], \end{aligned} \tag{4.31}$$

where $m_B^{(2)}$ and $m_{B'}^{(2)}$ are the corresponding LO SU(3) corrections to octet baryon masses given in Eq. (4.24).

4.1.3 Virtual decuplet contributions

Up to N^{3}LO, the octet baryon masses with the virtual decuplet contributions can be written as

$$m_B = m_0 + m_B^{(2)} + m_B^{(3)} + m_B^{(4)} + m_B^{(D)}, \tag{4.32}$$

Table 4.3: Coefficients of the N^{3}LO tree contribution to the self-energy of octet baryons [Eq. (4.27)].

	N	Λ	Σ	Ξ
$\xi_{B,\pi}^{(c)}$	$-4(4d_1+2d_5+d_7+3d_8)$	$-4(4d_3+\frac{8}{3}d_4+d_7+3d_8)$	$-4(4d_3+d_7+3d_8)$	$-4(4d_1-2d_5+d_7+3d_8)$
$\xi_{B,K}^{(c)}$	$-16\,(d_1-d_2+d_3 -d_5+d_7+d_8)$	$-16(\frac{8}{3}d_3+\frac{2}{3}d_4+d_7+d_8)$	$-16(d_7+d_8)$	$-16\,(d_1+d_2+d_3 +d_5+d_7+d_8)$
$\xi_{B,\pi K}^{(c)}$	$8\,(4d_1-2d_2-d_5 -2d_7+2d_8)$	$16(\frac{8}{3}d_3+\frac{4}{3}d_4-d_7+d_8)$	$-16(d_7-d_8)$	$8\,(4d_1+2d_2+d_5 -2d_7+2d_8)$

Table 4.4: Coefficients of the tadpole contribution to the self-energy of octet baryons [Eq. (4.27)].

	N	Λ	Σ	Ξ
$\xi^{(d,1)}_{B,\pi}$	$-3(2b_0+b_D+b_F)m_\pi^2$	$-2(3b_0+b_D)m_\pi^2$	$-6(b_0+b_D)m_\pi^2$	$-3(2b_0+b_D-b_F)m_\pi^2$
$\xi^{(d,1)}_{B,K}$	$-2(4b_0+3b_D-b_F)m_K^2$	$-\frac{4}{3}(6b_0+5b_D)m_K^2$	$-4(2b_0+b_D)m_K^2$	$-2(4b_0+3b_D+b_F)m_K^2$
$\xi^{(d,1)}_{B,\eta}$	$-\frac{1}{3}\left[8(b_0+b_D-b_F)m_K^2 -(2b_0+3b_D-5b_F)m_\pi^2\right]$	$-\frac{2}{9}\left[4(3b_0+4b_D)m_K^2 -(3b_0+7b_D)m_\pi^2\right]$	$-\frac{2}{3}\left[4b_0m_K^2 +(b_D-b_0)m_\pi^2\right]$	$-\frac{1}{3}\left[8(b_0+b_D+b_F)m_K^2 -(2b_0+3b_D+5b_F)m_\pi^2\right]$
$\xi^{(d,2)}_{B,\pi}$	$3(b_1+b_2+b_3+2b_4)$	$2(2b_2+3b_4)$	$2(4b_1+2b_2+3b_4)$	$3(b_1+b_2-b_3+2b_4)$
$\xi^{(d,2)}_{B,K}$	$2(3b_1+3b_2-b_3+4b_4)$	$\frac{4}{3}(9b_1+b_2+6b_4)$	$4(b_1+b_2+2b_4)$	$2(3b_1+3b_2+b_3+4b_4)$
$\xi^{(d,2)}_{B,\eta}$	$\frac{1}{3}(9b_1+b_2-3b_3+6b_4)$	$2(2b_2+b_4)$	$\frac{2}{3}(2b_2+3b_4)$	$\frac{1}{3}(9b_1+b_2+3b_3+6b_4)$
$\xi^{(d,3)}_{B,\pi}$	$6(b_5+b_6+b_7+2b_8)$	$4(2b_7+3b_8)$	$4(4b_5+2b_7+3b_8)$	$6(b_5-b_6+b_7+2b_8)$
$\xi^{(d,3)}_{B,K}$	$4(3b_5-b_6+3b_7+4b_8)$	$\frac{8}{3}(9b_5+b_7+6b_8)$	$8(b_5+b_7+2b_8)$	$4(3b_5+b_6+3b_7+4b_8)$
$\xi^{(d,3)}_{B,\eta}$	$\frac{2}{3}(9b_5-3b_6+b_7+6b_8)$	$4(2b_7+b_8)$	$\frac{4}{3}(2b_7+3b_8)$	$\frac{2}{3}(9b_5+3b_6+b_7+6b_8)$

Table 4.5: Coefficients of the loop contributions (Fig. 4.1e) to the self-energy of octet baryons [Eq. (4.27)].

N	Λ	Σ	Ξ
$\xi^{(e)}_{NN\pi}=\frac{3}{4}(D+F)^2$	$\xi^{(e)}_{\Lambda NK}=\frac{1}{6}(D+3F)^2$	$\xi^{(e)}_{\Sigma NK}=\frac{1}{2}(D-F)^2$	$\xi^{(e)}_{\Xi\Lambda K}=\frac{1}{12}(D-3F)^2$
$\xi^{(e)}_{NN\eta}=\frac{1}{12}(D-3F)^2$	$\xi^{(e)}_{\Lambda\Lambda\eta}=\frac{1}{3}D^2$	$\xi^{(e)}_{\Sigma\Lambda\pi}=\frac{1}{3}D^2$	$\xi^{(e)}_{\Xi\Sigma K}=\frac{3}{4}(D+F)^2$
$\xi^{(e)}_{N\Lambda K}=\frac{1}{12}(D+3F)^2$	$\xi^{(e)}_{\Lambda\Sigma\pi}=D^2$	$\xi^{(e)}_{\Sigma\Sigma\pi}=2F^2$	$\xi^{(e)}_{\Xi\Xi\pi}=\frac{3}{4}(D-F)^2$
$\xi^{(e)}_{N\Sigma K}=\frac{3}{4}(D-F)^2$	$\xi^{(e)}_{\Lambda\Xi K}=\frac{1}{6}(D-3F)^2$	$\xi^{(e)}_{\Sigma\Sigma\eta}=\frac{1}{3}D^2$	$\xi_{\Xi\Xi\eta}=\frac{1}{12}(D+3F)^2$
		$\xi^{(e)}_{\Sigma\Xi K}=\frac{1}{2}(D+F)^2$	

where $m_B^{(D)}$ denotes the contributions of virtual decuplet resonances up to N^{3}LO. After calculating the Feynman diagrams shown in Fig. 4.2 and subtracting the PCB terms with the EOMS scheme, the virtual decuplet contributions to the octet baryon masses can be expressed as

$$m_B^{(D)} = \frac{1}{(4\pi F_\phi)^2}\sum_{\phi=\pi,\ K,\ \eta}\xi^{(a)}_{BD,\phi}H^{(a)}_{B,D}(M_\phi) + \frac{1}{(4\pi F_\phi)^2}\sum_{\substack{\phi=\pi,\ K,\ \eta\\ D'=\Delta,\ \Sigma^*,\ \Xi^*,\ \Omega^-}}\xi^{(b/c)}_{BD',\phi}H^{(b/c)}_{B,D'}(M_\phi). \tag{4.33}$$

The first term of Eq. (4.33) is the NNLO contributions of Feynman diagram Fig. 4.2(a). The corresponding coefficients $\xi^{(a)}_{BD,\phi}$ are listed in Table 4.6 and the loop function $H^{(a)}_{B,D}(M_\phi)$ is

$$\begin{aligned} H^{(a)}_{B,D}(M_\phi) &= \frac{1}{24m_0m_D^2}M_\phi^2\left[2m_0^4+4m_0^3m_D-7m_0^2M_\phi^2-4m_0m_D(m_D^2+M_\phi^2)\right.\\ &\left.\quad -2(m_D^4+3m_D^2M_\phi^2-M_\phi^4)\right]\\ &\quad -\frac{1}{12m_0^3m_D^2}M_\phi^4\ln\left(\frac{M_\phi}{m_D}\right)\left[6m_0^4+6m_0^3m_D+m_0^2(6m_D^2-4M_\phi^2)\right.\\ &\left.\quad +m_0(6m_D^3-2m_DM_\phi^2)+6m_D^4-4m_D^2M_\phi^2+M_\phi^4\right] \end{aligned}$$

$$
\begin{aligned}
&+\frac{1}{12m_0^3m_D^2}(m_0-m_D)(m_0+m_D)^3\ln\left(\frac{m_DM_\phi}{m_D^2-m_0^2}\right)\\
&\quad\times\left[m_0^4-2m_0^2(m_D^2+2M_\phi^2)+2m_0m_DM_\phi^2+m_D^4-4m_D^2M_\phi^2\right]\\
&-\frac{1}{12m_0^3m_D^2\sqrt{\mathcal{W}}}(m_0^2-2m_0m_D+m_D^2-M_\phi^2)^2(m_0^2+2m_0m_D+m_D^2-M_\phi^2)^3\\
&\times\left[\arctan\left(\frac{m_0^2+m_D^2-M_\phi^2}{\mathcal{W}}\right)-\arctan\left(\frac{m_0^2-m_D^2+M_\phi^2}{\mathcal{W}}\right)\right], \qquad (4.34)
\end{aligned}
$$

where $\mathcal{W}=-m_0^4-(m_D^2-M_\phi^2)^2+2m_0^2(m_D^2+M_\phi^2)$.

The next term is the virtual decuplet contribution at $\mathcal{O}(p^4)$ from the one-loop diagram of Fig. 4.2(b) and the wave function renormalization diagrams of Fig. 4.2(c). The Clebsch-Gordan coefficients $\xi^{(b/c)}_{BD',\phi}$ are tabulated in Table 4.7, and the loop function $H^{(b/c)}_{B,D'}(M_\phi)$ has the following form:

$$
\begin{aligned}
H^{(b/c)}_{B,D}(M_\phi) \;=\;& \frac{1}{24m_0^2m_D^2}m_B^{(2)}M_\phi^2\left[2(11m_0^2+8m_0m_D+9m_D^2)\right.\\
&\left.\times(m_0^2-m_D^2)+(5m_0^2+8m_0m_D+18m_D^2)M_\phi^2-6M_\phi^4\right]\\
&+\frac{1}{36m_0m_D^3}m_D^{(2)}M_\phi^2\left[-34m_0^4-24m_0^3m_D+30m_D^4\right.\\
&\left.-6m_D^2M_\phi^2-6M_\phi^4+6m_0m_D(4m_D^2+M_\phi^2)+3m_0^2(4m_D^2+7M_\phi^2)\right]\\
&-\frac{1}{12m_0^4m_D^2}m_B^{(2)}M_\phi^2\ln\left(\frac{M_\phi}{m_D}\right)\left[12m_D^5(m_0+m_D)\right.\\
&\left.+6(m_0^4-m_0^2m_D^2-2m_0m_D^3-3m_D^4)M_\phi^2+4(m_0^2+m_0m_D+3m_D^2)M_\phi^4-3M_\phi^6\right]\\
&+\frac{1}{6m_0^3m_D^3}m_D^{(2)}M_\phi^2\ln\left(\frac{M_\phi}{m_D}\right)\left[m_D^5(9m_0+8m_D)\right.\\
&\left.+3(m_0^2-m_D^2)(2m_0^2+m_0m_D+2m_D^2)M_\phi^2-m_0(4m_0+m_D)M_\phi^4+M_\phi^6\right]\\
&-\frac{1}{12m_0^4m_D^3}M_\phi^2(m_0-m_D)^2(m_0+m_D)^4\ln\left(\frac{m_DM_\phi}{m_D^2-m_0^2}\right)\\
&\times\left[m_D\left(-5m_0^2+2m_0m_D-3m_D^2\right)m_B^{(2)}+2m_0\left(m_0^2-m_0m_D+3m_D^2\right)m_D^{(2)}\right]\\
&-\frac{1}{6m_D^3}m_0M_\phi^4\ln\left(\frac{m_DM_\phi}{\mu^2}\right)\left[6m_D(m_0+m_D)m_B^{(2)}-m_0(4m_0+3m_D)m_D^{(2)}\right]\\
&+\frac{1}{12m_0^4m_D^3\sqrt{\mathcal{W}}}(m_0^2-2m_0m_D+m_D^2-M_\phi^2)(m_0^2+2m_0m_D+m_D^2-M_\phi^2)^2\\
&\times\left[3m_D(m_D^2-M_\phi^2)^2m_B^{(2)}-2m_0(m_D^2-M_\phi^2)\left((3m_D^2+M_\phi^2)m_D^{(2)}+m_D^2m_B^{(2)}\right)\right.
\end{aligned}
$$

Table 4.6: Coefficients of the NNLO virtual decuplet contribution to the self-energy of octet baryons [Eq. (4.33)].

	N	Λ	Σ	Ξ
$\xi^{(a)}_{BD,\pi}$	$\frac{16}{3}\mathcal{C}^2$	$4\mathcal{C}^2$	$\frac{8}{9}\mathcal{C}^2$	$\frac{4}{3}\mathcal{C}^2$
$\xi^{(a)}_{BD,K}$	$\frac{4}{3}\mathcal{C}^2$	$\frac{8}{3}\mathcal{C}^2$	$\frac{40}{9}\mathcal{C}^2$	$4\mathcal{C}^2$
$\xi^{(a)}_{BD,\eta}$	0	0	$\frac{4}{3}\mathcal{C}^2$	$\frac{4}{3}\mathcal{C}^2$

Table 4.7: Coefficients of loop diagrams (Fig. 4.2(b/c)) to the self-energy of octet baryons [Eq. (4.33)].

N	Λ	Σ	Ξ
$\xi^{(b/c)}_{N\Delta,\pi} = 4\mathcal{C}^2$	$\xi^{(b/c)}_{\Lambda\Sigma^*,\pi} = 3\mathcal{C}^2$	$\xi^{(b/c)}_{\Sigma\Delta,K} = \frac{8}{3}\mathcal{C}^2$	$\xi^{(b/c)}_{\Xi\Sigma^*,K} = \mathcal{C}^2$
$\xi^{(b/c)}_{N\Sigma^*,K} = \mathcal{C}^2$	$\xi^{(b/c)}_{\Lambda\Xi^*,K} = 2\mathcal{C}^2$	$\xi^{(b/c)}_{\Sigma\Sigma^*,\pi} = \frac{2}{3}\mathcal{C}^2$	$\xi^{(b/c)}_{\Xi\Xi^*,\pi} = \mathcal{C}^2$
		$\xi^{(b/c)}_{\Sigma\Sigma^*,\eta} = \mathcal{C}^2$	$\xi^{(b/c)}_{\Xi\Xi^*,\eta} = \mathcal{C}^2$
		$\xi^{(b/c)}_{\Sigma\Xi^*,K} = \frac{2}{3}\mathcal{C}^2$	$\xi^{(b/c)}_{\Xi\Delta^-,K} = 2\mathcal{C}^2$

Table 4.8: Coefficients of LO contribution to the self-energy of decuplet baryons [Eq. (4.36)].

	Δ	Σ^*	Ξ^*	Ω^-
$\xi_{D,\pi}$	$t_0 + 3t_D$	$t_0 + t_D$	$t_0 - t_D$	$t_0 - 3t_D$
$\xi_{D,K}$	$2t_0$	$2t_0 + 2t_D$	$2t_0 + 4t_D$	$2t_0 + 6t_D$

$$
\begin{aligned}
&+2m_0^2 m_D^2 (m_D^2 + M_\phi^2)(m_B^{(2)} + m_D^{(2)}) + 2m_0^3 \left(2(m_D^2 - M_\phi^2) m_D^{(2)} + m_D^2 m_B^{(2)}\right) \\
&-m_0^4 m_D \left(5m_B^{(2)} + 2m_D^{(2)}\right) + 2m_0^5 m_D^{(2)}\Big] \\
&\times \left[\arctan\left(\frac{m_0^2 + m_D^2 - M_\phi^2}{\mathcal{W}}\right) + \arctan\left(\frac{m_0^2 - m_D^2 + M_\phi^2}{\mathcal{W}}\right)\right], \qquad (4.35)
\end{aligned}
$$

where the NLO octet baryon mass, $m_B^{(2)}$, is given in Eq. (4.32) and the NLO decuplet baryon mass is

$$
m_D^{(2)} = -\sum_{\phi=\pi,K} \xi^{(2)}_{D,\phi} M_\phi^2. \qquad (4.36)
$$

The corresponding coefficients $\xi^{(2)}_{D,\phi}$ are listed in Table 4.8. It should be noted that in order to obtain the results of Eq. (4.33), the decuplet-octet mass difference, $\delta = m_D - m_0$, is considered up to all orders [56]. Here we want to mention that there are two diagrams (presented in Fig. 4.3) contributed to the octet baryon masses up to N^{3}LO. In Ref. [207], it was pointed that their contributions are small and should be started at $\mathcal{O}(p^5)$ in EOMS BChPT. Therefore, we do not include them in this work.

At N^{3}LO, a replacement of meson masses by their $\mathcal{O}(p^4)$ counterparts in $m_B^{(2)}$ generates N^{3}LO contributions to $m_B^{(4)}$. The corresponding Nambu-Goldstone boson masses up to $\mathcal{O}(p^4)$

Figure 4.3: Two feynman diagrams contributing to the octet baryon masses with the intermediate decuplet resonances. The other notations are the same as Fig. 4.2.

can be found in Ref. [34], which read as

$$M_{\pi,4}^2 = M_{\pi,2}^2\left\{1+\frac{M_{\pi,2}^2}{32\pi^2F_\phi^2}\ln\left(\frac{M_{\pi,2}^2}{\mu^2}\right)-\frac{M_{\eta,2}^2}{96\pi^2F_\phi^2}\ln\left(\frac{M_{\eta,2}^2}{\mu^2}\right)\right.$$
$$\left.+\frac{16}{F_\phi^2}\left[\left(\frac{M_{\pi,2}^2}{2}+M_{K,2}^2\right)(2L_6^r-L_4^r)+\frac{M_{\pi,2}^2}{2}(2L_8^r-L_5^r)\right]\right\}, \tag{4.37}$$

$$M_{K,4}^2 = M_{K,2}^2\left\{1+\frac{M_{\eta,2}^2}{48\pi^2F_\phi^2}\ln\left(\frac{M_{\eta,2}^2}{\mu^2}\right)\right.$$
$$\left.+\frac{16}{F_\phi^2}\left[\left(\frac{M_{\pi,2}^2}{2}+M_{K,2}^2\right)(2L_6^r-L_4^r)+\frac{M_{K,2}^2}{2}(2L_8^r-L_5^r)\right]\right\}, \tag{4.38}$$

$$M_{\eta,4}^2 = M_{\pi,2}^2\left[\frac{M_{\eta,2}^2}{96\pi^2F_\phi^2}\ln\left(\frac{M_{\eta,2}^2}{\mu^2}\right)-\frac{M_{\pi,2}^2}{32\pi^2F_\phi^2}\ln\left(\frac{M_{\pi,2}^2}{\mu^2}\right)+\frac{M_{K,2}^2}{48\pi^2F_\phi^2}\ln\left(\frac{M_{K,2}^2}{\mu^2}\right)\right]$$
$$+M_{\eta,2}^2\left[1+\frac{M_{K,2}^2}{16\pi^2F_\phi^2}\ln\left(\frac{M_{K,2}^2}{\mu^2}\right)-\frac{M_{\eta,2}}{24\pi^2F_\phi^2}\ln\left(\frac{M_{\eta,2}}{\mu^2}\right)\right.$$
$$\left.+\frac{16}{F_\phi^2}\left(\frac{M_{\pi,2}^2}{2}+M_{K,2}^2\right)(2L_6^r-L_4^r)+8\frac{M_{\eta,2}^2}{F_\phi^2}(2L_8^r-L_5^r)\right]$$
$$+\frac{128}{9}\frac{(M_{K,2}^2-M_{\pi,2}^2)^2}{F_\phi^2}(3L_7^r+L_8^r). \tag{4.39}$$

The empirical values of $2L_6^r-L_4^r=-0.17\times10^{-3}$ and $2L_8^r-L_5^r=-0.22\times10^{-3}$, and $3L_7^r+L_8^r=-0.15\times10^{-3}$ are taken from the latest global fit [208], which are evaluated at the renormalization scale $\mu=0.77$ GeV. [2] To be consistent with our renormalization scale used for the one-baryon sector, we have re-evaluated the L_i^r's at $\mu=1$ GeV.

4.2 Finite-volume corrections

Because lattice QCD simulations are performed in a finite hypercube, the momenta of virtual particles are discretized. As a result, the simulated results are different from those of infinite space-time. The difference is termed as finite-volume corrections. In cases where $M_\phi L\gg1$, the so-called p-regime, ChPT provides a model-independent framework to study FVCs [77, 78].

Physically, finite-volume corrections can be easily understood. Because of the existence of space-time boundaries, the allowed momenta of virtual particles become discretized, i.e, one has to replace a momentum integral by a finite sum of discretized momenta,

$$\int_{-\infty}^{\infty}dk\rightarrow\sum_{n=-N+1}^{N}\left(\frac{2\pi}{L}\right)n, \tag{4.40}$$

[2] It should be noted that the uncertainties of the L_i^r are quite large. Because the effects of their contributions are found to be small, we do not take into account the uncertainties of these LECs in our fit of LQCD mass data.

with $N = L/(2a)$ (assuming periodical boundary conditions). In LQCD simulations of zero-temperature physics, the temporal extent is generally larger than the spatial extent such that the integral in temporal dimension can be treated as if it extends from $-\infty$ and ∞. As a result, only the integral in spatial dimensions should be replaced by an infinite sum. Furthermore, it is obvious that only loop diagrams are affected by the existence of space-time boundaries.

In the following, we take the one-loop diagram of Fig. 4.1(c) as an example to present the details of FVCs calculation. The definition of FVCs is the following difference:

$$\delta G_B^{(c)} = G_B^{(c)}(L) - G_B^{(c)}(\infty), \tag{4.41}$$

where $G_B^{(c)}(L)$ and $G_B^{(c)}(\infty)$ denote the integrals calculated in a finite hypercube and in an infinite space-time, respectively. These quantities have several features that make calculations more feasible than a direct computation of $G_B^{(c)}(L)$. First, because $G_B^{(c)}(L)$ and $G_B^{(c)}(\infty)$ have the same ultraviolet behavior, $\delta G_B^{(c)}$ are finite and can therefore be calculated in four dimensions. Second, the unwelcome PCB terms appearing in a covariant baryon ChPT calculation are absent because they emerge from short-distance physics while such short-distance properties are the same in $G_B^{(c)}(L)$ and $G_B^{(c)}(\infty)$. As a result, PCB terms vanish in the differences $\delta G_B^{(c)}$ and no power-counting-restoration schemes, such as EOMS or IR, are needed to calculate $\delta G_B^{(c)}$.

Using the Feynman parameterization, one obtains

$$\begin{aligned} G_B^{(c)}(\infty) &= i\int_0^1 dx \int \frac{d^4k}{(2\pi)^4}\frac{\not{k}(\not{k}-\not{p}+m_0)\not{k}}{((k-px)^2-\mathcal{M}_B^2)^2} \\ &= i\int_0^1 dx \int \frac{d^4k}{(2\pi)^4}\frac{\not{k}(k^2-2k\cdot p)+2k^2M_0}{((k-px)^2-\mathcal{M}_B^2)^2}, \end{aligned} \tag{4.42}$$

where $\mathcal{M}_B^2 = x^2m_0^2+(1-x)M_\phi^2-i\varepsilon$. Calculating the integral [Eq. (4.42)] in a finite hypercube requires treating the temporal and spatial dimensions differently. We choose to work in the baryon rest frame, i.e., $p^\mu = (m_0, \vec{0})$. In this frame,

$$G_B^{(c)} = i\int_0^1 dx \int \frac{dk_0}{2\pi}\int\frac{d\vec{k}}{(2\pi)^3}\frac{(\gamma^0k_0-\vec{\gamma}\cdot\vec{k})(k_0^2-\vec{k}^2-2k_0m_0)+2(k_0^2-\vec{k}^2)m_0}{\left[(k_0-xm_0)^2-\vec{k}^2-\mathcal{M}_B^2\right]^2}. \tag{4.43}$$

This can be easily calculated by performing a shift in k_0 ($k_0 \to k_0' + xm_0$), Wick rotating k_0' ($k_0' \to ik_0'$), and then performing the integration over k_0'. The result is

$$\begin{aligned} G_B^{(c)} = \int_0^1 dx\int\frac{d\vec{k}}{(2\pi)^3}&\left[\frac{1}{2}m_0(2x+1)\left(\frac{1}{\vec{k}^2+\mathcal{M}_B^2}\right)^{1/2}\right. \\ &\left.-\frac{1}{4}m_0(m_0^2x^3+\mathcal{M}_B^2(x+2))\left(\frac{1}{\vec{k}^2+\mathcal{M}_B^2}\right)^{3/2}\right]. \end{aligned} \tag{4.44}$$

After utilizing the master formula [209], one can easily obtain

$$\delta G_B^{(c)} = \int_0^1 dx\left[\frac{1}{2}m_0(2x+1)\delta_{1/2}(\mathcal{M}_B^2)\right.$$

$$-\frac{1}{4}m_0(m_0^2x^3+\mathcal{M}_B^2(x+2))\delta_{3/2}(\mathcal{M}_B^2)\Big], \tag{4.45}$$

where

$$\delta_r(\mathcal{M}^2)=\frac{2^{-1/2-r}(\sqrt{\mathcal{M}^2})^{3-2r}}{\pi^{3/2}\Gamma(r)}\sum_{\vec{n}\neq 0}(L\sqrt{\mathcal{M}^2}|\vec{n}|)^{-3/2+r}K_{3/2-r}(L\sqrt{\mathcal{M}^2}|\vec{n}|), \tag{4.46}$$

where $K_n(z)$ is the modified Bessel function of the second kind, and $\sum_{\vec{n}\neq 0}\equiv\sum_{n_x=-\infty}^{\infty}\sum_{n_y=-\infty}^{\infty}\sum_{n_z=-\infty}^{\infty}(1-\delta(|\vec{n}|,0))$ with $\vec{n}=(n_x,n_y,n_z)$.

In a similar way, one can calculate FVCs of Fig. 4.1(d,e)

$$\delta G_B^{(d,1)}(M_\phi)=\frac{1}{2}\delta_{1/2}\left(M_\phi^2\right), \tag{4.47}$$

$$\delta G_B^{(d,2)}(M_\phi)=\frac{M_\phi^2}{2}\delta_{1/2}\left(M_\phi^2\right), \tag{4.48}$$

$$\delta G_B^{(d,3)}(M_\phi)=\frac{m_0}{2}\delta_{-1/2}\left(M_\phi^2\right), \tag{4.49}$$

$$\begin{aligned}\delta G_{B,B'}^{(e)} \;=\; & \int_0^1 dx\left\{-\frac{1}{2}(2xm_B^{(2)}+m_{B'}^{(2)})\;\delta_{1/2}(\mathcal{M}_B^2)\right.\\ & -\frac{1}{4}\Big[M_\phi^2(x-1)\left(m_B^{(2)}(1+x)+m_{B'}^{(2)}\right)\\ & \quad -2xm_0^2\left(m_B^{(2)}(5x^2-3)+m_{B'}^{(2)}(4x+3)\right)\Big]\;\delta_{3/2}(\mathcal{M}_B^2)\\ & -\frac{1}{4}\Big[6m_0^4(x+1)x^3\left(m_B^{(2)}(x-1)+m_{B'}^{(2)}\right)-3m_0^2M_\phi^2\\ & \quad\left.\times\;x(x-1)(x+2)\left(m_B^{(2)}(x-1)+m_{B'}^{(2)}\right)\Big]\;\delta_{5/2}(\mathcal{M}_B^2)\right\}.\end{aligned} \tag{4.50}$$

In addition, when the virtual decuplet baryon contributions are taken into account, the FVCs to the loop results of Fig. 4.2(a,b,c) are

$$\begin{aligned}\delta G_{B,D}^{(a)} \;=\; & \frac{3}{4}\int_0^1 dx\left[\frac{m_0^2\left(m_0(1-x)+m_D\right)}{6m_D^2}\delta_{1/2}\left(\mathcal{M}_D^2\right)\right.\\ & \left.-\frac{m_0^2\left(m_0(1-x)+m_D\right)\mathcal{M}_D^2}{6m_D^2}\delta_{3/2}\left(\mathcal{M}_D^2\right)\right],\end{aligned} \tag{4.51}$$

and

$$\begin{aligned}\delta G_{B,D}^{(b/c)} \;=\; & \frac{m_0}{6m_D^3}\int_0^1 dx\left\{\Big[2m_0^2(x-1)m_D^{(2)}\right.\\ & -m_0m_D\left(m_D^{(2)}+3m_B^{(2)}(x-1)\right)+2m_D^2m_B^{(2)}\Big]\;\delta_{1/2}\left(\mathcal{M}_D^2\right)\\ & +\Big[3m_0^3m_Dx(x-1)^2m_B^{(2)}-2m_0^2\mathcal{M}_D^2(x-1)m_D^{(2)}\\ & +3m_0^2m_D^2x(x-1)\left(m_D^{(2)}-m_B^{(2)}\right)+m_0m_D\mathcal{M}_D^2\\ & \times\left(3m_B^{(2)}(x-1)+m_D^{(2)}\right)-3m_0m_D^3m_D^{(2)}x-2m_D^2\mathcal{M}_D^2m_B^{(2)}\Big]\;\delta_{3/2}\left(\mathcal{M}_D^2\right)\end{aligned}$$

$$+3m_0 m_D \mathcal{M}_D^2 x \left[-m_0^2(x-1)^2 m_B^{(2)} \right.$$
$$\left. +m_0 m_D (x-1) \left(m_B^{(2)} - m_D^{(2)} \right) + m_D^2 m_D^{(2)} \right] \delta_{5/2}\left(\mathcal{M}_D^2\right) \Big\}, \tag{4.52}$$

respectively, with $\mathcal{M}_D^2 = x^2 m_0^2 - x(m_0^2 - m_D^2) + (1-x)M_\phi^2 - i\varepsilon$.

4.3 Finite lattice spacings discretization effects

To apply ChPT to the study of lattice simulations, in principle, one should first take the continuum limit of LQCD data, since ChPT describes continuum QCD and is not valid for nonzero lattice spacing. However, nowadays it is a common practice to assume that lattice spacing artifacts for current LQCD setups of $a \approx 0.1$ fm are small and can be treated as systematic uncertainties.

In order to study discretization effects on LQCD simulations, one can first write down Symanzik's effective field theory [82–85], a continuum effective field theory which describes the lattice field theory close to the continuum limit, and then one can extend ChPT to be consistent with this EFT with additional symmetry breaking parameters. In this way, the chiral expansion results can naturally encode lattice spacing effects (see, e.g. Ref. [210]). Sharpe and Singleton [211] and Lee and Sharpe [212] first extended ChPT to include finite lattice spacing effects up to $\mathcal{O}(a)$ for Wilson fermions [17] (WChPT) and staggered fermions [137, 139] (SChPT), respectively. Later, Munster and Schmidt [213] applied WChPT to the study of discretization artifacts of twisted mass fermions (tmChPT) [141, 142].

In the past decade, discretization effects on the ground-state meson/baryon properties, such as masses, decay constants, electromagnetic form factors, etc., have been extensively studied in WChPT. In the mesonic sector, the masses and decay constants of the Nambu-Glodstone mesons were first studied up to $\mathcal{O}(m_q^2)$ and $\mathcal{O}(a)$ for the Wilson action [86] and for the mixed action [87], where Wilson sea quarks and Ginsparg-Wilson valence quarks are employed. These studies were subsequently extended to next-to-leading order (up to $\mathcal{O}(a^2)$) [88, 89]. In the one-baryon sector, a systematic study of the nucleon properties up to $\mathcal{O}(a)$ was first performed by Beane and Savage for both the mixed and the unmixed action [90]. The electromagnetic properties of the octet mesons as well as of the octet and decuplet baryons were also studied up to $\mathcal{O}(a)$ for both the mixed and the unmixed action [93]. Discretization effects on the nucleon and Δ masses [91] as well as on the vector meson masses [92] were also studied up to $\mathcal{O}(a^2)$. The EFT for the anisotropic Wilson lattice action has been formulated up to $\mathcal{O}(a^2)$ [94] as well.

In this subsection, we aim to study the discretization effects of the LQCD simulations of the ground-state octet baryon masses up to $\mathcal{O}(a^2)$ in covariant BChPT with the EOMS renormalization scheme. Firstly, we briefly review the continuum effective action up to and including $\mathcal{O}(a^2)$. After, we follow closely the procedure and notations of Ref. [91] and construct for the first time the chiral Lagrangians incorporating a finite lattice spacing for the Wilson action in the u, d, and s three-flavor one-baryon sector.

4.3.1 Continuum effective action

Close to the continuum limit, LQCD can be described by an effective action, the 'Symanzik action' [82, 83], which is expanded in powers of the lattice spacing a as

$$\begin{aligned} S_{\text{eff}} &= S_0 + aS_1 + a^2 S_2 + \cdots \\ &= \int d^4x(\mathcal{L}^{(4)} + a\mathcal{L}^{(5)} + a^2\mathcal{L}^{(6)} + \cdots), \end{aligned} \tag{4.53}$$

where the index $i = 4, 5, ...$ denotes the dimension mass. The $\mathcal{L}^{(4)}$ is the normal (continuum) QCD Lagrangian and the two new terms $\mathcal{L}^{(5)}$ and $\mathcal{L}^{(6)}$ are introduced to include the discretization effects of LQCD. The Lagrangian $\mathcal{L}^{(5)}$ contains chiral breaking terms only, while $\mathcal{L}^{(6)}$ contains both chiral invariant and breaking terms. In the u, d, and s three-flavor sector, QCD Lagrangian is

$$\mathcal{L}^{(4)} = \bar{\psi}_q(i\not{D} - \mathcal{M})\psi_q, \tag{4.54}$$

with the quark field ψ_q and the quark mass matrix $\mathcal{M} = \text{diag}(m_l, m_l, m_s)$ in the isospin limit ($m_u = m_d \equiv m_l$), and $\not{D} = D_\mu\gamma^\mu$ with D_μ the covariant derivative.

At $\mathcal{O}(a)$, there is only the Pauli term left by using equations of motion to redefine the effective fields [85]

$$a\mathcal{L}^{(5)} = ac_{\text{SW}}\bar{\psi}\sigma^{\mu\nu}G_{\mu\nu}\omega_q\psi, \tag{4.55}$$

where $G_{\mu\nu} = [D_\mu, D_\nu]$ and c_{SW} is the Sheikholeslami-Wohlert (SW) [84] coefficient that must be determined numerically. The ω_q ($q = u,\ d,\ s$) is a constant which is determined by the kind of lattice fermions employed in LQCD simulations: $\omega_q = 1$ for Wilson fermions [17] and $\omega_q = 0$ for Ginsparg-Wilson (GW) fermions [143]. Similar to the quark masses, the ω_q's are usually collected in the Wilson matrix,

$$\mathcal{W} = \text{diag}(\omega_l, \omega_l, \omega_s), \tag{4.56}$$

with conserved isospin symmetry ($\omega_u = \omega_d \equiv \omega_l$). This term breaks chiral symmetry in precisely the same way as the quark mass term. It should be noted that the Pauli term can be canceled by adding the clover term to the lattice action [89], resulting in the $\mathcal{O}(a)$-improved Wilson fermion action [84, 85, 214, 215].

Up to $\mathcal{O}(a^2)$, the Symanzik action for Wilson fermions has been extensively studied in Refs. [84, 88, 89]. In total, there are 18 operators appearing in $\mathcal{L}^{(6)}$. They can be classified into operators of the following five types according to whether or not they break chiral symmetry and the $O(4)$ rotation symmetry [91]:

- $\mathcal{L}_1^{(6)}$: quark bilinear operators that conserve chiral symmetry,

$$\bar{\psi}\not{D}^3\psi, \quad \bar{\psi}(D_\mu D_\mu\not{D} + \not{D}D_\mu D_\mu)\psi, \quad \bar{\psi}D_\mu\not{D}D_\mu\psi. \tag{4.57}$$

- $\mathcal{L}_2^{(6)}$: quark bilinear operators that break chiral symmetry,

$$\bar{\psi}m_q D_\mu D_\mu\psi, \quad \langle m_q\rangle\bar{\psi}D_\mu D_\mu\psi, \quad \bar{\psi}m_q i\sigma_{\mu\nu}G_{\mu\nu}\psi, \quad \langle m_q\rangle\bar{\psi}i\sigma_{\mu\nu}G_{\mu\nu}\psi. \tag{4.58}$$

- $\mathcal{L}_3^{(6)}$: four-quark operators that conserve chiral symmetry,

$$(\bar{\psi}\gamma_\mu\psi)^2, \quad (\bar{\psi}\gamma_\mu\gamma_5\psi)^2, \quad (\bar{\psi}t^a\gamma_\mu\psi)^2, \quad (\bar{\psi}t^a\gamma_\mu\gamma_5\psi)^2, \tag{4.59}$$

  where t^a are the SU(3) generators, $a = 1, \cdots, 8$.

- $\mathcal{L}_4^{(6)}$: four-quark operators that break chiral symmetry,

$$(\bar{\psi}\psi)^2, \quad (\bar{\psi}\gamma_5\psi)^2, \quad (\bar{\psi}\sigma_{\mu\nu}\psi)^2, \quad (\bar{\psi}t^a\psi)^2, \quad (\bar{\psi}t^a\gamma_5\psi)^2, \quad (\bar{\psi}t^a\sigma_{\mu\nu}\psi)^2. \tag{4.60}$$

- $\mathcal{L}_5^{(6)}$: quark bilinear operators that break the $O(4)$ rotation symmetry,

$$\bar{\psi}\gamma_\mu D_\mu D_\mu D_\mu\psi. \tag{4.61}$$

It should be noted that fermionic operators that conserve chiral symmetry first appear at $\mathcal{O}(a^2)$.

4.3.2 Wilson chiral Lagrangians

In order to construct the chiral Lagrangians of WChPT, one has to write down the most general Lagrangians that are invariant under the symmetries of the continuum EFT. This can be done by following the standard procedure of spurion analysis [88, 89]. In practice, in order to obtain the corresponding a-dependent chiral Lagrangians, one only needs to know which symmetries are broken and how [91]. Before writing down the chiral Lagrangians up to $\mathcal{O}(a^2)$, one has to first specify a chiral power-counting scheme, which should be enlarged to include the lattice spacing a. In LQCD simulations, the following hierarchy of energy scales is satisfied:

$$m_q \ll \Lambda_{\mathrm{QCD}} \ll \frac{1}{a}. \tag{4.62}$$

If one assumes that the size of chiral symmetry breaking due to light-quark masses and discretization effects are of comparable size, as done in Refs. [89–91], one has the following expansion parameters:

$$\varepsilon^2 \sim \frac{m_q}{\Lambda_{\mathrm{QCD}}} \sim a\Lambda_{\mathrm{QCD}}, \tag{4.63}$$

where ε denotes a generic small quantity and $\Lambda_{\mathrm{QCD}} \approx 300$ MeV denotes the typical low energy scale of QCD. Up to $\mathcal{O}(a^2)$, the a-dependent chiral Lagrangians contain terms of $\mathcal{O}$ (a, am_q, a^2) and can be written as

$$\begin{aligned}\mathcal{L}_a^{\mathrm{eff}} &= \mathcal{L}^{\mathcal{O}(a)} + \mathcal{L}^{\mathcal{O}(am_q)} \\ &\quad + \mathcal{L}_1^{\mathcal{O}(a^2)} + \mathcal{L}_2^{\mathcal{O}(a^2)} + \mathcal{L}_3^{\mathcal{O}(a^2)} + \mathcal{L}_4^{\mathcal{O}(a^2)} + \mathcal{L}_5^{\mathcal{O}(a^2)},\end{aligned} \tag{4.64}$$

and $\mathcal{L}_i^{\mathcal{O}(a^2)} (i = 1, \ldots, 5)$ are the five classes of chiral Lagrangians corresponding to the previous five types of operators appearing in the Symanzik action at $\mathcal{O}(a^2)$.

The chiral Lagrangian at $\mathcal{O}(a)$ can be written as

$$\mathcal{L}^{\mathcal{O}(a)} = \bar{b}_0\langle\bar{B}B\rangle\langle\rho_+\rangle + \bar{b}_D\langle\bar{B}[\rho_+, B]_-\rangle + \bar{b}_F\langle\bar{B}[\rho_+, B]_+\rangle, \tag{4.65}$$

where $\bar{b}_0$, $\bar{b}_D$, and $\bar{b}_F$ are the unknown LECs of dimension mass^{-1}. The new operator $\rho_+ = u^\dagger\rho u^\dagger + u\rho^\dagger u$ and ρ_+ transforms under chiral rotation (R), parity transformation (P), charge conjugation transformation (C) and hermitic conjugation transformation in the following way: $\rho_+ \xrightarrow{R} h\rho_+ h^\dagger$ with $h \in \mathrm{SU}(3)_V$, $\rho_+ \xrightarrow{P} \rho_+$, $\rho_+ \xrightarrow{C} \rho_+^T$, and $\rho_+ \xrightarrow{h.c.} \rho_+$. The matrix ρ is related to the Wilson matrix [Eq. (4.56)] via [86]

$$\rho = 2ac_{\mathrm{SW}}W_0\mathcal{W}, \tag{4.66}$$

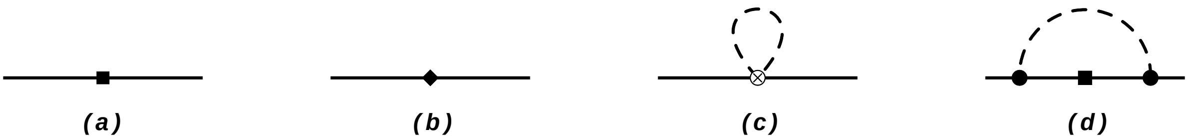

Figure 4.4: Feynman diagrams contributing to the a-dependence of octet baryon masses up to $\mathcal{O}(a^2)$. The solid lines represent octet baryons and the dashed lines denote pseudoscalar mesons. The boxes (diamonds) indicate the $\mathcal{O}(a)$ ($\mathcal{O}(a^2)$) vertices. The circle-cross is an insertion from the $\mathcal{L}^{\mathcal{O}(a)}$. The wave function renormalization diagrams are not explicitly shown but included in the calculation.

which introduces explicit chiral symmetry breaking because of the finite lattice spacing a. The constant $W_0 = -\langle 0|\bar{q}\sigma_{\mu\nu}G_{\mu\nu}q|0\rangle/F_\phi^2$ is an unknown dimensional quantity that is related to the scale Λ_χ.

The $\mathcal{O}(am_q)$ Lagrangian has the following form:

$$\begin{aligned}\mathcal{L}^{\mathcal{O}(am_q)} &= \bar{b}_1\langle\bar{B}\chi_+\rho_+B\rangle + \bar{b}_2\langle\bar{B}\chi_+B\rho_+\rangle + \bar{b}_3\langle\bar{B}\rho_+B\chi_+\rangle + \bar{b}_4\langle\bar{B}B\chi_+\rho_+\rangle \\ &\quad + \bar{b}_5\langle\bar{B}\chi_+\rangle\langle\rho_+B\rangle + \bar{b}_6\langle\bar{B}\rho_+\rangle\langle\chi_+B\rangle + \bar{b}_7\langle\bar{B}[\chi_+,B]\rangle\langle\rho_+\rangle \\ &\quad + \bar{b}_8\langle\bar{B}\{\chi_+,B\}\rangle\langle\rho_+\rangle + \bar{b}_9\langle\bar{B}[\rho_+,B]\rangle\langle\chi_+\rangle + \bar{b}_{10}\langle\bar{B}\{\rho_+,B\}\rangle\langle\chi_+\rangle \\ &\quad + \bar{b}_{11}\langle\bar{B}B\rangle\langle\chi_+\rangle\langle\rho_+\rangle + \bar{b}_{12}\langle\bar{B}B\rangle\langle\chi_+\rho_+\rangle, \end{aligned} \tag{4.67}$$

where $\bar{b}_{1,\ldots,12}$ are unknown LECs of dimension mass^{-3}. One can eliminate the $\bar{b}_3$ term by use of the following identity valid for any 3×3 matrix A derived from the Cayley-Hamilton identity [216]:

$$\begin{aligned}&\sum_{\text{perm}=6}\langle A_1A_2A_3A_4\rangle - \sum_{\text{perm}=8}\langle A_1A_2A_3\rangle\langle A_4\rangle - \sum_{\text{perm}=3}\langle A_1A_2\rangle\langle A_3A_4\rangle \\ &+ \sum_{\text{perm}=6}\langle A_1A_2\rangle\langle A_3\rangle\langle A_4\rangle - \langle A_1\rangle\langle A_2\rangle\langle A_3\rangle\langle A_4\rangle = 0, \end{aligned} \tag{4.68}$$

where 'perm' stands for permutation number. In the end, there are 11 independent terms left.

At $\mathcal{O}(a^2)$, the previous five operators in the Symanzik action can be mapped into the EFT with five classes of chiral Lagrangians $\mathcal{L}_i^{\mathcal{O}(a^2)}$ ($i = 1,\ldots,5$). Following the notation of Ref. [91], the first class of chiral Lagrangians can be written as

$$\mathcal{L}_1^{\mathcal{O}(a^2)} = a^2c_{\rm SW}^2W_0^2\left[\bar{c}_1\langle\bar{B}B\rangle + \bar{c}_2\langle\mathcal{O}_+\rangle\langle\bar{B}B\rangle + \bar{c}_3\langle\bar{B}[\mathcal{O}_+,B]_+\rangle + \bar{c}_4\langle\bar{B}[\mathcal{O}_+,B]_-\rangle\right], \tag{4.69}$$

where the operator $\mathcal{O}_+$ is defined as

$$\mathcal{O}_+ = 2\left[u^\dagger(\mathcal{W}-\overline{\mathcal{W}})u + u(\mathcal{W}-\overline{\mathcal{W}})u^\dagger\right], \tag{4.70}$$

with $\overline{\mathcal{W}} = 1-\mathcal{W} = \mathrm{diag}(1-\omega_l, 1-\omega_l, 1-\omega_s)$, and $\bar{c}_{1,\ldots,4}$ are the unknown LECs of dimension mass^{-3}.

Because the second type of operators have an insertion of the quark mass m_q, the chiral order of the corresponding chiral Lagrangians is at least $\mathcal{O}(p^6)$, which is beyond the present work and will not be shown.

There are seven independent terms in the third class of chiral Lagrangians

$$\mathcal{L}_3^{\mathcal{O}(a^2)} = a^2c_{\rm SW}^2W_0^2\left[\bar{e}_1\langle\bar{B}[\mathcal{O}_+,[\mathcal{O}_+,B]]\rangle + \bar{e}_2\langle\bar{B}[\mathcal{O}_+,\{\mathcal{O}_+,B\}]\rangle\right.$$

$$
\begin{aligned}
&+\bar{e}_3\langle\bar{B}\{\mathcal{O}_+,\{\mathcal{O}_+,B\}\}\rangle+\bar{e}_4\langle\bar{B}\mathcal{O}_+\rangle\langle\mathcal{O}_+B\rangle \\
&+\bar{e}_5\langle\bar{B}[\mathcal{O}_+,B]\rangle\langle\mathcal{O}_+\rangle+\bar{e}_6\langle\bar{B}\{\mathcal{O}_+,B\}\rangle\langle\mathcal{O}_+\rangle \\
&+\bar{e}_7\langle\bar{B}B\rangle\langle\mathcal{O}_+\rangle^2+\bar{e}_8\langle\bar{B}B\rangle\langle\mathcal{O}_+^2\rangle\big]\,, \qquad (4.71)
\end{aligned}
$$

where the $\bar{e}_i$ are the unknown LECs of dimension mass^{-3}. Furthermore, we can eliminate the $\bar{e}_6$ term by use of the Cayley-Hamilton identity [216]:

$$
\langle\bar{B}\{X^2,B\}\rangle+\langle\bar{B}XBX\rangle-\frac{1}{2}\langle\bar{B}B\rangle\langle X^2\rangle-\langle\bar{B}X\rangle\langle BX\rangle=0, \qquad (4.72)
$$

with $X=\mathcal{O}_+-\frac{1}{3}\langle\mathcal{O}_+\rangle$ being a 3×3 traceless matrix.

Four-quark operators that break chiral symmetry can be mapped into the following chiral Lagrangian:

$$
\begin{aligned}
\mathcal{L}_4^{\mathcal{O}(a^2)} &= \bar{d}_1\langle\bar{B}[\rho_+,[\rho_+,B]]\rangle+\bar{d}_2\langle\bar{B}[\rho_+,\{\rho_+,B\}]\rangle \\
&+\bar{d}_3\langle\bar{B}\{\rho_+,\{\rho_+,B\}\}\rangle+\bar{d}_4\langle\bar{B}\rho_+\rangle\langle\rho_+B\rangle \\
&+\bar{d}_5\langle\bar{B}[\rho_+,B]\rangle\langle\rho_+\rangle+\bar{d}_7\langle\bar{B}B\rangle\langle\rho_+\rangle^2 \\
&+\bar{d}_8\langle\bar{B}B\rangle\langle\rho_+^2\rangle, \qquad (4.73)
\end{aligned}
$$

with the seven unknown LECs $\bar{d}_i$ of dimension mass^{-3}. Because the chiral transformation properties of ρ_+ and χ_+ are the same, the chiral Lagrangian has the same form as the corresponding fourth-order chiral Lagrangian of ChPT.

For the $O(4)$ breaking operators, the mapped chiral Lagrangian can be written as

$$
\begin{aligned}
\mathcal{L}_5^{\mathcal{O}(a^2)} &= a^2c_{\rm SW}^2W_0^2\left[\bar{f}_1\langle\bar{B}D_\mu D_\mu D_\mu D_\mu B\rangle+\bar{f}_2\langle\mathcal{O}_+\rangle\langle\bar{B}D_\mu D_\mu D_\mu D_\mu B\rangle\right. \\
&\left.+\bar{f}_3\langle\bar{B}D_\mu D_\mu D_\mu D_\mu[\mathcal{O}_+,B]_+\rangle+\bar{f}_4\langle\bar{B}D_\mu D_\mu D_\mu D_\mu[\mathcal{O}_+,B]_-\rangle\right], \qquad (4.74)
\end{aligned}
$$

where the $\bar{f}_i$ are the unknown LECs of dimension mass^{-3}. Their contributions to the octet baryon masses can be absorbed by the terms of class one, i.e., Eq. (4.69).

4.3.3 Discretization effects up to $\mathcal{O}(a^2)$

The octet baryon masses up to N^{3}LO and with finite lattice spacing a contributions up to $\mathcal{O}(a^2)$ can be expressed as

$$
m_B=m_0+m_B^{(2)}+m_B^{(3)}+m_B^{(4)}+m_B^{(a)}, \qquad (4.75)
$$

where $m_B^{(a)}$ denotes the discretization effects up to $\mathcal{O}(a^2)$. In our power-counting scheme, it contains the following three contributions:

$$
m_B^{(a)}=m_B^{\mathcal{O}(a)}+m_B^{\mathcal{O}(am_q)}+m_B^{\mathcal{O}(a^2)}. \qquad (4.76)
$$

Here, we need to mention that virtual decuplet contributions are not explicitly included, since their effects on the chiral extrapolation and the finite-volume corrections are relatively small [65].

In the case of unmixed Wilson action, where the u, d, and s quarks are all Wilson fermions, the Wilson matrix can be written as $\mathcal{W}=\mathrm{diag}(1,1,1)$. One can easily compute the $\mathcal{O}(a)$ contributions of the diagram Fig. 4.4(a) to the octet baryon masses,

$$
m_B^{\mathcal{O}(a)}=-4ac_{\rm SW}W_0(3\bar{b}_0+2\bar{b}_D). \qquad (4.77)
$$

Table 4.9: Coefficients of the $\mathcal{O}(am_q)$ contributions to octet baryon masses (Eq. 4.78).

	ξ_l	ξ_s
N	$\bar{B}_1 + 2\bar{B}_3$	$\bar{B}_2 + \bar{B}_3$
Λ	$\frac{1}{3}(\bar{B}_1 + \bar{B}_2 + 6\bar{B}_3)$	$\frac{1}{3}(2\bar{B}_1 + 2\bar{B}_2 + 3\bar{B}_3)$
Σ	$\bar{B}_1 + \bar{B}_2 + 2\bar{B}_3$	$\bar{B}_3$
Ξ	$\bar{B}_2 + 2\bar{B}_3$	$\bar{B}_1 + \bar{B}_3$

The $\mathcal{O}(am_q)$ contributions can be written as

$$\begin{aligned} m_B^{\mathcal{O}(am_q)} &= -16ac_{\mathrm{SW}}W_0B_0(\xi_l m_l + \xi_s m_s) \\ &= -8ac_{\mathrm{SW}}W_0\left(\xi_l M_\pi^2 + \xi_s(2M_K^2 - M_\pi^2)\right), \end{aligned} \tag{4.78}$$

and the coefficients ξ_l and ξ_s are tabulated in Table 4.9. We have introduced the following combinations of LECs: $\bar{b}_1+\bar{b}_2+3\bar{b}_7+3\bar{b}_8 = \bar{B}_1$, $\bar{b}_4-3\bar{b}_7+3\bar{b}_8 = \bar{B}_2$, and $2\bar{b}_{10}+3\bar{b}_{11}+\bar{b}_{12} = \bar{B}_3$. Hence, there are 3 independent combinations. In obtaining the above results, the light-quark masses have been replaced by the leading-order pseudoscalar meson masses: $m_l = \frac{1}{2B_0}M_\pi^2$ and $m_s = \frac{1}{2B_0}(2M_K^2 - M_\pi^2)$.

The $\mathcal{O}(a^2)$ contributions are not only from the fourth-order tree-level diagram Fig. 4.4(b), but also from the one-loop diagrams of Fig. 4.4(c,d)

$$\begin{aligned} m_B^{\mathcal{O}(a^2)} &= -a^2c_{\mathrm{SW}}^2W_0^2\left(\bar{C} + 16\bar{D} + 16\bar{E}\right) \\ &\quad -\frac{1}{(4\pi F_\phi)^2}ac_{\mathrm{SW}}W_0\sum_{\pi,\ K,\ \eta}\xi_{B,\phi}^{(c)}H_B^{(c)}(M_\phi) \\ &\quad +\frac{1}{(4\pi F_\phi)^2}\sum_{\pi,\ K,\ \eta}\xi_{BB',\phi}^{(d)}H_{B,B'}^{(d)}(M_\phi), \end{aligned} \tag{4.79}$$

where $\bar{C} = \bar{c}_1 + 4(3\bar{c}_2 + 2\bar{c}_3)$, $\bar{D} = 4\bar{d}_3 + 9\bar{d}_7 + 3\bar{d}_8$, and $\bar{E} = 4\bar{e}_3 + 9\bar{e}_7 + 3\bar{e}_8$. We introduce $\bar{C} + 16\bar{D} + 16\bar{E} = 16\bar{X}$ as one free LEC in the fitting process. The second line of Eq. (4.79) is for the contributions from the tadpole diagram of Fig. 4.4c, and the corresponding coefficients $\xi_{B,\phi}^{(c)}$ are listed in Table 4.10. The last term is for the contributions from the one-loop diagram of Fig. 4.4d, and the coefficients $\xi_{BB',\phi}^{(d)}$ are already given in Table 4.5. The loop diagrams $H_B^{(c)}(M_\phi)$ and $H_{BB'}^{(d)}(M_\phi)$ read

$$H_B^{(c)}(M_\phi) = M_\phi^2\left[1 + \ln\left(\frac{\mu^2}{M_\phi^2}\right)\right], \tag{4.80}$$

$$\begin{aligned} H_{BB'}^{(d)}(M_\phi) &= m_B^{\mathcal{O}(a)}\left[\frac{2M_\phi^5}{m_0^2\sqrt{4m_0^2 - M_\phi^2}}\arccos\left(\frac{M_\phi}{2m_0}\right) + \frac{M_\phi^4}{m_0^2}\ln\left(\frac{M_\phi^2}{m_0^2}\right)\right. \\ &\quad \left. +2M_\phi^2\ln\left(\frac{m_0^2}{\mu^2}\right)\right], \end{aligned} \tag{4.81}$$

where the $m_B^{\mathcal{O}(a)}$ is for the leading-order discretization effects of Eq. (4.77).

Table 4.10: Coefficients of the tadpole diagram contributions to octet baryon masses (Eq. (4.79)).

	N	Λ	Σ	Ξ
$\xi^{(c)}_{B,\pi}$	$6(2\bar{b}_0+\bar{b}_D+\bar{b}_F)$	$4(3\bar{b}_0+\bar{b}_D)$	$12(\bar{b}_0+\bar{b}_D)$	$6(2\bar{b}_0+\bar{b}_D-\bar{b}_F)$
$\xi^{(c)}_{B,K}$	$4(4\bar{b}_0+3\bar{b}_D-\bar{b}_F)$	$\frac{8}{3}(6\bar{b}_0+5\bar{b}_D)$	$8(2\bar{b}_0+\bar{b}_D)$	$4(4\bar{b}_0+3\bar{b}_D+\bar{b}_F)$
$\xi^{(c)}_{B,\eta}$	$\frac{2}{3}(6\bar{b}_0+5\bar{b}_D-3\bar{b}_F)$	$4(\bar{b}_0+\bar{b}_D)$	$\frac{4}{3}(3\bar{b}_0+\bar{b}_D)$	$\frac{2}{3}(6\bar{b}_0+5\bar{b}_D+3\bar{b}_F)$

Chapter 5

Systematic study of lattice octet baryon masses

In this chapter, we discuss a systematic study of the lattice octet baryon masses by performing the chiral extrapolation of LQCD data, self-consistently including finite-volume corrections and finite lattice spacing discretization effects of LQCD. In order to fix all the unknown LECs and test the consistency of current lattice simulations, we perform a simultaneous fit of all the publicly available $n_f = 2+1$ LQCD data from the PACS-CS, LHPC, HSC, QCDSF-UKQCD and NPLQCD collaborations. The contributions of virtual decuplet baryons are also explicitly taken into account to study their effects on the chiral extrapolation of octet baryon masses and finite-volume corrections.

5.1 Chiral extrapolation of octet baryon masses

In this section, we study light quark mass dependence of lowest-lying octet baryon masses using the N^{3}LO EOMS-BChPT mass formulas [Eq. (4.20)] by fitting $n_f = 2+1$ LQCD simulation results. As mentioned above, there are 19 unknown LECs, which cannot be fully determined by the lattice data of a single LQCD simulation. Therefore, we decided to fit all the published lattice results of ground-state octet baryon masses obtained by different collaborations, including the PACS-CS [23], LHPC [25], HSC [26], QCDSF-UKQCD [28] and NLPQCD [29] collaborations. In performing such a study, we can test the consistency of all these lattice simulations, which used totally different setups.

In the fit process, we use the meson decay constant $F_\phi = 0.0871$ GeV [217]. In principle at N^{3}LO one can use either the chiral limit value $F_\phi = 0.0871$ GeV obtained from a two-loop ChPT calculation [217], or the SU(3) averaged value, $F_\phi = 1.17F_\pi$ with $F_\pi = 0.0924$ GeV as in Ref. [56]. The difference is of higher chiral order. In practice, we found that at N^{3}LO the results are not sensitive to these two options while at NNLO the SU(3) averaged value is preferred by the LQCD data. For the baryon axial coupling constants D and F, we use the standard value $D = 0.8$ and $F = 0.46$ with $D + F = 1.26$ as determined from nuclear beta decay. We have allowed D and F to vary in the fits and found that the optimal values determined by the lattice data are consistent with the phenomenological values. The renormalization scale μ is set at 1 GeV, as in Ref. [56].

As mentioned in Chapter 2, the fitted lattice data should fulfil $M_\pi < 500$ MeV and $M_\phi L > 4$ to ensure that the N^{3}LO BChPT is valid for these pion (light-quark) masses and lattice volumes. After selection, there are 11 data sets from the PACS-CS, LHPC, HSC, QCDSF-UKQCD and NPLQCD collaborations, respectively. The results of different collaborations are not correlated with each other, but the data from the same collaboration are partially correlated by the uncertainties propagated from the determination of the lattice spacing. Therefore, in order

Table 5.1: Values of the LECs and fit-χ^2/d.o.f. from the best fits. We have performed fits to the LQCD and experimental data at $\mathcal{O}(p^2)$, $\mathcal{O}(p^3)$, and $\mathcal{O}(p^4)$, without ($\not{D}$) and with (D) the explicit contributions of the virtual decuplet baryons.

	$\not{D}$-$\mathcal{O}(p^2)$	$\not{D}$-$\mathcal{O}(p^3)$	$\not{D}$-$\mathcal{O}(p^4)$	D-$\mathcal{O}(p^4)$
m_0 [MeV]	900(6)	767(6)	880(22)	908(24)
b_0 [GeV^{-1}]	−0.273(6)	−0.886(5)	−0.609(19)	−0.744(16)
b_D [GeV^{-1}]	0.0506(17)	0.0482(17)	0.225(34)	0.355(20)
b_F [GeV^{-1}]	−0.179(1)	−0.514(1)	−0.404(27)	−0.552(28)
b_1 [GeV^{-1}]	–	–	0.550(44)	1.08(6)
b_2 [GeV^{-1}]	–	–	−0.706(99)	0.431(93)
b_3 [GeV^{-1}]	–	–	−0.674(115)	−1.83(15)
b_4 [GeV^{-1}]	–	–	−0.843(81)	−1.57(4)
b_5 [GeV^{-2}]	–	–	−0.555(144)	−0.355(74)
b_6 [GeV^{-2}]	–	–	0.160(95)	−0.423(117)
b_7 [GeV^{-2}]	–	–	1.98(18)	2.79(15)
b_8 [GeV^{-2}]	–	–	0.473(65)	−1.73(6)
d_1 [GeV^{-3}]	–	–	0.0340(143)	0.0157(130)
d_2 [GeV^{-3}]	–	–	0.296(53)	0.445(57)
d_3 [GeV^{-3}]	–	–	0.0431(304)	0.328(18)
d_4 [GeV^{-3}]	–	–	0.234(67)	−0.117(59)
d_5 [GeV^{-3}]	–	–	−0.328(60)	−0.853(77)
d_7 [GeV^{-3}]	–	–	−0.0358(269)	−0.425(39)
d_8 [GeV^{-3}]	–	–	−0.107(32)	−0.557(56)
χ^2/d.o.f.	11.8	8.6	1.0	1.0

to correctly calculate the χ^2 we incorporate the inverse of the resulting correlation matrix $C_{ij} = \sigma_i\sigma_j\delta_{ij} + \Delta a_i\Delta a_j$ for each lattice ensemble (see Ref. [56]) , where the σ_i are the lattice statistical errors and the Δa_i are the fully-correlated errors propagated from the determination of lattice spacing a_i. The FVCs to the baryon masses are consistently calculated in the EOMS-BChPT framework as explained in Section 4.3.

We perform a χ^2 fit to the lattice data and the physical octet baryon masses by varying the 19 LECs. The so-obtained values of the LECs from the best fits are listed in Table 5.1. We remark that in the following the experimental octet baryon masses are always included in the fit unless otherwise stated. This way, the fitted values of LECs are better constrained.

For the sake of comparison, we have fitted lattice data using the NLO and NNLO EOMS-BChPT. It should be noted that since at NLO, ChPT does not generate any FVCs, we have shifted LQCD data by subtracting FVCs calculated by N^{3}LO EOMS-BChPT with the LECs determined from the corresponding best fit. The values of the LECs b_0, b_D, b_F, and m_0 are tabulated in Table 5.1. An order-by-order improvement is clearly seen, with decreasing χ^2/d.o.f. at each increasing order. Apparently, only using the $\mathcal{O}(p^3)$ chiral expansion, we cannot give a good description of the lattice data from the five collaborations. The corresponding χ^2/d.o.f. is about 8.6. On the other hand, in the N^{3}LO fit of lattice data and experimental octet baryon

Table 5.2: Finite-volume corrections (in units of MeV) to lattice octet baryon masses in covariant BChPT up to N^{3}LO.

	M_π	δm_N	δm_Λ	δm_Σ	δm_Ξ	$M_\pi L$	$M_K L$	$M_\eta L$
PACS-CS	296	7	2	5	2	4.3	8.7	9.8
	384	3	1	2	1	5.7	8.6	9.3
	411	2	0	1	1	6.0	9.3	10.2
LHPC	356	11	6	7	5	4.5	7.6	8.4
	495	2	1	1	1	7.5	8.6	9.0
HSC	383	3	2	2	1	5.7	8.1	8.8
	449	29	26	21	21	4.5	5.8	6.2
QCDSF-UKQCD	320	16	13	12	11	4.1	5.8	6.2
NPLQCD	388	10	7	6	6	4.8	6.8	7.3
	388	3	1	2	1	5.8	8.1	9.8
	388	0	0	0	9	7.7	10.8	11.7

masses, χ^2/d.o.f. = 1.0. In addition, the values of the fitted LECs all look very natural. [1] It should be noted that the baryon mass in the chiral limit, $m_0 = 880$ MeV, seems to be consistent with the SU(2)-BChPT value [81, 218].

Finally, it is important to point out that including the FVCs is important to understand the LQCD results in ChPT at N^{3}LO. In Table 5.2, we tabulate the values of FVCs calculated in N^{3}LO BChPT for each lattice ensemble in our fit. We can see that, in the SU(3) sector, FVCs are sizable even $M_\phi L > 4$. Without FVCs taken into account, the best fit to lattice data yields χ^2/d.o.f. ~ 1.9.

In Fig. 5.1, setting the strange-quark mass to its physical value, we plot the light-quark mass evolution of N, Λ, Σ and Ξ as functions of M_π^2 using the LECs from Table 5.1. We can see that the NNLO fitting results are more curved and do not describe well lattice data. On the contrary the N^{3}LO fit can give both a good description of lattice data and experimental results. The rather linear dependence of the lattice data on M_π^2 at large light quark masses, which are exhibited both by the lattice data [25] and reported by other groups, is clearly seen.

5.2 Virtual decuplet contributions

In this section, we perform a systematic study of virtual decuplet effects on the chiral extrapolation of octet baryon masses and the corresponding finite-volume corrections of lattice by explicitly including their contributions and comparing the fitting results with the octet-only ones.

Light-quark mass dependence of the octet baryon masses

Up to N^{3}LO, there are 19 unknown LECs (m_0, b_0, b_D, b_F, b_{1-8}, and $d_{1-5,\,7,\,8}$) in the octet-only EOMS BChPT [Eq. (4.20)]. To take into account the contributions of the decuplet

[1] We have checked that removing from lattice data the two lattice points of LHPC and HSC with $M_\pi > 400$ MeV and $M_K > 580$ MeV does not change qualitatively our results.

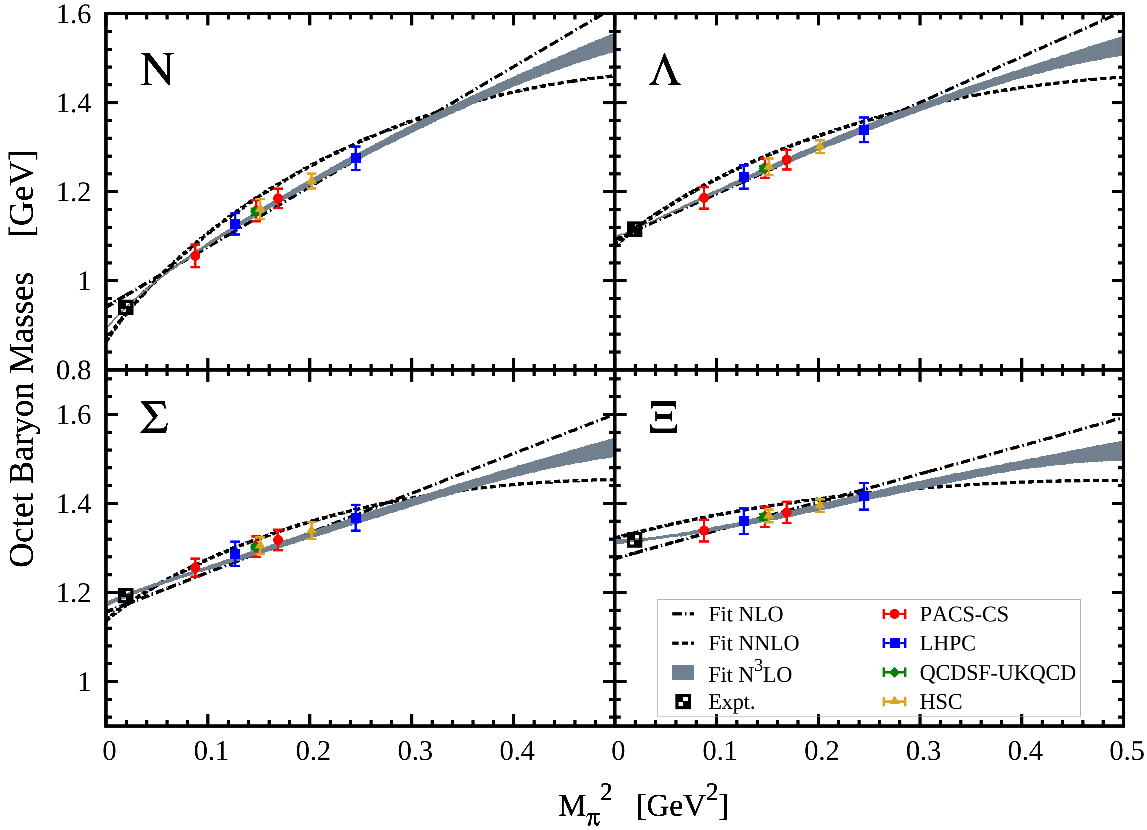

Figure 5.1: The lowest-lying baryon octet masses as functions of the pion mass. The dot-dashed lines and the dotted lines are the best NLO and NNLO fits to lattice data. The bands correspond to the best N^{3}LO fits to lattice results. In obtaining the ChPT results, the strangeness quark mass has been fixed at its physical value. The lattice data points are obtained from the original ones by setting the strange quark mass at its physical value.

baryons, one has to introduce four more LECs, m_D, t_0, t_D and $\mathcal{C}$ [Eq. (4.33)]. The ϕBD coupling constant $\mathcal{C}$ can be fixed to the SU(3)-average value among the different decuplet-to-octet pionic decay channels, i.e., $\mathcal{C} = 0.85$ [119] [2]. A moderate variation of $\mathcal{C}$ has no significant effects on our final results. The LECs t_0, t_D, and m_D can be fixed by fitting the NLO decuplet mass formula $M_D = m_D - m_D^{(2)}$ to the physical decuplet baryon masses. Because t_0 and m_D cannot be disentangled at the physical point, one only obtains a combination of m_D and t_0 with $m_D^{\text{eff}} = m_D - t_0(2M_K^2 + M_\pi^2) = 1.215$ GeV and $t_D = -0.326$ GeV^{-1}. In the following, the octet-decuplet mass splitting $\delta = m_D - m_0$ is fixed to be 0.231 GeV — the average mass gap between the octet and decuplet baryons. Therefore, one can fix the four LECs in the following way: $m_D = m_0 + 0.231$ GeV, $t_0 = (m_0 - 0.984)/0.507$ GeV^{-1}, $t_D = -0.326$ GeV^{-1} and $\mathcal{C} = 0.85$. As a result, the same 19 LECs as those in the octet-only BChPT need to be determined. The other fixed coupling constants are the same as previous section: the meson

[2] In Refs. [56, 118] the value of $\mathcal{C}$ is fixed from the $\Delta(1232) \to \pi N$ decay rate, which yields $\mathcal{C} = 1.0$. But in our previous study of the NPLQCD data, this coupling turned out to be somewhat smaller [57].

decay constant $F_\phi = 0.0871$ GeV, the baryon axial coupling constants $D = 0.8$, $F = 0.46$ and the renormalization scale $\mu = 1$ GeV.

We utilize the formulas of Eq. (4.32) to fit the lattice octet baryon masses and the experimental values [161]. The LQCD data to be studied are taken from the PACS-CS [23], LHPC [25], HSC [26], QCDSF-UKQCD [28] and NPLQCD [29] data satisfying $M_\pi < 500$ MeV and $M_\phi L > 4$, the same data set as previous section. The so-obtained values of the LECs from the best fit and the corresponding χ^2/d.o.f. are tabulated in Table 5.1. For χ^2/d.o.f., from the comparison with the octet-only best fit results, one can conclude that the inclusion of virtual decuplet baryons does not change the description of LQCD data. On the other hand, the values of LECs have changed a lot, as can be clearly seen from Table 5.1 [3]. This confirms the assumption that using only octet baryon mass data, one cannot disentangle virtual decuplet contributions from those of virtual octet baryons and tree-level diagrams [64]. In other words, for the static properties of octet baryons, most contributions of the virtual decuplet are hidden in the relevant LECs, as one naively expects. Below, we will see that their inclusion, however, does improve the description of the volume-dependence of LQCD data, as also noted in Ref. [57].

In Fig. 5.2, setting the strange-quark mass to its physical value, we show the pion mass dependence of octet baryon masses in the N^{3}LO EOMS BChPT with and without virtual decuplet baryon contributions. It is clear that the two N^{3}LO fits give the same description of lattice data, as can be inferred from the same χ^2/d.o.f. shown in Table 5.3.

Finite-volume corrections to the octet baryon masses

In Ref. [57], we have studied the FVCs to lowest-lying octet baryon masses using the EOMS BChPT up to NNLO, and found that finite-volume effects are very important and cannot be neglected. Therefore, in this work FVCs are self-consistently included in Eq. (4.32) to analyze the lattice data. The NPLQCD [29] simulation is performed with the same pion mass of $M_\pi \simeq 390$ MeV and at four different lattice sizes $L \sim 2.0,\ 2.5,\ 3.0$ and 3.9 fm. Therefore, it provides a good opportunity to study FVCs to the octet-baryon masses.

In Fig. 5.3, we contrast the NPLQCD data with the N^{3}LO EOMS BChPT using the LECs from Table 5.1. As stated in Ref. [64], three sets of the NPLQCD data with $M_\phi L > 4$ are included in lattice data and denoted by solid points in Fig. 5.3. Another set with $M_\pi L = 3.86$ (hollow points) is not included. Both the octet-only and the octet plus decuplet (O+D) BChPT can give a reasonable description of the FVCs. In the $e^{-m_\pi L}/(m_\pi L) \leq 0.2$ region, these two fits give essentially the same results. With the increase of $e^{-m_\pi L}/(m_\pi L)$ (the decrease of lattice size L), the O+D BChPT results are in better agreement the NPLQCD data, especially for the nucleon mass. It seems that the virtual decuplet baryons can help to improve the description of the FVCs, although the BChPT results are still a bit larger than the LQCD data at small $M_\phi L$. It is also indicated that including $M_\phi L = 3.86$ could give a better description of FVCs. Therefore, in the following, we would like to slightly loose the constraint of $M_\phi L$ with $M_\phi L > 3.8$.

[3] The same phenomenon has been observed in the studies of octet baryon magnetic moments [118] and octet baryon masses up to NNLO [119].

5.3 Continuum extrapolation of lattice data

In this section, we employ the octet baryon masses obtained in Wilson covariant BChPT up to N^{3}LO [Eq. (4.75)] to estimate discretization effects of the current LQCD simulations by performing a simultaneous fit of the latest $n_f = 2+1$ LQCD data, which are obtained with the $\mathcal{O}(a)$-improved Wilson action.

At present, most LQCD simulations employ a single lattice spacing a and take discretization effects as systematic uncertainties. A similar strategy has been adopted by theoretical studies. On the other hand, one may combine the LQCD simulations from different collaborations and perform a quantitative study of the discretization effects. Among the latest LQCD simulations, several collaborations employed the $\mathcal{O}(a)$-improved or 'clover' Wilson action, e.g. PACS-CS (with $a = 0.0907(14)$ fm and $c_{\mathrm{SW}} = 1.715$), QCDSF-UKQCD (with $a = 0.0795(3)$ fm and $c_{\mathrm{SW}} = 2.65$), HSC and NPLQCD (with $a_s = 0.1227(8)$ fm, $a_t = 0.03506(23)$ fm, $c^s_{\mathrm{SW}} = 2.6$, and $c^t_{\mathrm{SW}} = 1.8$) collaborations. These simulations are performed at three different values of lattice spacing a and with different light-quark masses and, therefore, in principle allow for a quantitative study of the discretization effects on the octet baryon masses.

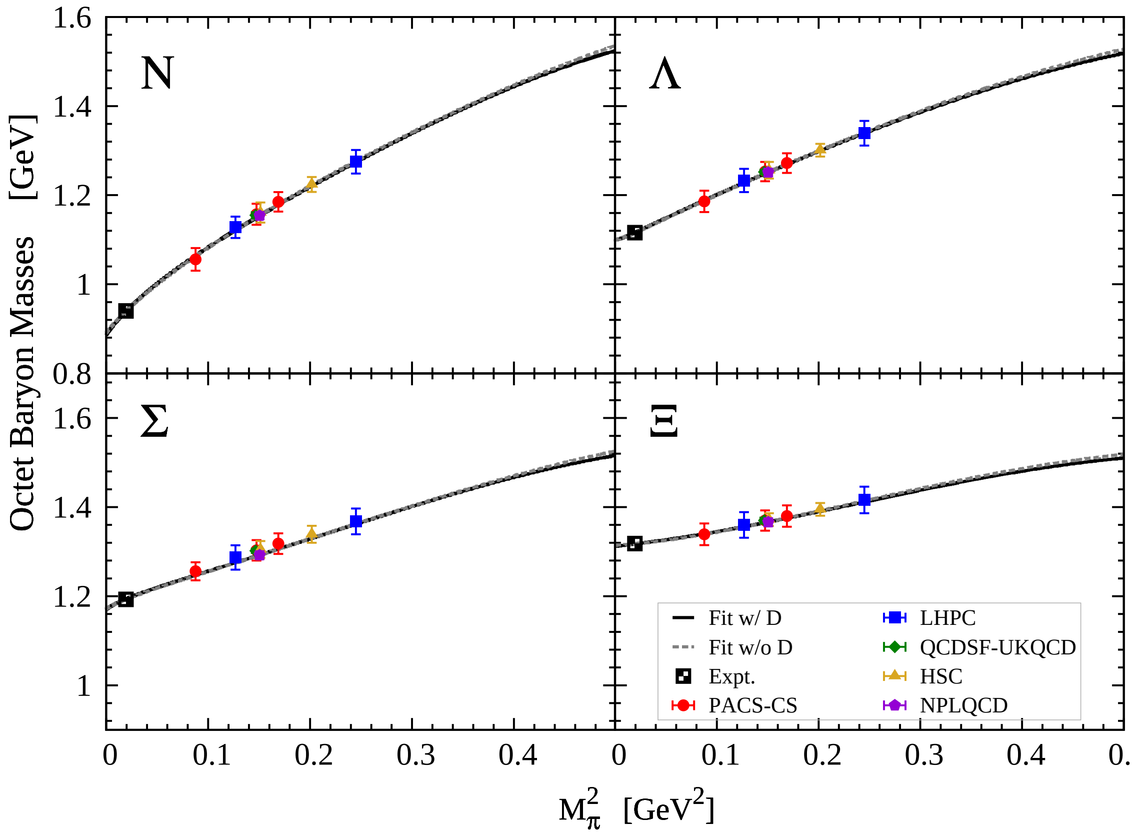

Figure 5.2: Pion mass dependence of the LQCD data in comparison with the best fits of the EOMS BChPT up to N^{3}LO with (solid lines) and without (dashed lines) the virtual decuplet contributions. The lattice data have been extrapolated to the physical strange-quark mass and infinite space-time.

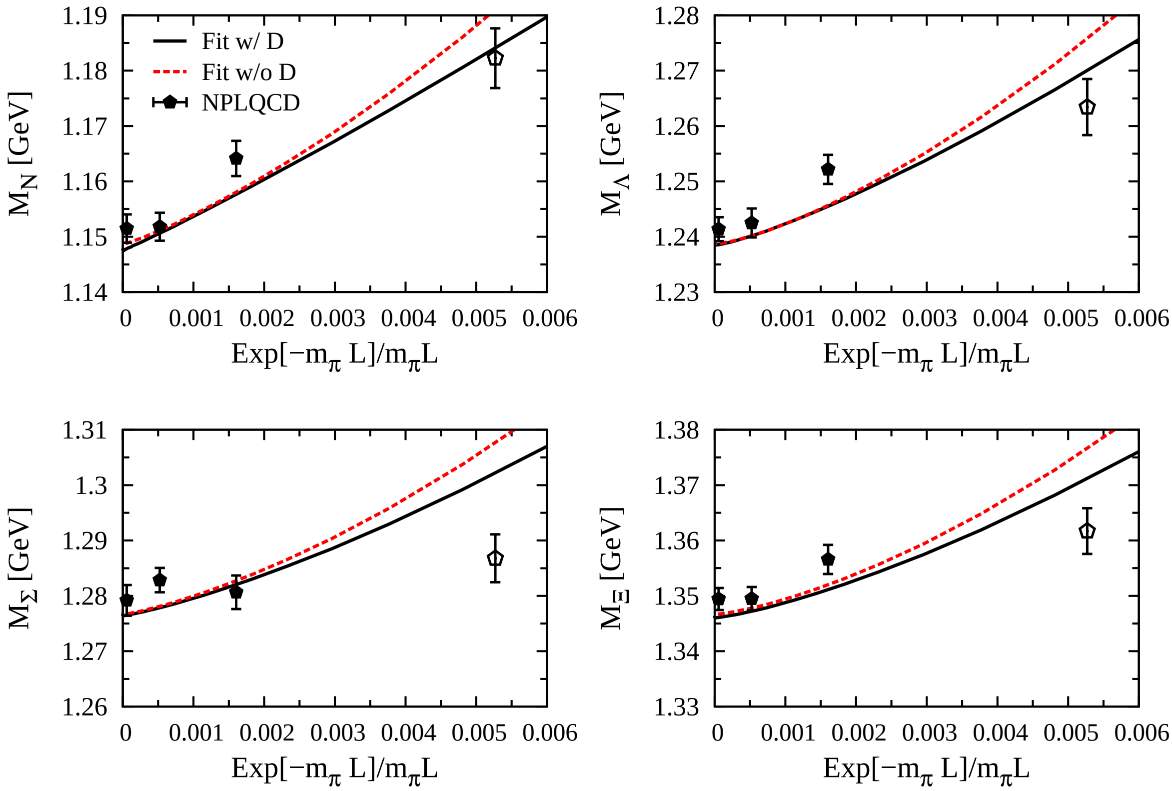

Figure 5.3: Lattice volume dependence of the NPLQCD data in comparison with the EOMS BChPT up to N^{3}LO with (solid lines) and without (dashed lines) the virtual decuplet contributions. The full black points with $M_\phi L > 4$ are included in the fit data sets, while the hollow point with $M_\phi L = 3.86$ are not.

It should be noted that both the HSC [26] and the NPLQCD [29] simulations employed the anisotropic clover fermion action [219]. In this action, the temporal lattice spacing is chosen to be much smaller than the spatial lattice spacing. The EFT for such a LQCD setup has been worked out in Ref. [94]. It is in principle more appropriate for the study of lattice data of HSC and NPLQCD collaborations. On the other hand, this EFT contains more LECs to discriminate the temporal and spatial lattice spacing effects. As we will see, present limited LQCD data do not allow us to perform such a study. Therefore, in our study we assume that these simulations are performed with a single lattice spacing, a_s, and we treat the difference between a_s and a_t as higher-order effects.

As in Refs. [65, 66], we focus on LQCD data from the above four collaborations with $M_\pi < 500$ MeV and $M_\phi L > 3.8$ to ensure the applicability of SU(3) covariant BChPT. In total, there are 12 sets of LQCD data from the PACS-CS (3 sets), QCDSF-UKQCD (2 sets), HSC (3 sets), and NPLQCD (4 sets). In order to better ascertain the values of LECs, the experimental octet baryon masses are also included in the fits.

In the $\mathcal{O}(a)$-improved Wilson action, the Pauli term $a\mathcal{L}^{(5)}$ is eliminated. As a result, discretization effects originate only from the $\mathcal{O}(am_q)$ and $\mathcal{O}(a^2)$ terms. Therefore, only the fourth-order tree-level diagrams contribute, while the leading order tree-level diagram and the

Table 5.3: Values of the LECs from the best fit to the LQCD data and the experimental data at $\mathcal{O}(p^4)$ with and without discretization effects.

	BChPT	WBChPT		BChPT	WBChPT
m_0 [MeV]	910(20)	915(20)	d_1 [GeV^{-3}]	0.0295(124)	−0.0196(121)
b_0 [GeV^{-1}]	−0.579(56)	−0.557(50)	d_2 [GeV^{-3}]	0.342(65)	0.230(58)
b_D [GeV^{-1}]	0.211(56)	0.201(48)	d_3 [GeV^{-3}]	−0.0314(63)	−0.0557(56)
b_F [GeV^{-1}]	−0.434(43)	−0.359(41)	d_4 [GeV^{-3}]	0.372(114)	0.304(1008)
b_1 [GeV^{-1}]	0.730(10)	0.810(8)	d_5 [GeV^{-3}]	−0.401(110)	−0.237(88)
b_2 [GeV^{-1}]	−1.21(18)	−0.819(26)	d_7 [GeV^{-3}]	−0.0913(58)	−0.104(48)
b_3 [GeV^{-1}]	−0.340(153)	−0.357(12)	d_8 [GeV^{-3}]	−0.132(79)	−0.0417(67)
b_4 [GeV^{-1}]	−0.776(16)	−0.780(15)	$\bar{B}_1$ [GeV^{-3}]$\times 10^{-2}$	–	−0.121(103)
b_5 [GeV^{-2}]	−1.15(287)	−1.34(23)	$\bar{B}_2$ [GeV^{-3}]$\times 10^{-2}$	–	−0.467(109)
b_6 [GeV^{-2}]	0.778(390)	0.889(199)	$\bar{B}_3$ [GeV^{-3}]$\times 10^{-2}$	–	0.344(267)
b_7 [GeV^{-2}]	0.899(26)	0.787(14)	$\bar{X}$ [GeV^{-3}]$\times 10^{-4}$	–	0.606(5723)
b_8 [GeV^{-2}]	0.627(37)	0.817(28)			
χ^2	30.0	28.0	χ^2/d.o.f.	0.91	0.97

tadpole/one-loop diagrams do not contribute. In the end, the discretization effects refer to the Eq. (4.78) and Eq. (4.79),

$$\begin{aligned} m_B^{(a)} &= m_B^{\mathcal{O}(am_q)} + m_B^{\mathcal{O}(a^2)} \\ &= -8ac_{\rm SW}W_0\left(\xi_l M_\pi^2 + \xi_s(2M_K^2 - M_\pi^2)\right) - 16a^2c_{\rm SW}^2W_0^2\bar{X}, \end{aligned} \tag{5.1}$$

only contain 4 new independent combinations of LECs, i.e., $\bar{B}_1$, $\bar{B}_2$, $\bar{B}_3$, and $\bar{X}$. Together with the 19 unknown LECs appearing in the octet baryon masses in the continuum, there are in total 23 free LECs that need to be fixed [4]. The other parameters are fixed as the same as before: $F_\phi = 0.0871$ GeV, $D = 0.8$, $F = 0.46$, and $\mu = 1$ GeV.

In order to study the discretization effects on the octet baryon masses, we perform two fits. First, we use the continuum octet baryon mass formulas to fit the LQCD and experimental data. Second, the mass formulas of Eq. (4.75) with discretization effects taken into account are employed to fit the same data. In both fits, the finite-volume corrections to the LQCD simulations are always taken into account self-consistently [64]. The LECs, together with the χ^2/d.o.f., obtained from the two best fits are tabulated in Table 5.3. It is clear that the 19 LECs remain similar whether or not discretization effects are taken into account. The total χ^2 changes from 30 for the first fit to 28 for the second fit, indicating that the data can be described slightly better. On the other hand, the χ^2/d.o.f. slightly increases from 0.91 to 0.97, implying that discretization effects do not play an important role in describing the present LQCD data.[5] This justifies their treatment as systematic uncertainties without being taken into account explicitly in the fitting, as done in most previous theoretical and LQCD studies. It should be noted that the one-sigma uncertainties of the LECs $\bar{B}_1$, $\bar{B}_2$, $\bar{B}_3$, and, particularly, $\bar{X}$ are rather large. This shows clearly the need to perform LQCD simulations at multiple lattice spacings in order to pin down more precisely discretization effects, which has long been

[4] In our fits, we set W_0 at 1 GeV^3. Later a more proper value will be used to check the naturalness of the resulting LECs, $\bar{B}_1$, $\bar{B}_2$, $\bar{B}_3$, and $\bar{X}$.

[5] This is in contrast with the finite-volume effects. In Ref. [64], it is shown that a self-consistent treatment of finite-volume effects is essential to obtain a χ^2/d.o.f. about 1.

Table 5.4: Extrapolated octet baryon masses (in units of MeV) to physical point with the LECs determined by fitting to LQCD data alone.

	BChPT	WBChPT	Exp. [161]
χ^2/d.o.f.	0.89	1.0	–
m_N	889(21)	865(39)	940(2)
m_Λ	1113(17)	1087(41)	1116(1)
m_Σ	1163(19)	1139(42)	1193(5)
m_Ξ	1333(16)	1309(41)	1318(4)

recognized [220].

In the above fits we have included the experimental data to better constrain the large number of LECs appearing at N^{3}LO. We can of course drop the experimental data, redo the fit, and calculate the octet baryon masses at the physical point. Such a procedure should be taken with caution, however, for the following reasons. First, we have a large number of unknown LECs (about 20). Second, the lightest LQCD data point has a M_π about 300 MeV, and it is still a bit away from the physical point. Third, all the χ^2/d.o.f. are close to 1. These factors can make the extrapolations unstable with respect to moderate changes of the LECs. In Table 5.4, we tabulate the extrapolated octet baryon masses with two sets of LECs, determined from the fits in which finite lattice spacing effects are either taken into account or neglected. It is clear that the extrapolated masses agree within uncertainties, and so do the corresponding LECs (not shown). Nevertheless, the extrapolated nucleon mass still deviates about 60-80 MeV from its physical value, calling for LQCD simulations with smaller light-quark masses (than studied in the present work).

In Fig. 5.4, we show the evolution of discretization effects as a function of the lattice spacing for three different pion masses with the relevant LECs determined from the second fit. It is seen that the discretization effects increase almost linearly with increasing lattice spacing a for fixed pion mass. For fixed a, they increase with increasing pion mass as well. Furthermore, essentially no curvature is observed. It is clear that in our present work the $\mathcal{O}(am_q)$ terms dominate over the $\mathcal{O}(a^2)$ terms [6]. It should be stressed that the LEC $\bar{X}$ is consistent with zero and a fit without the $\mathcal{O}(a^2)$ contributions would have yielded very similar results as shown in Table 5.3 and Fig. 5.4. For a lattice spacing up to $a = 0.15$ fm, the finite lattice spacing effects on the baryon masses are less than 2%, consistent with the LQCD study of Ref. [221].

The above results can be naively understood in the following way. Recall that $m_q/\Lambda_{\rm QCD} \sim a\Lambda_{\rm QCD}$ in our power-counting scheme. If we take $m_s = 100$ MeV, $\Lambda_{\rm QCD} = 300$ MeV, and $a = 0.1$ fm, we obtain $m_q/\Lambda_{\rm QCD} \approx 0.3$ and $a\Lambda_{\rm QCD} \approx 0.15$. If we further assume that all the LECs are of natural size, i.e., ~ 1, we then expect $\mathcal{O}(m_q^2) : \mathcal{O}(am_q) : \mathcal{O}(a^2) = 4 : 2 : 1$. Remember that the quark masses are larger than their physical values while the lattice spacing is fixed to be around 0.1 fm in the LQCD simulations, our actual numerical results seem to support this naive argument. Furthermore, we would like to point out that the a-dependent LECs $\bar{B}_1$, $\bar{B}_2$, $\bar{B}_3$, and $\bar{X}$ are of natural size. The values in Table 5.3 appear to be small

[6] In Ref. [207], Alvarez-Ruso *et al.* performed a phenomenological study of the continuum extrapolation of the LQCD simulations of the nucleon mass by considering only $\mathcal{O}(a^2)$ terms, and they showed that finite-volume corrections and finite lattice spacing effects are of similar size. In our present work we find that they are indeed of similar size, but the $\mathcal{O}(am_q)$ contributions are larger than the $\mathcal{O}(a^2)$ ones.

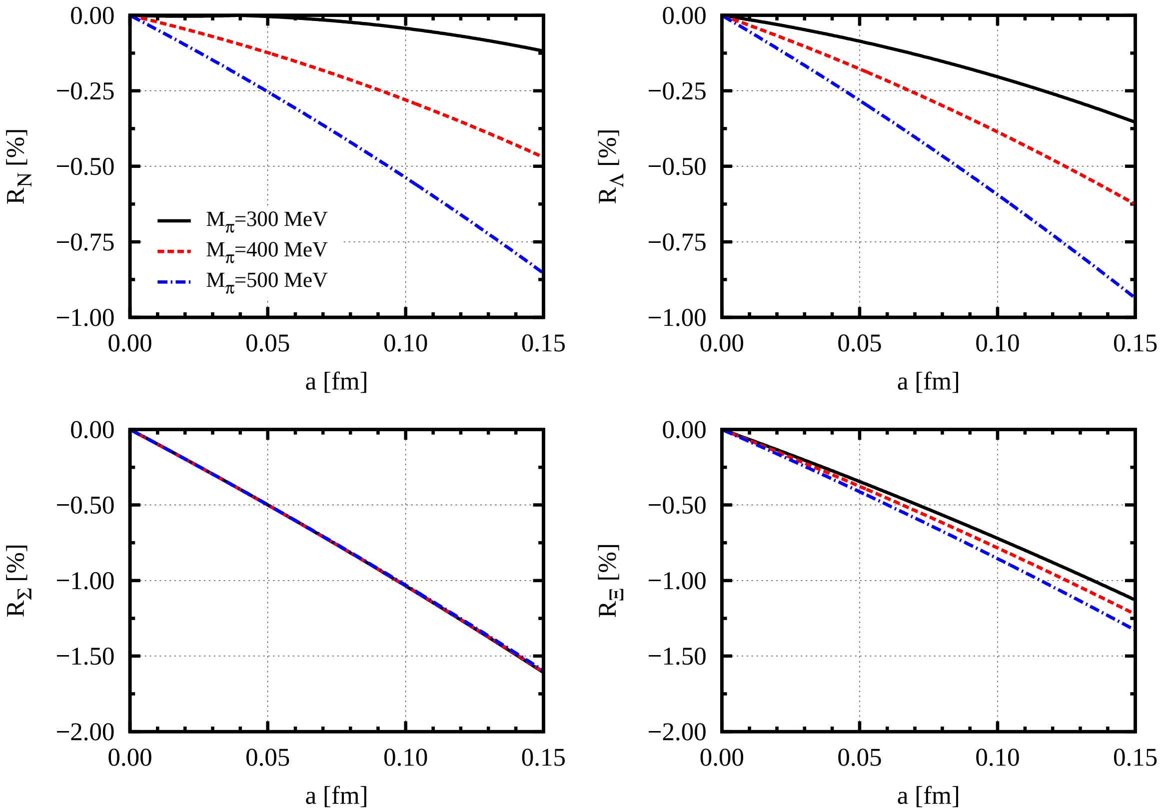

Figure 5.4: (color online). Finite lattice spacing effects on the octet baryon masses, $R_B = m_B^{(a)}/m_B$, as functions of lattice spacing a for $M_\pi = 300, 400$, and 500 MeV, respectively. The SW coefficient is set at $c_{\rm SW} = 1.715$, the value of the PACS-CS Collaboration. The strange quark mass is fixed at its physical value dictated by the leading order ChPT.

because we have set the dimensional quantity W_0 to be 1 GeV^3. Its more 'proper' value can be estimated by noting the following relations $W_0 a \sim B_0 m_q$ and $M_\pi^2 \propto 2B_0 m_q$ (in the leading-order ChPT), which yields $W_0 \approx 0.02$ GeV^3. With this value, the LECs turn out to be $\bar{B}_1 = -0.0605$ GeV^{-3}, $\bar{B}_2 = -0.234$ GeV^{-3}, $\bar{B}_3 = 0.172$ GeV^{-3}, and $\bar{X} = 0.152$ GeV^{-3}, which are of natural size as expected.

Chapter 6

Octet baryon sigma terms

In Chapter 4, we have obtained the chiral expansion of octet baryon masses. As an application, we would like to utilize the Feynman-Hellmann theorem to predict the octet baryon sigma terms by analyzing the high-statistics $n_f = 2 + 1$ lattice QCD data. In order to perform an accurate prediction of sigma terms, several key factors are systematically taken into account and clarified for the first time, including the effects of lattice scale setting, systematic uncertainties originating from chiral expansion truncations, and constraint of strong-interaction isospin breaking effects.

6.1 Introduction

Understanding the sea-quark structure of nucleon has long been a central topic in nuclear physics [222]. Of particular interest are the contributions of the $s\bar{s}$ component since nucleon contains no valence strange quarks, e.g., the strangeness contribution to proton spin [223] and to electric and magnetic form factors [224]. In this context, the strangeness-nucleon sigma term, $\sigma_{sN} = m_s\langle N|\bar{s}s|N\rangle$, plays an important role as it relates to the scalar strangeness content of nucleon, the composition of nucleon mass, KN scatterings, counting rates in Higgs boson searches [225], and the precise measurement of the Standard Model parameters in pp collisions at LHC [226]. Furthermore, the uncertainty in σ_{sN} is the principal source in predicting the cross section of certain candidate dark matter particles interacting with nucleons [227].

Although the pion-nucleon sigma term $\sigma_{\pi N} = m_l\langle N|\bar{u}u + \bar{d}d|N\rangle$ can be determined from pion-nucleon scattering [228, 229], historically the strangeness-nucleon sigma term has been determined indirectly via the nonsinglet matrix element $\sigma_0 = m_l\langle N|\bar{u}u+\bar{d}d-2\bar{s}s|N\rangle$, which yields a value ranging from 0 to 300 MeV [119]. In principle, LQCD provides a model independent way in the determination of baryon sigma terms by either computing three-point [230–237] or two-point correlation functions (the so-called spectrum method) [58, 64, 200, 235, 238–242]. Although tremendous efforts have been made in this endeavor, due to the many systematic and statistical uncertainties inherent in these studies, no consensus has been reached on the value of the scalar strangeness content of nucleon.

The most important sources of systematic uncertainties originate from the so-called chiral extrapolations. In the u, d, and s flavor sector, a proper formulation of baryon chiral perturbation theory that satisfies all symmetry and analyticity constraints is known to be essential to properly describe the nonperturbative regime of QCD. In this sense, the extended-on-mass-shell formulation [71] has shown a number of both formal and practical advantages, whose applications have solved a number of long-existing puzzles in the one-baryon sector [199]. Its applications in the studies of the LQCD octet baryon masses turn out to be very successful as well [64–66]. Furthermore, as demonstrated recently, mass dependent and mass independent lattice scale setting methods can result in a σ_{sN} different by a factor of three [240, 243].

Therefore, it casts doubts on the determination of σ_{sN} from a single data set with a particular scale setting method. To say the least, systematic uncertainties might be well underestimated.

In this chapter, utilizing the latest and high-statistics $n_f = 2+1$ LQCD simulations of the octet baryon masses from the PACS-CS [23], LHPC [25], and QCDSF-UKQCD [28] collaborations and the Feynman-Hellmann theorem, paying special attention to the lattice scale setting, we report a determination of the baryon sigma terms, particularly the strangeness-nucleon sigma term, in covariant BChPT up to N^{3}LO.

The Feynman-Hellmann theorem [244] dictates that in the isospin limit the baryon sigma terms can be calculated from the quark mass dependence of the octet baryon masses, m_B, in the following way:

$$\sigma_{\pi B} = m_l\langle B|\bar{u}u + \bar{d}d|B\rangle \equiv m_l \frac{\partial m_B}{\partial m_l}, \tag{6.1}$$

$$\sigma_{sB} = m_s\langle B|\bar{s}s|B\rangle \equiv m_s \frac{\partial m_B}{\partial m_s}. \tag{6.2}$$

The chiral expansion of octet baryon masses up to N^{3}LO, m_B, is already given in Eq. (4.20) of Chapter 4. The virtual decuplet contributions are not explicitly included, since their effects on the chiral extrapolation and FVCs are shown to be relatively small [65]. For convenience in the following discussion, we would like to mention that there are 19 unknown LECs: m_0, b_0, b_D, b_F, b_{1-8}, $d_{1-5,7,8}$ to be determined by fitting the LQCD data [64], and the others are fixed at the following values: $D = 0.8$, $F = 0.46$ [245], $F_\phi = 0.0871$ GeV [217], and $\mu = 1$ GeV.

6.2 Three key factors for accurate determination

In order to obtain an accurate determination of baryon sigma terms, a careful examination of LQCD data is essential, since not all of them are of the same quality though they are largely consistent with each other as shown in Refs. [64, 201]. For instance, the statistics of the HSC simulations needs to be improved [26] while the NPLQCD simulations are performed at one single combination of light-quark and strange-quark masses [29], which offers little constraint on the quark mass dependence of baryon masses. The BMW simulations [22], though of high quality, are not publicly available. This leaves the PACS-CS [23], LHPC [25], and QCDSF-UKQCD [28] data for our study. It is important to note that most LQCD simulations fix the strange-quark mass close to its physical value and vary the light-quark masses. As a result, they are suitable to study the light-quark mass dependence but not the strange-quark mass dependence. In this respect, the QCDSF-UKQCD simulations are of particular importance because they provide a dependence of baryon masses on the strange-quark mass in a region not accessible in other simulations. In order to stay within the application region of BChPT, we only choose LQCD data satisfying the following two criteria: $M_\pi < 500$ MeV [1] and $M_\phi L > 3.8$, as in Refs. [65, 67]. It should be noted that the later criterium is relaxed for the QCDSF-UKQCD data (the smallest $M_\phi L$ taken into account is 2.932) since their FVCs are small because of the use of ratio method [28].

[1] We have checked that reducing the cut on M_π down to $M_\pi = 400$ MeV or $M_\pi = 360$ MeV has little effect on our numerical results, but since our χ^2/d.o.f. (see Table 6.1) is already about 1, there is no need to further decrease the cut on M_π.

Table 6.1: Values of the LECs from the best fits to LQCD and experimental octet baryon masses up to N^{3}LO. The lattice scale in each simulation is determined using both the mass independent scale setting (MIS) and the MDS methods. In the MIS, both the original lattice spacings determined by the LQCD collaborations themselves "a fixed" and the self-consistently determined lattice spacings "a free" are used (see text for details).

	MIS		MDS
	a fixed	a free	
m_0 [MeV]	884(11)	877(10)	887(10)
b_0 [GeV^{-1}]	−0.998(2)	−0.967(6)	−0.911(10)
b_D [GeV^{-1}]	0.179(5)	0.188(7)	0.039(15)
b_F [GeV^{-1}]	−0.390(17)	−0.367(21)	−0.343(37)
b_1 [GeV^{-1}]	0.351(9)	0.348(4)	−0.070(23)
b_2 [GeV^{-1}]	0.582(55)	0.486(11)	0.567(75)
b_3 [GeV^{-1}]	−0.827(107)	−0.699(169)	−0.553(214)
b_4 [GeV^{-1}]	−0.732(27)	−0.966(8)	−1.30(4)
b_5 [GeV^{-2}]	−0.476(30)	−0.347(17)	−0.513(89)
b_6 [GeV^{-2}]	0.165(158)	0.166(173)	−0.0397(1574)
b_7 [GeV^{-2}]	−1.10(11)	−0.915(26)	−1.27(8)
b_8 [GeV^{-2}]	−1.84(4)	−1.13(7)	0.192(30)
d_1 [GeV^{-3}]	0.0327(79)	0.0314(72)	0.0623(116)
d_2 [GeV^{-3}]	0.313(26)	0.269(42)	0.325(54)
d_3 [GeV^{-3}]	−0.0346(87)	−0.0199(81)	−0.0879(136)
d_4 [GeV^{-3}]	0.271(30)	0.230(24)	0.365(23)
d_5 [GeV^{-3}]	−0.350(28)	−0.302(50)	−0.326(66)
d_7 [GeV^{-3}]	−0.435(10)	−0.352(8)	−0.322(7)
d_8 [GeV^{-3}]	−0.566(24)	−0.456(30)	−0.459(33)
χ^2/d.o.f.	0.87	0.88	0.53

A second issue relates to the scale setting of LQCD simulations as mentioned in Chapter 2. For the spectrum determination of baryon sigma terms, it was pointed out in Ref. [240, 243] that using the Sommer scale r_0 [152] to fix the lattice spacing of the PACS-CS data can change the prediction of the strangeness-nucleon sigma term by a factor of two to three in the FRR BChPT up to NNLO. However, in our following studies, we found that the scale setting effects on sigma terms are small. It was claimed that using Sommer scale r_1 for the purpose of lattice scale setting is preferred in the LHPC simulations [246] as well. As a result, it is necessary to understand how different scale setting methods for the same simulations affect the prediction of the baryon sigma terms. Unfortunately, such a systematic study is still missing. In addition, instead of relying on the scale determined by the LQCD collaborations themselves, one can fix the lattice scale self-consistently in the BChPT study of the LQCD dimensionless data, as recently done in Ref. [201]. In the present work, all the three alternative ways of lattice scale setting will be studied and their effects on the predicted sigma terms examined and quantified.

At N^{3}LO, the large number of unknown LECs should be better constrained in order to give a reliable prediction of the baryon sigma terms. In this work, we employ the latest LQCD results on the strong isospin-splitting effects on octet baryon masses to further constrain the LECs. The following values are used: $\delta m_N = -2.50(50)$ MeV, $\delta m_\Sigma = -7.67(79)(105)$ MeV and $\delta m_\Xi = -5.87(76)(43)$ MeV at the physical point. The δm_N is chosen such as to cover all the recent results [247, 248], while the δm_Σ and δm_Ξ are taken from Ref. [248]. It should be pointed out that no new unknown LECs need to be introduced to calculate isospin-breaking corrections up to the order at which we work. For more details about the strong isospin-splitting effects on octet baryon masses, please refer to Appendix D.

6.3 Predicted baryon sigma terms

In the mass formulas of octet baryon, the LQCD and experimental meson masses are described by NLO ChPT [34] with the LECs of Ref. [249]. FVCs [250] are taken into account but found to play a negligible role. In Table 6.1, we tabulate the values of LECs and the corresponding χ^2/d.o.f. from three best fits to lattice and experimental octet baryon masses. In the first fit, we use the lattice spacings a determined by LQCD collaborations themselves to obtain the hadron masses in physical units as done in Ref. [64]. In the second fit, we determine the lattice spacings a self-consistently. Interestingly, we find that the so-determined lattice spacings a are close to the ones determined by LQCD collaborations themselves. Specifically, the PACS-CS deviation is 2.5%, the LHPC deviation is 4.1%, and the QCDSF-UKQCD deviation is 2.1%. The corresponding χ^2/d.o.f. also look similar. While in the third fit, we adopt the so-called mass dependent scale setting (MDS), either from r_0 for the PACS-CS data with $r_0(\text{phys.}) = 0.465(12)$ fm [251], r_1 for the LHPC data with $r_1(\text{phys.}) = 0.31174(20)$ fm [242] [2], or $X_\pi = \sqrt{(M_\pi^2 + 2M_K^2)/3}$ for the QCDSF-UKQCD data with $X_\pi(\text{phys.}) = 0.4109$ GeV [28]. The third fit yields a smaller χ^2/d.o.f. and different LECs compared to the other two fits.

In Fig. 6.1, we show octet baryon masses as functions of M_π^2 and $2M_K^2 - M_\pi^2$ using the LECs from Table 6.1 with the physical light- (right panel) and strange-quark (left panel) masses. In

Table 6.2: Predicted pion- and strangeness-sigma terms of the octet baryons (in units of MeV) by the N^{3}LO BChPT with the LECs of Table 6.1.

	MIS		MDS
	a fixed	a free	
$\sigma_{\pi N}$	55(1)(4)	54(1)	51(2)
$\sigma_{\pi\Lambda}$	32(1)(2)	32(1)	30(2)
$\sigma_{\pi\Sigma}$	34(1)(3)	33(1)	37(2)
$\sigma_{\pi\Xi}$	16(1)(2)	18(2)	15(3)
σ_{sN}	27(27)(4)	23(19)	26(21)
$\sigma_{s\Lambda}$	185(24)(17)	192(15)	168(14)
$\sigma_{s\Sigma}$	210(26)(42)	216(16)	252(15)
$\sigma_{s\Xi}$	333(25)(13)	346(15)	340(13)

[2]Technically, this scale setting should be classified as a mass independent scale setting. Here, we slightly misuse the terminology to distinguish it from the one used in the LHPC original publication [25].

Table 6.3: The strangeness content and the "dimensionless sigma terms" of the octet baryons at the physical point. The first error is statistical and the second one is systematic, estimated by taking half the difference between the N^{3}LO result and the NNLO result.

	y_B	$f_{\pi B}$	f_{sB}
N	0.041(41)(7)	0.059(1)(0)	0.029(29)(4)
Λ	0.48(6)(5)	0.029(0)(1)	0.166(22)(15)
Σ	0.51(7)(11)	0.028(0)(3)	0.176(22)(35)
Ξ	1.73(17)(23)	0.012(0)(2)	0.253(19)(10)

order to cross-check the validity of our N^{3}LO BChPT fit, the BMW collaboration data [238] are shown as well. It is clear that our three fits yield similar results and are all consistent with the high-quality BMW data, which are not included in our fits.

Using the best fit LECs, we predict the sigma terms of the octet baryons and tabulate the results in Table 6.2. Our predictions given by LECs of Table 6.1 are consistent with each other within uncertainties, and the scale setting effects on the sigma terms seem to be small. Therefore, we take the central values from the fit to the mass independent a fixed LQCD simulations as our final results, and treat the difference between three lattice scale settings as systematic uncertainties, which are given in the second parenthesis of the second column of Table 6.2. It is clear that for $\sigma_{\pi N}$, uncertainties due to scale setting are dominant, while for σ_{sN} statistics errors are much larger, calling for improved LQCD simulations. It should be noted that we have studied the effects of virtual decuplet baryons and variation of the LECs D, F, F_ϕ, and found that the induced uncertainties are negligible compared to those shown in Table 6.2. We want to mention that, as shown in Ref. [67], continuum extrapolations have no visible effects on the predicted sigma terms. Furthermore, there are also other related quantities, which often appear in the literature, including the strangeness content (y_B) and the so-called "dimensionless sigma terms" ($f_{\pi B}$, f_{sB}):

$$y_B = \frac{2\langle B|\bar{s}s|B\rangle}{\langle B|\bar{u}u+\bar{d}d|B\rangle} = \frac{m_l}{m_s}\frac{2\sigma_{sB}}{\sigma_{\pi B}}, \tag{6.3}$$

$$f_{\pi B} = \frac{m_l\langle B|\bar{u}u+\bar{d}d|B\rangle}{M_B} = \frac{\sigma_{\pi B}}{M_B}, \tag{6.4}$$

$$f_{sB} = \frac{m_s\langle B|\bar{s}s|B\rangle}{M_B} = \frac{\sigma_{sB}}{M_B}, \tag{6.5}$$

are also calculated and tabulated in Table 6.3.

The pion-nucleon sigma term, $\sigma_{\pi N} = 55(1)(4)$ MeV, is in reasonable agreement with the latest πN scattering study, $\sigma_{\pi N} = 59(7)$ MeV [229], and also the systematic study of $n_f = 2+1$ LQCD simulations on the nucleon mass, $\sigma_{\pi N} = 52(3)(8)$ MeV [207], but larger than that of Ref. [201], $\sigma_{\pi N} = 39^{+2}_{-1}$ MeV. Our predicted σ_{sN} is compared with those of earlier studies in Fig. 6.2, classified into three groups according to the methods by which they are determined. The first group is the results reported by the $n_f = 2+1$ LQCD simulations, while the second and third groups are predicted by the NNLO and N^{3}LO BChPT, respectively. Our results are consistent with the latest LQCD determinations and those of NNLO BChPT studies. However, the prediction of the only other N^{3}LO study in the partial summation approach [201] is not

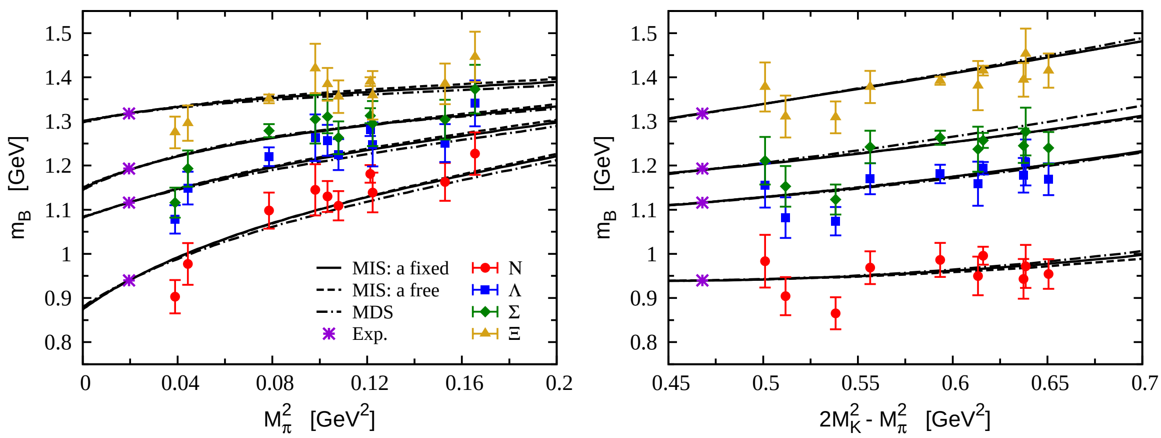

Figure 6.1: Octet baryon masses as a function of M_π^2 and $2M_K^2 - M_\pi^2$ vs the BMW LQCD data (data points are taken from Fig. [2] of Ref. [238]). The solid, dashed, and dot-dashed lines are obtained with the LECs from the three fits of Table 6.1. On the left and right panels, the strange-quark mass and the light-quark mass are fixed at their respective physical values.

consistent with our result and most LQCD results. It should be noted that, in last two months, the BMW and χQCD collaborations have updated their nucleon sigma terms. More surprisingly, the latest nucleon strangeness sigma term from the BMW Collaboration changes from $\sigma_{sN} = 34(15)(25)$ [238] to $\sigma_{sN} = 105(41)(37)$ MeV [252], while the χQCD result only changes a little bit ($\sigma_{sN} = 32.3(4.7)(4.9)$ MeV [253]). Therefore, one has to put more efforts to clarify this large distinction of σ_{sN}.

A note of caution is in order. Clearly, using the spectrum method to determine baryon sigma terms depends critically on the details of LQCD simulations. Lattice scale setting is just one of the sources for potentially large systematic errors. We have studied three common alternative strategies and found that the resulting predictions remain almost the same. Nevertheless, our studies do not exclude the possibility that predictions can change in more rare scenarios. In addition, other LQCD artifacts (such as lattice spacing discretization effects) not addressed in the present work that affect little the baryon masses may have an impact on the predicted baryon sigma terms, which is, however, beyond the scope of present work.

Given the fact that BChPT plays an important role in predicting baryon sigma terms, it is of particular importance to assess the uncertainties of truncating chiral expansions. It becomes even more important in the u, d, and s three-flavor sector, where convergence is governed by the relative large ratio of $m_K/\Lambda_{\rm ChPT} \approx 0.5$. Previous studies either stayed at NNLO or N^{3}LO and, therefore, were unable to perform such an analysis except those of Refs. [64, 65], which, however, focused on a global study of baryon masses and did not include all the QCDSF-UKQCD data that provide further constraints on the strange-quark mass dependence of the octet baryon masses.

To understand quantitatively the convergence issue, we have studied at NNLO the octet baryon masses of the PACS-CS, LHPC and QCDSF-UKQCD data obtained with the lattice spacings a given by the LQCD collaborations themselves. We have allowed the LEC F_ϕ to vary to get an estimation of the induced variation. All the obtained χ^2/d.o.f. is larger than 1, indicating that higher-order chiral contributions need to be taken into account. In addition,

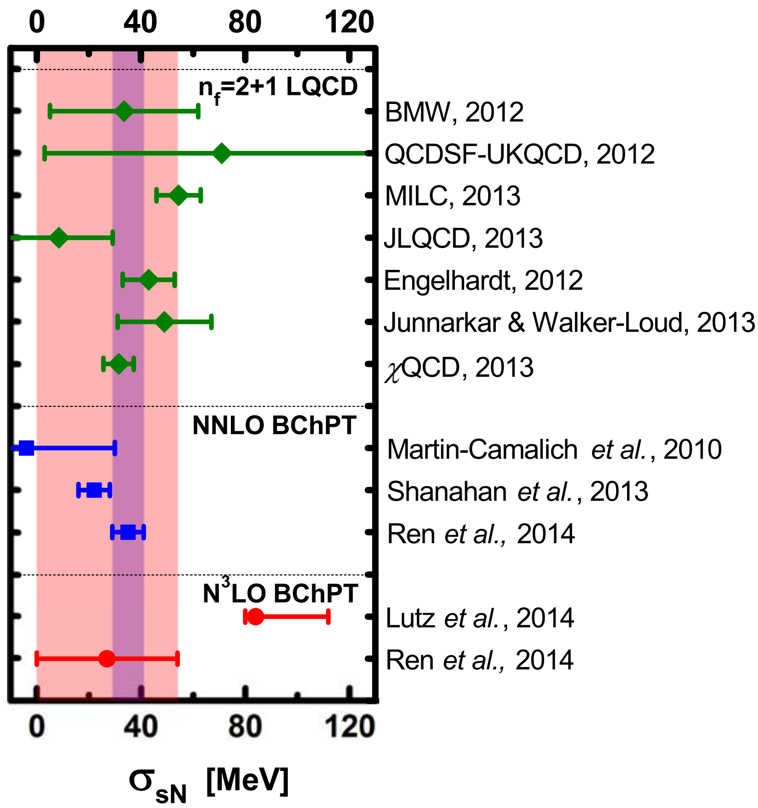

Figure 6.2: Strangeness-nucleon sigma term determined from different studies. The purple and pink bands are our NNLO and N^{3}LO results, respectively. Data points are taken from the following references: BMW [238], QCDSF-UKQCD [239], MILC(2013) [254], JLQCD [235], Engelhardt [234], Junnarkar & Walker-Loud [242], χQCD [236], Martin-Camalich *et al.* [56], Shanahan *et al.* [240], Lutz *et al.* [201].

we have employed the FRR method, which is known to converge relatively faster, to study the same data and found no qualitative difference with the EOMS approach. We noted that if one allows the F_ϕ to deviate from the chiral limit value to take into account SU(3) breaking effects, the so-obtained F_ϕ is close to its SU(3) average $1.17 f_\pi$ with $f_\pi = 92.1$ MeV [161]. The predicted strangeness-nucleon sigma term is shown in Fig. 6.2. It is clear that the NNLO result has a much smaller uncertainty compared to the N^{3}LO one mainly because LECs are over constrained by LQCD simulations. It should be mentioned that in the Feynman-Hellmann method the large m_s multiplying the derivative enhances the uncertainty in the determination of strangeness-baryon sigma term, which seems to dominate the uncertainty and therefore puts an upper limit in the precision one can achieve.

To summarize, we have determined the octet baryon sigma terms using covariant baryon chiral perturbation theory up to next-to-next-to-next-to-leading order. We found $\sigma_{\pi N} = 55(1)(4)$ MeV and $\sigma_{sN} = 27(27)(4)$ MeV. Special attention was paid to uncertainties induced by the lattice scale setting method, which, however, were found to be small, in contrast with previous studies. Other uncertainties, such as those induced by truncating chiral expansions and variations of LECs were also studied in detail. In addition, we have used the strong-interaction isospin-splitting effects from the LQCD simulations to further constrain the relevant LECs. Our results indicate a small scalar strangeness content in nucleon, consistent with the strangeness contribution to proton spin and to the electromagnetic form factors of nucleon.

Chapter 7

Decuplet baryon masses in ChPT

As a natural extension, in this chapter, we present an analysis of lowest-lying decuplet baryon masses in covariant baryon chiral perturbation theory with the extended-on-mass-shell scheme up to next-to-next-to-next-to-leading order. In order to determine the unknown low-energy constants, we perform a simultaneous fit of $n_f = 2+1$ lattice data from the PACS-CS, QCDSF-UKQCD, and HSC collaborations, self-consistently including finite-volume corrections. We also tentatively explore the convergence of the SU(3) BChPT. In addition, the pion- and strangeness-sigma terms of decuplet baryons are predicted using the Feynman-Hellmann theorem.

7.1 Introduction

In the past few years several studies of lowest-lying baryon decuplet masses have been performed on the lattice [22–29]. Just like the baryon octet case, under the limitation of computing resources, decuplet baryon masses from LQCD should be extrapolated to the physical point with the help of chiral perturbation theory. At present, the ground-state octet baryon masses have been studied rather extensively in baryon chiral perturbation theory up to N^{3}LO [56–58, 61–65, 200]. In contrast, there are only a few studies of $n_f = 2 + 1$ LQCD decuplet baryon masses [25, 61, 63, 76, 200], despite many studies limited either to the SU(2) sector or to the quenched LQCD data [47, 49, 56, 60, 76, 106, 255–266]. In Refs. [25, 76], it was shown that HB ChPT at NNLO cannot describe the LHPC and PACS-CS decuplet baryon masses. In Ref. [56], the PACS-CS and LHPC decuplet baryon data were also studied by using EOMS BChPT up to NNLO and a reasonable description of the LQCD data was achieved, contrary to the HBChPT studies of Refs. [25, 76]. In Refs. [61], Semeke and Lutz studied the BMW [22] lattice data for octet and decuplet baryon masses up to N^{3}LO in BChPT with the partial summation scheme. It was shown that the light-quark mass dependence of decuplet baryon masses can be well described. However, FVCs to lattice data are not taken into account self-consistently. Whereas, in our previous studies [57, 64, 65], it has been shown that FVCs need to be taken into account self-consistently in order to achieve a χ^2/d.o.f about 1 in the description of current $n_f = 2 + 1$ LQCD octet baryon masses.

Given the fact that a simultaneous description of $n_f = 2+1$ LQCD decuplet baryon masses with FVCs taken into account self-consistently is still missing and that the EOMS BChPT can describe lattice octet baryon masses rather well [56, 57, 64, 65], it is timely to perform a thorough study of lowest-lying decuplet baryon masses in EOMS BChPT up to N^{3}LO.

7.2 Chiral correction to decuplet baryon masses

In this section, we collect the relevant chiral effective Lagrangians. For convenience of the following discussion, we would like to keep the relevant notations, which are already given in Chapter 4. After that, we calculate the chiral corrections to decuplet baryon masses and the corresponding FVCs in covariant BChPT up to N^{3}LO.

7.2.1 Chiral effective Lagrangians

The chiral effective Lagrangians relevant to the present study can be written as the sum of a mesonic part and a meson-baryon part:

$$\mathcal{L}_{\text{eff}} = \mathcal{L}_{\phi}^{(2)} + \mathcal{L}_{\phi}^{(4)} + \mathcal{L}_{\phi D}^{(1)} + \mathcal{L}_{\phi D}^{(2)} + \mathcal{L}_{\phi D}^{(4)}. \tag{7.1}$$

The Lagrangians $\mathcal{L}_{\phi}^{(2)}$ and $\mathcal{L}_{\phi}^{(4)}$ of the mesonic sector are given in Eq. (3.38) of Chapter 3 and Eq. (4.2) of Chapter 4, respectively. For the decuplet baryon fields in the ChPT, the construction principles can be seen in Chapter 4. The leading-order meson-baryon Lagrangian is

$$\mathcal{L}_{\phi D}^{(1)} = \mathcal{L}_{D} + \mathcal{L}_{\phi BD}^{(1)} + \mathcal{L}_{\phi DD}^{(1)}, \tag{7.2}$$

where $\mathcal{L}_D$ denotes the covariant free Lagrangian, and $\mathcal{L}_{\phi BD}^{(1)}$ and $\mathcal{L}_{\phi DD}^{(1)}$ describe the interaction of the octet- and decuplet-baryons with the pseudoscalar mesons. The expressions of $\mathcal{L}_D$ and $\mathcal{L}_{\phi BD}^{(1)}$ are given in Eq. (4.14) and Eq. (4.17), respectively. And, $\mathcal{L}_{\phi DD}^{(1)}$ has the following form:

$$\mathcal{L}_{\phi DD}^{(1)} = \frac{i\mathcal{H}}{m_D F_\phi} \bar{T}_{\mu}^{abc} \gamma^{\mu\nu\rho\sigma} \gamma_5 \left(\partial_\rho T_{\nu}^{abd}\right) \partial_\sigma \phi_d^c, \tag{7.3}$$

where we have used the so-called "consistent" coupling scheme for the meson-octet-decuplet vertices [205, 206].

The meson-baryon Lagrangian at order $\mathcal{O}(p^2)$ can be written as

$$\mathcal{L}_{\phi D}^{(2)} = \mathcal{L}_{\phi B}^{(2,\ \text{sb})} + \mathcal{L}_{\phi D}^{(2,\ \text{sb})} + \mathcal{L}_{\phi D}^{(2)\,\prime}. \tag{7.4}$$

The first and second terms, $\mathcal{L}_{\phi B}^{(2,\ \text{sb})}$ and $\mathcal{L}_{\phi D}^{(2,\ \text{sb})}$, denote the explicit chiral symmetry breaking part. Their expressions are given in Eq. (4.5) and Eq. (4.16) of Chapter 4, respectively. For the chiral symmetry conserving part, $\mathcal{L}_{\phi D}^{(2)\,\prime}$, one has nine terms, following the conventions of Refs. [61, 267],

$$\begin{aligned}
\mathcal{L}_{\phi D}^{(2)\,\prime} = \frac{1}{F_\phi^2} \Big\{ & t_1 \bar{T}_{\mu}^{abc} g^{\mu\nu} \left(\partial^\sigma \phi \partial_\sigma \phi\right)_c^d T_{\nu}^{abd} + t_2 \bar{T}_{\mu}^{abc} \left[\left(\partial^\mu \phi \partial_\nu \phi\right)_c^d + \left(\partial_\nu \phi \partial^\mu \phi\right)_c^d\right] T^{\nu,abd} \\
& + t_3 \bar{T}_{\mu,abc} \partial_\nu \phi_d^a \varepsilon^{bde} T^{\mu,fgc} \partial^\nu \phi_f^h \varepsilon_{ghe} \\
& + t_4 \bar{T}_{\mu,abc} \left[\partial^\mu \phi_d^a \varepsilon^{bde} \partial_\nu \phi_f^h \varepsilon_{ghe} + \partial_\nu \phi_d^a \varepsilon^{bde} \partial^\mu \phi_f^h \varepsilon_{ghe}\right] T^{\nu,fgc} \\
& + t_5 \bar{T}_{\mu}^{abc} g^{\mu\nu} T_{\nu}^{abc} \langle \partial^\sigma \phi \partial_\sigma \phi \rangle + t_6 \bar{T}_{\mu}^{abc} T^{\nu,abc} \langle \partial^\mu \phi \partial_\nu \phi \rangle \\
& + t_7 \left[\left(\bar{T}_{\alpha}^{abc} \left(\partial_\mu \phi \partial_\nu \phi\right)_c^d i\gamma^\mu \partial^\nu T^{\alpha,abd} + \bar{T}_{\alpha}^{abc} \left(\partial_\nu \phi \partial_\mu \phi\right)_c^d i\gamma^\mu \partial^\nu T^{\alpha,abd}\right) + \text{H.c.}\right] \\
& + t_8 \left[\left(\bar{T}_{\alpha,abc} \partial_\mu \phi_d^a \varepsilon^{bde} i\gamma^\mu \partial^\nu T^{\alpha,fgc} \partial_\nu \phi_f^h \varepsilon_{ghe}\right.\right.
\end{aligned}$$

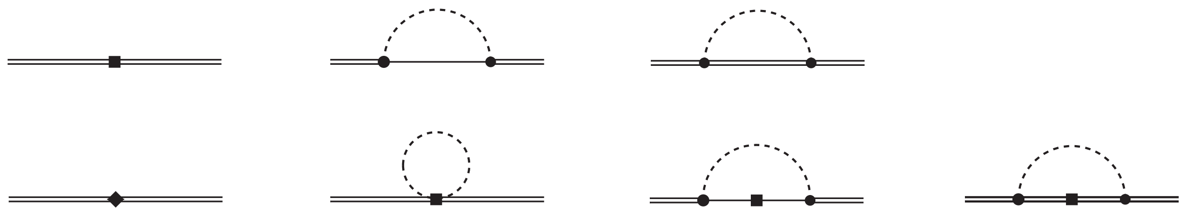

Figure 7.1: Feynman diagrams contributing to the decuplet-baryon masses up to $\mathcal{O}(p^4)$ in EOMS BChPT. The single lines correspond to octet-baryons, double lines to decuplet baryons and dashed lines to mesons. The black boxes (diamond) indicate second (fourth) order couplings. The solid dot indicates an insertion from the dimension one meson-baryon Lagrangians. Wave function renormalization diagrams are not explicitly shown but included in the calculation.

$$
\begin{aligned}
&+\bar{T}_{\alpha,abc}\partial_\nu\phi^a_d\varepsilon^{bde}i\gamma^\mu\partial^\nu T^{\alpha,fgc}\partial_\mu\phi^h_f\varepsilon_{ghe}\Big) + \text{H.c.}\Big] \\
&+t_9\left[\bar{T}^{abc}_\alpha i\gamma^\mu\partial^\nu T^{\alpha,abc}\langle\partial_\mu\phi\partial_\nu\phi\rangle + \text{H.c.}\right]\Big\}, \qquad (7.5)
\end{aligned}
$$

where $t_{1,\ldots,6}$ have dimension mass^{-1} and $t_{7,\ldots,9}$ have dimension mass^{-2}.

The fourth order chiral effective Lagrangians contain five LECs (see also Refs. [61, 263]):

$$
\begin{aligned}
\mathcal{L}^{(4)}_{\phi D} \;=\;& e_1\bar{T}^{abc}_\mu g^{\mu\nu}\left(\chi^2_+\right)^c_d T^{abd}_\nu + e_2\left(\bar{T}^{abc}_\mu\left(\chi_+\right)^d_c\right)g^{\mu\nu}\left(\left(\chi_+\right)^b_e T^{aed}_\nu\right) \\
&+e_3\bar{T}^{abc}_\mu g^{\mu\nu}\left(\chi_+\right)^c_d T^{abd}_\nu\langle\chi_+\rangle + e_4\bar{T}^{abc}_\mu g^{\mu\nu}T^{abc}_\nu\langle\chi_+\rangle^2 \\
&+e_5\bar{T}^{abc}_\mu g^{\mu\nu}T^{abc}_\nu\langle\chi^2_+\rangle, \qquad (7.6)
\end{aligned}
$$

where e_{1-5} are the unknown LECs.

7.2.2 Decuplet baryon self-energies

In this subsection, decuplet baryon masses are calculated in the limit of exact isospin symmetry. Formally, up to $\mathcal{O}(p^4)$ baryon masses can be written as

$$
M_D = m_D + m^{(2)}_D + m^{(3)}_D + m^{(4)}_D, \qquad (7.7)
$$

where $m^{(2)}_D$, $m^{(3)}_D$, and $m^{(4)}_D$ are the LO, NLO, and NNLO SU(3)-breaking corrections to decuplet baryon masses, respectively. The corresponding Feynman diagrams are shown in Fig. 7.1, and the explicit expression of decuplet baryon masses is

$$
\begin{aligned}
M_D \;=\;& m_D + \xi^{(a)}_{D,\pi}M^2_\pi + \xi^{(a)}_{D,K}M^2_K \\
&+\frac{1}{(4\pi F_\phi)^2}\sum_{\phi=\pi,K,\eta}\left[\xi^{(b)}_{D,\phi}H^{(b)}_D(M_\phi) + \xi^{(c)}_{D,\phi}H^{(c)}_D(M_\phi)\right] \\
&+\xi^{(d)}_{D,\pi}M^4_\pi + \xi^{(d)}_{D,K}M^4_K + \xi^{(d)}_{D,\pi K}M^2_\pi M^2_K \\
&+\frac{1}{(4\pi F_\phi)^2}\sum_{\phi=\pi,\ K,\ \eta}\left[\xi^{(e,1)}_{D,\phi}H^{(e,1)}_D(M_\phi) + \xi^{(e,2)}_{D,\phi}H^{(e,2)}_D(M_\phi) + \xi^{(e,3)}_{D,\phi}H^{(e,3)}_D(M_\phi)\right]
\end{aligned}
$$

$$
\begin{aligned}
&-\frac{1}{(4\pi F_\phi)^2}\sum_{\substack{\phi=\pi,\ K,\ \eta\\ B=N,\ \Lambda,\ \Sigma,\ \Xi}}\xi^{(f)}_{DB,\phi}H^{(f)}_{D,B}(M_\phi)\\
&-\frac{1}{(4\pi F_\phi)^2}\sum_{\substack{\phi=\pi,\ K,\ \eta\\ D'=\Delta,\ \Sigma^*,\ \Xi^*,\ \Omega^-}}\xi^{(g)}_{DD',\phi}H^{(g)}_{D,D'}(M_\phi),
\end{aligned}
\tag{7.8}
$$

where $\xi^{(i)}$'s and $H^{(i)}$'s are the corresponding coefficients and loop functions with the subscript i denoting the corresponding diagrams shown in Fig. 7.1. The $\xi^{(i)}$'s are tabulated in Tables 7.1 and 7.2.

Table 7.1: Coefficients of the NLO and NNLO contributions to decuplet baryon masses [Eq. (7.8)].

	Δ	Σ^*	Ξ^*	Ω^-
$\xi^{(a)}_{D,\pi}$	t_0+3t_D	t_0+t_D	t_0-t_D	t_0-3t_D
$\xi^{(a)}_{D,K}$	$2t_0$	$2t_0+2t_D$	$2t_0+4t_D$	$2t_0+6t_D$
$\xi^{(b)}_{D,\pi}$	$\frac{4}{3}\mathcal{C}^2$	$\frac{10}{9}\mathcal{C}^2$	$\frac{2}{3}\mathcal{C}^2$	0
$\xi^{(b)}_{D,K}$	$\frac{4}{3}\mathcal{C}^2$	$\frac{8}{9}\mathcal{C}^2$	$\frac{4}{3}\mathcal{C}^2$	$\frac{8}{3}\mathcal{C}^2$
$\xi^{(b)}_{D,\eta}$	0	$\frac{2}{3}\mathcal{C}^2$	$\frac{2}{3}\mathcal{C}^2$	0
$\xi^{(c)}_{D,\pi}$	$\frac{50}{27}\mathcal{H}^2$	$\frac{80}{81}\mathcal{H}^2$	$\frac{10}{27}\mathcal{H}^2$	0
$\xi^{(c)}_{D,K}$	$\frac{20}{27}\mathcal{H}^2$	$\frac{160}{81}\mathcal{H}^2$	$\frac{20}{9}\mathcal{H}^2$	$\frac{40}{27}\mathcal{H}^2$
$\xi^{(c)}_{D,\eta}$	$\frac{10}{27}\mathcal{H}^2$	0	$\frac{10}{27}\mathcal{H}^2$	$\frac{40}{27}\mathcal{H}^2$

In Eq. (7.8), the loop functions $H^{(b)}_D$, $H^{(c)}_D$, $H^{(e,1)}_D$, $H^{(e,2)}_D$, $H^{(e,3)}_D$, $H^{(f)}_{D,B}$ and $H^{(g)}_{D,D'}$ are obtained by using the $\overline{\text{MS}}$ renormalization scheme to remove the divergent pieces and the EOMS renormalization scheme to remove the PCB terms [71, 72, 199]. The explicit expressions of $H^{(b)}_D$, $H^{(c)}_D$, $H^{(e)}_D$, $H^{(f)}_{D,B}$, $H^{(g)}_{D,D'}$ are given in the following:

$$
\begin{aligned}
H^{(b)}_D(M_\phi) &= \frac{1}{48m_D^3}M_\phi^2\left[M_\phi^2(6m_0^2+4m_0m_D+7m_D^2)\right.\\
&\quad\left.+2(m_0-m_D)(m_0+m_D)^3-2M_\phi^4\right]\\
&+\frac{1}{24m_D^5}M_\phi^4\log\frac{M_\phi}{m_0}\left[-2M_\phi^2(2m_0^2+m_0m_D+2m_D^2)\right.\\
&\quad\left.+6(m_0^4+m_0^3m_D+m_0^2m_D^2+m_0m_D^3+m_D^4)+M_\phi^4\right]\\
&+\frac{1}{24m_D^5}(m_0-m_D)(m_0+m_D)^3\log\left(\frac{m_0M_\phi}{m_0^2-m_D^2}\right)\\
&\quad\times\left[2M_\phi^2(-2m_0^2+m_0m_D-2m_D^2)+(m_0^2-m_D^2)^2\right]\\
&-\frac{1}{24m_D^5\sqrt{\mathcal{W}}}(m_0^2-2m_0m_D+m_D^2-M_\phi^2)^2(m_0^2+2m_0m_D+m_D^2-M_\phi^2)^3\\
&\quad\times\left[\arctan\left(\frac{m_0^2-m_D^2-M_\phi^2}{\sqrt{\mathcal{W}}}\right)-\arctan\left(\frac{m_0^2+m_D^2-M_\phi^2}{\sqrt{\mathcal{W}}}\right)\right],
\end{aligned}
\tag{7.9}
$$

Table 7.2: Coefficients of the N^{3}LO contributions to decuplet baryon masses [Eq. (7.8)], with the following notations: $\tilde{t}_1 = 2t_1+t_2$, $\tilde{t}_2 = 2t_3+t_4$, and $\tilde{t}_3 = 4t_5 + t_6$.

	Δ	Σ^*	Ξ^*	Ω^-
$\xi^{(d)}_{D,\pi}$	$4(e_1+e_2+e_3+e_4+3e_5)$	$\frac{4}{3}(3e_1-e_2+e_3+3e_4+9e_5)$	$\frac{4}{3}(3e_1-e_2-e_3+3e_4+9e_5)$	$4(e_1+e_2-e_3+e_4+3e_5)$
$\xi^{(d)}_{D,K}$	$16(e_4+e_5)$	$\frac{16}{3}(e_1+e_3+3e_4+3e_5)$	$\frac{16}{3}(2e_1+e_2+2e_3+3e_4+3e_5)$	$16(e_1+e_2+e_3+e_4+e_5)$
$\xi^{(d)}_{D,\pi K}$	$8(e_3+2e_4-2e_5)$	$-\frac{16}{3}(e_1-e_2-e_3-3e_4+3e_5)$	$-\frac{8}{3}(4e_1-e_3-6e_4+6e_5)$	$-16(e_1+e_2-e_4+e_5)$
$\xi^{(e,1)}_{D,\pi}$	$\frac{3}{2}(2t_0+3t_D)M_\pi^2$	$3(t_0+t_D)M_\pi^2$	$\frac{3}{2}(2t_0+t_D)M_\pi^2$	$3t_0M_\pi^2$
$\xi^{(e,1)}_{D,K}$	$(4t_0+3t_D)M_K^2$	$4(t_0+t_D)M_K^2$	$(4t_0+5t_D)M_K^2$	$2(2t_0+3t_D)M_K^2$
$\xi^{(e,1)}_{D,\eta}$	$\frac{1}{6}\left[8t_0M_K^2-(2t_0-3t_D)M_\pi^2\right]$	$\frac{1}{3}(t_0+t_D)(4M_K^2-M_\pi^2)$	$\frac{1}{6}\left[8(t_0+2t_D)M_K^2-(2t_0+7t_D)M_\pi^2\right]$	$\frac{1}{3}\left[4(t_0+3t_D)M_K^2-(t_0+6t_D)M_\pi^2\right]$
$\xi^{(e,2)}_{D,\pi}$	$-\frac{1}{2}(3\tilde{t}_1+2\tilde{t}_2+3\tilde{t}_3)$	$-\frac{1}{6}(6\tilde{t}_1+5\tilde{t}_2+9\tilde{t}_3)$	$-\frac{1}{2}(\tilde{t}_1+\tilde{t}_2+3\tilde{t}_3)$	$-\frac{3}{2}\tilde{t}_3$
$\xi^{(e,2)}_{D,K}$	$-(\tilde{t}_1+\tilde{t}_2+2\tilde{t}_3)$	$-\frac{2}{3}(2\tilde{t}_1+\tilde{t}_2+3\tilde{t}_3)$	$-\frac{1}{3}(5\tilde{t}_1+3\tilde{t}_2+6\tilde{t}_3)$	$-2(\tilde{t}_1+\tilde{t}_2+\tilde{t}_3)$
$\xi^{(e,2)}_{D,\eta}$	$-\frac{1}{6}(\tilde{t}_1+3\tilde{t}_3)$	$-\frac{1}{6}(2\tilde{t}_1+3\tilde{t}_2+3\tilde{t}_3)$	$-\frac{1}{2}(\tilde{t}_1+\tilde{t}_2+\tilde{t}_3)$	$-\frac{1}{6}(4\tilde{t}_1+3\tilde{t}_3)$
$\xi^{(e,3)}_{D,\pi}$	$-4(3t_7+2t_8+3t_9)$	$-\frac{4}{3}(6t_7+5t_8+9t_9)$	$-4(t_7+t_8+3t_9)$	$-12t_9$
$\xi^{(e,3)}_{D,K}$	$-8(t_7+t_8+2t_9)$	$-\frac{16}{3}(2t_7+t_8+3t_9)$	$-\frac{8}{3}(5t_7+3t_8+6t_9)$	$-16(t_7+t_8+t_9)$
$\xi^{(e,3)}_{D,\eta}$	$-\frac{4}{3}(t_7+3t_9)$	$-\frac{4}{3}(2t_7+3t_8+3t_9)$	$-4(t_7+t_8+t_9)$	$-\frac{4}{3}(4t_7+3t_9)$
$\xi^{(f)}_{DN,\{\pi,K,\eta\}}$	$\{2\mathcal{C}^2,0,0\}$	$\{0,\frac{2}{3}\mathcal{C}^2,0\}$	$\{0,0,0\}$	$\{0,0,0\}$
$\xi^{(f)}_{D\Lambda,\{\pi,K,\eta\}}$	$\{0,0,0\}$	$\{\mathcal{C}^2,0,0\}$	$\{0,\mathcal{C}^2,0\}$	$\{0,0,0\}$
$\xi^{(f)}_{D\Sigma,\{\pi,K,\eta\}}$	$\{0,2\mathcal{C}^2,0\}$	$\{\frac{2}{3}\mathcal{C}^2,0,\mathcal{C}^2\}$	$\{0,\mathcal{C}^2,0\}$	$\{0,0,0\}$
$\xi^{(f)}_{D\Xi,\{\pi,K,\eta\}}$	$\{0,0,0\}$	$\{0,\frac{2}{3}\mathcal{C}^2,0\}$	$\{\mathcal{C}^2,0,\mathcal{C}^2\}$	$\{0,0,4\mathcal{C}^2\}$
$\xi^{(g)}_{D\Delta,\{\pi,K,\eta\}}$	$\{\frac{5}{3}\mathcal{H}^2,0,\frac{1}{3}\mathcal{H}^2\}$	$\{0,\frac{8}{9}\mathcal{H}^2,0\}$	$\{0,0,0\}$	$\{0,0,0\}$
$\xi^{(g)}_{D\Sigma^*,\{\pi,K,\eta\}}$	$\{0,\frac{2}{3}\mathcal{H}^2,0\}$	$\{\frac{8}{9}\mathcal{H}^2,0,0\}$	$\{0,\frac{4}{3}\mathcal{H}^2,0\}$	$\{0,0,0\}$
$\xi^{(g)}_{D\Xi^*,\{\pi,K,\eta\}}$	$\{0,0,0\}$	$\{0,\frac{8}{9}\mathcal{H}^2,0\}$	$\{\frac{1}{3}\mathcal{H}^2,0,\frac{1}{3}\mathcal{H}^2\}$	$\{0,\frac{4}{3}\mathcal{H}^2,0\}$
$\xi^{(g)}_{D\Omega^-,\{\pi,K,\eta\}}$	$\{0,0,0\}$	$\{0,0,0\}$	$\{0,\frac{2}{3}\mathcal{H}^2,0\}$	$\{0,0,\frac{4}{3}\mathcal{H}^2\}$

$$
\begin{aligned}
H_D^{(c)}(M_\phi) &= \frac{5M_\phi^3}{72m_D^5}(4m_D^2-M_\phi^2)^{5/2} \\
&\quad\times\left[\arctan\left(\frac{M_\phi}{\sqrt{4m_D^2-M_\phi^2}}\right)+\arctan\left(\frac{2m_D^2-M_\phi^2}{M_\phi\sqrt{4m_D^2M_\phi^2-M_\phi^4}}\right)\right] \\
&\quad+\frac{5M_\phi^4}{144m_D^5}\left[17m_D^4-2m_D^2M_\phi^2+2(30m_D^4-10m_D^2M_\phi^2+M_\phi^4)\log\frac{M_\phi}{m_0}\right], \qquad (7.10)
\end{aligned}
$$

$$
\begin{aligned}
H_D^{(e,1)}(M_\phi) &= M_\phi^2\left[1+\ln\left(\frac{\mu^2}{M_\phi^2}\right)\right], && (7.11)\\
H_D^{(e,2)}(M_\phi) &= M_\phi^4\left[1+\ln\left(\frac{\mu^2}{M_\phi^2}\right)\right], && (7.12)\\
H_D^{(e,3)}(M_\phi) &= m_D\left\{\frac{M_\phi^4}{4}\left[1+\ln\left(\frac{\mu^2}{M_\phi^2}\right)\right]+\frac{1}{8}M_\phi^4\right\}, && (7.13)
\end{aligned}
$$

$$
\begin{aligned}
H_{D,B}^{(f)}(M_\phi) &= \frac{1}{144m_D^4}m_D^{(2)}M_\phi^2\left[90m_0^4+96m_0^3m_D+36m_0^2m_D^2+48m_0m_D^3-22m_D^4\right. \\
&\quad\left.-3\left(30m_0^2+16m_0m_D+19m_D^2\right)M_\phi^2+30M_\phi^4\right] \\
&\quad-\frac{1}{12m_D^3}m_B^{(2)}M_\phi^2\left[8m_0^3+8m_0^2m_D+4m_0m_D^2+7m_D^3-(4m_0+m_D)M_\phi^2\right] \\
&\quad+\frac{1}{24m_D^6}m_D^{(2)}M_\phi^2\left[-6(5m_0^4+4m_0^3m_D+3m_0^2m_D^2+2m_0m_D^3+m_D^4)M_\phi^2\right. \\
&\quad\left.+4m_0^5(5m_0+6m_D)+4(5m_0^2+2m_0m_D+3m_D^2)M_\phi^4-5M_\phi^6\right]\log\frac{M_\phi}{m_0} \\
&\quad-\frac{1}{12m_D^5}m_B^{(2)}M_\phi^2\left[3m_0^4(4m_0+5m_D)\right. \\
&\quad\left.-3(4m_0^3+3m_0^2m_D+2m_0m_D^2+m_D^3)M_\phi^2+(4m_0+m_D)M_\phi^4\right]\log\frac{M_\phi}{m_0} \\
&\quad+\frac{1}{24m_D^6}(m_0-m_D)^2(m_0+m_D)^4\left[\log(m_0M_\phi)-\log(m_0^2-m_D^2)-i\pi\right] \\
&\quad\times\left[2m_Dm_B^{(2)}(4m_0-m_D)-m_D^{(2)}(5m_0^2-2m_0m_D+3m_D^2)\right] \\
&\quad+\frac{1}{12}M_\phi^2\left(3m_B^{(2)}+2m_D^{(2)}\right)\log\frac{m_0M_\phi}{\mu^2} \\
&\quad+\frac{1}{24m_D^6\sqrt{\mathcal{W}}}(m_0^2-2m_0m_D+m_D^2-M_\phi^2)(m_0^2+2m_0m_D+m_D^2-M_\phi^2)^2 \\
&\quad\times\left[5m_0^4m_D^{(2)}-2m_0^2\left(5M_\phi^2m_D^{(2)}+m_D^2\left(m_D^{(2)}-m_B^{(2)}\right)\right)\right. \\
&\quad-2m_0^3m_D\left(m_D^{(2)}+4m_B^{(2)}\right)+2m_0m_D(m_D^2+M_\phi^2)\left(m_D^{(2)}+4m_B^{(2)}\right) \\
&\quad\left.-(m_D^2-M_\phi^2)\left(5M_\phi^2m_D^{(2)}+m_D^2\left(3m_D^{(2)}+2m_B^{(2)}\right)\right)\right] \\
&\quad\times\left[\arctan\left(\frac{m_0^2-m_D^2-M_\phi^2}{\sqrt{\mathcal{W}}}\right)-\arctan\left(\frac{m_0^2+m_D^2-M_\phi^2}{\sqrt{\mathcal{W}}}\right)\right], \qquad (7.14)
\end{aligned}
$$

$$
\begin{aligned}
H^{(g)}_{D,D'}(M_\phi) &= \frac{M_\phi^2}{432 m_D^4}\left[4m_D^4\left(132 m_D^{(2)} - 97 m_{D'}^{(2)}\right)\right.\\
&\quad \left. +30 M_\phi^4\left(3m_D^{(2)} + 2m_{D'}^{(2)}\right) - 15 m_D^2 M_\phi^2\left(31 m_D^{(2)} + 14 m_{D'}^{(2)}\right)\right]\\
&\quad +\frac{5M_\phi^2}{72 m_D^6}\log\frac{M_\phi}{m_D}\left[-30 m_D^4 M_\phi^2 m_D^{(2)} + 48 m_D^6\left(m_D^{(2)} - m_{D'}^{(2)}\right)\right.\\
&\quad \left. +10 m_D^2 M_\phi^4\left(2m_D^{(2)} + m_{D'}^{(2)}\right) - M_\phi^6\left(3m_D^{(2)} + 2m_{D'}^{(2)}\right)\right]\\
&\quad +\frac{5M_\phi^2}{36}\left(12 m_D^{(2)} - 7 m_{D'}^{(2)}\right)\log\frac{m_D^2}{\mu^2} - \frac{5}{72 m_D^6} M_\phi^3 (4m_D^2 - M_\phi^2)^{3/2}\\
&\quad \times\left[2m_D^2\left(m_D^{(2)} - m_{D'}^{(2)}\right) - M_\phi^2\left(3m_D^{(2)} + 2m_{D'}^{(2)}\right)\right]\\
&\quad \times\left[\arctan\frac{M_\phi}{\sqrt{4m_D^2 - M_\phi^2}} + \arctan\frac{2m_D^2 - M_\phi^2}{M_\phi\sqrt{4m_D^2 - M_\phi^2}}\right]. \qquad (7.15)
\end{aligned}
$$

In Eqs. (7.10,7.14,7.15), $\mathcal{W} = -m_0^4 - (m_D^2 - M_\phi^2)^2 + 2m_0^2(m_D^2 + M_\phi^2)$, $m_D^{(2)}$ and $m_B^{(2)}$ are the NLO decuplet and octet baryon masses, where $m_D^{(2)}$ is given in Eq. (7.8), and $m_B^{(2)}$ has the following form:

$$
m_B^{(2)} = \sum_{\phi=\pi,\ K} \xi^{(2)}_{B,\phi} M_\phi^2 \qquad (7.16)
$$

with the corresponding coefficients $\xi^{(2)}_{B,\phi}$ listed in Table 7.3.

It should be noted that in the evaluation of diagrams Fig. 7.1(f,g), we have only kept terms linear in $M_D^{(2)}$ and $M_B^{(2)}$, in accordance with our power-counting. At N^{3}LO, the pesudoscalar meson masses, appearing in $m_D^{(2)}$, should be replaced by their $\mathcal{O}(p^4)$ counterparts. The explicit expressions of the meson masses up to $\mathcal{O}(p^4)$ are given in Eqs. (4.37-4.39) of Chapter 4. The empirical values of the LECs L_i^r $(i = 1,\ldots,10)$ are taken from the latest global fit [208]. In order to be consistent with our renormalization scale used for the baryon sector, we have re-evaluated the LECs at $\mu = 1$ GeV. The details can be found in Ref. [64].

7.2.3 Finite-volume corrections

As emphasized in Refs. [57, 64, 65], finite-volume corrections have to be taken into account in studying the current LQCD data. In the case of decuplet baryon masses, they have been studied up to NNLO in EOMS BChPT [56] and in HB ChPT [76]. In the following, we extend the study up to N^{3}LO in EOMS BChPT.

The FVCs can be easily evaluated following the standard technique. One chooses the baryon rest frame, i.e., $p^\mu = (m_D, \vec{0})$, performs a momentum shift and Wick rotation, integrates over

Table 7.3: Coefficients of the NLO contributions to octet baryon masses [Eq. (7.16)].

	N	Λ	Σ	Ξ
$\xi^{(a)}_{B,\pi}$	$-(2b_0+4b_F)$	$\frac{-2}{3}(3b_0-2b_D)$	$-(2b_0+4b_D)$	$-(2b_0-4b_F)$
$\xi^{(a)}_{B,K}$	$-(4b_0+4b_D-4b_F)$	$\frac{-2}{3}(6b_0+8b_D)$	$-4b_0$	$-(4b_0+4b_D+4b_F)$

the temporal dimension, and obtains the results expressed in terms of the master formulas given in Ref. [209]. The details can be seen in Section 4.2 of Chapter 4.

To proceed with the above procedure, one should note that since Lorentz invariance is lost in finite volume, the mass term in the loop functions is identified as the term having the structure of δ_{ij}. This can be easily seen by noticing that in the rest frame the zero component of decuplet baryon field vanishes because of the on-shell condition $p_\mu T^\mu = 0$. For instance, the loop function of diagram Fig. 7.1(b), after Feynman parameterisation, becomes:

$$G_D^{(b)} \propto \int \frac{d^4k}{(2\pi)^4} \frac{(m_D(x-1)-m_B)k^\alpha k^\beta}{\left(k^2-\mathcal{M}_D^{(b)2}\right)^2}, \tag{7.17}$$

where $\mathcal{M}_D^{(b)2} = (x^2-x)m_D^2 + xm_0^2 + (1-x)M_\phi^2 - i\varepsilon$. To evaluate its contribution to the decuplet baryon mass, one simply replaces $k^\alpha k^\beta$ with $\delta_{ij}\vec{k}^2/3$ in the numerator. Following the procedure specified above, one can then easily obtain the FVCs to the loop function of diagram Fig. 7.1(b),

$$\begin{aligned} \delta G_D^{(b)}(M_\phi) &\equiv G_D^{(b)}(L) - G_D^{(b)}(\infty) \\ &= \frac{-1}{12}\int_0^1 dx\,[m_0 - m_D(x-1)]\left[\delta_{1/2}(\mathcal{M}_D^{(b)2}) - \mathcal{M}_D^{(b)2}\delta_{3/2}(\mathcal{M}_D^{(b)2})\right], \end{aligned} \tag{7.18}$$

where the "master" formula $\delta_r(\mathcal{M}^2)$ is defined as

$$\delta_r(\mathcal{M}^2) = \frac{2^{-1/2-r}(\sqrt{\mathcal{M}^2})^{3-2r}}{\pi^{3/2}\Gamma(r)}\sum_{\vec{n}\neq 0}(L\sqrt{\mathcal{M}^2}|\vec{n}|)^{-3/2+r}K_{3/2-r}(L\sqrt{\mathcal{M}^2}|\vec{n}|), \tag{7.19}$$

where $K_n(z)$ is the modified Bessel function of the second kind, and $\sum_{\vec{n}\neq 0} \equiv \sum_{n_x=-\infty}^{\infty}\sum_{n_y=-\infty}^{\infty}\sum_{n_z=-\infty}^{\infty}(1-\delta(|\vec{n}|,0))$ with $\vec{n}=(n_x,n_y,n_z)$.

One also can obtain the FVCs of other loop diagrams in Fig. 7.1. For the NNLO one-loop diagram of Fig. (7.1c), one obtains

$$\delta G_D^{(c)}(M_\phi) = \frac{5}{36}\int_0^1 dx\; m_D(x-2)\left[\delta_{1/2}(\mathcal{M}_D^{(c)2}) - \mathcal{M}_D^{(c)2}\delta_{3/2}(\mathcal{M}_D^{(c)2})\right], \tag{7.20}$$

with $\mathcal{M}_D^{(c)2} = x^2 m_D^2 + (1-x)M_\phi^2 - i\varepsilon$. Taking the limit of $m_D \to \infty$, Eq. (7.18) and Eq. (7.20) reduce to

$$\delta G_D^{(b)}(M_\phi)_{\rm HB} = -\frac{1}{8}\int_0^\infty dx\left[\delta_{1/2}(\beta_\Delta^2) - \beta_\Delta^2\delta_{3/2}(\beta_\Delta^2)\right], \tag{7.21}$$

$$\delta G_D^{(c)}(M_\phi)_{\rm HB} = \frac{1}{2}\int_0^\infty dx\left[\delta_{1/2}(\beta^2) - \beta^2\delta_{3/2}(\beta^2)\right], \tag{7.22}$$

where $\beta_\Delta = x^2 - 2x\delta + M_\phi^2$ and $\beta = x^2 + M_\phi^2$. They agree with the HB ChPT results of Ref. [76].

FVCs to the N^{3}LO one-loop diagrams Fig. 7.1 (e,f,g) have the following form:

$$\delta G_D^{(e,1)}(M_\phi) = \frac{1}{2}\delta_{1/2}(M_\phi^2), \tag{7.23}$$

$$\delta G_D^{(e,2)}(M_\phi) = \frac{1}{2} M_\phi^2 \delta_{1/2}(M_\phi^2), \tag{7.24}$$

$$\delta G_D^{(e,3)}(M_\phi) = \frac{1}{2} m_D \delta_{-1/2}(M_\phi^2), \tag{7.25}$$

$$\begin{aligned}
\delta G_{D,B}^{(f)}(M_\phi) = & \frac{1}{12}\int_0^1 dx \left\{ \left[m_D^{(2)}(x-1) - m_B^{(2)} \right] \cdot \delta_{1/2}({\mathcal{M}_D^{(b)}}^2) \right. \\
& + \left[(1-x) m_D^{(2)} \left(2{\mathcal{M}_D^{(b)}}^2 + M_\phi^2(x-1) \right. \right. \\
& \quad \left. - (m_0+m_D)(m_0+2m_D)x + 2m_D^2 x^2 \right) \\
& \quad \left. + \left({\mathcal{M}_D^{(b)}}^2 + 3m_0 x(m_0 + m_D(1-x)) \right) m_B^{(2)} \right] \cdot \delta_{3/2}({\mathcal{M}_D^{(b)}}^2) \\
& + {\mathcal{M}_D^{(b)}}^2 \left[(x-1) m_D^{(2)} \left({\mathcal{M}_D^{(b)}}^2 + M_\phi^2 (x-1) \right. \right. \\
& \quad \left. -(m_0+m_D)(m_0+2m_D)x + 2m_D^2 x^2 \right) \\
& \quad \left. \left. -3m_0 x(m_0 + m_D(1-x)) m_B^{(2)} \right] \cdot \delta_{5/2}({\mathcal{M}_D^{(b)}}^2) \right\},
\end{aligned} \tag{7.26}$$

$$\begin{aligned}
\delta G_{D,D'}^{(g)}(M_\phi) = & \frac{5}{36}\int_0^1 dx \left\{ \left[(3x-5) m_D^{(2)} + (3-2x) m_{D'}^{(2)} \right] \cdot \delta_{1/2}({\mathcal{M}_D^{(c)}}^2) \right. \\
& + \left[\left({\mathcal{M}_D^{(c)}}^2 (10-6x) + 2m_D^2 x(2x-3) + M_\phi^2(-3x^2+8x-5) \right) m_D^{(2)} \right. \\
& \quad \left. + \left({\mathcal{M}_D^{(c)}}^2 (2x-3) - 3m_D^2(x^2-2x) \right) m_{D'}^{(2)} \right] \cdot \delta_{3/2}({\mathcal{M}_D^{(c)}}^2) \\
& + \left[{\mathcal{M}_D^{(c)}}^2 \left(m_D^2(6x-4x^2) + {\mathcal{M}_D^{(c)}}^2 (3x-5) + M_\phi^2 (x-1)(3x-5) \right) m_D^{(2)} \right. \\
& \quad \left. \left. + 3{\mathcal{M}_D^{(c)}}^2 m_D^2 (x^2-2x) m_{D'}^{(2)} \right] \cdot \delta_{5/2}({\mathcal{M}_D^{(c)}}^2) \right\}.
\end{aligned} \tag{7.27}$$

There is a technical problem in computing $\delta G_{D,B}^{(f)}(M_\phi)$ with the master formula [Eq. (7.19)], because ${\mathcal{M}_D^{(b)}}^2$, appearing in Eq. (7.18) and Eq. (7.26), can become negative for $m_D > m_0 + M_\phi$ in $x \in [0,1]$, i.e., when baryon can decay into the intermediate channel. In order to deal with this problem, we adopt the strategy proposed in Ref. [268] and replace the original $\delta_r(\mathcal{M}^2)$ with three parts by introducing a new scale μ satisfying $\mu < m_0 + M_\phi$, i.e.,

$$\delta_r(\mathcal{M}^2) = g_1^r - g_2^r + g_3^r, \tag{7.28}$$

where the $g_{1,2,3}^r$ are

$$g_1^r = \frac{1}{L^3}\sum_{\vec{k}} \left\{ \frac{1}{\left[\frac{4\pi^2\vec{n}^2}{L^2} + \mathcal{M}^2(m_D^2)\right]^r} - \frac{1}{\left[\frac{4\pi^2\vec{n}^2}{L^2} + \mathcal{M}^2(\mu^2)\right]^r} + \frac{r(x^2-x)(m_D^2-\mu^2)}{\left[\frac{4\pi^2\vec{n}^2}{L^2} + \mathcal{M}^2(\mu^2)\right]^{r+1}} \right\},$$

$$g_2^r = \int_0^{+\infty} \frac{k^2 dk}{2\pi^2} \left\{ \frac{1}{\left[\vec{k}^2 + \mathcal{M}^2(m_D^2)\right]^r} - \frac{1}{\left[\vec{k}^2 + \mathcal{M}^2(\mu^2)\right]^r} + \frac{r(x^2-x)(m_D^2-\mu^2)}{\left[\vec{k}^2 + \mathcal{M}^2(\mu^2)\right]^{r+1}} \right\},$$

$$g_3^r = \delta_r\left(\mathcal{M}^2(\mu^2)\right) - r(x^2-x)(m_D^2-\mu^2)\delta_{r+1}\left(\mathcal{M}^2(\mu^2)\right), \tag{7.29}$$

and

$$\mathcal{M}^2(m_D^2) = (x^2-x)m_D^2 + xm_0^2 + (1-x)M_\phi^2 - i\varepsilon, \tag{7.30}$$
$$\mathcal{M}^2(\mu^2) = (x^2-x)\mu^2 + xm_0^2 + (1-x)M_\phi^2 - i\varepsilon. \tag{7.31}$$

To take into account of FVCs in the study of the LQCD data, one simply replaces the loop functions H of Eq. (7.8) by $\tilde{H} = H + \delta G$ with the δGs calculated above.

7.3 Systematic study of lattice decuplet baryon masses

In this section, we perform a simultaneous fit of the $n_f = 2+1$ LQCD data from the PACS-CS [23], QCDSF-UKQCD [28], and HSC [26] Collaborations and the experimental data [161] to determine the 17 unknown LECs, m_D, t_D, $t_{0\cdots 9}$, and $e_{1\cdots 5}$. Since t_1, t_2, t_3, t_4, t_5, and t_6 appear in combinations, effectively we have only 14 independent LECs. The pion or light-quark mass dependence of the decuplet baryon masses is studied in the NLO, NNLO, and N^{3}LO EOMS BChPT. Using the so-obtained LECs, we also carry out a detailed study on the QCDSF-UKQCD and LHPC data to test the applicability of the N^{3}LO BChPT and the consistency between different LQCD simulations. Furthermore, the pion- and strangeness-baryon sigma terms are predicted by the use of the Feynman-Hellmann theorem.

7.3.1 Lattice data of decuplet baryon masses

Up to now, five collaborations have reported $n_f = 2+1$ simulations of the decuplet baryon masses, i.e., the BMW [22], PACS-CS [23], LHPC [25], HSC [26], and QCDSF-UKQCD [28] collaborations. Because the BMW data are not publicly available and the data of the LHPC Collaboration seem to suffer some systematic errors, as shown in their chiral extrapolation result on the $\Delta(1232)$ mass, which is much higher than its physical value [25], we will concentrate on the data of the PACS-CS, QCDSF-UKQCD, and HSC collaborations. Following the criteria used in our previous studies [65], we only select the LQCD data that satisfy $M_\pi < 0.5$ GeV and $M_\phi L > 3.8$. As a result, there are eight sets of data from the PACS-CS (3 sets), QCDSF-UKQCD (2 sets), and HSC (3 sets) Collaborations. Among the eight LQCD data sets studied, only in the ensemble with $M_\pi = 296$ MeV from the PACS-CS Collaboration, can the decay $\Delta \to N + \pi$ happen. It should be noted that the PACS-CS Collaboration measured the lowest energy levels of the vector meson and decuplet baryon channels, which are different from the true resonance masses. The resulting difference for the ρ meson is estimated to be 5 percent using Lüscher's formula [23]. We will comment on this later.

It should be mentioned that the $\mathcal{O}(a)$-improved Wilson action was used by all the above collaborations except the LHPC Collaboration, which employed a mixed action. The $\mathcal{O}(a)$-improved action has the favorable property that the leading order corrections from the finite lattice spacing are eliminated. The finite lattice spacing corrections of the mixed action of the LHPC Collaboration were also shown to be small [25]. Therefore, in the present work we assume that the discretization artifacts of the present LQCD simulations are small and can be ignored, and will leave a detailed study on finite lattice spacing artifacts to a future study (for a recent study of the discretization effects on the octet baryon masses, see Ref. [67]).

Before we perform a simultaneous fit of LQCD data, we specify our strategy to fix some of the LECs in the N^{3}LO BChPT mass formulas Eq. (7.8). For the meson decay constant, we use $F_\phi = 0.0871$ GeV. The ϕBD coupling is fixed to the SU(3)-average value among the different decuplet-to-octet pionic decay channels, $\mathcal{C} = 0.85$ [119]. The ϕDD coupling $\mathcal{H}$ is barely known, and we fix it using the large N_c relation $H_A = (9/5)g_A$, where g_A and H_A are the nucleon and Δ axial charges. With $g_A = 1.26$, this yields the ϕDD coupling $\mathcal{H} = H_A/2 = 1.13$. In the loop function Eq. (7.27), the LO corrections to virtual octet masses are included, therefore, there are 4 more LECs m_0, b_0, b_D, and b_F related to octet baryon masses up to $\mathcal{O}(p^2)$. Similar to the determination of decuplet baryon masses at $\mathcal{O}(p^2)$ in Chapter 5, their values can be obtained by fitting the physical octet baryon masses with the NLO octet mass formula $M_B = m_0 - m_B^{(2)}$. Because at the same pion masses, the m_0 and b_0 cannot be disentangled, we only obtain $m_0^{\text{eff}} = m_0 - b_0(4M_K^2 + 2M_\pi^2)$, $b_D = 0.06$ GeV^{-1}, and $b_F = -0.231$ GeV^{-1}. The octet-decuplet mass splitting $\delta = 0.231$ GeV is taken as the average physical masses gap. As a result, m_0 and b_0 can be expressed as $m_0 = m_D - 0.231$ GeV and $b_0 = (m_D - 1.423)/1.014$ GeV^{-1}.

In the fitting process, we incorporate the inverse of the correlation matrix $C_{ij} = \sigma_i\sigma_j\delta_{ij} + \Delta a_i \Delta a_j$ for each lattice ensemble to calculate the χ^2, where σ_i are the lattice statistical errors and Δa_i are the fully-correlated errors propagated from the determination of a_i. This is because the data from different collaborations are not correlated with each other, but the data form the same collaboration are partially correlated by the uncertainties propagated from the determination of lattice spacing a.

7.3.2 Chiral extrapolation

In this subsection, we proceed to study the eight sets of lattice data for decuplet baryon masses by using the N^{3}LO BChPT mass formulas [Eq. (7.8)]. In order to constrain better the values of LECs, we include the corresponding experimental data in the fits. The obtained 14 LECs from the best fits are tabulated in Table 7.4. For the sake of comparison, we also perform fits at NLO [1] and NNLO. Up to NNLO, there are only three LECs, i.e., m_D, t_0, and t_D.

It is clear that the NLO fit (without loop contributions) already describe the LQCD simulations very well. The description becomes a bit worse at NNLO. [2] The χ^2/d.o.f. for the N^{3}LO is as low as 0.20. Therefore we confirm that the PACS-CS, QCDSF-UKQCD, and HSC data are consistent with each other, although their setups are different. Furthermore, it seems that lattice decuplet baryon masses are almost linear in M_π^2, as demonstrated by the good fit obtained at NLO, $\chi^2/\text{d.o.f.}^* = 0.44$.

The values of 14 LECs seem very natural, except that the LECS $\tilde{t}_1$, $\tilde{t}_2$, $\tilde{t}_3$, and t_7 might be slightly large. If we had constrained their values to lie between -1 to 1 in the fitting process, we would have obtained a $\chi^2/\text{d.o.f.} = 0.26$, instead of 0.20. It seems that the present LQCD simulations are not precise enough or are too limited to put a stringent constraint on the values of all the LECs appearing up to N^{3}LO, because the NLO fit already yields a χ^2/d.o.f. smaller than 1. This is further confirmed by the relatively large correlation observed between some of the LECs, e.g., between $\tilde{t}_1$ and $\tilde{t}_2$, among t_7, t_8, and t_9, and among e_1, e_3, and e_5. We found

[1] Because at $\mathcal{O}(p^2)$, BChPT does not generate any FVCs, we have adjusted lattice data by subtracting the FVCs calculated by the N^{3}LO EOMS BChPT with virtual octet contributions taken into account.

[2] Without the contributions of the virtual octet baryons, the NNLO description would be much better, with a $\chi^2/\text{d.o.f.} \approx 2$.

Table 7.4: Values of LECs from the best fits to the lattice and experimental data with different fitting strategies at $\mathcal{O}(p^2)$, $\mathcal{O}(p^3)$, and $\mathcal{O}(p^4)$, respectively. The estimator for the fits with and without the experimental decuplet masses, χ^2/d.o.f. and χ^2/d.o.f.*, are given in the last two rows (see text for details).

	NLO	NNLO	N^{3}LO
m_D [MeV]	1135(14)	870(12)	1152(25)
t_0 [GeV^{-1}]	0.167(27)	1.36(2)	0.0710(59)
t_D [GeV^{-1}]	0.322(2)	0.785(3)	0.318(16)
$\tilde{t}_1$ [GeV^{-1}]	–	–	5.90(24)
$\tilde{t}_2$ [GeV^{-1}]	–	–	−2.26(29)
$\tilde{t}_3$ [GeV^{-1}]	–	–	−3.67(45)
t_7 [GeV^{-2}]	–	–	−2.37(8)
t_8 [GeV^{-2}]	–	–	0.298(156)
t_9 [GeV^{-2}]	–	–	1.21(13)
e_1 [GeV^{-3}]	–	–	−0.00386(11689)
e_2 [GeV^{-3}]	–	–	0.194(47)
e_3 [GeV^{-3}]	–	–	−0.167(117)
e_4 [GeV^{-3}]	–	–	0.0767(480)
e_5 [GeV^{-3}]	–	–	−0.0182(734)
χ^2/d.o.f.	4.4	9.5	0.20
χ^2/d.o.f.*	0.44	1.7	0.18

that putting some of them to zero only slightly increases the χ^2/d.o.f.. In short, the values of the N^{3}LO LECs should be viewed in the present context and used with care.

As mentioned earlier, the lightest lattice point with $m_\pi = 296$ MeV of the PACS-CS Collaboration suffers from potentially large systematic errors. If we had performed the fit without this point, we would have obtained a $\chi^2/\text{d.o.f.} = 0.24$, slightly larger than the $\chi^2/\text{d.o.f.} = 0.20$ of Table 7.4. In addition, the values of the corresponding LECs would change moderately. On the other hand, the extrapolations with the LECs determined from the fit excluding physical masses became much worse. This seems to suggest that the inclusion of the lightest PACS-CS point is reasonable, keeping in mind the caveat that they suffer from potentially large systematic errors. This is also the strategy adopted by the PACS-CS collaboration [76] and other similar studies [200].

In Fig. 7.2, we show the Δ, Σ^*, Ξ^*, and Ω^- masses as functions of M_π^2, where the strange quark mass is set to its physical value. It is clear that lattice data are rather linear in M_π^2 . The $\mathcal{O}(p^3)$ BChPT results show strong curvature and cannot describe LQCD data. A good description can only be achieved up to N^{3}LO. [3] In Fig. 7.2, we also show those data of the PACS-CS and HSC collaborations, which are excluded from the fit. The $\mathcal{O}(p^4)$ BChPT can describe reasonably well those data as well.

It should be emphasised that the setups of the QCDSF-UKQCD simulations are rather

[3] In principle, at NNLO, we can use for the meson decay constant its SU(3) average, $F_\phi = 1.17 f_\pi$ with $f_\pi = 92.4$ MeV. This improves a lot the NNLO fit.

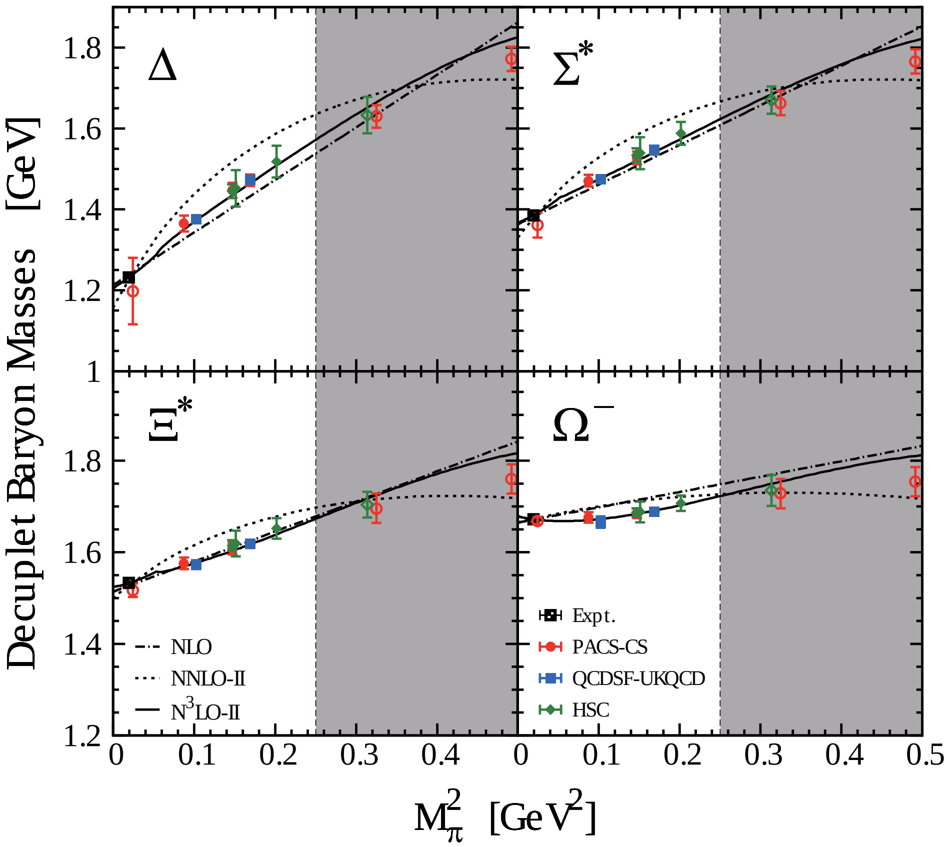

Figure 7.2: (Color online). Pion mass dependences of the lowest-lying decuplet baryon masses. Filled (open) symbols denote the lattice data points included in (excluded from) the fits, which are projected to have the physical strange-quark mass. The dot-dashed, the dashed, and the solid lines are the best NLO, NNLO and N^{3}LO fits to the lattice data, respectively. In obtaining the BChPT results, the strange quark mass has been set to its physical value. The lattice points in the shaded region are not included in the fits.

different from those of the PACS-CS and HSC collaborations. Most LQCD simulations fix the strange quark mass at (or close to) its physical value and gradually moving u/d quark masses to their physical values. The QCDSF-UKQCD Collaboration adopted an alternative method by starting at a point on the SU(3) flavor symmetric line ($m_{u/d} = m_s$) and holding the sum of the quark masses $\bar{m} = (2m_{u/d} + m_s)/3$ constant [27]. In this way, the corresponding kaon and eta masses can be smaller than the pion mass. On the other hand, the FVCs from the kaon and eta loops can become comparable or even larger than that induced by the pion loop, because the $M_\phi L$ can simultaneously become smaller than 4. Therefore, the QCDSF-UKQCD data provide us an opportunity to test BChPT in the world of small strange quark masses and small lattice volumes.

In Fig. 7.3, the QCDSF-UKQCD lattice data are compared with the N^{3}LO BChPT. The lattice points included in the fit are denoted by solid points and those excluded from the fit by hollow points. All lattice points are shifted by FVCs and the kaon mass is fixed using the function $M_K^2 = a + bM_\pi^2$ for the lattice ensemble with a and b determined in Appendix II of Ref. [64]. It is clear that the N^{3}LO BChPT can describe reasonably well the QCDSF-UKQCD

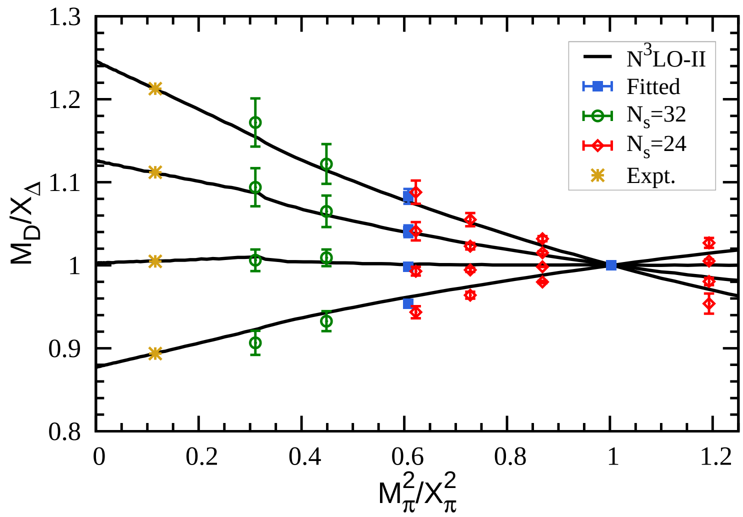

Figure 7.3: The QCDSF-UKQCD lattice data [27] in comparison with the N^{3}LO BChPT. The lattice data denoted by the blue filled squares are included in the fit; those by the green opened circles (with $N_s = 32$) and the red diamonds (with $N_s = 24$) are not. FVCs of the lattice results have been subtracted. The two flavour singlet quantities, X_π and X_Δ, are defined as: $X_\pi = \sqrt{(M_\pi^2 + 2M_K^2)/3}$, $X_\Delta = (2m_\Delta + m_{\Omega^-})/3$, respectively [27].

data obtained in both large ($N_s = 32$) and small ($N_s = 24$) volumes with both heavy and light pion masses. However, it should be pointed out that the ratio method eliminates to a large extent the FVCs. In other words, to plot/study the data this way one can neglect FVCs, as noticed in Ref. [28].

We would like to point out that in the above fits we have not included the LHPC data, while in Refs. [64, 65] we have studied their data for octet baryon masses. The reason is that the LHPC decuplet baryon data do not seem to be consistent with those of the PACS-CS, QCDSF-UKQCD, and HSC collaborations. This is clearly demonstrated in Fig. 7.4, where the LHPC data are contrasted with the N^{3}LO BChPT with the LECs of N^{3}LO-II tabulated in Table I, and the corresponding kaon mass is fixed using $M_K^2 = a + bM_\pi^2$ with a and b determined in Ref. [64]. It is clear that the dependence of lattice data on M_π^2 seems to be flatter than suggested by N^{3}LO BChPT. In Ref. [25], it was noticed that it is difficult to extrapolate lattice data to the physical $\Delta(1232)$ mass. Our study seems to confirm their finding. If we had included the LHPC data [4](three sets of them satisfying our selection criteria), we would have obtained a $\chi^2/\text{d.o.f.} = 2.4$.

Finite-volume corrections play an important role in describing LQCD data as pointed out in the present context in Refs. [57, 64]. In Table 7.5, we show the finite-volume corrections calculated in N^{3}LO BChPT with the LECs determined above. Not surprisingly, the finite-volume corrections to the QCDSF-UKQCD data are the largest, which can be easily understood from the arguments given above.

Furthermore, in order to quantify the effects of loop contributions involving virtual octet

[4]It needs to be mentioned that in Ref. [246], a different way of setting the lattice scale has been used to obtain the decuplet baryon masses of the LHPC Collaboration [25] in physical units.

Table 7.5: Finite-volume corrections (in units of MeV) to LQCD decuplet baryon masses in covariant BChPT up to N^{3}LO.

	M_π	δm_Δ	δm_{Σ^*}	δm_{Ξ^*}	δm_{Ω^-}	$M_\pi L$	$M_K L$	$M_\eta L$
PACS-CS	296	14	5	0	-3	4.3	8.7	9.8
	384	5	2	1	1	5.7	8.6	9.3
	411	4	2	0	1	6.0	9.3	10.2
QCDSF-UKQCD	320	20	13	8	4	4.1	5.8	6.2
	411	50	50	50	50	3.95	3.95	3.95
HSC	383	4	2	1	0	5.7	8.1	8.8
	389	42	27	14	3	3.9	5.4	5.9
	449	28	19	11	4	4.5	5.8	6.2

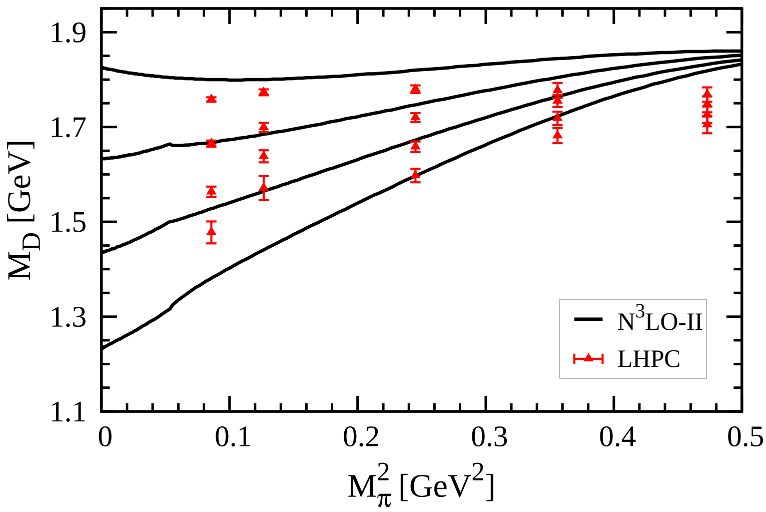

Figure 7.4: Comparison between the N^{3}LO BChPT and the LHPC data [25].

and decuplet baryons, one can allow $\mathcal{C}$ and $\mathcal{H}$ to vary in the fitting. The corresponding best fit-χ^2/d.o.f. is 0.27 with $\mathcal{C} = 0.75$ and $\mathcal{H} = 1.0$. It is clear that the values are consistent with the phenomenological values we used above, which can be seen as evidence for the existence of non-analytical chiral contributions following the argument given in Ref. [246]. One should note that because of the small difference between the χ^2/d.o.f. obtained here and the χ^2/d.o.f. obtained by putting $\mathcal{C}$ and $\mathcal{H}$ to zero, this evidence is rather weak in the present case.

7.3.3 Convergence of SU(3) EOMS BChPT

Convergence of BChPT in the u, d, and s three-flavor sector has been under debate for many years. See, e.g., Refs.[73, 74, 199, 269] and references cited therein.[5] One prominent example is

[5]For related discussions in the mesonic sector, see, e.g., Refs. [270, 271], where the so-called resummed chiral perturbation theory has been shown to exhibit better convergence than conventional chiral perturbation theory. To our knowledge, no similar studies exist in the one-baryon sector.

the magnetic moments of octet baryons. In Ref. [196], it has been shown that compared to HB ChPT and IR BChPT, EOMS BChPT converges relatively faster. The same has been found for octet baryon masses [56]. Nevertheless, even in EOMS BChPT, convergence is relatively slow because of the large expansion parameter, $M_K/\Lambda_{\mathrm{ChPT}}$. Naively, each higher order contribution is only suppressed by about one half at the physical point, which can even be further reduced for LQCD simulations with larger light-quark masses.

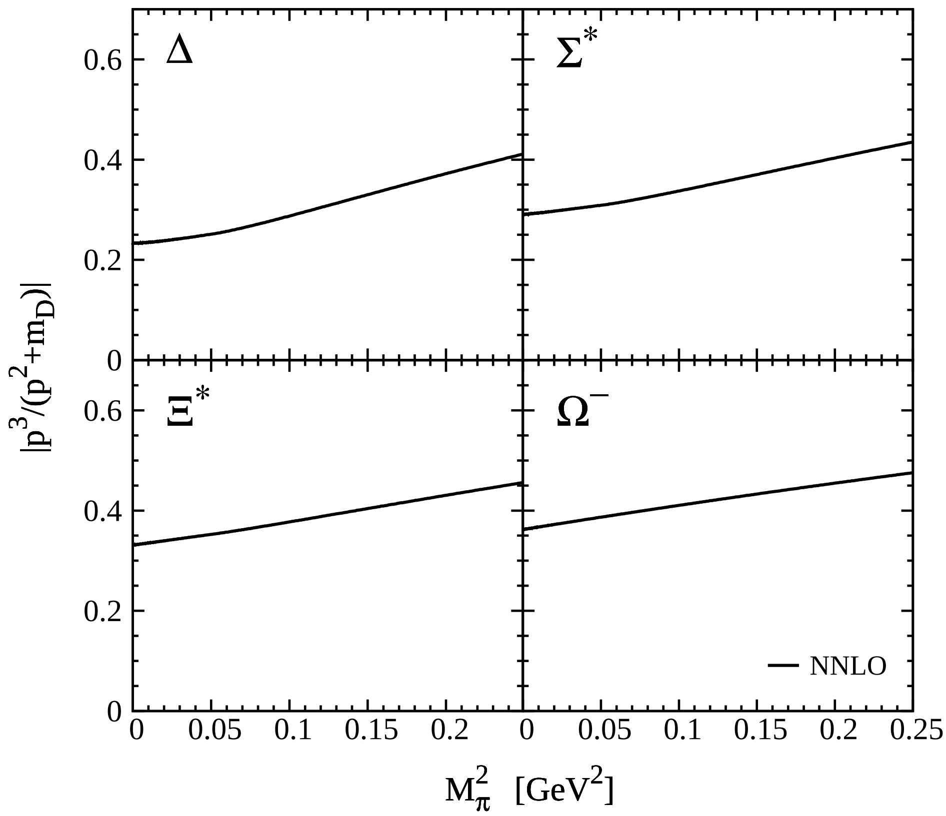

Figure 7.5: Ratio of one-loop and tree contributions to the decuplet baryon masses, $\left|p^3/(p^2+m_D)\right|$, as a function of pion mass. The strange quark mass is set at its physical value.

In the following, we would like to examine the contributions of different chiral orders. In Table 7.4 and Fig. 7.2, one notices that the NLO BChPT can already describe LQCD data very well, but experimental data are missed a little bit. If the chiral expansions work, one

Table 7.6: Contributions of different chiral order to the decuplet baryon masses at the physical point (in units of GeV).

		Δ			Σ^*			Ξ^*			Ω^-		
	m_D	p^2	p^3	p^4	p^2	p^3	p^4	p^2	p^3	p^4	p^2	p^3	p^4
NLO	1.135	0.104	–	–	0.248	–	–	0.392	–	–	0.537	–	–
NNLO	0.870	0.737	−0.383	–	1.089	−0.582	–	1.441	−0.785	–	1.793	−0.991	–
N^{3}LO	1.152	0.046	−0.429	0.463	0.158	−0.652	0.728	0.270	−0.878	0.988	0.382	−1.106	1.244

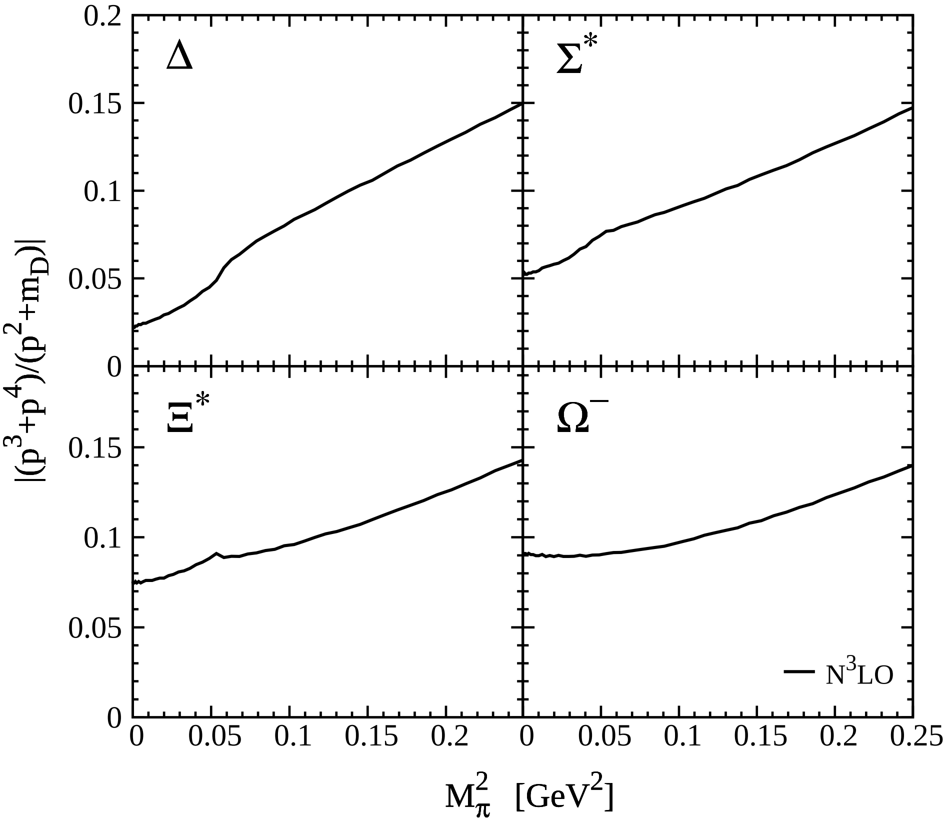

Figure 7.6: Ratio of one-loop and tree contributions to the decuplet baryon masses, $\left|(p^3+p^4)/(p^2+m_D)\right|$, as a function of pion mass. The strange quark mass is set at its physical value.

should expect a smaller χ^2/d.o.f. at NNLO and N^{3}LO. This is indeed the case. Since the NLO results already describe LQCD data very well, it is not surprising that up to NNLO and N^{3}LO, there should be some reshuffling of contributions of different order. This can be clearly seen from Table 7.6, where contributions of different chiral order to decuplet baryon masses at the physical point are tabulated. Once loop diagrams are included, a naive comparison of p^0 (m_D), p^2, p^3, and p^4 contributions turns out to be a disaster. At NNLO, the p^2 contributions can be a factor of 2 larger than m_D, while at N^{3}LO, the p^3 and p^4 contributions are opposite and become comparable to or even larger than the p^2 contributions, particularly for the decuplet baryons containing strangeness.

On the other hand, up to one-loop level, it might be more proper to judge convergence by comparing tree and loop contributions. In Figs. 7.5 and 7.6 $\left|p^3/(p^2+m_D)\right|$ and $\left|(p^3+p^4)/(p^2+m_D)\right|$ are shown as a function of M_π^2. At NNLO, the p^3 contributions can reach about 50% of the tree contributions, while at N^{3}LO the loop contributions become about 10% $\sim$ 20% of the tree contributions. These results suggest that the chiral expansions are convergent as expected.

Table 7.7: Pion- and strangeness-sigma terms of the decuplet baryons at the physical point. The first error is statistical and the second is systematic, estimated by taking half the difference between the N^{3}LO result and the NNLO result.

	$\mathcal{O}(p^3)$			$\mathcal{O}(p^4)$		
	w/o octet	w/ octet	Ref. [56]	w/o octet	w/ octet	Ref. [200]
$\sigma_{\pi\Delta}$	50(1)	64(1)	55(4)(18)	42(1)(4)	28(1)(8)	34(3)
$\sigma_{\pi\Sigma^*}$	32(1)	44(1)	39(3)(13)	24(1)(4)	22(2)(9)	28(2)
$\sigma_{\pi\Xi^*}$	17(1)	26(1)	22(3)(7)	8(2)(5)	11(2)(6)	18(4)
$\sigma_{\pi\Omega^-}$	6(1)	8(1)	5(2)(1)	−5(2)(6)	5(2)(2)	10(4)
$\sigma_{s\Delta}$	70(13)	93(12)	56(24)(1)	99(24)(15)	88(22)(3)	41(41)
$\sigma_{s\Sigma^*}$	198(13)	181(13)	160(28)(7)	233(23)(18)	243(24)(31)	211(44)
$\sigma_{s\Xi^*}$	298(13)	258(14)	274(32)(9)	375(24)(39)	391(24)(67)	373(53)
$\sigma_{s\Omega^-}$	370(14)	326(15)	360(34)(26)	507(25)(69)	528(26)(101)	510(50)

7.4 Pion- and strangeness-decuplet baryon sigma terms

The baryon sigma terms are important quantities in understanding the chiral condensate and the composition of the baryons. At present, there are no direct LQCD simulation of these quantities for decuplet baryons (In Ref. [272], the very preliminary studies of the decuplet baryon sigma terms was reported.). On the other hand, one can calculate the decuplet baryon sigma terms $\sigma_{\pi D}$ and σ_{sD} using BChPT, once the relevant LECs are fixed, via the Feynman-Hellmann theorem. See, e.g., Refs. [64] for relevant formulas.

Using the LECs given in Table 7.4, we calculate the sigma terms of the baryon decuplet at the physical point, and the results are listed in Table 7.7. For comparison, we also tabulate the results of Refs. [56, 200]. The difference between our $\mathcal{O}(p^3)$ predictions with those of Ref. [56] reflects the influence of the LQCD data and the fitting strategy. However, our N^{3}LO results are consistent with those of Ref. [200] within uncertainties.

Chapter 8

Roper mass and width in ChPT

With the development of computer techniques, the baryon masses of excited states are becoming available in lattice QCD, especially for the Roper. In this chapter, the nucleon, Delta, and Roper masses and widths are calculated in chiral perturbation theory up to next-to-next-to-leading order. The effects of the mixing between the nucleon and the Roper are taken into account for the first time. We also tentatively perform an analysis of the lattice Roper masses to explore the quark mass dependence. Here, we want to mention that this work is still in progress, and the obtained results should be thought as preliminary.

8.1 Introduction

The light-quark spectrum provides a great opportunity to study QCD in its nonperturbative regime. In particular, the first even-parity excited state of the nucleon, the $J^P = (1/2)^+$ Roper resonance $N(1440)$ or $P_{11}(1440)$, has been a puzzle since its discovery [162]. In the constituent quark model, the Roper, as an S-wave excitation, tends to be above the first odd-parity excited state $N(1530)$ or $S_{11}(1530)$, a P-wave excitation, a problem that is ameliorated if Goldstone-boson exchange is introduced. Several exotic interpretations have been proposed, such as a hybrid baryon [273, 274], a pentaquark state [275], and a breathing mode of the ground state [276]. This puzzle has made the Roper a focus of the N^* program at JLab, and in Bonn, Mainz, and Japan [277–279].

The recent outburst of interest in lattice QCD has not resolved this puzzle. The low-lying hadron spectrum is now well understood within controllable lattice artifacts [128], but lattice simulations of excited states have not yet reached the same level of maturity. Several LQCD collaborations have published results for the Roper mass at various values of the pion mass m_π [150, 163, 164, 166, 167, 280]. Except for the χQCD collaboration [167] which finds relatively small masses with a chiral behavior similar to that of nucleons, most of the results are in broad agreement. For $m_\pi \leq 500$ MeV, the proton is light enough for the Roper to be unstable, yet, it is treated as a stable particle. Taken at face value, however, these results imply that there is a strong decrease in the Roper mass as m_π approaches the physical point. This, in turn, suggests that the Roper could be considerably closer to the nucleon in the chiral limit than in the real world.

There are other clues that indicate an important role for the Roper with respect to chiral symmetry. The importance of the Delta isobar $\Delta(1232)$ in low-energy phenomena stems from the relatively small Delta-nucleon mass difference $\delta_{\Delta N} = m_\Delta - m_N \simeq 290$ MeV, at least compared to most mesons. The Roper-nucleon mass difference $\delta_{RN} = m_R - m_N \simeq 490$ MeV is less than twice as large, and the ratio of Roper-to-Delta widths is roughly of the order of $(\delta_{RN}/\delta_{\Delta N})^3$, as one might expect from widths that come primarily from a one-pion-loop self-energy [281]. Moreover, the nucleon, Delta and Roper nearly saturate the Adler-Weisberger sum rule, which can be understood if they act as chiral partners in a reducible representation of the chiral symmetry group $SU(2)_L \times SU(2)_R$ [282].

Much work has been carried out in ChPT including explicitly pions, nucleons and Deltas — for a comprehensive review, see for example Ref. [45]. In contrast, the next nucleon excited state, the Roper, has received considerably less attention. The Roper-nucleon splitting is still somewhat smaller than Λ_χ at the physical pion mass, and could decrease towards the chiral limit. Therefore, it can be included as an explicit degree of freedom in ChPT. Various quantities and processes have been studied from this point of view, including: Roper octet contributions to decuplet masses and magnetic moments [261]; virtual Roper contributions to $\pi N \to \pi\pi N$ threshold amplitudes [283] and to elastic πN scattering [281, 284]; chiral corrections to the Roper self-energy [285, 286]; and Roper magnetic moment [287]. The Roper has also been included indirectly via resonance saturation of LECs in the calculations of baryon self-energies [50] and of nonleptonic hyperon decays [288], and explicitly in the chiral unitarity approach to study meson-baryon dynamics [289].

Perhaps the most noticeable effect of the Roper in ChPT is, not surprisingly, in the reaction that led to its discovery [162], elastic πN scattering. In ChPT, whether without [290–295] or with [194, 284, 296–298] an explicit Delta, the empirical near-threshold behavior of the P_{11} phase shift is reproduced in lowest orders, with a monotonically decreasing function of energy. Yet the empirical phase shift turns up and crosses zero in the Delta region, which can only be achieved if a nominally higher-order effect provides an opposite contribution to cancels those of lowest orders. This lack of convergence is not a problem when the Delta region is considered beyond the range of EFT, but needs to be addressed as we extend this range [298]. Once the Roper is included explicitly as a low-energy degree of freedom, Roper pole diagrams, suppressed only by the relatively small energy difference $\delta_{\Delta N} - \delta_{RN}$, appear already at the lowest non-trivial order and naturally produce the observed phase-shift behavior [281].

The goal of the present work is to initiate a systematic study of nucleon, Delta and Roper properties within ChPT. As LQCD continues to pick up momentum, we can anticipate increasingly precise data for a variety of baryon properties at pion masses from Λ_χ down to the physical value, and perhaps below. Over such a broad range, the simplest approach is to treat the baryon mass differences in the same footing as the pion mass, and consider momenta $Q \sim m_\pi \sim \delta_{\Delta N} \sim \delta_{RN}$. We express observables as expansions in Q/Λ_χ. In this way, we generalize the simpler countings of ChPT without [69] and with [116] Deltas, where $\delta_{\Delta N}$ and/or δ_{RN} are considered high scales and the effects of Deltas and/or Ropers are relegated to LECs.

As a first step, we reconsider the Roper self-energy [285, 286] to next-to-next-to-leading order including explicitly the pion-mass dependence of the mixing between nucleon and Roper. We also calculate the virtual Roper effects on the nucleon and Delta self-energies to the same order. Thus, we obtain the full one-loop corrections to the nucleon mass, and Delta and Roper masses and widths. Many LQCD studies exist already of nucleon and Delta masses, indicating a relatively good convergence of ChPT, see for example Ref. [299]. We hope our results will prove useful in similar analysis of upcoming data.

8.2 Chiral effective Lagrangians in SU(2) sector

In this section, we present the effective Lagrangian relevant for the chiral corrections to the nucleon, Delta, and Roper self-energies up to NNLO. Further background and references can be found in Ref. [45].

The nonrelativistic nature of nucleons in the regime of validity of the EFT means that we can integrate out antinucleons and limit ourselves to interactions with at most one baryon. We can split the effective Lagrangian as

$$\mathcal{L} = \mathcal{L}_{\pi} + \mathcal{L}_{\pi N} + \mathcal{L}_{\pi N\Delta} + \mathcal{L}_{\pi NR} + \mathcal{L}_{\pi\Delta R}, \tag{8.1}$$

which describe, respectively, interactions among pions, between pions and nucleons, of Deltas with pions and nucleons, of Ropers with pions and nucleons, and of Ropers with pions and Deltas. We do not consider electromagnetic effects nor isospin violation stemming from the quark mass difference, but extension is straightforward.

The effective Lagrangian can be ordered,

$$\mathcal{L} = \sum_{n_{\mathrm{ChPT}}} \mathcal{L}^{(n_{\mathrm{ChPT}})}, \tag{8.2}$$

according to the (integer) chiral index [32, 300]

$$n_{\mathrm{ChPT}} = d + f/2 - 2 \geq 0, \tag{8.3}$$

where d and f are, respectively, the number of derivatives and low-energy scales, and the number of fermion fields entering each interaction. In the mesonic and one-baryon sectors [1] the chiral index tracks the number of powers of Λ_χ^{-1} expected from the naive dimensional analysis (NDA) [168] that underlies the EFT expansion. It exhibits the lowest order where the corresponding interaction appears. The lower bound in Eq. (8.3) stems from the pattern of chiral-symmetry breaking in QCD, and guarantees that there is a leading order from which the expansion can be constructed.

In the next subsections we describe each term in Eq. (8.1), making specific choices of fields. At a given order, results can only depend on these choices up to higher-order terms, that is, results for different choices must fall within the theoretical error bars. The choice of fields is guided by the symmetries we want to implement, namely chiral symmetry and Lorentz invariance in the nonrelativistic regime.

Each interaction with symmetry transformation properties (*i.e.*, invariant or transforming like the quark mass terms in the QCD Lagrangian) introduces a LEC. The LECs can be determined by fitting LQCD data at different values of m_π, and particular combinations can be obtained from experimental data at the physical point. We assume that throughout the low-mass region we have two small expansion parameters $\delta_{N\Delta}/\Lambda_\chi$ and δ_{NR}/Λ_χ in addition to m_π/Λ_χ. Thus all LECs, which are defined in the chiral limit ($m_\pi = 0$), can be written as series in these parameters. The coefficients of these series cannot be determined from experiment or LQCD, except perhaps if QCD is deformed with the introduction of further independent parameters such as the number of colors. For simplicity we leave these series implicit.

[1] Note that Lagrangians in these sectors are frequently labeled not by n_{ChPT} but by d, for example $\mathcal{L}_\pi^{(n_{\mathrm{ChPT}}+2)}$ and $\mathcal{L}_{\pi N}^{(n_{\mathrm{ChPT}}+1)}$.

Pion Lagrangian

We use an exponential realization of the pion fields ($\pi^0,\ \pi^\pm$),

$$u = \exp\left[i\frac{\Phi}{2f_\pi}\right], \qquad \Phi = \tau_a\pi^a = \begin{pmatrix} \pi^0 & \sqrt{2}\pi^+ \\ \sqrt{2}\pi^- & -\pi^0 \end{pmatrix}, \tag{8.4}$$

where τ_a is the isospin Pauli matrix and $f_\pi = 92.1$ MeV [279] is the pion decay constant in the chiral limit.

The chiral lagrangian is built from covariant combinations of pion fields such as the pion vector and axial currents

$$\Gamma_\mu = \frac{1}{2}\left(u^\dagger\partial_\mu u + u\partial_\mu u^\dagger\right) = \frac{1}{2}\tau_a\langle\tau^a\Gamma_\mu\rangle, \quad u_\mu = i\left(u^\dagger\partial_\mu u - u\partial_\mu u^\dagger\right) = \frac{1}{2}\tau_a\langle\tau^a u_\mu\rangle, \tag{8.5}$$

and

$$\chi_\pm = u^\dagger\chi u^\dagger \pm u\chi^\dagger u, \tag{8.6}$$

where $\langle\cdots\rangle$ denotes the trace in flavor space, and $\chi = 2B_0\mathcal{M}$, $\mathcal{M} = \mathrm{diag}(m_u, m_d)$, represents the explicit breaking of chiral symmetry by the up- and down quark masses m_u and m_d. Here $B_0 = -\langle\bar{q}q\rangle/f_\pi^2$ is related to the quark condensate $\langle\bar{q}q\rangle_0$ in the chiral limit.

From the pion Lagrangian, we need only the $n_{\mathrm{ChPT}} = 0$ part, which can be written as

$$\mathcal{L}_\pi^{(0)} = \frac{f_\pi^2}{4}\left[\langle u_\mu u^\mu\rangle + \langle\chi_+\rangle\right]. \tag{8.7}$$

The first term includes the pion kinetic energy while the second gives rise to the pion mass,

$$m_\pi^2 = \frac{1}{4}\langle(\chi + \chi^\dagger)\rangle. \tag{8.8}$$

In the following only the pion propagator obtained from Eq. (8.7) appears.

Nucleon Chiral Lagrangian

Since the nucleon mass in the chiral limit M_{N0} is of the order of the breakdown scale of the EFT, we use a heavy nucleon field

$$N = \begin{pmatrix} p \\ n \end{pmatrix} \tag{8.9}$$

which does not have a trivial evolution factor $\exp(-iM_{N0}v\cdot x)$, where v_μ is the nucleon velocity ($v_\mu = (1,\vec{0})$ in the rest frame). This amounts to measuring nucleon energies with respect to the nucleon rest energy in the chiral limit, M_{N0}. With this choice of field, all spin physics enters through the covariant spin-operator $S_\mu = i\gamma_5\sigma_{\mu\nu}v^\nu/2$, with the basic properties

$$S\cdot v = 0, \quad \{S_\mu, S_\nu\} = \frac{1}{2}(v_\mu v_\nu - g_{\mu\nu}), \quad [S_\mu, S_\nu] = i\varepsilon_{\mu\nu\alpha\beta}v^\alpha S^\beta, \tag{8.10}$$

in the convention $\varepsilon_{0123} = 1$. Lorentz invariance at a given order is ensured by $1/M_{N0}$ corrections introduced via reparametrization invariance [189]. Interactions with pions are written with the chiral covariant derivative

$$D_\mu N = \partial_\mu N + \Gamma_\mu N. \tag{8.11}$$

The pion-nucleon effective Lagrangian with lowest chiral index can be written as

$$\mathcal{L}^{(0)}_{\pi N} = \bar{N}(iv \cdot D + g_A S \cdot u)N, \tag{8.12}$$

where $g_A = \mathcal{O}(1)$ is the axial vector coupling at the chiral limit. This Lagragian gives rise to a static nucleon propagator and the usual derivative pion-nucleon coupling. At the next order we have recoil corrections, the sigma term, and new interactions,

$$\begin{aligned}\mathcal{L}^{(1)}_{\pi N} &= \frac{1}{M_{N0}}\bar{N}\left[(v \cdot D)^2 - D^2 - ig_A\{S \cdot D, v \cdot u\}\right]N \\ &+c_{N1}\langle\chi_+\rangle\bar{N}N - c_{N2}\langle(v \cdot u)^2\rangle\bar{N}N + \frac{c_{N3}}{2}\langle u \cdot u\rangle\bar{N}N + \cdots,\end{aligned} \tag{8.13}$$

with $c_{N1},\ c_{N2},\ c_{N3}$ unknown LECs expected to be of $\mathcal{O}(1/\Lambda_\chi)$. The term with LEC c_{N1} gives an m_π^2 correction to the nucleon mass, while the $c_{N1},\ c_{N2},\ c_{N3}$ terms provide seagull vertices. For our purposes we also require the m_π^4 correction to the mass contained in the third-order Lagrangian [2],

$$\begin{aligned}\mathcal{L}^{(3)}_{\pi N} &= e_{38}\langle\chi_+\rangle^2\bar{N}N + e_{115}\langle\chi\chi^\dagger\rangle\bar{N}N + e_{116}(\det\chi + \det\chi^\dagger)\bar{N}N + \cdots \\ &= e_{N1}m_\pi^4\bar{N}N + \cdots,\end{aligned} \tag{8.15}$$

where $e_{N1} = (16e_{38} + 2e_{115} + 2e_{116})$ is a combination of the three LECs e_{38}, e_{115}, and e_{116} of Ref. [301]. We expect $e_{N1} = \mathcal{O}(1/\Lambda_\chi^3)$.

Delta Chiral Lagrangian

The Delta is a spin-3/2, isospin-3/2 resonance and, therefore, it is described by a field

$$\Delta_\mu = \begin{pmatrix}\Delta_\mu^{++} \\ \Delta_\mu^{+} \\ \Delta_\mu^{0} \\ \Delta_\mu^{-}\end{pmatrix} \tag{8.16}$$

where each charge state has four spin components. In order to construct isospin conserving interactions we need the isospin 3/2 analogs of the Pauli matrices,

$$\mathcal{T}^1 = \frac{2}{3}\begin{pmatrix} 0 & \sqrt{3}/2 & 0 & 0 \\ \sqrt{3}/2 & 0 & 1 & 0 \\ 0 & 1 & 0 & \sqrt{3}/2 \\ 0 & 0 & \sqrt{3}/2 & 0 \end{pmatrix}, \tag{8.17}$$

$$\mathcal{T}^2 = \frac{2i}{3}\begin{pmatrix} 0 & -\sqrt{3}/2 & 0 & 0 \\ \sqrt{3}/2 & 0 & -1 & 0 \\ 0 & 1 & 0 & -\sqrt{3}/2 \\ 0 & 0 & \sqrt{3}/2 & 0 \end{pmatrix}, \quad \mathcal{T}^3 = \begin{pmatrix} 1 & 0 & 0 & 0 \\ 0 & 1/3 & 0 & 0 \\ 0 & 0 & -1/3 & 0 \\ 0 & 0 & 0 & -1 \end{pmatrix} \tag{8.18}$$

[2]Sometimes further terms, such as

$$\mathcal{L}^{(2)}_{\pi N} = \bar{N}(B_{32}\delta^3_{\Delta N} + B_{23}\delta_{\Delta N}\langle\chi_+\rangle)N, \tag{8.14}$$

are written explicitly [256]. Here they are absorbed in the LECs M_{N0} and c_{N1} in the ciral limit.

with $\mathcal{T}^a\mathcal{T}^a = \frac{5}{3}$, as well as the isospin 1/2-to-3/2 transition matrices,

$$t^1 = \frac{1}{\sqrt{6}}\begin{pmatrix} -\sqrt{3} & 0 & 1 & 0 \\ 0 & -1 & 0 & \sqrt{3} \end{pmatrix},\ t^2 = \frac{-i}{\sqrt{6}}\begin{pmatrix} \sqrt{3} & 0 & 1 & 0 \\ 0 & 1 & 0 & \sqrt{3} \end{pmatrix},\ t^3 = \sqrt{\frac{2}{3}}\begin{pmatrix} 0 & 0 & 1 & 0 \\ 0 & 0 & 1 & 0 \end{pmatrix}, \tag{8.19}$$

with $t^a t^{b\dagger} = \delta^{ab} - \frac{1}{3}\tau^a\tau^b$.

Since Delta excitation requires only $\delta_{\Delta N}$ in energy, we choose the phase of the field so that the same factor $M_{N0} v\cdot x$ is absent. As a consequence, Delta energies are also measured with respect to the nucleon's. The Delta is then also a static field, but with a residual mass.

The chiral Lagrangian for the Delta and its transition to the nucleon has a parallel form to the Lagrangian of the previous subsection. The chiral covariant derivative on Delta field is written as

$$D_\nu\Delta_\mu = \partial_\nu\Delta_\mu + \mathcal{T}_a\langle\tau^a\Gamma_\nu\rangle\Delta_\mu. \tag{8.20}$$

At lowest index,

$$\mathcal{L}^{(0)}_{\pi N\Delta} = -\bar{\Delta}_\mu(iv\cdot D - \delta_{N\Delta})\Delta^\mu - H_A\bar{\Delta}_\mu S^\nu\mathcal{T}_a\langle\tau^a u_\nu\rangle\Delta^\mu - \frac{1}{4}h_A\left(\bar{\Delta}^\mu t_a\langle\tau^a u_\mu\rangle N + \text{H.c.}\right). \tag{8.21}$$

The first term provides the Delta propagator

$$S^{\mu\nu}(k) = -\frac{i}{v\cdot k - \delta_{N\Delta} + i\varepsilon}\left[v^\mu v^\nu - g^{\mu\nu} - \frac{4}{3}S^\mu S^\nu\right], \tag{8.22}$$

where $\delta_{N\Delta} = M_{\Delta 0} - M_{N0}$ is the mass splitting between Delta and nucleon in the chiral limit. The LECs $H_A, h_A = \mathcal{O}(1)$ are axial vector couplings of the Delta and of the Delta-nucleon transition, respectively. At next order we again need recoil corrections and seagull vertices,

$$\begin{aligned}\mathcal{L}^{(1)}_{\pi N\Delta} \;=\; & -\frac{1}{M_{N0}}\bar{\Delta}_\mu\left[(v\cdot D)^2 - D^2\right]\Delta^\mu \\ & +\frac{iH_A}{M_{N0}}\bar{\Delta}_\mu\{S\cdot D, v^\nu\mathcal{T}_a\langle\tau^a u_\nu\rangle\}\Delta^\mu + \frac{h_A}{4M_{N0}}\left(i\bar{\Delta}^\mu\overleftarrow{D}_\mu v^\nu t_a\langle\tau^a u_\nu\rangle N + \text{H.c.}\right) \\ & -\bar{\Delta}_\mu\left[c_{\Delta 1}\langle\chi_+\rangle - c_{\Delta 2}\langle(v\cdot u)^2\rangle + \frac{c_{\Delta 3}}{2}\langle u^2\rangle\right]\Delta^\mu + \cdots,\end{aligned} \tag{8.23}$$

where $c_{\Delta 1}, c_{\Delta_2}, c_{\Delta 3} = \mathcal{O}(1/\Lambda_\chi)$ are LECs [3]. As in the nucleon sector, of higher orders we need only the m_π^4 correction to the baryon mass,

$$\mathcal{L}^{(3)}_{\pi N\Delta} = -e_{\Delta 1}m_\pi^4\bar{\Delta}_\mu\Delta^\mu + \cdots, \tag{8.25}$$

with $e_{\Delta 1} = \mathcal{O}(1/\Lambda_\chi^3)$ yet another LEC.

[3] Note that in covariant ChPT there are two more terms [302] in $\mathcal{L}^{(1)}_{\pi N\Delta}$ which are relevant in the study of baryon masses up to NNLO [207, 256],

$$\mathcal{L}^{(1)}_{\pi N\Delta} = -ib_3\bar{N}T^a\omega^{a,\mu\nu}\gamma_\mu\Delta_\nu - \frac{b_6}{M_\Delta}\bar{N}T^a(\partial_\mu\Delta_\nu)\omega^{a,\mu\nu} + \text{H.c.}, \tag{8.24}$$

with $\omega^a_{\mu\nu} = \frac{1}{2}\langle\tau^a[D_\mu, u_\nu]\rangle$. However these terms are redundant in the heavy baryon expansion [303, 304].

Roper Chiral Lagrangian

The Roper has the same spin/isospin numbers as the nucleon, just a higher mass. The machinery we employ to build the interactions of its field

$$R = \begin{pmatrix} R^+ \\ R^0 \end{pmatrix} \tag{8.26}$$

is the same as for the nucleon. The only differences are that *i)* it has a residual mass in the chiral limit, and *ii)* it can mix with the nucleon with a mixing angle that depends on the quark masses.

We define the nucleon and Roper fields such that they are mass eigenstates in the chiral limit. Then we can simply add to the LO nucleon Lagrangian Eq. (8.12) the lowest-order Roper terms

$$\mathcal{L}^{(0)}_{\pi NR} = \bar{R}(iv \cdot D - \delta_{RN} + g_R S \cdot u)R + g_{NR}\left(\bar{N} S \cdot u R + \text{h.c.}\right), \tag{8.27}$$

where $\delta_{RN} = M_{R0} - M_{N0}$ denotes the mass splitting between nucleon and Roper in the chiral limit, $g_R = \mathcal{O}(1)$ is the axial-vector coupling of the Roper, and $g_{NR} = \mathcal{O}(1)$ the axial-vector transition coupling between Roper and nucleon. Terms at next order have a form familiar from Eq. (8.13),

$$\begin{aligned} \mathcal{L}^{(1)}_{\pi NR} &= \frac{1}{M_{N0}}\bar{R}\left[(v\cdot D)^2 - D^2 - ig_R\{S\cdot D, v\cdot u\}\right]R \\ &\quad + c_{R1}\langle\chi_+\rangle\bar{R}R - c_{R2}\langle(v\cdot u)^2\rangle\bar{R}R + \frac{c_{R3}}{2}\langle u\cdot u\rangle\bar{R}R \qquad (8.28)\\ &\quad + c_{NR}\left(\langle\chi_+\rangle\bar{N}R + \text{h.c.}\right) - \frac{ig_{NR}}{M_{N0}}\bar{R}\{S\cdot D, v\cdot u\}N + \text{h.c.} + \cdots, \qquad (8.29)\end{aligned}$$

where $c_{R1}, c_{R_2}, c_{R3} = \mathcal{O}(1/\Lambda_\chi)$ are LECs to be fixed. Noteworthy is the Roper-nucleon mixing linear in the quark masses with LEC $c_{NR} = \mathcal{O}(1/\Lambda_\chi)$, which we kep here explicit in contrast to what is done in Ref. [285]. When one is interested in Roper effects at a fixed pion mass, for example at its physical value (*e.g.* Refs. [281, 283, 284]), we can perform a new rotation to re-diagonalize the fields at that mass and eliminate c_{NR}. Here we keep track of its effects as the pion mass is varied. As before, the only higher-order term we need is

$$\mathcal{L}^{(3)}_{\pi NR} = e_{R1} m_\pi^4 \bar{R}R + \ldots. \tag{8.30}$$

with $e_{R1} = \mathcal{O}(1/\Lambda_\chi^3)$ another LEC.

In addition we need the Roper-Delta transitions at the two lowest orders,

$$\mathcal{L}^{(0)}_{\pi\Delta R} = -\frac{1}{4}g_{\Delta R}\left(\bar{\Delta}^\mu t_a\langle\tau^a u_\mu\rangle R + \text{H.c.}\right) \tag{8.31}$$

and

$$\mathcal{L}^{(1)}_{\pi\Delta R} = \frac{ig_{\Delta R}}{4M_{N0}}\left(\bar{\Delta}^\mu \overleftarrow{D}_\mu v^\nu t_a\langle\tau^a u_\nu\rangle R + \text{H.c.}\right), \tag{8.32}$$

where $g_{\Delta R} = \mathcal{O}(1)$ is the axial-vector transition coupling.

8.3 Baryon mass and width matrices

8.3.1 Perturbatively calculation of the baryon self-energies

Firstly, let us consider the two-point function of the baryon field $B(x)$

$$S_0(x) = -i\langle 0|T[B(x)\bar{B}(0)]|0\rangle = \frac{1}{p^0 - \delta - \Sigma(p^0)}, \tag{8.33}$$

where the momentum matrix p^0, the mass splitting matrix δ and the self-energy matrix $\Sigma(p^0)$, respectively, can be written as

$$p^0 = \begin{pmatrix} p^0_{NN} & 0 & p^0_{NR} \\ 0 & p^0_{\Delta\Delta} & 0 \\ p^0_{RN} & 0 & p^0_{RR} \end{pmatrix}, \quad \delta = \begin{pmatrix} 0 & 0 & 0 \\ 0 & \delta_{N\Delta} & 0 \\ 0 & 0 & \delta_{NR} \end{pmatrix}, \tag{8.34}$$

$$\Sigma(p^0) = \begin{pmatrix} \Sigma_{NN}(p^0_{NN}) & 0 & \Sigma_{NR}(p^0_{NR}) \\ 0 & \Sigma_{\Delta\Delta}(p^0_{\Delta\Delta}) & 0 \\ \Sigma_{RN}(p^0_{RN}) & 0 & \Sigma_{RR}(p^0_{RR}) \end{pmatrix}, \tag{8.35}$$

where the elements of self-energy matrix, $\Sigma_{BB'}(p^0_{BB'})$ with $B, B' = N,\ \Delta,\ R$, can be expanded up to fourth order

$$\Sigma_{BB'}(p^0_{BB'}) = \Sigma^{(2)}_{BB'} + \Sigma^{(3)}_{BB'}(p^0_{BB'}) + \Sigma^{(4)}_{BB'}(p^0_{BB'}) + \cdots . \tag{8.36}$$

The baryon masses are defined as $M_B = M_{N0} + \mathrm{Re}[p^0]$ at the pole with $p^0 = \delta + \Sigma(p^0)$. And the corresponding widths are defined as $\Gamma_B = -2\mathrm{Im}[\Sigma(p^0)]$. In order to obtain the baryon masses and widths, one has to calculate the matrix equation perturbatively in terms of the expansion of p^0,

$$p^0 = p^{0(1)} + p^{0(2)} + p^{0(3)} + p^{0(4)} + \cdots, \tag{8.37}$$

with

$$p^{0(1)} = \delta = \begin{pmatrix} 0 & 0 & 0 \\ 0 & \delta_{N\Delta} & 0 \\ 0 & 0 & \delta_{NR} \end{pmatrix}, \quad p^{0(2)} = \begin{pmatrix} \Sigma^{(2)}_{NN} & 0 & \Sigma^{(2)}_{NR} \\ 0 & \Sigma^{(2)}_{\Delta\Delta} & 0 \\ \Sigma^{(2)}_{RN} & 0 & \Sigma^{(2)}_{RR} \end{pmatrix}, \tag{8.38}$$

$$p^{0(3)} = \begin{pmatrix} \Sigma^{(3)}_{NN}(0) & 0 & \Sigma^{(3)}_{NR}(0) \\ 0 & \Sigma^{(3)}_{\Delta\Delta}(\delta_{N\Delta}) & 0 \\ \Sigma^{(3)}_{RN}(0) & 0 & \Sigma^{(3)}_{RR}(\delta_{NR}) \end{pmatrix}, \tag{8.39}$$

and

$$\begin{aligned} p^{0(4)} \quad = & \begin{pmatrix} \Sigma^{(2)}_{NN}\, {\Sigma^{(3)}_{NN}}'(0) & 0 & \Sigma^{(2)}_{NR}\, {\Sigma^{(3)}_{NR}}'(0) \\ 0 & \Sigma^{(2)}_{\Delta\Delta}\, {\Sigma^{(3)}_{\Delta\Delta}}'(\delta_{N\Delta}) & 0 \\ \Sigma^{(2)}_{RN}\, {\Sigma^{(3)}_{RN}}'(0) & 0 & \Sigma^{(2)}_{RR}\, {\Sigma^{(3)}_{RR}}'(\delta_{NR}) \end{pmatrix} \\ & + \begin{pmatrix} \Sigma^{(4)}_{NN}(0) & 0 & \Sigma^{(4)}_{NR}(0) \\ 0 & \Sigma^{(4)}_{\Delta\Delta}(\delta_{N\Delta}) & 0 \\ \Sigma^{(4)}_{RN}(0) & 0 & \Sigma^{(4)}_{RR}(\delta_{NR}) \end{pmatrix} \end{aligned}$$

$$\equiv \left(\begin{array}{ccc} \tilde{\Sigma}^{(4)}_{NN}(0) & 0 & \tilde{\Sigma}^{(4)}_{NR}(0) \\ 0 & \tilde{\Sigma}^{(4)}_{\Delta\Delta}(\delta_{N\Delta}) & 0 \\ \tilde{\Sigma}^{(4)}_{RN}(0) & 0 & \tilde{\Sigma}^{(4)}_{RR}(\delta_{NR}) \end{array} \right). \tag{8.40}$$

Here we would like to mention that the mixed terms Σ_{NR} and Σ_{RN} are the same.

The baryon mass matrix, $M_B = M_{N0} + \mathrm{Re}[p^0]$, can be expressed as

$$M_B = \left(\begin{array}{ccc} M_{NN} & 0 & M_{NR} \\ 0 & M_{\Delta\Delta} & 0 \\ M_{RN} & 0 & M_{RR} \end{array} \right), \tag{8.41}$$

with the diagonal terms M_{NN}, $M_{\Delta\Delta}$, and M_{RR}

$$\begin{aligned} M_{NN} &= M_{N0} + M^{(2)}_{NN} + M^{(3)}_{NN} + M^{(4)}_{NN} + \cdots, \\ M_{\Delta\Delta} &= M_{N0} + \delta_{N\Delta} + M^{(2)}_{\Delta\Delta} + M^{(3)}_{\Delta\Delta} + M^{(4)}_{\Delta\Delta} + \cdots, \\ M_{RR} &= M_{N0} + \delta_{NR} + M^{(2)}_{RR} + M^{(3)}_{RR} + M^{(4)}_{RR} + \cdots, \end{aligned} \tag{8.42}$$

and the mixed terms M_{NR} and M_{RN}

$$\begin{aligned} M_{NR} &= M^{(2)}_{NR} + M^{(3)}_{NR} + M^{(4)}_{NR} + \cdots, \\ M_{RN} &= M^{(2)}_{RN} + M^{(3)}_{RN} + M^{(4)}_{RN} + \cdots, \end{aligned} \tag{8.43}$$

where $M^{(i)}_{BB'}$ are the real parts of baryon self-energies:

$$M^{(2)}_{BB'} = \Sigma^{(2)}_{BB'}, \quad M^{(3)}_{BB'} = \mathrm{Re}\left[\Sigma^{(3)}_{BB'}({p^0_{BB'}}^{(1)})\right], \quad M^{(4)}_{BB'} = \mathrm{Re}\left[\tilde{\Sigma}^{(4)}_{BB'}({p^0_{BB'}}^{(1)})\right]. \tag{8.44}$$

Similarly, we also can define the matrix of baryon widths

$$\Gamma_B = \left(\begin{array}{ccc} \Gamma_{NN} & 0 & \Gamma_{NR} \\ 0 & \Gamma_{\Delta\Delta} & 0 \\ \Gamma_{RN} & 0 & \Gamma_{RR} \end{array} \right), \tag{8.45}$$

with the diagonal terms Γ_{NN}, $\Gamma_{\Delta\Delta}$, and Γ_{RR}

$$\begin{aligned} \Gamma_{NN} &= \Gamma^{(3)}_{NN} + \Gamma^{(4)}_{NN} + \cdots = -2\mathrm{Im}[\Sigma^{(3)}_{NN}(0)] - 2\mathrm{Im}[\tilde{\Sigma}^{(4)}_{NN}(0)] + \cdots, \\ \Gamma_{\Delta\Delta} &= \Gamma^{(3)}_{\Delta\Delta} + \Gamma^{(4)}_{\Delta\Delta} + \cdots = -2\mathrm{Im}[\Sigma^{(3)}_{\Delta\Delta}(\delta_{N\Delta})] - 2\mathrm{Im}[\tilde{\Sigma}^{(4)}_{\Delta\Delta}(\delta_{N\Delta})] + \cdots, \\ \Gamma_{RR} &= \Gamma^{(3)}_{RR} + \Gamma^{(4)}_{RR} + \cdots = -2\mathrm{Im}[\Sigma^{(3)}_{RR}(\delta_{NR})] - 2\mathrm{Im}[\tilde{\Sigma}^{(4)}_{RR}(\delta_{NR})] + \cdots, \end{aligned} \tag{8.46}$$

and the mixed terms Γ_{NR} and Γ_{RN}

$$\begin{aligned} \Gamma_{NR} &= \Gamma^{(3)}_{NR} + \Gamma^{(4)}_{NR} + \cdots = -2\mathrm{Im}[\Sigma^{(3)}_{NR}(0)] - 2\mathrm{Im}[\tilde{\Sigma}^{(4)}_{NR}(0)] + \cdots, \\ \Gamma_{RN} &= \Gamma^{(3)}_{RN} + \Gamma^{(4)}_{RN} + \cdots = -2\mathrm{Im}[\Sigma^{(3)}_{RN}(0)] - 2\mathrm{Im}[\tilde{\Sigma}^{(4)}_{RN}(0)] + \cdots. \end{aligned} \tag{8.47}$$

Because the nucleon is the lightest baryon state, the imaginary part of self-energies $\Sigma_{NN}(0)$ and $\Sigma_{NR}(0) = \Sigma_{RN}(0)$ should be zero, therefore,

$$\Gamma_{NN} = \Gamma_{NR} = \Gamma_{RN} \equiv 0. \tag{8.48}$$

8.3.2 Diagonalization of the baryon mass and width matrices

In order to obtain the masses and widths of nucleon, Delta, and Roper, one should diagonalize the above two matrices [Eq. (8.41) and Eq. (8.45)] simultaneously. We encode the baryon mass and width matrices into a single matrix

$$\begin{aligned} M_B - i\frac{\Gamma_B}{2} &\equiv \begin{pmatrix} M_{NN} - i\frac{\Gamma_{NN}}{2} & 0 & M_{NR} - i\frac{\Gamma_{NR}}{2} \\ 0 & M_{\Delta\Delta} - i\frac{\Gamma_{\Delta\Delta}}{2} & 0 \\ M_{RN} - i\frac{\Gamma_{RN}}{2} & 0 & M_{RR} - i\frac{\Gamma_{RR}}{2} \end{pmatrix} \\ &= \begin{pmatrix} M_{NN} & 0 & M_{NR} \\ 0 & M_{\Delta\Delta} - i\frac{\Gamma_{\Delta\Delta}}{2} & 0 \\ M_{RN} & 0 & M_{RR} - i\frac{\Gamma_{RR}}{2} \end{pmatrix}. \end{aligned} \tag{8.49}$$

After diagnolizing the baryon mass and width matrices, we obtain the three eigenvalues represent the nucleon, Delta and Roper masses and widths,

$$M_N - i\frac{\Gamma_N}{2} = \frac{1}{2}\left[M_{NN} + M_{RR} - \sqrt{\mathcal{W}} - i\frac{\Gamma_{RR}}{2}\right], \tag{8.50}$$

$$M_\Delta - i\frac{\Gamma_\Delta}{2} = M_{\Delta\Delta} - i\frac{\Gamma_{\Delta\Delta}}{2}, \tag{8.51}$$

$$M_R - i\frac{\Gamma_R}{2} = \frac{1}{2}\left[M_{NN} + M_{RR} + \sqrt{\mathcal{W}} - i\frac{\Gamma_{RR}}{2}\right], \tag{8.52}$$

with

$$\mathcal{W} = (M_{NN} - M_{RR})^2 + 4M_{NR}M_{RN} + i(M_{NN} - M_{RR})\Gamma_{RR} - \frac{\Gamma_{RR}^2}{4}. \tag{8.53}$$

The corresponding three eigenvectors after normalization are

$$V_N = \begin{pmatrix} -\frac{|M_{RN}|}{M_{RN}}\frac{\sqrt{\mathcal{W}} - M_{NN} + M_{RR} - i\frac{\Gamma_{RR}}{2}}{\sqrt{4M_{RN}^2 + (\sqrt{\mathcal{W}} - M_{NN} + M_{RR} - i\frac{\Gamma_{RR}}{2})^2}} \\ 0 \\ \frac{2|M_{RN}|}{\sqrt{4M_{RN}^2 + (\sqrt{\mathcal{W}} - M_{NN} + M_{RR} - i\frac{\Gamma_{RR}}{2})^2}} \end{pmatrix}, \quad V_\Delta = \begin{pmatrix} 0 \\ 1 \\ 0 \end{pmatrix}, \tag{8.54}$$

$$V_R = \begin{pmatrix} \frac{|M_{RN}|}{M_{RN}}\frac{\sqrt{\mathcal{W}} + M_{NN} - M_{RR} + i\frac{\Gamma_{RR}}{2}}{\sqrt{4M_{RN}^2 + (\sqrt{\mathcal{W}} + M_{NN} - M_{RR} + i\frac{\Gamma_{RR}}{2})^2}} \\ 0 \\ \frac{2|M_{RN}|}{\sqrt{4M_{RN}^2 + (\sqrt{\mathcal{W}} + M_{NN} - M_{RR} + i\frac{\Gamma_{RR}}{2})^2}} \end{pmatrix}. \tag{8.55}$$

Expanding $\sqrt{\mathcal{W}}$ up to NNLO,

$$\begin{aligned} \sqrt{\mathcal{W}} \approx\ & M_{RR} - M_{NN} - \frac{2}{\delta_{NR}}\left(M_{NR}^{(2)}M_{RN}^{(2)} - M_{NR}^{(2)}M_{RN}^{(3)} - M_{RN}^{(2)}M_{NR}^{(3)}\right) \\ & + \frac{2}{\delta_{NR}^2}\left(M_{NR}^{(2)}M_{RN}^{(2)}(M_{RR}^{(2)} - M_{NN}^{(2)})\right) - i\frac{\Gamma_{RR}}{2}, \end{aligned} \tag{8.56}$$

the expressions of baryon masses and widths are

$$\begin{aligned} M_N - i\frac{\Gamma_N}{2} \approx\ & M_{N0} + M_{NN}^{(2)} + M_{NN}^{(3)} + M_{NN}^{(4)} \\ & + \frac{1}{\delta_{NR}}\left(M_{NR}^{(2)}M_{RN}^{(2)} - M_{NR}^{(2)}M_{RN}^{(3)} - M_{RN}^{(2)}M_{NR}^{(3)}\right) \end{aligned}$$

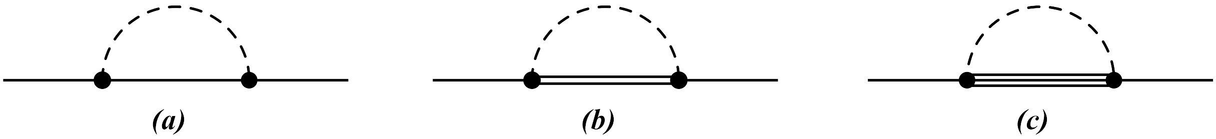

Figure 8.1: One loop self-energy diagrams contributing to $M_{NN}^{(3)}$. The dashed, solid, double-solid, and triple-solid lines correspond to the pion, nucleon, Δ, and Roper, respectively. Black dots indicate an insertion from the dimension one chiral Lagrangians.

$$+\frac{1}{\delta_{NR}^2}\left(M_{NR}^{(2)}M_{RN}^{(2)}(M_{NN}^{(2)}-M_{RR}^{(2)})\right), \tag{8.57}$$

$$M_\Delta - i\frac{\Gamma_\Delta}{2} \approx M_{N0}+\delta_{N\Delta}+M_{\Delta\Delta}^{(2)}+M_{\Delta\Delta}^{(3)}+M_{\Delta\Delta}^{(4)}-i\frac{\Gamma_{\Delta\Delta}^{(3)}+\Gamma_{\Delta\Delta}^{(4)}}{2}, \tag{8.58}$$

$$\begin{aligned} M_R - i\frac{\Gamma_R}{2} \approx\ & M_{N0}+\delta_{NR}+M_{RR}^{(2)}+M_{RR}^{(3)}+M_{RR}^{(4)} \\ & -\frac{1}{\delta_{NR}}\left(M_{NR}^{(2)}M_{RN}^{(2)}-M_{NR}^{(2)}M_{RN}^{(3)}-M_{RN}^{(2)}M_{NR}^{(3)}\right) \\ & -\frac{1}{\delta_{NR}^2}\left(M_{NR}^{(2)}M_{RN}^{(2)}(M_{NN}^{(2)}-M_{RR}^{(2)})\right)-i\frac{\Gamma_{RR}^{(3)}+\Gamma_{RR}^{(4)}}{2}. \end{aligned} \tag{8.59}$$

Therefore, in order to obtain the explicit expressions of baryon masses and widths, one needs the diagonal terms of baryon self-energies up to NNLO and the mixed terms between nucleon and Roper up to NLO.

8.4 Baryon self-energies up to NNLO

Diagonal terms of the nucleon self-energy

The leading order contribution to the nucleon self-energy is

$$\Sigma_{NN}^{(2)} = -4c_{N1}m_\pi^2. \tag{8.60}$$

At $\mathcal{O}(\varepsilon^3)$, the contributing loop diagrams are collected in Fig. 8.1. After calculating the diagrams using the HBChPT, we can obtain the chiral corrections to the nucleon self-energy

$$\Sigma_{NN}^{(3)}(0) = -\frac{3g_A^2}{32\pi f_\pi^2}m_\pi^3-\frac{h_A^2}{12\pi^2 f_\pi^2}\delta_{N\Delta}^3\mathcal{F}\left(\frac{m_\pi}{\delta_{N\Delta}}\right)-\frac{3g_{NR}^2}{(4\pi f_\pi)^2}\delta_{NR}^3\mathcal{F}\left(\frac{m_\pi}{\delta_{NR}}\right), \tag{8.61}$$

where the loop function $\mathcal{F}(x)$ is defined as

$$\mathcal{F}(x) = \frac{1}{4}x^2 + \frac{1}{2}(1-\frac{3}{2}x^2)\log\frac{x^2}{4} + \begin{cases} (1-x^2)^{3/2}\log\left(\frac{1}{x}+\sqrt{\frac{1}{x^2}-1}\right), & 0\le x<1, \\ (x^2-1)^{3/2}\arccos\frac{1}{x}, & |x|\ge 1, \\ -(1-x^2)^{3/2}\left[i\pi-\log\left(\frac{-1}{x}+\sqrt{\frac{1}{x^2}-1}\right)\right], & -1<x<0. \end{cases} \tag{8.62}$$

The evolution of $\mathcal{F}(x)$ is illustrated in Fig. 8.2. There are six different values of $\mathcal{F}(x)$ with $x=\pm m_\pi/\delta$ ($\delta=\delta_{N\Delta}$, $\delta=\delta_{\Delta R}$ and $\delta=\delta_{NR}$) at the physical point are presented. We also investigate the limit behavior of $\mathcal{F}(x)$: when $x\to 0$, the loop function $\mathcal{F}(x)\to 0$ and when $x\to\infty$, the loop function $\mathcal{F}(x)\to\frac{\pi}{2}x^3$.

Up to NNLO, the needed one loop diagrams are collected in Fig. 8.3, and the corresponding chiral correction to the nucleon self-energy can be expressed as

$$\begin{aligned}\tilde{\Sigma}^{(4)}_{NN}(0) = & -e_{N1}m_\pi^4 + \frac{3}{64\pi^2 f_\pi^2}(8c_{N1}-c_{N2}-4c_{N3})m_\pi^4\log\frac{m_\pi^2}{\mu^2} + \frac{3c_{N2}}{128\pi^2 f_\pi^2}m_\pi^4 \\ & -\frac{3}{4(4\pi f_\pi)^2}\frac{g_A^2}{M_{N0}}\left(\log\frac{m_\pi^2}{\mu^2}+1\right)m_\pi^4 \\ & +\frac{h_A^2}{4\pi^2 f_\pi^2}(c_{N1}-c_{\Delta 1})\left[m_\pi^2\delta_{N\Delta}^2\mathcal{J}\left(\frac{m_\pi}{\delta_{N\Delta}},\frac{\delta_{N\Delta}}{\mu}\right)+m_\pi^4\right] \\ & -\frac{5}{8(4\pi f_\pi)^2}\frac{h_A^2}{M_{N0}}\left(\log\frac{m_\pi^2}{\mu^2}+\frac{9}{10}\right)m_\pi^4 - \frac{h_A^2}{24\pi^2 f_\pi^2}\frac{\delta_{N\Delta}^4}{M_{N0}}\mathcal{F}\left(\frac{m_\pi}{\delta_{N\Delta}}\right)\end{aligned}$$

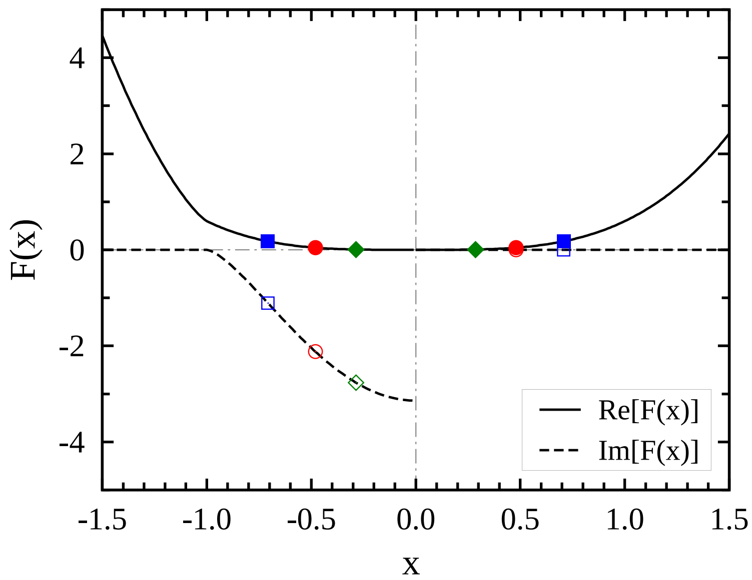

Figure 8.2: The evolution of $\mathcal{F}(x)$. Solid (dash) line corresponds to the real (imaginary) part of $\mathcal{F}(x)$. Red circles denote $\mathcal{F}(x)$ with $x=\pm m_\pi^{\text{phys.}}/\delta_{N\Delta}^{\text{phys.}}$, blue squares and green diamonds are the results with $x=\pm m_\pi^{\text{phys.}}/\delta_{\Delta R}^{\text{phys.}}$ ($\delta_{\Delta R}^{\text{phys.}}=m_\Delta^{\text{phys.}}-m_R^{\text{phys.}}$) and $x=\pm m_\pi^{\text{phys.}}/\delta_{NR}^{\text{phys.}}$. The full and hollow symbols are the real and imaginary results of $\mathcal{F}(x)$, respectively.

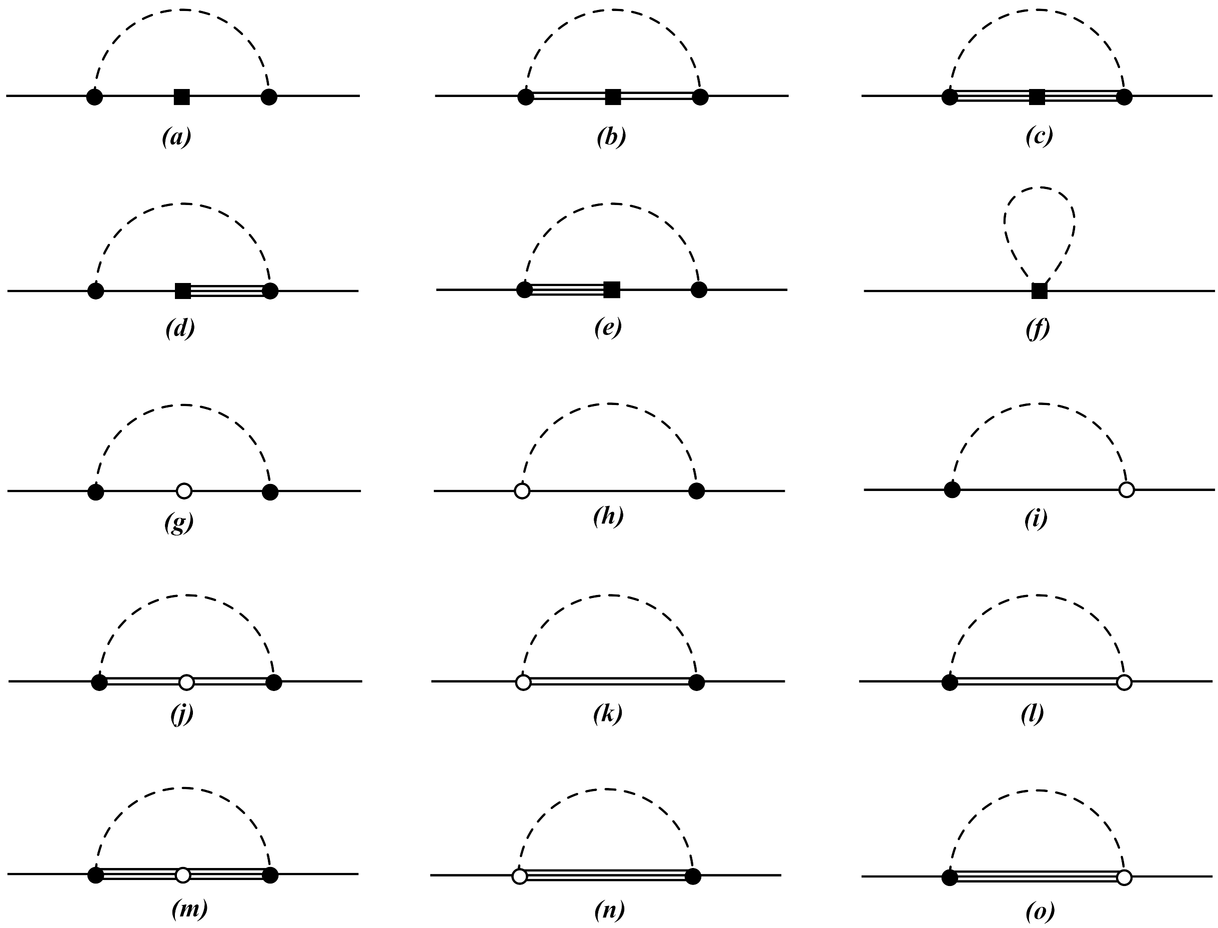

Figure 8.3: One loop self-energy diagrams contributing to $M_{NN}^{(4)}$. The dashed, solid, double-solid, and triple-solid lines correspond to the pion, nucleon, Δ, and Roper, respectively. The filled circles denote an insertion from the dimension one chiral Lagrangians, the black boxes indicate $\mathcal{O}(p^2)$ mass insertions, and the empty circles are the couplings from the $1/M_B$ correction Lagrangains. Wave function renormalization diagrams are not explicitly shown but included in the calculation.

$$
\begin{aligned}
&+\frac{9g_{NR}^2}{(4\pi f_\pi)^2}(c_{N1}-c_{R1})\left[m_\pi^2\delta_{NR}^2\mathcal{J}\left(\frac{m_\pi}{\delta_{NR}},\frac{\delta_{NR}}{\mu}\right)+\frac{2}{3}m_\pi^4\right]\\
&-\frac{3}{4(4\pi f_\pi)^2}\frac{g_{NR}^2}{M_{N0}}\left(\log\frac{m_\pi^2}{\mu^2}+1\right)m_\pi^4-\frac{9g_{NR}^2}{2(4\pi f_\pi)^2}\frac{\delta_{NR}^4}{M_{N0}}\mathcal{F}\left(\frac{m_\pi}{\delta_{NR}}\right)\\
&-\frac{3}{4\pi^2 f_\pi^2}c_{NR}g_A g_{NR}\left[m_\pi^2\delta_{NR}^2\mathcal{H}\left(\frac{m_\pi}{\delta_{NR}},\frac{\delta_{NR}}{\mu}\right)+m_\pi^4\right], \qquad (8.63)
\end{aligned}
$$

where the function, $\mathcal{J}(x,y)$, from loop diagrams Fig. 8.3(a,b,c), is defined as

$$
\begin{aligned}
\mathcal{J}(x,y) &= x^2\log(x^2y^2)+2\log\frac{4}{x^2}\\
&-\begin{cases}
4\sqrt{1-x^2}\log\left(\frac{1}{x}+\sqrt{\frac{1}{x^2}-1}\right), & 0<x<1,\\
(-4)\sqrt{x^2-1}\arccos\frac{1}{x}, & |x|\geq 1,\\
(-4)\sqrt{1-x^2}\left[i\pi-\log\left(\frac{-1}{x}+\sqrt{\frac{1}{x^2}-1}\right)\right], & -1<x<0.
\end{cases} \qquad (8.64)
\end{aligned}
$$

The asymptotic behavior of $\mathcal{J}(x,y)$ is: $\mathcal{J}(x,y)\to -x^2+x^2\log(4y^2)$ when $x\to 0$ and $\mathcal{J}(x,y)\to x^2\log(x^2y^2)$ when $x\to\infty$.

Due to the mixing between nucleon and Roper fields, two new loop diagrams [Fig. 8.3(d,e)] should be taken into account. The corresponding three-point function $\mathcal{H}(x,y)$ is defined as

$$\begin{aligned}\mathcal{H}(x,y) &= \frac{3}{2}x^2\log(x^2y^2)+\pi x^3+\log\frac{4}{x^2}\\ &- \begin{cases} 2(1-x^2)^{3/2}\log\left(\frac{1}{x}+\sqrt{\frac{1}{x^2}-1}\right), & 0<x<1,\\ 2(x^2-1)^{3/2}\arccos\frac{1}{x}, & |x|\geq 1,\\ -2(1-x^2)^{3/2}\left[i\pi-\log\left(\frac{-1}{x}+\sqrt{\frac{1}{x^2}-1}\right)\right], & -1<x<0.\end{cases}\end{aligned} \tag{8.65}$$

Furthermore, the limit behavior is: $\mathcal{H}(x,y)\to -\frac{1}{2}x^2+\frac{3}{2}x^2\log(4y^2)$ when $x\to 0$ and $\mathcal{H}(x,y)\to \frac{3}{2}x^2\log(x^2y^2)$ when $x\to\infty$.

Diagonal terms of the Delta self-energy

In order to obtain the chiral corrections to the self-energy of Delta, one has to calculate the one-loop diagrams shown in Figs. 8.4 and 8.5. The LO, NLO and NNLO contributions are

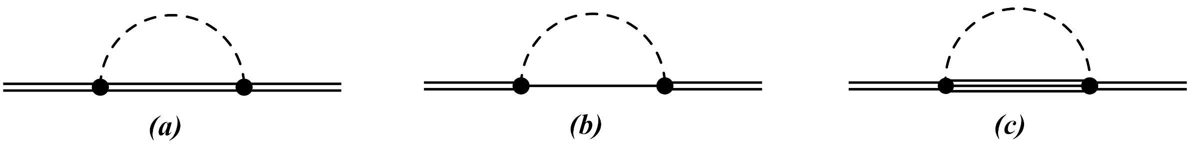

Figure 8.4: One loop self-energy diagrams contributing to $M^{(3)}_{\Delta\Delta}$. Other notations are the same as in Fig. 8.1.

$$\Sigma^{(2)}_{\Delta\Delta} = -4c_{\Delta 1}m_\pi^2, \tag{8.66}$$

$$\Sigma^{(3)}_{\Delta\Delta}(\delta_{N\Delta}) = -\frac{25H_A^2}{864\pi f_\pi^2}m_\pi^3+\frac{h_A^2}{3(4\pi f_\pi)^2}\delta^3_{N\Delta}\mathcal{F}(-\frac{m_\pi}{\delta_{N\Delta}})-\frac{g^2_{\Delta R}}{3(4\pi f_\pi)^2}\delta^3_{\Delta R}\mathcal{F}(\frac{m_\pi}{\delta_{\Delta R}}), \tag{8.67}$$

$$\begin{aligned}\tilde\Sigma^{(4)}_{\Delta\Delta}(\delta_{N\Delta}) &= -e_{\Delta 1}m_\pi^4+\frac{3}{64\pi^2 f_\pi^2}(8c_{\Delta 1}-c_{\Delta 2}-4c_{\Delta 3})m_\pi^4\log\frac{m_\pi^2}{\mu^2}+\frac{3c_{\Delta 2}}{128\pi^2 f_\pi^2}m_\pi^4\\ &-\frac{25}{96(4\pi f_\pi)^2}\frac{H_A^2}{M_{N0}}\left(\log\frac{m_\pi^2}{\mu^2}+\frac{19}{10}\right)m_\pi^4\\ &+\frac{h_A^2}{(4\pi f_\pi)^2}(c_{\Delta 1}-c_{N1})m_\pi^2\delta^2_{N\Delta}\mathcal{J}(-\frac{m_\pi}{\delta_{N\Delta}},-\frac{\delta_{N\Delta}}{\mu})\\ &-\frac{5}{32(4\pi f_\pi)^2}\frac{h_A^2}{M_{N0}}\left(\log\frac{m_\pi^2}{\mu^2}-\frac{1}{10}\right)m_\pi^4-\frac{5h_A^2}{6(4\pi f_\pi)^2}\frac{\delta^4_{N\Delta}}{M_{N0}}\mathcal{F}(-\frac{m_\pi}{\delta_{N\Delta}})\\ &+\frac{g^2_{\Delta R}}{(4\pi f_\pi)^2}(c_{\Delta 1}-c_{R1})m_\pi^2\delta^2_{\Delta R}\mathcal{J}(\frac{m_\pi}{\delta_{\Delta R}},\frac{\delta_{\Delta R}}{\mu})\\ &-\frac{5}{32(4\pi f_\pi)^2}\frac{g^2_{\Delta R}}{M_{N0}}\left(\log\frac{m_\pi^2}{\mu^2}-\frac{1}{10}\right)m_\pi^4-\frac{5g^2_{\Delta R}}{6(4\pi f_\pi)^2}\frac{\delta^4_{\Delta R}}{M_{N0}}\mathcal{F}(\frac{m_\pi}{\delta_{\Delta R}})\\ &-\frac{2}{(4\pi f_\pi)^2}c_{NR}h_A g_{\Delta R}\left[\mathcal{G}(m_\pi,\delta_{N\Delta},\delta_{NR},\mu)-\frac{4}{3}m_\pi^4\right],\end{aligned} \tag{8.68}$$

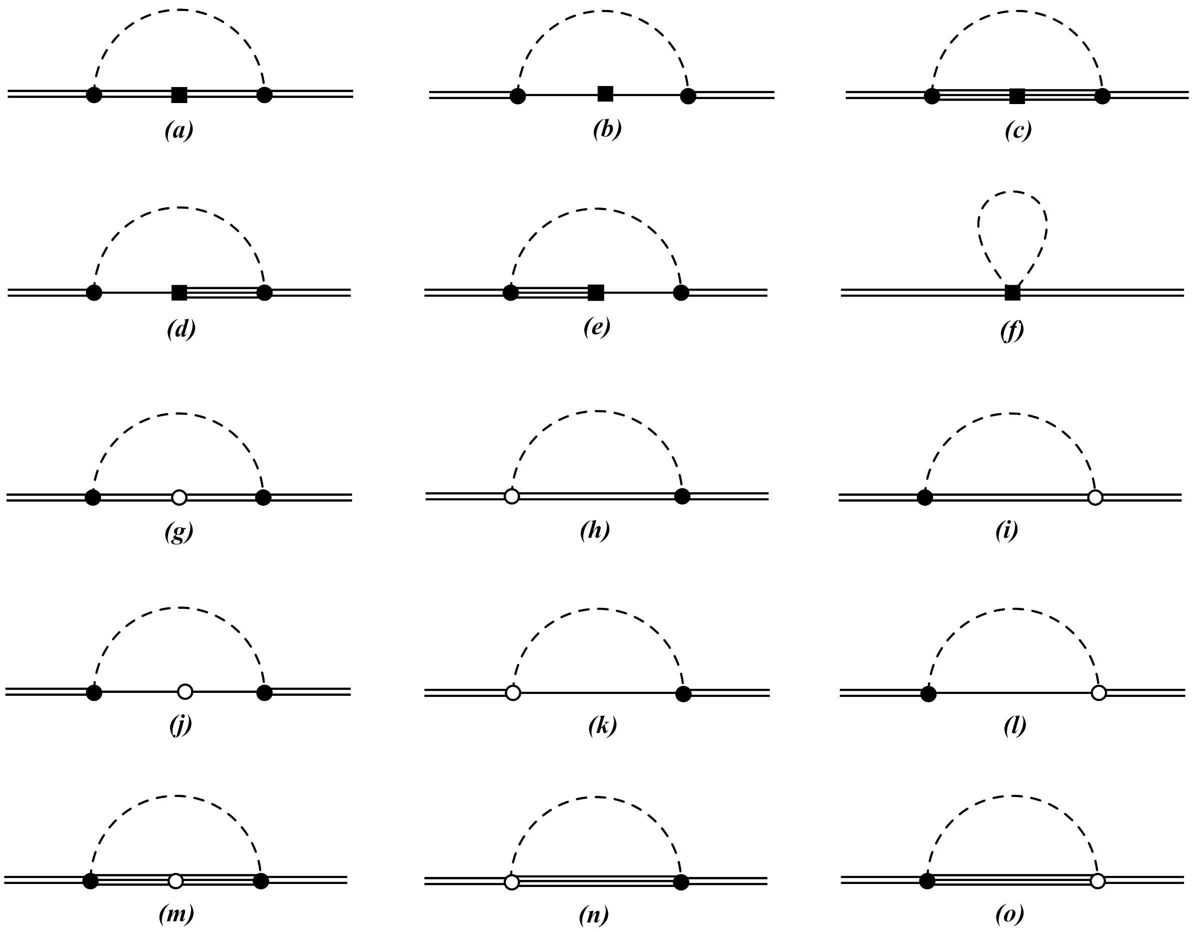

Figure 8.5: One loop self-energy diagrams contributing to $M^{(4)}_{\Delta\Delta}$. Other notations are the same as in Fig. 8.3.

where the new loop function $\mathcal{G}(m_\pi, \delta_{ND}, \delta_{NR}, \mu)$, from Fig. 8.5(d,e), is defined as

$$\begin{aligned}
\mathcal{G}(m_\pi, \delta_{N\Delta}, \delta_{\Delta R}, \mu) &= m_\pi^4 \log\frac{m_\pi^2}{\mu^2} + \frac{2}{3}\frac{\delta_{N\Delta}^3 m_\pi^2}{\delta_{N\Delta}+\delta_{\Delta R}} \log\frac{4\delta_{N\Delta}^2}{m_\pi^2} + \frac{2}{3}\frac{m_\pi^2 \delta_{\Delta R}^3}{\delta_{N\Delta}+\delta_{\Delta R}} \log\frac{4\delta_{\Delta R}^2}{m_\pi^2} \\
&+\frac{4}{3}\frac{m_\pi^2}{\delta_{N\Delta}+\delta_{\Delta R}} \begin{cases} -(\delta_{N\Delta}^2 - m_\pi^2)^{3/2} \log\left(\frac{\delta_{N\Delta}}{m_\pi} + \sqrt{\frac{\delta_{N\Delta}^2}{m_\pi^2}-1}\right), & \delta_{N\Delta} > m_\pi, \\ (m_\pi^2 - \delta_{N\Delta})^{3/2} \arccos\frac{-\delta_{N\Delta}}{m_\pi}, & |\delta_{N\Delta}| < m_\pi, \\ -(\delta_{N\Delta}^2 - m_\pi^2)^{3/2} \left[i\pi - \log\left(\frac{-\delta_{N\Delta}}{m_\pi} + \sqrt{\frac{\delta_{N\Delta}^2}{m_\pi^2}-1}\right)\right], & \delta_{N\Delta} < -m_\pi, \end{cases} \\
&-\frac{4}{3}\frac{m_\pi^2}{\delta_{N\Delta}+\delta_{\Delta R}} \begin{cases} -(\delta_{\Delta R}^2 - m_\pi^2)^{3/2} \log\left(\frac{-\delta_{\Delta R}}{m_\pi} + \sqrt{\frac{\delta_{\Delta R}^2}{m_\pi^2}-1}\right), & \delta_{\Delta R} > m_\pi, \\ (m_\pi^2 - \delta_{\Delta R}^2)^{3/2} \arccos\frac{\delta_{\Delta R}}{m_\pi}, & |\delta_{\Delta R}| < m_\pi, \\ -(\delta_{\Delta R}^2 - m_\pi^2)^{3/2} \left[i\pi - \log\left(\frac{\delta_{\Delta R}}{m_\pi} + \sqrt{\frac{\delta_{\Delta R}^2}{m_\pi^2}-1}\right)\right], & \delta_{\Delta R} < -m_\pi. \end{cases}
\end{aligned} \tag{8.69}$$

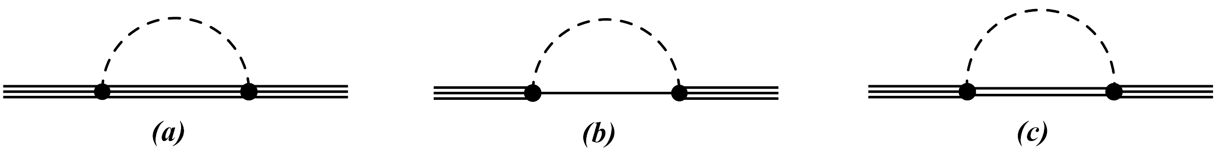

Figure 8.6: One loop self-energy diagrams contributing to $M_{RR}^{(3)}$. Other notations are the same as in Fig. 8.1.

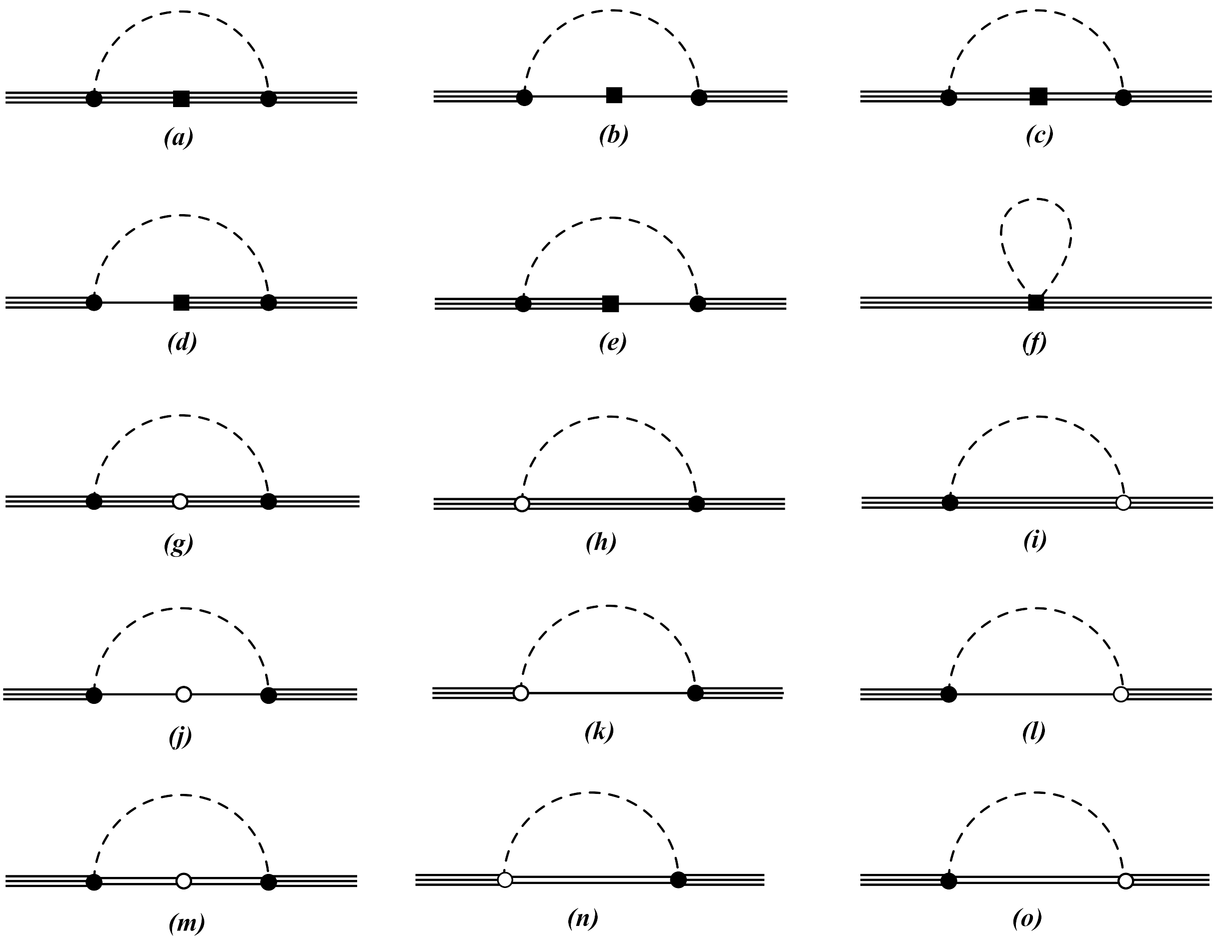

Figure 8.7: One loop diagrams self-energy contributing to $M_{RR}^{(4)}$. Other notations are the same as in Fig. 8.3.

Diagonal terms of the Roper self-energy

Just the same as the case of the nucleon, all the loop diagrams that contribute to the self-energy of Roper up to and including NNLO are presented in Figs. (8.6-8.7). The different order contributions to the Roper self-energy are

$$\Sigma_{RR}^{(2)} = -4c_{R1}m_\pi^2, \tag{8.70}$$

$$\Sigma_{RR}^{(3)}(\delta_{NR}) = -\frac{3g_R^2}{32\pi f_\pi^2}m_\pi^3 + \frac{3g_{NR}^2}{(4\pi f_\pi)^2}\delta_{NR}^3\mathcal{F}(-\frac{m_\pi}{\delta_{NR}}) + \frac{g_{\Delta R}^2}{12\pi^2 f_\pi^2}\delta_{\Delta R}^3\mathcal{F}(-\frac{m_\pi}{\delta_{\Delta R}}), \tag{8.71}$$

$$\tilde{\Sigma}_{RR}^{(4)}(\delta_{NR}) = -e_{R1}m_\pi^4 + \frac{3}{64\pi^2 f_\pi^2}(8c_{R1} - c_{R2} - 4c_{R3})m_\pi^4 \log\frac{m_\pi^2}{\mu^2} + \frac{3c_{R2}}{128\pi^2 f_\pi^2}m_\pi^4$$

$$
\begin{aligned}
&-\frac{3}{4(4\pi f_\pi)^2}\frac{g_R^2}{M_{N0}}\left(\log\frac{m_\pi^2}{\mu^2}+1\right)m_\pi^4 \\
&+\frac{9g_{NR}^2}{(4\pi f_\pi)^2}(c_{R1}-c_{N1})\left[m_\pi^2\delta_{NR}^2\mathcal{J}(-\frac{m_\pi}{\delta_{NR}},-\frac{\delta_{NR}}{\mu})+\frac{2}{3}m_\pi^4\right] \\
&-\frac{3}{4(4\pi f_\pi)^2}\frac{g_{NR}^2}{M_{N0}}\left(\log\frac{m_\pi^2}{\mu^2}+1\right)m_\pi^4-\frac{9g_{NR}^2}{2(4\pi f_\pi)^2}\frac{\delta_{NR}^4}{M_{N0}}\mathcal{F}(-\frac{m_\pi}{\delta_{NR}}) \\
&+\frac{g_{\Delta R}^2}{4\pi^2 f_\pi^2}(c_{R1}-c_{\Delta1})\left[m_\pi^2\delta_{\Delta R}^2\mathcal{J}(-\frac{m_\pi}{\delta_{\Delta R}},-\frac{\delta_{\Delta R}}{\mu})+m_\pi^4\right] \\
&-\frac{5}{8(4\pi f_\pi)^2}\frac{g_{\Delta R}^2}{M_{N0}}\left(\log\frac{m_\pi^2}{\mu^2}+\frac{9}{10}\right)m_\pi^4-\frac{g_{\Delta R}^2}{24\pi^2 f_\pi^2}\frac{\delta_{\Delta R}^4}{M_{N0}}\mathcal{F}(-\frac{m_\pi}{\delta_{\Delta R}}) \\
&-\frac{3}{4\pi^2 f_\pi^2}c_{NR}g_R g_{NR}\left[m_\pi^2\delta_{NR}^2\mathcal{H}(-\frac{m_\pi}{\delta_{NR}},-\frac{\delta_{NR}}{\mu})+m_\pi^4\right]. \qquad (8.72)
\end{aligned}
$$

Mixed terms between nucleon and Roper

Figure 8.8: Leading order diagrams of mixed terms between nucleon and Roper. Other notations are the same as in Fig. 8.3.

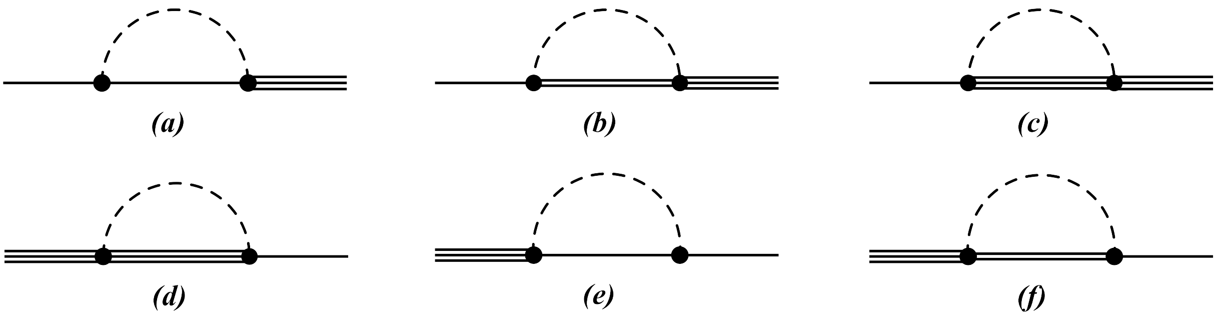

Figure 8.9: Next-to-leading order diagrams of mixed terms between nucleon and Roper. Other notations are the same as in Fig. 8.1.

Because Roper, as the first excitation state of nucleon, has the same quantum numbers as nucleon, there exists mixing between nucleon and Roper which is allowed by chiral symmetry. According to the mass formulas of nucleon [Eq. (8.57)] and Roper [Eq. (8.59)], we only need the mixed contributions up to NLO, including $\Sigma_{NR}^{(2)}$, $\Sigma_{RN}^{(2)}$, $\Sigma_{NR}^{(3)}$, and $\Sigma_{RN}^{(3)}$. As illustrated in Fig. (8.8), the mixed term up to leading order is

$$\Sigma_{NR}^{(2)}=\Sigma_{RN}^{(2)}=-4c_{NR}m_\pi^2. \qquad (8.73)$$

At $\mathcal{O}(\varepsilon^3)$, the one-loop diagrams contributing to the mixed terms $\Sigma_{NR}^{(3)}$ and $\Sigma_{RN}^{(3)}$ are shown in Fig. 8.9. The mixed terms $\Sigma_{NR}^{(3)}$ and $\Sigma_{RN}^{(3)}$ have the same loop structure as $\Sigma_{NN}^{(3)}$, and can be expressed as

$$\Sigma_{NR}^{(3)}(0) \;=\; \Sigma_{RN}^{(3)}(0)$$

$$= -\frac{3g_A g_{NR}}{32\pi f_\pi^2} m_\pi^3 - \frac{h_A g_{\Delta R}}{12\pi^2 f_\pi^2} \delta_{N\Delta}^3 \mathcal{F}(\frac{m_\pi}{\delta_{N\Delta}}) - \frac{3g_{NR} g_R}{(4\pi f_\pi)^2} \delta_{NR}^3 \mathcal{F}(\frac{m_\pi}{\delta_{NR}}). \quad (8.74)$$

8.5 Results and Discussion

Up to now, we have obtained the chiral expansions of the self-energies of nucleon, Delta, and Roper up to NNLO. Now, we can give explicit expressions of the baryon masses and widths. As a tentative application, we would like to simultaneously analyze the lattice data of nucleon, Delta, and Roper masses to explore the quark mass dependence of Roper mass and the nucleon-Roper mixing effects.

8.5.1 Nucleon, Delta and Roper masses

In terms of Eqs. (8.57-8.59), we could explicitly write out the expressions of nucleon, Delta and Roper masses at $\mathcal{O}(\varepsilon^4)$.

- The nucleon mass M_N is

$$\begin{aligned}
M_N \;=\;& M_{N0} - 4c_{N1} m_\pi^2 - \frac{3g_A^2}{32\pi f_\pi^2} m_\pi^3 - \left(e_{N1} - \frac{16c_{NR}^2}{\delta_{NR}}\right) m_\pi^4 \\
&+ \frac{1}{128\pi^2 f_\pi^2}\left[3c_{N2} + 32(c_{N1} - c_{\Delta 1})h_A^2 + 48(c_{N1} - c_{R1})g_{NR}^2 - 96c_{NR} g_A g_{NR}\right] m_\pi^4 \\
&- \frac{3}{256\pi^2 f_\pi^2 M_{N0}}(4g_A^2 + 3h_A^2 + 4g_{NR}^2) m_\pi^4 - \frac{3c_{NR} g_A g_{NR}}{4\pi f_\pi^2 \delta_{NR}} m_\pi^5 - \frac{64c_{NR}^2 (c_{N1} - c_{R1})}{\delta_{NR}^2} m_\pi^6 \\
&+ \frac{1}{128\pi^2 f_\pi^2}\left[6(8c_{N1} - c_{N2} - 4c_{N3}) - \frac{1}{M_{N0}}(6g_A^2 + 5h_A^2 + 6g_{NR}^2)\right] m_\pi^4 \log\frac{m_\pi^2}{\mu^2} \\
&- \frac{1}{24\pi^2 f_\pi^2}\delta_{N\Delta}^3\left(2h_A^2 + \frac{h_A^2 \delta_{N\Delta}}{M_{N0}} + \frac{16c_{NR} h_A g_{\Delta R} m_\pi^2}{\delta_{NR}}\right)\mathcal{F}(\frac{m_\pi}{\delta_{N\Delta}}) \\
&- \frac{3}{32\pi^2 f_\pi^2}\delta_{NR}^3\left(2g_{NR}^2 + \frac{3g_{NR}^2\delta_{NR}}{M_{N0}} + \frac{16c_{NR} g_{NR} g_R m_\pi^2}{\delta_{NR}}\right)\mathcal{F}(\frac{m_\pi}{\delta_{NR}}) \\
&+ \frac{h_A^2}{4\pi^2 f_\pi^2}(c_{N1} - c_{\Delta 1}) m_\pi^2 \delta_{N\Delta}^2 \mathcal{J}\left(\frac{m_\pi}{\delta_{N\Delta}}, \frac{\delta_{N\Delta}}{\mu}\right) \\
&+ \frac{9g_{NR}^2}{(4\pi f_\pi)^2}(c_{N1} - c_{R1}) m_\pi^2 \delta_{NR}^2 \mathcal{J}\left(\frac{m_\pi}{\delta_{NR}}, \frac{\delta_{NR}}{\mu}\right) \\
&- \frac{3g_A g_{NR}}{4\pi^2 f_\pi^2} c_{NR} m_\pi^2 \delta_{NR}^2 \mathcal{H}\left(\frac{m_\pi}{\delta_{NR}}, \frac{\delta_{NR}}{\mu}\right). \quad (8.75)
\end{aligned}$$

- The Delta mass M_Δ is

$$\begin{aligned}
M_\Delta \;=\;& M_{N0} + \delta_{N\Delta} - 4c_{\Delta 1} m_\pi^2 - \frac{25H_A^2}{864\pi f_\pi^2} m_\pi^3 - e_{\Delta 1} m_\pi^4 \\
&+ \frac{1}{384\pi^2 f_\pi^2}(9c_{\Delta 2} + 64c_{NR} h_A g_{\Delta R}) m_\pi^4 - \frac{1}{3072\pi^2 f_\pi^2 M_{N0}}\left[95H_A^2 - 3(h_A^2 + g_{\Delta R}^2)\right] m_\pi^4 \\
&+ \frac{1}{1536\pi^2 f_\pi^2}\left[72(8c_{\Delta 1} - c_{\Delta 2} - 4c_{\Delta 3}) - \frac{5}{M_{N0}}(5H_A^2 + 3h_A^2 + 3g_{\Delta R}^2)\right] m_\pi^4 \log\frac{m_\pi^2}{\mu^2} \\
&+ \frac{h_A^2}{6(4\pi f_\pi)^2}\left(2\delta_{N\Delta}^3 - \frac{5\delta_{N\Delta}^4}{M_{N0}}\right)\mathcal{F}(-\frac{m_\pi}{\delta_{N\Delta}}) - \frac{g_{\Delta R}^2}{6(4\pi f_\pi)^2}\left(2\delta_{\Delta R}^3 + \frac{5\delta_{\Delta R}^4}{M_{N0}}\right)\mathcal{F}(\frac{m_\pi}{\delta_{\Delta R}})
\end{aligned}$$

$$
\begin{aligned}
&+\frac{h_A^2}{(4\pi f_\pi)^2}(c_{\Delta 1}-c_{N1})m_\pi^2\delta_{N\Delta}^2\mathcal{J}(-\frac{m_\pi}{\delta_{N\Delta}},-\frac{\delta_{N\Delta}}{\mu})\\
&+\frac{g_{\Delta R}^2}{(4\pi f_\pi)^2}(c_{\Delta 1}-c_{R1})m_\pi^2\delta_{\Delta R}^2\mathcal{J}(\frac{m_\pi}{\delta_{\Delta R}},\frac{\delta_{\Delta R}}{\mu})\\
&-\frac{2h_A g_{\Delta R}}{(4\pi f_\pi)^2}c_{NR}\mathcal{G}(m_\pi,\delta_{N\Delta},\delta_{NR},\mu).
\end{aligned}
\tag{8.76}
$$

- The Roper mass M_R is

$$
\begin{aligned}
M_R \;=\;& M_{N0}+\delta_{NR}-4c_{R1}m_\pi^2-\frac{3g_R^2}{32\pi f_\pi^2}m_\pi^3-\left(e_{R1}+\frac{16c_{NR}^2}{\delta_{NR}}\right)m_\pi^4\\
&+\frac{1}{128\pi^2 f_\pi^2}\left[3c_{R2}+32(c_{R1}-c_{\Delta 1})g_{\Delta R}^2+48(c_{R1}-c_{N1})g_{NR}^2-96c_{NR}g_R g_{NR}\right]m_\pi^4\\
&-\frac{3}{256\pi^2 f_\pi^2 M_{N0}}(4g_R^2+4g_{NR}^2+3g_{\Delta R}^2)m_\pi^4+\frac{3c_{NR}g_A g_{NR}}{4\pi f_\pi^2\delta_{NR}}m_\pi^5-\frac{64c_{NR}^2(c_{R1}-c_{N1})}{\delta_{NR}^2}m_\pi^6\\
&+\frac{1}{128\pi^2 f_\pi^2}\left[6(8c_{R1}-c_{R2}-4c_{R3})-\frac{1}{M_{N0}}(6g_R^2+6g_{NR}^2+5g_{\Delta R}^2)\right]m_\pi^4\log\frac{m_\pi^2}{\mu^2}\\
&+\frac{3}{32\pi^2 f_\pi^2}\delta_{NR}^3\left[g_{NR}^2\left(2-\frac{3\delta_{NR}}{M_{N0}}\right)\mathcal{F}(-\frac{m_\pi}{\delta_{NR}})+\frac{16c_{NR}g_R g_{NR}m_\pi^2}{\delta_{NR}}\mathcal{F}(\frac{m_\pi}{\delta_{NR}})\right]\\
&+\frac{1}{24\pi^2 f_\pi^2}\delta_{\Delta R}^3\left[g_{\Delta R}^2\left(2-\frac{\delta_{\Delta R}}{M_{N0}}\right)\mathcal{F}(-\frac{m_\pi}{\delta_{\Delta R}})+\frac{16c_{NR}h_A g_{\Delta R}m_\pi^2}{\delta_{NR}}\mathcal{F}(\frac{m_\pi}{\delta_{N\Delta}})\right]\\
&+\frac{9g_{NR}^2}{(4\pi f_\pi)^2}(c_{R1}-c_{N1})m_\pi^2\delta_{NR}^2\mathcal{J}\left(-\frac{m_\pi}{\delta_{NR}},-\frac{\delta_{NR}}{\mu}\right)\\
&+\frac{g_{\Delta R}^2}{4\pi^2 f_\pi^2}(c_{R1}-c_{\Delta 1})m_\pi^2\delta_{\Delta R}^2\mathcal{J}\left(-\frac{m_\pi}{\delta_{\Delta R}},-\frac{\delta_{\Delta R}}{\mu}\right)\\
&-\frac{3g_R g_{NR}}{4\pi^2 f_\pi^2}c_{NR}m_\pi^2\delta_{NR}^2\mathcal{H}\left(-\frac{m_\pi}{\delta_{NR}},-\frac{\delta_{NR}}{\mu}\right).
\end{aligned}
\tag{8.77}
$$

We want to mention that, the chiral expansions of nucleon, Delta and Roper masses have been carried out in Refs. [73, 81, 256, 259, 285, 286, 305]. Our nucleon mass, without the virtual Delta and Roper contributions, is the same as Eq.(11) of Ref. [73] and Eq.(A.1) of Ref. [305]. But, for the nucleon and Delta masses, even without the virtual Roper contributions, our results are different with Ref. [259], which did not perform the expansion in $\delta_{\Delta N}$ and δ_{RN}.

8.5.2 Delta and Roper widths

The width of resonance can be obtained by the imaginary of self-energy with $\Gamma_B = -2\mathrm{Im}[\Sigma_B]$. By using the Eq. (8.58) and Eq. (8.59), we obtain:

- The width of Delta Γ_Δ

$$
\begin{aligned}
\Gamma_\Delta \;=\;& \frac{\pi}{3}\frac{h_A^2}{(4\pi f_\pi)^2}(\delta_{N\Delta}^2-m_\pi^2)^{3/2}\left(2-\frac{5\delta_{N\Delta}}{M_{N0}}\right)\\
&-8\pi\frac{h_A^2}{(4\pi f_\pi)^2}(c_{\Delta 1}-c_{N1})\delta_{N\Delta}m_\pi^2\sqrt{\delta_{N\Delta}^2-m_\pi^2}\\
&+\frac{16\pi}{3}\frac{h_A g_{\Delta R}}{(4\pi f_\pi)^2}c_{NR}\frac{m_\pi^2}{\delta_{NR}}((\delta_{N\Delta}-\delta_{NR})^2-m_\pi^2)^{3/2}.
\end{aligned}
\tag{8.78}
$$

- The width of Roper Γ_R

$$
\begin{aligned}
\Gamma_R &= \frac{3\pi g_{NR}}{(4\pi f_\pi)^2}\left(2g_{NR} - \frac{3g_{NR}\delta_{NR}}{M_{N0}} + 16 g_R c_{NR}\frac{m_\pi^2}{\delta_{NR}}\right)(\delta_{NR}^2 - m_\pi^2)^{3/2} \\
&+ \frac{g_{\Delta R}^2}{12\pi f_\pi^2}\left(2 - \frac{\delta_{\Delta R}}{M_{N0}}\right)(\delta_{\Delta R}^2 - m_\pi^2)^{3/2} \\
&- 24\pi\frac{3g_{NR}^2}{(4\pi f_\pi)^2}(c_{R1} - c_{N1})m_\pi^2\delta_{NR}\sqrt{\delta_{NR}^2 - m_\pi^2} \\
&- 32\pi\frac{g_{\Delta R}^2}{(4\pi f_\pi)^2}(c_{R1} - c_{\Delta 1})m_\pi^2\delta_{\Delta R}\sqrt{\delta_{\Delta R}^2 - m_\pi^2}.
\end{aligned} \tag{8.79}
$$

In the next subsection, we will employ the widths of Delta and Roper to determine/constrain the values of the related LECs.

8.5.3 Analysis of lattice data of nucleon, Delta and Roper masses

Due to the unstable Roper state with $m_\pi \leq 500$ MeV in LQCD, in principle, the lattice Roper mass is not suitable to be studied in ChPT. As illustration of our calculations, we would like to perform the chiral extrapolation of Roper mass by analyzing the lattice data.

However, because there is a large number of LECs (24) appearing in the nucleon, Delta, and Roper masses up to NNLO, we do not expect to determine all the LECs by just fitting the lattice baryon masses. In order to tentatively study the chiral extrapolation of Roper mass, we would like to utilize the NLO baryon masses, which contains 10 unknown LECs (m_0, $\delta_{\Delta N}$, Δ_{RN}, c_{N1}, $c_{\Delta 1}$, c_{R1}, c_{NR}, g_{NR}, $g_{\Delta R}$, and g_R), to simultaneously study the lattice data of nucleon, Delta, and Roper masses and their experimental results.

Table 8.1: Values of the LECs from the best fit to the nucleon, Delta, and Roper lattice data and experimental results.

	Fit-I	Fit-II
M_{N0}	853(2)	854(3)
$\delta_{\Delta N}$	304(11)	310(5)
δ_{RN}	237(141)	535(54)
c_{N1}	-1.36(1)	-1.35(2)
$c_{\Delta 1}$	-1.19(10)	-1.07(5)
c_{R1}	-5.79(2.97)	-0.450(486)
c_{NR}	0±0.147	0±0.231
g_{NR}	0.390(64)	0.391(64)
$g_{\Delta R}$	2.00(49)	2.03(48)
g_R	3.26(160)	0±3.69
χ^2-N	20.98	20.85
χ^2-Δ	4.66	4.28
χ^2-R	5.39	0.16
χ^2/d.o.f.	1.15	1.01

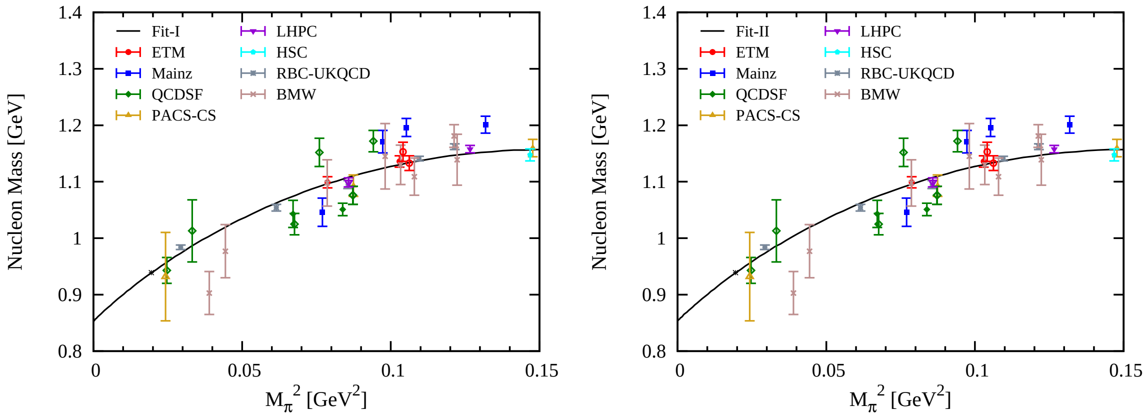

Figure 8.10: Chiral extrapolation of nucleon mass. Left panel and right panel are the results from Fit-I and Fit-II, respectively.

At present, there are many lattice simulations on the nucleon mass, such as the $n_f = 2$ simulations from the ETM [306], Mainz [307], QCDSF [308], and BGR [165] collaborations, and the $n_f = 2 + 1$ simulations from the PACS-CS [23], LHPC [25], HSC [26], RBC-UKQCD [241] and BMW [22] collaborations. For the lattice Delta masses, several collaborations have reported their results, the ETM [306] and BGR [165] collaborations with $n_f = 2$, and the PACS-CS [23], HSC [165] collaborations with $n_f = 2 + 1$. But the situation for the lattice Roper masses is unsatisfactory. As mentioned in Chapter 2, the lattice data of Roper masses from the CSSM [163], JLab [164], BGR [165], Cyprus [150] collaborations is large different with the results of χQCD [167] simulation. In the sense of the tentative study of lattice Roper masses, we could divide the lattice results of Roper masses into two groups: one group is from the CSSM, JLab, BGR, and Cyprus collaborations, another from χQCD Collaboration.

In the following, we perform a simultaneous fit of the nucleon, Delta, and Roper masses of the LQCD by using the chiral expansions of baryon masses at $\mathcal{O}(\varepsilon^3)$. The lattice data should fulfill $m_\pi^2 < 0.15$ GeV^2 to ensure the validity of NLO ChPT. After selection, the number of lattice points is 25 for the nucleon, 6 for the Delta, and 6(4) from group one (two) for the Roper. We denote the lattice data points of nucleon, Delta, and lattice data of Roper masses from group one as Set-I. And, Set-II contains the same nucleon and Delta lattice data as Set-I and the lattice Roper masses from group two. The pion decay constant f_π is taken its latest experimental result $f_\pi = 92.1$ MeV [15]. The nucleon-Delta coupling h_A is fixed as $h_A = 2.09$ by using the Delta width. And, the nucleon-Roper and Delta-Roper couplings g_{NR} and $g_{\Delta R}$ are constrained by the Breit-Wigner width of Roper $\Gamma_R = 350 \pm 100$ MeV.

We perform a χ^2 fit to the lattice data and the physical baryon masses. The obtained LECs and χ^2/d.o.f. from the best fits are tabulated in Table 8.1. Besides, the fit-χ^2 for nucleon, Delta, and Roper are also given. The two fit strategies, named as Fit-I and Fit-II, give essentially the same description of nucleon and Delta masses of LQCD. This is also illustrated in Fig. 8.10 and Fig. 8.11 of the chiral extrapolation of lattice data. Due to the large difference of the fitted Roper masses in Set-I and Set-II, we can see that the values of LECs related to Roper masses, e.g. δ_{RN}, c_{R1}, are very different. In Fig. 8.12, we present the quark mass dependence of Roper masses from Set-I (left panel) and Set-II (right panel). As we expected, the lattice data from

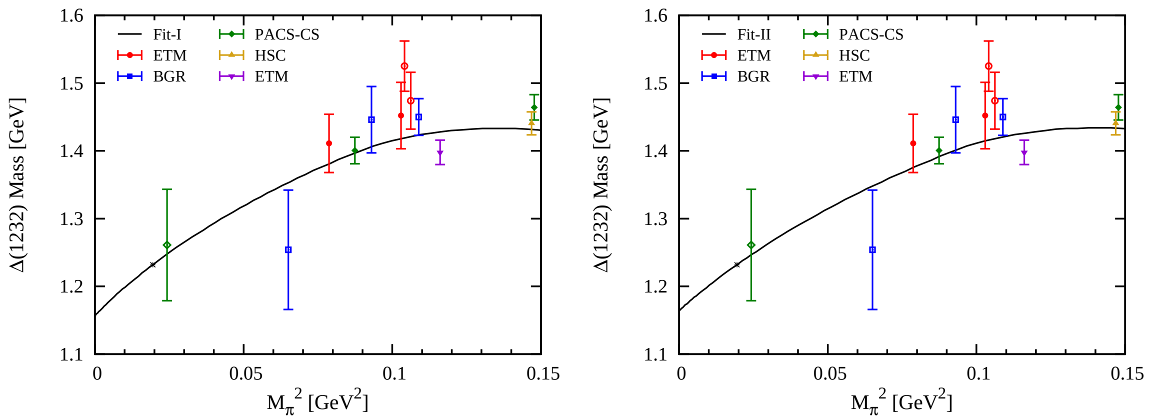

Figure 8.11: Chiral extrapolation of Delta mass. Left panel and right panel are the results from Fit-I and Fit-II, respectively.

the CSSM, JLab, BGR, Cyprus collaborations present a large chiral-log effect, whereas the χQCD results give a mild quark mass dependence of Roper mass. In Fit-I, as anticipated, the Roper-nucleon mass difference in the chiral limit is relatively small, and comparable to the Delta-nucleon splitting. The value of $c_{NR} \sim 0$ denotes that the mixed effects of nucleon and Roper are very small at $\mathcal{O}(p^3)$. But, on the other hand, the sizable error of c_{NR} also indicates the mixing effects should be carefully investigated when better lattice data becomes available. And, it would be interest to study its effects up to NNLO.

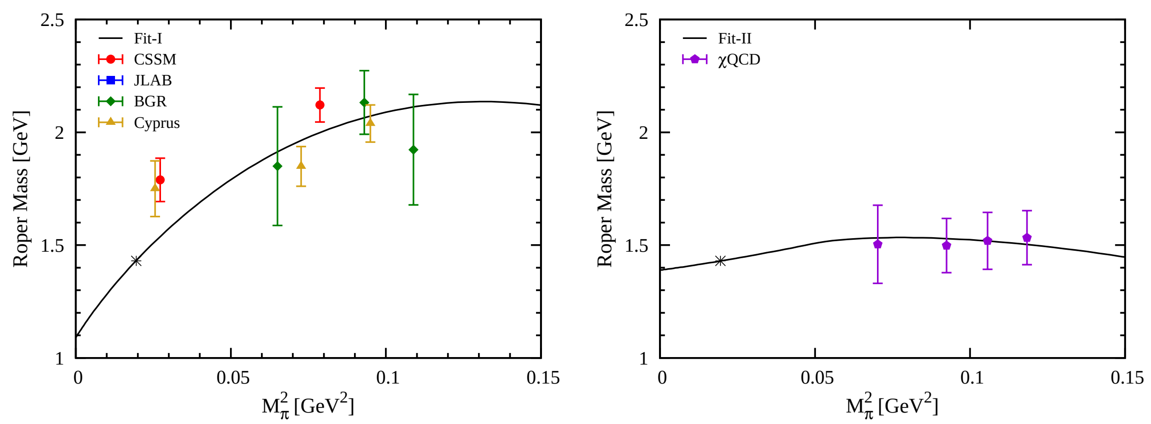

Figure 8.12: Chiral extrapolation of Roper mass. Left panel and right panel are the results from Fit-I and Fit-II, respectively.

Chapter 9

Conclusion

The origin of mass of ordinary matter is linked to the origin of nucleon masses. The components of a nucleon mass can be divided into two parts: one is the three valence quark masses from the Brout-Englert-Higgs mechanism, which can only provide 1% contributions, and the other is from the nonperturbative strong interaction, which accounts for $\sim$99% of the nucleon mass. In this dissertation, we present an integration of chiral perturbation theory and lattice QCD to study lattice baryon masses and to understand the mechanism of the origin of mass.

In the SU(3) sector, we performed a systematic study of the lattice results of lowest-lying octet and decuplet baryon masses in covariant baryon chiral perturbation theory with the extended-on-mass-shell renormalization scheme.

- For lowest-lying octet baryons, we calculated the baryon self-energies up to next-to-next-to-next-to-leading order in the chiral expansion by using EOMS BChPT. The corresponding finite-volume corrections to the lattice data were evaluated up to $\mathcal{O}(p^4)$. By constructing the discretized BChPT for Wilson fermions, we obtained the finite lattice spacing discretization effects of lattice QCD. Then, we performed a systematic study of lattice baryon masses from the PACS-CS, LHPC, QCDSF-UKQCD, HSC, and NPLQCD collaborations by exploring the chiral extrapolation of baryon masses, and evaluating finite-volume and finite lattice spacing discretization effects of LQCD.

  We confirmed that covariant BChPT in the three-flavor sector converges as expected, relatively slowly as dictated by $M_K/\Lambda_{\text{ChPT}}$ but with clear improvement order by order, at least concerning the octet baryon masses. A successful simultaneous fit of all the latest 2+1 flavors LQCD simulations indicates that the lattice octet baryon masses are consistent with each other, though their setups are quite different. We also found the finite-volume corrections of LQCD are important. And, for the lattice discretization effects, our studies showed that the treatment of discretization effects as systematic uncertainties in the previous studies of the LQCD octet baryon masses seems to be justified. It was shown that the discretization effects on the octet baryon masses are less than 2% for lattice spacings up to 0.15 fm, in agreement with other LQCD studies. Furthermore, it is also shown that the contributions of virtual decuplet baryons affect little the light-quark mass dependence of the octet baryon masses, indicating that their effects can be embodied in the LECs of the octet only version. On the other hand, a slightly better description of FVCs can be achieved once virtual decuplet baryons are taken into account.

- Applying the obtained chiral formulas for the octet baryon masses at $\mathcal{O}(p^4)$, we have performed an accurate prediction of the octet baryon sigma terms by systematically analyzing the high statistic lattice baryon masses from PACS-CS, LHPC, QCDSF-UKQCD collaborations. We found $\sigma_{\pi N} = 55(1)(4)$ MeV and $\sigma_{sN} = 27(27)(4)$ MeV. Special attention was paid to uncertainties induced by the lattice scale setting method, which, however, were found to be small, in contrast with previous studies. Other uncertainties, such as those induced by truncating chiral expansions and variations of LECs were also studied in detail. In addition, we have used the strong-interaction isospin-splitting effects from the LQCD simulations to further constrain the relevant LECs. Our results indicate a small scalar strangeness content in the nucleon, consistent with the strangeness contribution to the proton spin and to the electromagnetic form factors of the nucleon.

- As a natural extension, we have also studied the lowest-lying decuplet baryon masses in covariant baryon chiral perturbation theory with the extended-on-mass-shell scheme up to next-to-next-to-next-to-leading order. Through a simultaneous fit of the $n_f = 2+1$ lattice data from the PACS-CS, QCDSF-UKQCD, and HSC collaborations, the 14 unknown low-energy constants are determined. In fitting the lattice data, finite-volume corrections are taken into account self-consistently. A $\chi^2/\text{d.o.f.} = 0.23$ is achieved for the eight sets of lattice data satisfying $M_\pi^2 < 0.25$ GeV^2 and $M_\phi L > 3.8$.

  Our studies show that the chiral expansions are convergent as expected and the results of the PACS-CS, QCDSF-UKQCD, and HSC collaborations seem to be consistent with each other, but not those of the LHPC Collaboration which employs the hybrid action. We have predicted the sigma terms of the decuplet baryons by use of the Feynman-Hellmann theorem, which should be compared to the lattice data in the future. It should be noted that our present study suffers from the limited range of the LQCD data (in terms of the input parameters) and the rather large number of unknown low-energy constants. Future refined LQCD simulations with various light-quark and strange quark masses, lattice volume and lattice spacing will be extremely welcome to put covariant baryon chiral perturbation theory to a more stringent test than did in the present work.

From the above studies, we present a nice interplay of lattice QCD and chiral perturbation theory to study the lowest-lying baryon masses. By performing the chiral extrapolation of lattice baryon masses to the physical point, we could reproduce the baryon masses. This could confirm that the nonperturbative strong interaction can provide the 99% of nucleon (baryon) masses.

With the studies of excited states becoming popular in lattice simulations, we also explored the chiral corrections to the self-energies of Roper, the first excitation state of nucleon. We performed a systematic study of the nucleon, Delta and Roper masses and widths in an extension of chiral perturbation theory that includes the Delta-nucleon and Roper-nucleon mass differences as expansion degrees of freedom. The contributions due to the mixing between nucleon and Roper induced by explicit chiral symmetry breaking were taken into account explicitly. The virtual Roper effects on the nucleon and Delta masses were evaluated up to next-to-next-to-leading order, as well as the effects of the nucleon and Delta in the Roper mass and width.

Lattice QCD has been successful to calculate many physical properties of lowest-lying states. The ground-state hadron spectrum is well understood [128], and the corresponding numerical artifacts from continuum extrapolation and finite-volume corrections are well controlled. Therefore, computing the spectrum of excited mesons and baryons in lattice QCD becomes interesting. At present, there are several lattice collaborations which performed the study of excited hadron spectrum, such as the CSSM Collaboration [309–311], the BGR Collaboration [165, 312], the HSC Collaboration [313, 314], the Cyprus Collaboration [150, 166]. But, such calculations are still very challenging. Although, in this dissertation, we have studied Roper mass in chiral perturbation theory, the corresponding lattice Roper mass is not very clear and not suitable to perform the chiral extrapolation. We believe that, in the future, when the lattice QCD studies of Roper mass are mature, we can then use the same ideas to perform a systematic study of Roper mass by including the finite-volume corrections and finite lattice spacing discretization effects. Furthermore, we also want to study the nucleon axial charge g_A including the Roper effects and the Roper axial charge g_R in chiral perturbation theory.

In this dissertation, the isospin symmetry between u and d quarks is always taken exactly with $m_u = m_d \equiv m_l$ in the lattice baryon masses and the chiral corrections to baryon self-energies [1]. Although the difference between u, d quarks is very small, it plays important roles in the study of low-energy physics. If one understands the baryon mass splitting from isospin symmetry breaking, especially for the proton and neutron masses splitting, it would be very helpful to the study of β decay and to explore new physics [315]. More recently, with the advance of computer techniques and computational resources, the effects of isospin symmetry breaking are starting to be included in lattice simulations. There are several studies of nucleon and baryon masses combining QCD and QED [247, 248, 316–322]. In Ref. [323], Davoudi and Savage have studied the electromagnetic corrections to the masses of meson, baryon and nuclei in a finite volume. In a near future, we would like to construct chiral effective Lagrangians including virtual photons, and study the electromagnetic corrections to the octet baryon masses in chiral perturbation theory.

Furthermore, studies of hadron resonance structure become a hot topic with the discovery of the exotic (X, Y, and Z) hadron states by experiments. Although chiral perturbation theory is a powerful theoretical tool to study the low-energy physics, its application energy region is around 1 GeV. Therefore, unitary chiral perturbation theory (UChPT) [324, 325], which employs unitary techniques to conventional chiral perturbation theory, enables the study of higher-energy regions and describes low-lying resonances. With my collaborators, we have studied five different subjects: (1) We studied for the first time the antineutrino-proton reactions to produce the $\Lambda(1405)$ by using the UChPT, which generates two $\Lambda(1405)$ poles [326]; (2) We presented a new reaction $\eta_c(\eta_c(2S)) \to \phi K^* \bar{K}^*$ to generate the $h_1(1830)$ by using UChPT, which can provide a suggestion for experimentalists to confirm the existence of $h_1(1830)$ state [327]; (3) We calculated the interaction kernel up to $\mathcal{O}(p^2)$ to generate the lowest-lying axial-vector mesons in the UChPT to explore the effects of higher order contributions [328]; (4) We calculated the energy levels of the KK^* system in the $f_1(1285)$ channel in finite volume by utilizing the UChPT [329]; (5) With the three-body resonances drawing much attention, we also studied the ρ, D^*, $\bar{D}^*$ three-body system by using the fixed-center approximation to the Faddeev equation in Ref. [330]. Recently, With the discovery of pentaquark states $P_c(4380)^+$ and $P_c(4450)^+$ by LHCb [331], it would be interesting to explore the nature and the properties of pentaquark states with those methods.

[1] We want to mention that, in Appendix D, the strong isospin-breaking effects are calculated.

Appendix A

$N_f = 2 + 1$ Lattice QCD simulation results

In this section, we briefly summarize some key ingredients of the LQCD simulations of the PACS-CS [23], LHPC [25], HSC [26], QCDSF-UKQCD [28] and NPLQCD [29] collaborations, which are relevant to our study. In addition, we tabulate the simulated octet baryon masses in physical units, which satisfy $M_\pi^2 < 0.5$ GeV^2, $M_K^2 < 0.7$ GeV^2, and the pseudoscalar meson mass times lattice box size $M_\phi L > 3$.

PACS-CS [23]

The PACS-CS Collaboration employs the nonperturbatively $O(a)$-improved Wilson quark action and the Iwasaki gauge action. Numerical simulations are carried out at the lattice spacing of $a = 0.0907(14)$ fm, on a $32^3 \times 64$ lattice with the use of the domain-decomposed HMC algorithm to reduce the up-down quark mass, which is about 3 MeV. For the strange quark part they improve the PHMC algorithm with the UV-filtering procedure. Their simulation points cover from 701 MeV to 156 MeV, but the lightest point has a $M_\pi L \approx 2.9$, which might induce large finite volume corrections.

Table A.1: Masses of the pseudoscalar mesons and the octet baryons (in units of MeV) obtained by the PACS-CS Collaboration (TABLE III of Ref. [23].) The first number in the parentheses is the statistical uncertainty and second is that from the uncertainty of the lattice spacing. The lattice data sets with stars demand $M_\pi < 500$ MeV and $M_\phi L > 4$.

M_π	M_K	m_N	m_Λ	m_Σ	m_Ξ
155.8	553.7	932.1(78.3)(14.4)	1139.9(20.7)(17.6)	1218.4(21.5)(18.8)	1393.3(6.7)(21.5)
$*$ 295.7	593.5	1093.1(18.9)(16.9)	1253.8(14.1)(19.4)	1314.8(15.4)(20.3)	1447.7(10.0)(22.3)
$*$ 384.4	581.4	1159.7(15.4)(17.9)	1274.1(9.1)(19.7)	1316.5(10.4)(20.3)	1408.3(7.0)(21.7)
$*$ 411.2	635.0	1214.7(11.5)(18.7)	1350.4(7.8)(20.8)	1400.2(8.5)(21.6)	1503.1(6.5)(23.2)
569.7	713.2	1411.1(12.2)(21.8)	1503.8(9.8)(23.2)	1531.2(11.1)(23.6)	1609.5(9.4)(24.8)
701.4	789.0	1583.0(4.8)(24.4)	1643.9(5.0)(25.4)	1654.5(4.4)(25.5)	1709.6(5.4)(26.4)

LHPC [25]

The LHPC Collaboration calculates the light hadron spectrum in full QCD using a mixed action that exploits the lattice chiral symmetry provided by domain wall valence quarks (the

DWF valence quark action) and ensembles of computationally economical improved staggered sea quark configurations (the so-called asqtad action). The lattice spacing is determined to be $a = 0.12406(248)$ fm and the lattice volume is $20^3 \times 64$. The range of pion masses simulated in this work extends from 758 MeV down to 293 MeV.

Table A.2: Masses of the pseudoscalar mesons and the octet baryons (in units of MeV) obtained by the LHPC Collaboration (TABLE II, TABLE VI, TABLE VII of Ref. [25]). The uncertainties have the same origin as those in Table A.1.

M_π	M_K	m_N	m_Λ	m_Σ	m_Ξ
292.9	585.6	1098.9(8.0)(22.0)	1240.5(4.8)(24.8)	1321.6(6.4)(26.4)	1412.2(3.2)(28.2)
$*$ 355.9	602.9	1157.8(6.4)(23.1)	1280.2(4.8)(25.6)	1350.2(4.8)(27.0)	1432.9(3.2)(28.6)
$*$ 495.1	645.4	1288.2(6.4)(25.8)	1369.3(4.8)(27.4)	1409.1(6.4)(28.2)	1469.5(4.8)(29.4)
596.7	685.6	1394.8(6.4)(27.9)	1440.9(8.0)(28.8)	1463.1(9.5)(29.2)	1504.5(8.0)(30.1)
687.7	728.1	1502.9(11.1)(30.0)	1528.3(9.5)(30.6)	1536.3(9.5)(30.7)	1557.0(9.5)(31.1)

HSC [26]

The HSC Collaboration uses a Symanzik-improved action with tree-level tadpole-improved coefficients for the gauge sector and the anisotropic clover fermion action for the fermion sector. The lattice spacings are $a_s = 0.1227(8)$ fm and $a_t = 0.003506(23)$ fm in spatial and temporal directions, respectively. The simulations are performed at four different lattice volumes $12^3 \times 96$, $16^3 \times 96$, $16^3 \times 128$, and $24^3 \times 128$. The simulated pion masses range from 383 MeV to 1565 MeV. For our purposes, we only need those data with $M_\pi^2 \leq 0.5$ GeV^2. The pseudoscalar meson masses and corresponding octet baryon masses are listed in Table A.3.

Table A.3: Masses of the pseudoscalar mesons and the lowest-lying baryons (in units of MeV) obtained by the HSC Collaboration (TABLE VI and TABLE VII of Ref. [26]). The uncertainties have the same origin as those in Table A.1.

M_π	M_K	m_N	m_Λ	m_Σ	m_Ξ
$*$ 383.2	543.6	1147.5(10.7)(7.5)	1243.1(8.4)(8.2)	1287.0(8.4)(8.4)	1347.8(6.8)(8.8)
388.9	545.9	1164.9(22.5)(7.6)	1226.8(16.9)(8.0)	1288.7(16.9)(8.5)	1345.0(11.3)(8.8)
$*$ 448.5	580.8	1238.1(16.9)(8.1)	1328.1(11.3)(8.7)	1361.9(16.9)(8.9)	1412.5(10.7)(9.3)
560.5	646.6	1361.9(22.5)(8.9)	1440.6(16.9)(9.5)	1457.5(22.5)(9.6)	1496.9(16.9)(9.8)

QCDSF-UKQCD [28]

The QCDSF-UKQCD Collaboration employs the particular clover action, which has a single iterated mild stout smearing, and the (tree-level) Symanzik improved gluon action, which contains the gluon action and the three-flavor Wilson-Dirac fermion action. The simulations are carried out at the lattice spacing of $a = 0.075 - 0.078$ fm, on $16^3 \times 32$, $24^3 \times 48$ and $32^3 \times 64$

lattices. The resulting pion masses range from 229 MeV to 449 MeV. In the simulations, they kept the singlet quark mass fixed and tuned the quark masses to ensure that the kaon always has a mass less than the physical one. It should be noted that in Table A.4 we did not tabulate the $16^3 \times 32$ and the $32^3 \times 64$ three-flavor simulation results, which have meson masses out of the range specified above.

Table A.4: Masses of the pseudoscalar mesons and the lowest-lying baryons (in units of MeV) obtained by the QCDSF-UKQCD Collaboration (TABLE XX, TABLE XXII and TABLE XXIII of Ref. [28]). The uncertainties have the same origin as those in Table A.1.

M_π	M_K	m_N	m_Λ	m_Σ	m_Ξ
229.3	476.9	996.7(22.1)(3.8)	1181.5(16.1)(4.3)	1181.6(9.7)(4.5)	1263.7(4.7)(4.8)
274.9	462.7	1027.1(15.1)(3.9)	1119.3(14.4)(4.3)	1164.0(9.2)(4.4)	1233.7(5.2)(4.7)
$*$ 319.1	448.8	1059.0(12.4)(4.0)	1128.5(10.7)(4.3)	1165.6(8.2)(4.4)	1217.8(5.2)(4.6)
332.6	461.1	1108.4(16.4)(4.0)	1193.7(14.1)(4.4)	1201.9(10.4)(4.4)	1257.8(7.9)(4.6)
358.4	449.0	1153.5(11.4)(4.1)	1195.0(12.2)(4.3)	1218.5(8.9)(4.4)	1254.5(6.9)(4.5)
392.9	436.5	1175.6(16.9)(4.2)	1189.8(14.4)(4.3)	1208.9(13.6)(4.4)	1225.5(11.9)(4.4)
420.9	420.9	1194.0(8.2)(4.3)	1194.0(8.2)(4.3)	1194.0(8.2)(4.3)	1194.0(8.2)(4.3)
457.3	399.3	1234.9(6.2)(4.5)	1205.9(10.7)(4.4)	1189.0(7.7)(4.3)	1161.2(9.7)(4.2)

NPLQCD [29]

The NPLQCD Collaboration mainly studied finite-volume effects on the octet baryon masses. Simulations are performed with $n_f = 2+1$ anisotropic clover Wilson action in four lattice volumes with spatial extent $L \sim 2.0,\ 2.5,\ 3.0$ and 3.9 fm. The anisotropic lattice spacing in the spatial direction is $b_s \sim 0.123$ fm and $b_t = b_s/3.5$ in the time direction. The pion mass is fixed at $M_\pi \sim 390$ MeV.

Table A.5: Masses of the pseudoscalar mesons and the lowest-lying baryons (in units of MeV) obtained by the NPLQCD Collaboration (TABLE II of Ref. [29]). The uncertainties have the same origin as those in Table A.1.

M_π	M_K	m_N	m_Λ	m_Σ	m_Ξ
387.8	544.4	1182.1(5.4)(7.7)	1263.3(5.1)(8.2)	1286.6(4.3)(8.4)	1361.5(4.1)(8.9)
$*$ 387.8	544.4	1164.0(3.2)(7.6)	1252.0(2.6)(8.2)	1280.5(3.0)(8.3)	1356.4(2.6)(8.8)
$*$ 387.8	544.4	1151.6(2.5)(7.5)	1242.3(2.6)(8.1)	1282.7(2.2)(8.4)	1349.3(2.1)(8.8)
$*$ 387.8	544.4	1151.3(2.6)(7.5)	1241.2(2.2)(8.1)	1279.0(2.8)(8.3)	1349.2(2.0)(8.9)

Appendix B

Feynman Rules

Here we would like to collect the relevant Feynman rules in the calculation of octet and decuplet baryon masses.

Propagators

Pseudoscalar meson propagator:

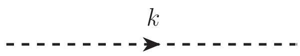

$$\frac{i}{k^2-m^2+i\varepsilon} \tag{B.1}$$

Octet baryon propagator:

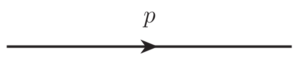

$$\frac{i}{\not{p}-m_0+i\varepsilon} \tag{B.2}$$

Decuplet baryon propagator:

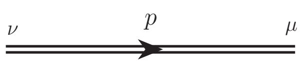

$$\frac{-i\mathcal{P}^{3/2}_{\mu\nu}(p)}{\not{p}-m_D+i\varepsilon}. \tag{B.3}$$

The covariant spin-3/2 projection operator is defined as

$$\mathcal{P}^{3/2}_{\mu\nu}(p) = g_{\mu\nu} - \frac{1}{d-1}\gamma_\mu\gamma_n u - \frac{1}{(d-1)m_D}(\gamma_\mu p_\nu + p_\mu\gamma_\nu) - \frac{d-2}{(d-1)m_D^2}p_\mu p_\nu, \tag{B.4}$$

in d dimensions.

Vertices

For the calculation of octet baryon masses

From $\mathcal{L}^{(1)}_{\phi B}$:

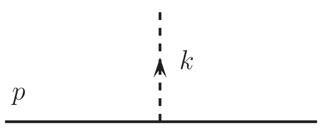

$$\propto \gamma^\mu\gamma_5 k_\mu. \tag{B.5}$$

From $\mathcal{L}^{(2)}_{\phi B}$:

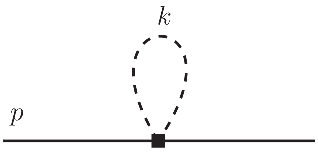

$$\propto 1, k_\mu k^\mu, k_\mu k_\nu p^\mu \gamma^\nu \tag{B.6}$$

From $\mathcal{L}^{(1)}_{\phi BD}$:

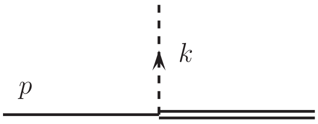

$$\propto k_\mu (p-k)_\nu \gamma^{\nu a \mu} \tag{B.7}$$

For the calculation of decuplet baryon masses

From $\mathcal{L}^{(1)}_{\phi D}$:

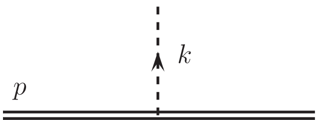

$$\propto \bar{T}_\rho k_\mu (p-k)_\nu \gamma_5 \gamma^{\sigma\rho\nu\mu} T_\sigma \tag{B.8}$$

From $\mathcal{L}^{(2)}_{\phi D}$:

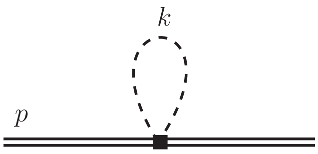

$$\propto 1, k_\mu k^\mu, k_\mu k_\nu p^\mu \gamma^\nu \tag{B.9}$$

From $\mathcal{L}^{(1)}_{\phi BD}$:

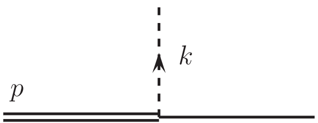

$$\propto k_\mu (p-k)_\nu \gamma^{\nu\rho\mu} T_\rho \tag{B.10}$$

Appendix C

Loop Integrals

Feynman parameterization

The Feynman parameterization is a way to fraction with a product in the denominator:

$$\frac{1}{A_1 A_2 \cdots A_n} = (n-1)! \int_0^1 dx_1 \int_0^1 dx_2 \cdots \int_0^1 dx_n \frac{\delta(1-x_1-x_2-\cdots-x_n)}{[A_1 x_1 + A_2 x_2 + \cdots + A_n x_n]^n}, \quad \text{(C.1)}$$

invented by Richard Feynman to calculate loop integrals.

In our studies, we use the following Feynman parameterization:

$$\frac{1}{AB} = \int_0^1 dx \frac{1}{[Ax + B(1-x)]^2}, \quad \text{(C.2)}$$

$$\frac{1}{ABC} = \int_0^1 dx \int_0^{1-x} dy \frac{1}{[Ax + By + C(1-x-y)]^3}. \quad \text{(C.3)}$$

Loop functions

In the calculation of the loop diagrams, we have used the d-dimension integrals in Minkowski space:

$$\int d^d k \frac{k^{\alpha_1} \cdots k^{\alpha_{2n}}}{(k^2 - \mathcal{M}^2)^\lambda} = i(-1)^\lambda \pi^{d/2} \frac{\Gamma(\lambda - n + \varepsilon - 2)}{2^n \Gamma(\lambda)} \frac{(-1)^n g_s^{\alpha_1 \cdots \alpha_{2n}}}{(\mathcal{M}^2)^{\lambda - n + \varepsilon - 2}}, \quad \text{(C.4)}$$

with $\varepsilon = (4-d)/2$. And, $g_s^{\alpha_1 \cdots \alpha_{2n}} = g^{\alpha_1 \alpha_2} \cdots g^{\alpha_{2n-1}\alpha_{2n}} + \cdots$ is a combination symmetric with respect to the permutation of any pair of indices. After expansion in powers of ε up to $\mathcal{O}(\varepsilon)$, we can easily obtain the following integral identities:

$$i\mu^{4-D} \int \frac{d^D l}{(2\pi)^D} \frac{1}{(l^2 - \mathcal{M}^2)^2} = -\frac{1}{16\pi^2} \left[R + \log\left(\frac{\mu^2}{\mathcal{M}^2}\right) \right], \quad \text{(C.5)}$$

$$i\mu^{4-D} \int \frac{d^D l}{(2\pi)^D} \frac{l^a l^b}{(l^2 - \mathcal{M}^2)^2} = -\frac{1}{16\pi^2} g_s^{(a,b)} \left[R + 1 + \log\left(\frac{\mu^2}{\mathcal{M}^2}\right) \right] \mathcal{M}^2, \quad \text{(C.6)}$$

$$i\mu^{4-D} \int \frac{d^D l}{(2\pi)^D} \frac{l^a l^b l^c l^d}{(l^2 - \mathcal{M}^2)^2} = -\frac{1}{32\pi^2} g_s^{(a,b,c,d)} \left[R + \frac{3}{2} + \log\left(\frac{\mu^2}{\mathcal{M}^2}\right) \right] \mathcal{M}^4, \quad \text{(C.7)}$$

$$i\mu^{4-D} \int \frac{d^D l}{(2\pi)^D} \frac{1}{(l^2 - \mathcal{M}^2)^3} = -\frac{1}{16\pi^2} \left[-\frac{1}{2\mathcal{M}^2} \right], \quad \text{(C.8)}$$

$$i\mu^{4-D} \int \frac{d^D l}{(2\pi)^D} \frac{l^a l^b}{(l^2 - \mathcal{M}^2)^3} = -\frac{1}{64\pi^2} g_s^{(a,b)} \left[R + \log\frac{\mu^2}{\mathcal{M}^2} \right], \quad \text{(C.9)}$$

$$i\mu^{4-D} \int \frac{d^D l}{(2\pi)^D} \frac{l^a l^b l^c l^d}{(l^2 - \mathcal{M}^2)^3} = -\frac{1}{128\pi^2} g_s^{(a,b,c,d)} \left[R + 1 + \log\frac{\mu^2}{\mathcal{M}^2} \right] \mathcal{M}^2, \quad \text{(C.10)}$$

where

$$R = \frac{1}{\varepsilon} + \log(4\pi) - \gamma, \tag{C.11}$$

$$g_s^{(a,b)} = \frac{1}{2} g^{ab}, \tag{C.12}$$

$$g_s^{(a,b,c,d)} = \frac{1}{4}(g^{ab}g^{cd} + g^{ac}g^{bd} + g^{ad}g^{bc}). \tag{C.13}$$

Appendix D

Strong isospin-breaking effects on octet baryon masses

In Chapter 5, the chiral expansions of octet baryon masses are obtained under the assumption that the isospin symmetry of u, d quarks is always conservation. Although the isospin breaking corrections to the octet baryon masses are small in comparison with octet baryon masses, as pointed in Ref. [332], their effects are of fundamental importance to describe the structure of ordinary matter.

There are two different sources of isospin symmetry breaking. One is from the small difference between the masses of u and d quarks, which are contributed by strong interaction. Another one is from the electric charge differences between u and d quarks. In this section, we would like to focus on the former one and calculate the strong isospin-breaking effects on the masses of pseudoscalar meson and octet baryon at $\mathcal{O}(p^4)$.

Isospin breaking effects to pseudoscalar meson masses

Expanding the lowest order meson Lagrangian [Eq. (3.38)] in powers of meson fields, one can obtain

$$\begin{aligned}\mathcal{L}_\phi^{(2)} &= B_0(m_u+m_d)(\pi^+\pi^-)+\frac{B_0}{2}(m_u+m_d)(\pi^0\pi^0)\\ &\quad +B_0(m_u+m_s)(K^+K^-)+B_0(m_d+m_s)(K^0\bar{K}^0)\\ &\quad +\frac{B_0}{6}(m_u+m_d+4m_s)(\eta^2)-\frac{1}{\sqrt{3}}(m_u-m_d)(\pi^0\eta)\end{aligned} \tag{D.1}$$

Because the masses difference between u and d quarks, mixing of π^0 and η would be appear. In order to remove the mixing to obtain the meson masses, one should rotate the meson field with

$$\begin{pmatrix}\pi^0\\ \eta\end{pmatrix}\to\begin{pmatrix}\cos(\varepsilon) & -\sin(\varepsilon)\\ \sin(\varepsilon) & \cos(\varepsilon)\end{pmatrix}\begin{pmatrix}\pi^0\\ \eta\end{pmatrix}, \tag{D.2}$$

where the lowest order mixing angel ε is

$$\tan(2\varepsilon)=\frac{\sqrt{3}(m_d-m_u)}{2m_s-m_u-m_d}. \tag{D.3}$$

Therefore, the meson masses can be expressed at leading order [1] as

$$M_{\pi^\pm}^2 = B_0(m_u+m_d)-\frac{2B_0}{3}(2m_s-m_u-m_d)\frac{\sin^2(\varepsilon)}{\cos(2\varepsilon)}, \tag{D.4}$$

[1] Under CPT symmetry, $M_{\pi^+}=M_{\pi^-}$, $M_{K^+}=M_{K^-}$, and $M_{K^0}=M_{\bar{K}^0}$.

$$M_{K^0}^2 = B_0(m_d+m_s), \tag{D.5}$$
$$M_{K^\pm}^2 = B_0(m_u+m_s), \tag{D.6}$$
$$M_\eta^2 = \frac{B_0}{3}(m_u+m_d+4m_s)+\frac{2B_0}{3}(2m_s-m_u-m_d)\frac{\sin^2(\varepsilon)}{\cos(2\varepsilon)}. \tag{D.7}$$

Up to next-to-leading order, the contributions to the meson masses by including the effects of isospin breaking read as

$$\begin{aligned} M_\phi^{2,4} = {} & \frac{1}{16\pi^2F_0^2}\frac{B_0}{36}\sum_{\phi'=\pi^\pm,\pi^0,\eta,K^\pm,K^0}\xi_{\phi,\phi'}H_\phi(M_{\phi'}^{2,2}) \\ & -\frac{8B_0^2}{F_0^2}\left(\xi_{\phi,uu}m_u^2+\xi_{\phi,dd}m_d^2+\xi_{\phi,ss}m_s^2+\right. \\ & \left.\xi_{\phi,ud}m_um_d+\xi_{\phi,us}m_um_s+\xi_{\phi,ds}m_dm_s\right), \end{aligned} \tag{D.8}$$

where $M_\phi^{2,2}$ and $M_\phi^{2,4}$ denote the M_ϕ^2 at the leading order and the next-to-leading order, respectively. The corresponding coefficients $\xi_{\phi,\phi'}$ and $\xi_{\phi,qq'}$ are listed in Tables (D.1-D.5) and Table D.6. The loop function H_ϕ is

$$H_\phi(M_{\phi'}^{2,2}) = M_{\phi'}^{2,2}\ln\left(\frac{\mu^2}{M_{\phi'}^{2,2}}\right). \tag{D.9}$$

Table D.1: The coefficients $\xi_{\phi,\phi'}$ in Eq. (D.8).

	$\pi^\pm$
$\xi_{\phi,\pi^\pm}$	0
ξ_{ϕ,π^0}	$-5m_u-5m_d-2m_s-12(m_u+m_d)\cos(2\varepsilon)-(m_u+m_d-2m_s)\cos(4\varepsilon)+\sqrt{3}(m_d-m_u)\sin(4\varepsilon)$
$\xi_{\phi,\eta}$	$-5m_u-5m_d-2m_s+12(m_u+m_d)\cos(2\varepsilon)-(m_u+m_d-2m_s)\cos(4\varepsilon)+\sqrt{3}(m_d-m_u)\sin(4\varepsilon)$
$\xi_{\phi,K^\pm}$	0
ξ_{ϕ,K^0}	0

Table D.2: The coefficients $\xi_{\phi,\phi'}$ in Eq. (D.8).

	π^0
$\xi_{\phi,\pi^\pm}$	$2\left(-5m_u-5m_d-2m_s-12(m_u+m_d)\cos(2\varepsilon)-(m_u+m_d-2m_s)\cos(4\varepsilon)+\sqrt{3}(m_d-m_u)\sin(4\varepsilon)\right)$
ξ_{ϕ,π^0}	$2\left(6(m_u+m_d+m_s)+4(m_u+m_d-2m_s)\cos(2\varepsilon)-(m_u+m_d-2m_s)\cos(4\varepsilon)-\sqrt{3}(m_d-m_u)(4\sin(2\varepsilon)+\sin(4\varepsilon))\right)$
$\xi_{\phi,\eta}$	$2\left(2(m_u+m_d+m_s)+(m_u+m_d-2m_s)\cos(4\varepsilon)+\sqrt{3}(m_d-m_u)\sin(4\varepsilon)\right)$
$\xi_{\phi,K^\pm}$	$2\left(-5m_u-2m_d-5m_s+6(m_u+m_s)\cos(2\varepsilon)-(m_d-2m_u+m_s)\cos(4\varepsilon)-\sqrt{3}\left((m_d-m_s)\sin(4\varepsilon)+6(m_u+m_s)\sin(2\varepsilon)\right)\right)$
ξ_{ϕ,K^0}	$2\left(-2m_u-5m_d-5m_s+6(m_d+m_s)\cos(2\varepsilon)-(m_u-2m_d+m_s)\cos(4\varepsilon)+\sqrt{3}\left((m_u-m_s)\sin(4\varepsilon)+6(m_d+m_s)\sin(2\varepsilon)\right)\right)$

Table D.3: The coefficients $\xi_{\phi,\phi'}$ in Eq. (D.8).

	η
$\xi_{\phi,\pi^\pm}$	$2\left(-5m_u-5m_d-2m_s+12(m_u+m_d)\cos(2\varepsilon)-(m_u+m_d-2m_s)\cos(4\varepsilon)+\sqrt{3}(m_d-m_u)\sin(4\varepsilon)\right)$
ξ_{ϕ,π^0}	$2\left(2(m_u+m_d+m_s)+(m_u+m_d-2m_s)\cos(4\varepsilon)+\sqrt{3}(m_d-m_u)\sin(4\varepsilon)\right)$
$\xi_{\phi,\eta}$	$2\left(6(m_u+m_d+m_s)-4(m_u+m_d-2m_s)\cos(2\varepsilon)-(m_u+m_d-2m_s)\cos(4\varepsilon)+\sqrt{3}(m_d-m_u)(4\sin(2\varepsilon)-\sin(4\varepsilon))\right)$
$\xi_{\phi,K^\pm}$	$2\left(-5m_u-2m_d-5m_s-6(m_u+m_s)\cos(2\varepsilon)-(m_d-2m_u+m_s)\cos(4\varepsilon)-\sqrt{3}\left((m_d-m_s)\sin(4\varepsilon)-6(m_u+m_s)\sin(2\varepsilon)\right)\right)$
ξ_{ϕ,K^0}	$2\left(-2m_u-5m_d-5m_s-6(m_d+m_s)\cos(2\varepsilon)-(m_u-2m_d+m_s)\cos(4\varepsilon)+\sqrt{3}\left((m_u-m_s)\sin(4\varepsilon)-6(m_d+m_s)\sin(2\varepsilon)\right)\right)$

Table D.4: The coefficients $\xi_{\phi,\phi'}$ in Eq. (D.8).

	$K^{\pm}$
$\xi_{\phi,\pi^{\pm}}$	0
ξ_{ϕ,π^0}	$-5m_u-2m_d-5m_s+6(m_u+m_s)\cos(2\varepsilon)-(m_d+m_s-2m_u)\cos(4\varepsilon)+\sqrt{3}\,((m_s-m_d)\sin(4\varepsilon)-6(m_u+m_s)\sin(2\varepsilon))$
$\xi_{\phi,\eta}$	$-5m_u-2m_d-5m_s-6(m_u+m_s)\cos(2\varepsilon)-(m_d+m_s-2m_u)\cos(4\varepsilon)+\sqrt{3}\,((m_s-m_d)\sin(4\varepsilon)+6(m_u+m_s)\sin(2\varepsilon))$
$\xi_{\phi,K^{\pm}}$	0
ξ_{ϕ,K^0}	0

Table D.5: The coefficients $\xi_{\phi,\phi'}$ in Eq. (D.8).

	K^0
$\xi_{\phi,\pi^{\pm}}$	0
ξ_{ϕ,π^0}	$-2m_u-5m_d-5m_s+6(m_d+m_s)\cos(2\varepsilon)-(m_u+m_s-2m_d)\cos(4\varepsilon)+\sqrt{3}\,((m_u-m_s)\sin(4\varepsilon)+6(m_d+m_s)\sin(2\varepsilon))$
$\xi_{\phi,\eta}$	$-2m_u-5m_d-5m_s-6(m_d+m_s)\cos(2\varepsilon)-(m_u+m_s-2m_d)\cos(4\varepsilon)+\sqrt{3}\,((m_u-m_s)\sin(4\varepsilon)-6(m_d+m_s)\sin(2\varepsilon))$
$\xi_{\phi,K^{\pm}}$	0
ξ_{ϕ,K^0}	0

Table D.6: The coefficients $\xi_{\phi,qq'}$ in Eq. (D.8).

	$\pi^{\pm}$	$K^{\pm}$	K^0
$\xi_{\phi,uu}$	$2L_4+L_5-4L_6-2L_8$	$2L_4+L_5-4L_6-2L_8$	0
$\xi_{\phi,dd}$	$2L_4+L_5-4L_6-2L_8$	0	$2L_4+L_5-4L_6-2L_8$
$\xi_{\phi,ss}$	0	$2L_4+L_5-4L_6-2L_8$	$2L_4+L_5-4L_6-2L_8$
$\xi_{\phi,ud}$	$4L_4+2L_5-8L_6-4L_8$	$2L_4-4L_6$	$2L_4-4L_6$
$\xi_{\phi,us}$	$2L_4-4L_6$	$4L_4+2L_5-8L_6-4L_8$	$2L_4-4L_6$
$\xi_{\phi,ds}$	$2L_4-4L_6$	$2L_4-4L_6$	$4L_4+2L_5-8L_6-4L_8$
	π^0		
$\xi_{\pi^0,uu}$	$\frac{1}{9}[6(2L_4+L_5-4L_6-4L_7-4L_8)+2\sqrt{3}\sin(2\varepsilon)(3L_4+2L_5-6L_6-6L_7-6L_8+L_5\cos(2\varepsilon))]$ $+\frac{1}{9}[2\cos(2\varepsilon)(3L_4+2L_5-6L_6-6L_7-6L_8)-\cos(4\varepsilon)L_5]$		
$\xi_{\pi^0,dd}$	$\frac{1}{9}[6(2L_4+L_5-4L_6-4L_7-4L_8)-2\sqrt{3}\sin(2\varepsilon)(3L_4+2L_5-6L_6-6L_7-6L_8+L_5\cos(2\varepsilon))]$ $+\frac{1}{9}[2\cos(2\varepsilon)(3L_4+2L_5-6L_6-6L_7-6L_8)-\cos(4\varepsilon)L_5]$		
$\xi_{\pi^0,ss}$	$\frac{8}{9}\sin^2(2\varepsilon)\,(3L_4+L_5-6L_6-6L_7-6L_8-L_5\cos(2\varepsilon))$		
$\xi_{\pi^0,ud}$	$\frac{2}{9}\,(3(4L_4+L_5-8L_6+4L_7)+2\cos(2\varepsilon)(3L_4+2L_5-6L_6+12L_7)+2\cos(4\varepsilon)L_5)$		
$\xi_{\pi^0,us}$	$\frac{2}{9}[3(4L_4+L_5-8L_6+4L_7)+\sqrt{3}\sin(2\varepsilon)(3L_4+2L_5-6L_6+12L_7-2L_5\cos(2\varepsilon))]$ $-\frac{2}{9}[\cos(2\varepsilon)(3L_4+2L_5-6L_6+12L_7)+\cos(4\varepsilon)L_5]$		
$\xi_{\pi^0,ds}$	$\frac{2}{9}[3(4L_4+L_5-8L_6+4L_7)-\sqrt{3}\sin(2\varepsilon)(3L_4+2L_5-6L_6+12L_7-2L_5\cos(2\varepsilon))]$ $-\frac{2}{9}[\cos(2\varepsilon)(3L_4+2L_5-6L_6+12L_7)+\cos(4\varepsilon)L_5]$		
	η		
$\xi_{\eta,uu}$	$\frac{1}{9}[6(2L_4+L_5-4L_6-4L_7-4L_8)-2\sqrt{3}\sin(2\varepsilon)(3L_4+2L_5-6L_6-6L_7-6L_8-L_5\cos(2\varepsilon))]$ $-\frac{1}{9}[2\cos(2\varepsilon)(3L_4+2L_5-6L_6-6L_7-6L_8)+\cos(4\varepsilon)L_5]$		
$\xi_{\eta,dd}$	$\frac{1}{9}[6(2L_4+L_5-4L_6-4L_7-4L_8)+2\sqrt{3}\sin(2\varepsilon)(3L_4+2L_5-6L_6-6L_7-6L_8-L_5\cos(2\varepsilon))]$ $-\frac{1}{9}[2\cos(2\varepsilon)(3L_4+2L_5-6L_6-6L_7-6L_8)+\cos(4\varepsilon)L_5]$		
$\xi_{\eta,ss}$	$\frac{8}{9}\cos^2(\varepsilon)\,(3L_4+L_5-6L_6-6L_7-6L_8+L_5\cos(2\varepsilon))$		
$\xi_{\eta,ud}$	$\frac{2}{9}\,(3(4L_4+L_5-8L_6+4L_7)-2\cos(2\varepsilon)(3L_4+2L_5-6L_6+12L_7)+2\cos(4\varepsilon)L_5)$		
$\xi_{\eta,us}$	$\frac{2}{9}[3(4L_4+L_5-8L_6+4L_7)-\sqrt{3}\sin(2\varepsilon)(3L_4+2L_5-6L_6+12L_7+2L_5\cos(2\varepsilon))]$ $+\frac{2}{9}[\cos(2\varepsilon)(3L_4+2L_5-6L_6+12L_7)-\cos(4\varepsilon)L_5]$		
$\xi_{\eta,ds}$	$\frac{2}{9}[3(4L_4+L_5-8L_6+4L_7)+\sqrt{3}\sin(2\varepsilon)(3L_4+2L_5-6L_6+12L_7+2L_5\cos(2\varepsilon))]$ $+\frac{2}{9}[\cos(2\varepsilon)(3L_4+2L_5-6L_6+12L_7)-\cos(4\varepsilon)L_5]$		

Strong isospin-breaking effects on octet baryon masses

The effective pseudoscalar meson-octet baryon Lagrangians have been given in Eq. (4.3) of Chatper 4. Due to the isospin breaking of u and d quarks, the quark mass matrix $\mathcal{M} ==\mathrm{diag}(m_l, m_l, m_s)$ (with $m_l \equiv m_u = m_d$) appeared in Eq. (4.3) should be replaced by $\mathcal{M} = \mathrm{diag}(m_u, m_d, m_s)$. After calculating the Feynman diagrams given in Fig. 4.1, we can obtain the strong isospin-breaking effects on octet baryon masses up to $\mathrm{N^3LO}$,

$$m_B = m_0 + m_B^{(2)} + m_B^{(3)} + m_B^{(4)}, \tag{D.10}$$

where the leading order contribution is

$$m_B^{(2)} = -\xi_{B,u}^{(a)} B_0 m_u - \xi_{B,d}^{(a)} B_0 m_d - \xi_{B,s}^{(a)} B_0 m_s, \tag{D.11}$$

with the coefficients $\xi_{B,u}^{(a)}$, $\xi_{B,d}^{(a)}$, and $\xi_{B,s}^{(a)}$ tabulated in Table D.7.

Table D.7: The coefficients $\xi_{B,u}^{(a)}$, $\xi_{B,d}^{(a)}$, and $\xi_{B,s}^{(a)}$ in Eq. (D.11).

B	$\xi_{B,u}^{(a)}$	$\xi_{B,d}^{(a)}$	$\xi_{B,s}^{(a)}$
p	$4(b_0+b_D+b_F)$	$4b_0$	$4(b_0+b_D-b_F)$
n	$4b_0$	$4(b_0+b_D+b_F)$	$4(b_0+b_D-b_F)$
Λ	$\frac{4}{3}(3b_0+b_D)$	$\frac{4}{3}(3b_0+b_D)$	$\frac{4}{3}(3b_0+4b_D)$
Σ^+	$4(b_0+b_D+b_F)$	$4(b_0+b_D-b_F)$	$4b_0$
Σ^0	$4(b_0+b_D)$	$4(b_0+b_D)$	$4b_0$
Σ^-	$4(b_0+b_D-b_F)$	$4(b_0+b_D+b_F)$	$4b_0$
Ξ^0	$4b_0$	$4(b_0+b_D-b_F)$	$4(b_0+b_D+b_F)$
Ξ^-	$4(b_0+b_D-b_F)$	$4b_0$	$4(b_0+b_D+b_F)$

At $\mathcal{O}(p^3)$, the chiral corrections to the baryon self-energies can be expressed as

$$m_B^{(3)} = \frac{1}{(4\pi F_\phi)^2} \sum_{\phi=\pi^{\pm,0},\ K^{\pm,0},\ \eta} \xi_{B,\phi}^{(b)} H_B^{(b)}(M_\phi), \tag{D.12}$$

where the loop function $H_B^{(b)}(M_\phi)$ is already given in Eq. (4.26), and the coefficients $\xi_{B,\phi}^{(b)}$ given in Table D.8.

Table D.8: The coefficients $\xi_{B,\phi}^{(b)}$ in Eq. (D.12).

	$\pi^\pm$	π^0	K^0	$K^\pm$	η
p	$(D+F)^2$	$\frac{1}{18}\left(\sqrt{3}(D-3F)\sin(\varepsilon)-3(D+F)\cos(\varepsilon)\right)^2$	$(D-F)^2$	$\frac{2}{3}(D^2+3F^2)$	$\frac{1}{18}\left(\sqrt{3}(D-3F)\cos(\varepsilon)+3(D+F)\sin(\varepsilon)\right)^2$
n	$(D+F)^2$	$\frac{1}{18}\left(\sqrt{3}(D-3F)\sin(\varepsilon)+3(D+F)\cos(\varepsilon)\right)^2$	$\frac{2}{3}(D^2+F^2)$	$(D-F)^2$	$\frac{1}{18}\left(\sqrt{3}(D-3F)\cos(\varepsilon)-3(D+F)\sin(\varepsilon)\right)^2$
Λ	$\frac{4}{3}D^2$	$\frac{2}{3}D^2$	$\frac{1}{3}(D^2+9F^2)$	$\frac{1}{3}(D^2+9F^2)$	$\frac{2}{3}D^2$
Σ^+	$\frac{2}{3}(D^2+3F^2)$	$\frac{2}{9}\left(\sqrt{3}D\sin(\varepsilon)+3F\cos(\varepsilon)\right)^2$	$(D-F)^2$	$(D+F)^2$	$\frac{2}{9}\left(\sqrt{3}D\cos(\varepsilon)-3F\sin(\varepsilon)\right)^2$
Σ^0	$4F^2$	$\frac{2}{3}D^2$	D^2+F^2	D^2+F^2	$\frac{2}{3}D^2$
Σ^-	$\frac{2}{3}(D^2+3F^2)$	$\frac{2}{9}\left(\sqrt{3}D\sin(\varepsilon)-3F\cos(\varepsilon)\right)^2$	$(D+F)^2$	$(D-F)^2$	$\frac{2}{9}\left(\sqrt{3}D\cos(\varepsilon)+3F\sin(\varepsilon)\right)^2$
Ξ^0	$(D-F)^2$	$\frac{1}{18}\left(\sqrt{3}(D+3F)\sin(\varepsilon)+3(D-F)\cos(\varepsilon)\right)^2$	$\frac{2}{3}(D^2+3F^2)$	$(D+F)^2$	$\frac{1}{18}\left(\sqrt{3}(D+3F)\cos(\varepsilon)-3(D-F)\sin(\varepsilon)\right)^2$
Ξ^-	$(D-F)^2$	$\frac{1}{18}\left(\sqrt{3}(D+3F)\sin(\varepsilon)-3(D-F)\cos(\varepsilon)\right)^2$	$(D+F)^2$	$\frac{2}{3}(D^2+3F^2)$	$\frac{1}{18}\left(\sqrt{3}(D+3F)\cos(\varepsilon)+3(D-F)\sin(\varepsilon)\right)^2$

Up to N^{3}LO, the contributions to octet baryon masses are

$$\begin{aligned}
m_B^{(4)} &= \xi^{(c)}_{B,u^2} B_0^2 m_u^2 + \xi^{(c)}_{B,d^2} B_0^2 m_d^2 + \xi^{(c)}_{B,s^2} B_0^2 m_s^2 \\
&+ \xi^{(c)}_{B,ud} B_0^2 m_u m_d + \xi^{(c)}_{B,us} B_0^2 m_u m_s + \xi^{(c)}_{B,ds} B_0^2 m_d m_s \\
&+ \frac{1}{(4\pi F_\phi)^2} \sum_{\phi=\pi^{\pm,0},\ K^{\pm,0},\ \eta} \left(\xi^{(d,1)}_{B,\phi} H_B^{(d,1)}(M_\phi) + \xi^{(d,2)}_{B,\phi} H_B^{(d,2)}(M_\phi) + \xi^{(d,3)}_{B,\phi} H_B^{(d,3)}(M_\phi) \right) \\
&+ \frac{1}{(4\pi F_\phi)^2} \sum_{\substack{\phi=\pi^{\pm,0},\ K^{\pm,0},\ \eta \\ B'=p,n,\Lambda,\Sigma^+,\Sigma^0,\Sigma^-,\Xi^0,\Xi^-}} \xi^{(e)}_{BB',\phi} \cdot H^{(e)}_{B,B'}(M_\phi),
\end{aligned} \tag{D.13}$$

where the loop functions are given in Eqs. (4.28) and (4.31), and the coefficients are listed in Tables (D.9-D.20).

Table D.9: The coefficients $\xi^{(c)}_{B,u^2}$, $\xi^{(c)}_{B,d^2}$, $\xi^{(c)}_{B,s^2}$, $\xi^{(c)}_{B,ud}$, $\xi^{(c)}_{B,us}$, and $\xi^{(c)}_{B,ds}$ in Eq. (D.13).

	$\xi^{(c)}_{B,u^2}$	$\xi^{(c)}_{B,d^2}$	$\xi^{(c)}_{B,s^2}$
p	$-16(d_1+d_2+d_3+d_5+d_7+d_8)$	$-16(d_7+d_8)$	$-16(d_1-d_2+d_3-d_5+d_7+d_8)$
n	$-16(d_7+d_8)$	$-16(d_1+d_2+d_3+d_5+d_7+d_8)$	$-16(d_1-d_2+d_3-d_5+d_7+d_8)$
Λ	$-\frac{8}{3}(4d_3+d_4+6d_7+6d_8)$	$-\frac{8}{3}(4d_3+d_4+6d_7+6d_8)$	$-\frac{8}{3}(16d_3+4d_4+6d_7+6d_8)$
Σ^+	$-16(d_1+d_2+d_3+d_5+d_7+d_8)$	$-16(d_1-d_2+d_3-d_5+d_7+d_8)$	$-16(d_7+d_8)$
Σ^0	$-8(4d_3+d_4+2d_7+2d_8)$	$-8(4d_3+d_4+2d_7+2d_8)$	$-16(d_7+d_8)$
Σ^-	$-16(d_1-d_2+d_3-d_5+d_7+d_8)$	$-16(d_1+d_2+d_3+d_5+d_7+d_8)$	$-16(d_7+d_8)$
Ξ^0	$-16(d_7+d_8)$	$-16(d_1-d_2+d_3-d_5+d_7+d_8)$	$-16(d_1+d_2+d_3+d_5+d_7+d_8)$
Ξ^-	$-16(d_1-d_2+d_3-d_5+d_7+d_8)$	$-16(d_7+d_8)$	$-16(d_1+d_2+d_3+d_5+d_7+d_8)$
	$\xi^{(c)}_{B,ud}$	$\xi^{(c)}_{B,us}$	$\xi^{(c)}_{B,ds}$
p	$-16(d_5+2d_7)$	$-16(-2d_1+2d_3+2d_7)$	$-16(2d_7-d_5)$
n	$-16(d_5+2d_7)$	$-16(2d_7-d_5)$	$-16(-2d_1+2d_3+2d_7)$
Λ	$-\frac{16}{3}(d_4+6d_7)$	$-\frac{32}{3}(3d_7-d_4)$	$-\frac{32}{3}(3d_7-d_4)$
Σ^+	$-32(-d_1+d_3+d_7)$	$-16(d_5+2d_7)$	$-16(2d_7-d_5)$
Σ^0	$-16(2d_7-d_4)$	$-32d_7$	$-32d_7$
Σ^-	$-32(-d_1+d_3+d_7)$	$-16(2d_7-d_5)$	$-16(d_5+2d_7)$
Ξ^0	$-16(2d_7-d_5)$	$-16(d_5+2d_7)$	$-32(-d_1+d_3+d_7)$
Ξ^-	$-16(2d_7-d_5)$	$-32(-d_1+d_3+d_7)$	$-16(d_5+2d_7)$

Table D.10: The coefficients $\xi^{(d,1)}_{B,\phi}$ in Eq. (D.13).

	π^0 $\quad \xi^{(d,1)}_{B,\pi^0} = \xi_{\pi^0,u} B_0 m_u + \xi_{\pi^0,d} B_0 m_d + \xi_{\pi^0,s} B_0 m_s$		
	$\xi_{\pi^0,u}$	$\xi_{\pi^0,d}$	$\xi_{\pi^0,s}$
p	$-\frac{2}{3}(b_0+b_D+b_F)\left(\sqrt{3}\sin(2\varepsilon)+\cos(2\varepsilon)+2\right)$	$-\frac{2}{3}b_0\left(-\sqrt{3}\sin(2\varepsilon)+\cos(2\varepsilon)+2\right)$	$-\frac{8}{3}(b_0+b_D-b_F)\sin^2(\varepsilon)$
n	$-\frac{2}{3}b_0\left(\sqrt{3}\sin(2\varepsilon)+\cos(2\varepsilon)+2\right)$	$-\frac{2}{3}(b_0+b_D+b_F)\left(-\sqrt{3}\sin(2\varepsilon)+\cos(2\varepsilon)+2\right)$	$-\frac{8}{3}(b_0+b_D-b_F)\sin^2(\varepsilon)$
Λ	$-\frac{2}{9}(3b_0+b_D)\left(\sqrt{3}\sin(2\varepsilon)+\cos(2\varepsilon)+2\right)$	$-\frac{2}{9}(3b_0+b_D)\left(-\sqrt{3}\sin(2\varepsilon)+\cos(2\varepsilon)+2\right)$	$-\frac{8}{9}(3b_0+4b_D)\sin^2(\varepsilon)$
Σ^+	$-\frac{2}{3}(b_0+b_D+b_F)\left(\sqrt{3}\sin(2\varepsilon)+\cos(2\varepsilon)+2\right)$	$-\frac{2}{3}(b_0+b_D-b_F)\left(-\sqrt{3}\sin(2\varepsilon)+\cos(2\varepsilon)+2\right)$	$-\frac{8}{3}b_0\sin^2(\varepsilon)$
Σ^0	$-\frac{2}{3}(b_0+b_D)\left(\sqrt{3}\sin(2\varepsilon)+\cos(2\varepsilon)+2\right)$	$-\frac{2}{3}(b_0+b_D)\left(-\sqrt{3}\sin(2\varepsilon)+\cos(2\varepsilon)+2\right)$	$-\frac{8}{3}b_0\sin^2(\varepsilon)$
Σ^-	$-\frac{2}{3}(b_0+b_D-b_F)\left(\sqrt{3}\sin(2\varepsilon)+\cos(2\varepsilon)+2\right)$	$-\frac{2}{3}(b_0+b_D+b_F)\left(-\sqrt{3}\sin(2\varepsilon)+\cos(2\varepsilon)+2\right)$	$-\frac{8}{3}b_0\sin^2(\varepsilon)$
Ξ^0	$-\frac{2}{3}b_0\left(\sqrt{3}\sin(2\varepsilon)+\cos(2\varepsilon)+2\right)$	$-\frac{2}{3}(b_0+b_D-b_F)\left(-\sqrt{3}\sin(2\varepsilon)+\cos(2\varepsilon)+2\right)$	$-\frac{8}{3}(b_0+b_D+b_F)\sin^2(\varepsilon)$
Ξ^-	$-\frac{2}{3}(b_0+b_D-b_F)\left(\sqrt{3}\sin(2\varepsilon)+\cos(2\varepsilon)+2\right)$	$-\frac{2}{3}b_0\left(-\sqrt{3}\sin(2\varepsilon)+\cos(2\varepsilon)+2\right)$	$-\frac{8}{3}(b_0+b_D+b_F)\sin^2(\varepsilon)$

	η $\quad \xi^{(d,1)}_{B,\eta} = \xi_{\eta,u} B_0 m_u + \xi_{\eta,d} B_0 m_d + \xi_{\eta,s} B_0 m_s$		
	$\xi_{\eta,u}$	$\xi_{\eta,d}$	$\xi_{\eta,s}$
p	$\frac{2}{3}(b_0+b_D+b_F)\left(\sqrt{3}\sin(2\varepsilon)+\cos(2\varepsilon)-2\right)$	$\frac{2}{3}b_0\left(-\sqrt{3}\sin(2\varepsilon)+\cos(2\varepsilon)-2\right)$	$-\frac{8}{3}(b_0+b_D-b_F)\cos^2(\varepsilon)$
n	$\frac{2}{3}b_0\left(\sqrt{3}\sin(2\varepsilon)+\cos(2\varepsilon)-2\right)$	$\frac{2}{3}(b_0+b_D+b_F)\left(-\sqrt{3}\sin(2\varepsilon)+\cos(2\varepsilon)-2\right)$	$-\frac{8}{3}(b_0+b_D-b_F)\cos^2(\varepsilon)$
Λ	$\frac{2}{9}(3b_0+b_D)\left(\sqrt{3}\sin(2\varepsilon)+\cos(2\varepsilon)-2\right)$	$\frac{2}{9}(3b_0+b_D)\left(-\sqrt{3}\sin(2\varepsilon)+\cos(2\varepsilon)-2\right)$	$-\frac{8}{9}(3b_0+4b_D)\cos^2(\varepsilon)$
Σ^+	$\frac{2}{3}(b_0+b_D+b_F)\left(\sqrt{3}\sin(2\varepsilon)+\cos(2\varepsilon)-2\right)$	$\frac{2}{3}(b_0+b_D-b_F)\left(-\sqrt{3}\sin(2\varepsilon)+\cos(2\varepsilon)-2\right)$	$-\frac{8}{3}b_0\cos^2(\varepsilon)$
Σ^0	$\frac{2}{3}(b_0+b_D)\left(\sqrt{3}\sin(2\varepsilon)+\cos(2\varepsilon)-2\right)$	$\frac{2}{3}(b_0+b_D)\left(-\sqrt{3}\sin(2\varepsilon)+\cos(2\varepsilon)-2\right)$	$-\frac{8}{3}b_0\cos^2(\varepsilon)$
Σ^-	$\frac{2}{3}(b_0+b_D-b_F)\left(\sqrt{3}\sin(2\varepsilon)+\cos(2\varepsilon)-2\right)$	$\frac{2}{3}(b_0+b_D+b_F)\left(-\sqrt{3}\sin(2\varepsilon)+\cos(2\varepsilon)-2\right)$	$-\frac{8}{3}b_0\cos^2(\varepsilon)$
Ξ^0	$\frac{2}{3}b_0\left(\sqrt{3}\sin(2\varepsilon)+\cos(2\varepsilon)-2\right)$	$\frac{2}{3}(b_0+b_D-b_F)\left(-\sqrt{3}\sin(2\varepsilon)+\cos(2\varepsilon)-2\right)$	$-\frac{8}{3}(b_0+b_D+b_F)\cos^2(\varepsilon)$
Ξ^-	$\frac{2}{3}(b_0+b_D-b_F)\left(\sqrt{3}\sin(2\varepsilon)+\cos(2\varepsilon)-2\right)$	$\frac{2}{3}b_0\left(-\sqrt{3}\sin(2\varepsilon)+\cos(2\varepsilon)-2\right)$	$-\frac{8}{3}(b_0+b_D+b_F)\cos^2(\varepsilon)$

	$\pi^\pm$	K^0	$K^\pm$
p	$-2(2b_0+b_D+b_F)(m_u+m_d)B_0$	$-2(2b_0+b_D-b_F)(m_d+m_s)B_0$	$-4(b_0+b_D)(m_u+m_s)B_0$
n	$-2(2b_0+b_D+b_F)(m_u+m_d)B_0$	$-4(b_0+b_D)(m_d+m_s)B_0$	$-2(2b_0+b_D-b_F)(m_u+m_s)B_0$
Λ	$-\frac{4}{3}(3b_0+b_D)(m_u+m_d)B_0$	$-\frac{2}{3}(6b_0+5b_D)(m_d+m_s)B_0$	$-\frac{2}{3}(6b_0+5b_D)(m_u+m_s)B_0$
Σ^+	$-4(b_0+b_D)(m_u+m_d)B_0$	$-2(2b_0+b_D-b_F)(m_d+m_s)B_0$	$-2(2b_0+b_D+b_F)(m_u+m_s)B_0$
Σ^0	$-4(b_0+b_D)(m_u+m_d)B_0$	$-2(2b_0+b_D)(m_d+m_s)B_0$	$-2(2b_0+b_D)(m_u+m_s)B_0$
Σ^-	$-4(b_0+b_D)(m_u+m_d)B_0$	$-2(2b_0+b_D+b_F)(m_d+m_s)B_0$	$-2(2b_0+b_D-b_F)(m_u+m_s)B_0$
Ξ^0	$-2(2b_0+b_D-b_F)(m_u+m_d)B_0$	$-4(b_0+b_D)(m_d+m_s)B_0$	$-2(2b_0+b_D+b_F)(m_u+m_s)B_0$
Ξ^-	$-2(2b_0+b_D-b_F)(m_u+m_d)B_0$	$-2(2b_0+b_D+b_F)(m_d+m_s)B_0$	$-4(b_0+b_D)(m_u+m_s)B_0$

Table D.11: The coefficients $\xi^{(d,2)}_{B,\phi}$ in Eq. (D.13).

	π^0
p	$\frac{1}{3}\left(2(3b_1+b_3+3b_4)+(-3b_1+3b_2+b_3)\cos(2\varepsilon)+\sqrt{3}(3b_1+b_2-b_3)\sin(2\varepsilon)\right)$
n	$\frac{1}{3}\left(2(3b_1+b_3+3b_4)+(-3b_1+3b_2+b_3)\cos(2\varepsilon)-\sqrt{3}(3b_1+b_2-b_3)\sin(2\varepsilon)\right)$
Λ	$\frac{2}{3}(4b_3+3b_4-2b_3\cos(2\varepsilon))$
Σ^+	$\frac{2}{3}\left(3b_1+b_3+3b_4+(3b_1-b_3)\cos(2\varepsilon)+\sqrt{3}b_2\sin(2\varepsilon)\right)$
Σ^0	$\frac{2}{3}(4b_3+3b_4+2b_3\cos(2\varepsilon))$
Σ^-	$\frac{2}{3}\left(3b_1+b_3+3b_4+(3b_1-b_3)\cos(2\varepsilon)-\sqrt{3}b_2\sin(2\varepsilon)\right)$
Ξ^0	$\frac{1}{3}\left(2(3b_1+b_3+3b_4)-(3b_1+3b_2-b_3)\cos(2\varepsilon)-\sqrt{3}(3b_1-b_2-b_3)\sin(2\varepsilon)\right)$
Ξ^-	$\frac{1}{3}\left(2(3b_1+b_3+3b_4)-(3b_1+3b_2-b_3)\cos(2\varepsilon)+\sqrt{3}(3b_1-b_2-b_3)\sin(2\varepsilon)\right)$
	η
p	$\frac{1}{3}\left(2(3b_1+b_3+3b_4)-(-3b_1+3b_2+b_3)\cos(2\varepsilon)-\sqrt{3}(3b_1+b_2-b_3)\sin(2\varepsilon)\right)$
n	$\frac{1}{3}\left(2(3b_1+b_3+3b_4)-(-3b_1+3b_2+b_3)\cos(2\varepsilon)+\sqrt{3}(3b_1+b_2-b_3)\sin(2\varepsilon)\right)$
Λ	$\frac{2}{3}(4b_3+3b_4+2b_3\cos(2\varepsilon))$
Σ^+	$\frac{2}{3}\left(3b_1+b_3+3b_4-(3b_1-b_3)\cos(2\varepsilon)-\sqrt{3}b_2\sin(2\varepsilon)\right)$
Σ^0	$\frac{2}{3}(4b_3+3b_4-2b_3\cos(2\varepsilon))$
Σ^-	$\frac{2}{3}\left(3b_1+b_3+3b_4-(3b_1-b_3)\cos(2\varepsilon)+\sqrt{3}b_2\sin(2\varepsilon)\right)$
Ξ^0	$\frac{1}{3}\left(2(3b_1+b_3+3b_4)+(3b_1+3b_2-b_3)\cos(2\varepsilon)+\sqrt{3}(3b_1-b_2-b_3)\sin(2\varepsilon)\right)$
Ξ^-	$\frac{1}{3}\left(2(3b_1+b_3+3b_4)+(3b_1+3b_2-b_3)\cos(2\varepsilon)-\sqrt{3}(3b_1-b_2-b_3)\sin(2\varepsilon)\right)$

	$\pi^\pm$	K^0	$K^\pm$
p	$2(b_1+b_2+b_3+2b_4)$	$2(b_1-b_2+b_3+2b_4)$	$4(b_1+b_3+b_4)$
n	$2(b_1+b_2+b_3+2b_4)$	$4(b_1+b_3+b_4)$	$2(b_1-b_2+b_3+2b_4)$
Λ	$\frac{4}{3}(2b_3+3b_4)$	$\frac{2}{3}(9b_1+b_3+6b_4)$	$\frac{2}{3}(9b_1+b_3+6b_4)$
Σ^+	$4(b_1+b_3+b_4)$	$2(b_1-b_2+b_3+2b_4)$	$2(b_1+b_2+b_3+2b_4)$
Σ^0	$4(2b_1+b_4)$	$2(b_1+b_3+2b_4)$	$2(b_1+b_3+2b_4)$
Σ^-	$4(b_1+b_3+b_4)$	$2(b_1+b_2+b_3+2b_4)$	$2(b_1-b_2+b_3+2b_4)$
Ξ^0	$2(b_1-b_2+b_3+2b_4)$	$4(b_1+b_3+b_4)$	$2(b_1+b_2+b_3+2b_4)$
Ξ^-	$2(b_1-b_2+b_3+2b_4)$	$2(b_1+b_2+b_3+2b_4)$	$4(b_1+b_3+b_4)$

Table D.12: The coefficients $\xi^{(d,3)}_{B,\phi}$ in Eq. (D.13).

	π^0
p	$\frac{2}{3}\left(3(b_5+b_6+b_7+2b_8)\cos(\varepsilon)+\sqrt{3}(3b_5+3b_6-b_7)\sin(\varepsilon)\right)$
n	$\frac{2}{3}\left(3(b_5+b_6+b_7+2b_8)\cos(\varepsilon)-\sqrt{3}(3b_5+3b_6-b_7)\sin(\varepsilon)\right)$
Λ	$\frac{4}{3}(2b_7+3b_8)\cos(\varepsilon)$
Σ^+	$4(2b_5+b_8)\cos(\varepsilon)$
Σ^0	$4(2b_7+b_8)\cos(\varepsilon)$
Σ^-	$4(2b_5+b_8)\cos(\varepsilon)$
Ξ^0	$\frac{2}{3}\left(3(b_5-b_6+b_7+2b_8)\cos(\varepsilon)-\sqrt{3}(3b_5-3b_6-b_7)\sin(\varepsilon)\right)$
Ξ^-	$\frac{2}{3}\left(3(b_5-b_6+b_7+2b_8)\cos(\varepsilon)+\sqrt{3}(3b_5-3b_6-b_7)\sin(\varepsilon)\right)$

	η
p	$\frac{2}{3}\left((9b_5-3b_6+b_7+6b_8)\cos(\varepsilon)-\sqrt{3}(3b_5-b_6-b_7)\sin(\varepsilon)\right)$
n	$\frac{2}{3}\left((9b_5-3b_6+b_7+6b_8)\cos(\varepsilon)+\sqrt{3}(3b_5-b_6-b_7)\sin(\varepsilon)\right)$
Λ	$4(2b_7+b_8)\cos(\varepsilon)$
Σ^+	$\frac{4}{3}\left((2b_7+3b_8)\cos(\varepsilon)-2\sqrt{3}b_6\sin(\varepsilon)\right)$
Σ^0	$\frac{4}{3}(2b_7+3b_8)\cos(\varepsilon)$
Σ^-	$\frac{4}{3}\left((2b_7+3b_8)\cos(\varepsilon)+2\sqrt{3}b_6\sin(\varepsilon)\right)$
Ξ^0	$\frac{2}{3}\left((9b_5+3b_6+b_7+6b_8)\cos(\varepsilon)+\sqrt{3}(3b_5+b_6-b_7)\sin(\varepsilon)\right)$
Ξ^-	$\frac{2}{3}\left((9b_5+3b_6+b_7+6b_8)\cos(\varepsilon)-\sqrt{3}(3b_5+b_6-b_7)\sin(\varepsilon)\right)$

	$\pi^\pm$	K^0	$K^\pm$
p	$4(b_5+b_6+b_7+2b_8)$	$4(b_5-b_6+b_7+2b_8)$	$8(b_5+b_7+b_8)$
n	$4(b_5+b_6+b_7+2b_8)$	$8(b_5+b_7+b_8)$	$4(b_5-b_6+b_7+2b_8)$
Λ	$\frac{8}{3}(2b_7+3b_8)$	$\frac{4}{3}(9b_5+b_7+6b_8)$	$\frac{4}{3}(9b_5+b_7+6b_8)$
Σ^+	$8(b_5+b_7+b_8)$	$4(b_5-b_6+b_7+2b_8)$	$4(b_5+b_6+b_7+2b_8)$
Σ^0	$8(2b_5+b_8)$	$4(b_5+b_7+2b_8)$	$4(b_5+b_7+2b_8)$
Σ^-	$8(b_5+b_7+b_8)$	$4(b_5+b_6+b_7+2b_8)$	$4(b_5-b_6+b_7+2b_8)$
Ξ^0	$4(b_5-b_6+b_7+2b_8)$	$8(b_5+b_7+b_8)$	$4(b_5+b_6+b_7+2b_8)$
Ξ^-	$4(b_5-b_6+b_7+2b_8)$	$4(b_5+b_6+b_7+2b_8)$	$8(b_5+b_7+b_8)$

Table D.13: The coefficients $\xi^{(e)}_{pB',\phi}$ in Eq. (D.13).

	$\pi^\pm$	π^0	K^0	$K^\pm$	η
p	0	$\frac{1}{36}\Big[3(D+F)\cos(\varepsilon)$ $-\sqrt{3}(D-3F)\sin(\varepsilon)\Big]^2$	0	0	$\frac{1}{36}\Big[3(D+F)\sin(\varepsilon)$ $+\sqrt{3}(D-3F)\cos(\varepsilon)\Big]^2$
n	$\frac{1}{2}(D+F)^2$	0	0	0	0
Λ	0	0	0	$\frac{1}{12}(D+3F)^2$	0
Σ^+	0	0	$\frac{1}{2}(D-F)^2$	0	0
Σ^0	0	0	0	$\frac{1}{4}(D-F)^2$	0
Σ^-	0	0	0	0	0
Ξ^0	0	0	0	0	0
Ξ^-	0	0	0	0	0

Table D.14: The coefficients $\xi^{(e)}_{nB',\phi}$ in Eq. (D.13).

	$\pi^{\pm}$	π^0	K^0	$K^{\pm}$	η
p	$\frac{1}{2}(D+F)^2$	0	0	0	0
n	0	$\frac{1}{36}\Big[3(D+F)\cos(\varepsilon)$ $+\sqrt{3}(D-3F)\sin(\varepsilon)\Big]^2$	0	0	$\frac{1}{36}\Big[3(D+F)\sin(\varepsilon)$ $-\sqrt{3}(D-3F)\cos(\varepsilon)\Big]^2$
Λ	0	0	$\frac{1}{12}(D+3F)^2$	0	0
Σ^+	0	0	0	0	0
Σ^0	0	0	$\frac{1}{4}(D-F)^2$	0	0
Σ^-	0	0	0	$\frac{1}{2}(D-F)^2$	0
Ξ^0	0	0	0	0	0
Ξ^-	0	0	0	0	0

Table D.15: The coefficients $\xi^{(e)}_{\Lambda B',\phi}$ in Eq. (D.13).

	$\pi^{\pm}$	π^0	K^0	$K^{\pm}$	η
p	0	0	0	$\frac{1}{12}(D+3F)^2$	0
n	0	0	$\frac{1}{12}(D+3F)^2$	0	0
Λ	0	$\frac{1}{3}D^2\sin^2(\varepsilon)$	0	0	$\frac{1}{3}D^2\cos^2(\varepsilon)$
Σ^+	$\frac{D^2}{3}$	0	0	0	0
Σ^0	0	$\frac{1}{3}D^2\cos^2(\varepsilon)$	0	0	$\frac{1}{3}D^2\sin^2(\varepsilon)$
Σ^-	$\frac{D^2}{3}$	0	0	0	0
Ξ^0	0	0	$\frac{1}{12}(D-3F)^2$	0	0
Ξ^+	0	0	0	$\frac{1}{12}(D-3F)^2$	0

Table D.16: The coefficients $\xi^{(e)}_{\Sigma^+ B',\phi}$ in Eq. (D.13).

	$\pi^{\pm}$	π^0	K^0	$K^{\pm}$	η
p	0	0	$\frac{1}{2}(D-F)^2$	0	0
n	0	0	0	0	0
Λ	$\frac{1}{3}D^2$	0	0	0	0
Σ^+	0	$\frac{1}{9}\left(3F\cos(\varepsilon)+\sqrt{3}D\sin(\varepsilon)\right)^2$	0	0	$\frac{1}{9}\left(3F\sin(\varepsilon)-\sqrt{3}D\cos(\varepsilon)\right)^2$
Σ^0	F^2	0	0	0	0
Σ^-	0	0	0	0	
Ξ^0	0	0	0	$\frac{1}{2}(D+F)^2$	0
Ξ^-	0	0	0	0	0

Table D.17: The coefficients $\xi^{(e)}_{\Sigma^0 B',\phi}$ in Eq. (D.13).

	$\pi^{\pm}$	π^0	K^0	$K^{\pm}$	η
p	0	0	0	$\frac{1}{4}(D-F)^2$	0
n	0	0	$\frac{1}{4}(D-F)^2$	0	0
Λ	0	$\frac{1}{3}D^2\cos^2(\varepsilon)$	0	0	$\frac{1}{3}D^2\sin^2(\varepsilon)$
Σ^+	F^2	0	0	0	0
Σ^0	0	$\frac{1}{3}D^2\sin^2(\varepsilon)$	0	0	$\frac{1}{3}D^2\cos^2(\varepsilon)$
Σ^-	F^2	0	0	0	0
Ξ^0	0	0	$\frac{1}{4}(D+F)^2$	0	0
Ξ^-	0	0	0	$\frac{1}{4}(D+F)^2$	0

Table D.18: The coefficients $\xi^{(e)}_{\Sigma^- B',\phi}$ in Eq. (D.13).

	$\pi^{\pm}$	π^0	K^0	$K^{\pm}$	η
p	0	0	0	0	0
n	0	0	0	$\frac{1}{2}(D-F)^2$	0
Λ	$\frac{1}{3}D^2$	0	0	0	0
Σ^+	0	0	0	0	0
Σ^0	F^2	0	0	0	0
Σ^-	0	$\frac{1}{9}\left(3F\cos(\varepsilon)-\sqrt{3}D\sin(\varepsilon)\right)^2$	0	0	$\frac{1}{9}\left(3F\sin(\varepsilon)+\sqrt{3}D\cos(\varepsilon)\right)^2$
Ξ^0	0	0	0	0	0
Ξ	0	0	$\frac{1}{2}(D+F)^2$	0	0

Table D.19: The coefficients $\xi^{(e)}_{\Xi^0 B',\phi}$ in Eq. (D.13).

	$\pi^{\pm}$	π^0	K^0	$K^{\pm}$	η
p	0	0	0	0	0
n	0	0	0	0	0
Λ	0	0	$\frac{1}{12}(D-3F)^2$	0	0
Σ^+	0	0	0	$\frac{1}{2}(D+F)^2$	0
Σ^0	0	0	$\frac{1}{4}(D+F)^2$	0	0
Σ^-	0	0	0	0	0
Ξ^0	0	$\frac{1}{36}\Big[3(D-F)\cos(\varepsilon)$ $+\sqrt{3}(D+3F)\sin(\varepsilon)\Big]^2$	0	0	$\frac{1}{36}\Big[3(D-F)\sin(\varepsilon)$ $-\sqrt{3}(D+3F)\cos(\varepsilon)\Big]^2$
Ξ^-	$\frac{1}{2}(D-F)^2$	0	0	0	0

Table D.20: The coefficients $\xi^{(e)}_{\Xi^- B',\phi}$ in Eq. (D.13).

	$\pi^{\pm}$	π^0	K^0	$K^{\pm}$	η
p	0	0	0	0	0
n	0	0	0	0	0
Λ	0	0	0	$\frac{1}{12}(D-3F)^2$	0
Σ^+	0	0	0	0	0
Σ^0	0	0	0	$\frac{1}{4}(D+F)^2$	0
Σ^-	0	0	$\frac{1}{2}(D+F)^2$	0	0
Ξ^0	$\frac{1}{2}(D-F)^2$	0	0	0	0
Ξ^-	0	$\frac{1}{36}\Big[3(D-F)\cos(\varepsilon) -\sqrt{3}(D+3F)\sin(\varepsilon)\Big]^2$	0	0	$\frac{1}{36}\Big[3(D-F)\sin(\varepsilon) +\sqrt{3}(D+3F)\cos(\varepsilon)\Big]^2$

Bibliography

[1] I. Newton, A. Motte, and J. Machin. *The Mathematical Principles of Natural Philosophy*. Number Volume 1 in The Mathematical Principles of Natural Philosophy. B. Motte, 1729.

[2] A. Einstein. Die grundlage der allgemeinen relativitätstheorie. *Annalen der Physik*, 354(7):769–822, 1916.

[3] R. v. Eötvös. *Mathematische und Naturwissenschaftliche Berichte aus Ungarn*, 8(65), 1890.

[4] F. Englert and R. Brout. Broken Symmetry and the Mass of Gauge Vector Mesons. *Phys.Rev.Lett.*, 13:321–323, 1964.

[5] P. W. Higgs. Spontaneous Symmetry Breakdown without Massless Bosons. *Phys.Rev.*, 145:1156–1163, 1966.

[6] G. Guralnik, C. Hagen, and T. Kibble. Global Conservation Laws and Massless Particles. *Phys.Rev.Lett.*, 13:585–587, 1964.

[7] G. Aad et al. Observation of a new particle in the search for the Standard Model Higgs boson with the ATLAS detector at the LHC. *Phys.Lett.*, B716:1–29, 2012.

[8] S. Chatrchyan et al. Observation of a new boson at a mass of 125 GeV with the CMS experiment at the LHC. *Phys.Lett.*, B716:30–61, 2012.

[9] J. Thomson. Cathode rays. *Phil.Mag.*, 44:293–316, 1897.

[10] E. Rutherford. The scattering of alpha and beta particles by matter and the structure of the atom. *Phil.Mag.*, 21:669–688, 1911.

[11] J. Chadwick. Possible Existence of a Neutron. *Nature*, 129:312, 1932.

[12] M. Gell-Mann. A Schematic Model of Baryons and Mesons. *Phys.Lett.*, 8:214–215, 1964.

[13] G. Zweig. An su(3) model for strong interaction symmetry and its breaking. version 2. pages 22–101, 1964.

[14] A. Einstein. Ist die trägheit eines körpers von seinem energieinhalt abhängig? *Annalen der Physik*, 323(13):639–641, 1905.

[15] K. Olive et al. Review of Particle Physics. *Chin.Phys.*, C38:090001, 2014.

[16] S. Bethke. Experimental tests of asymptotic freedom. *Prog. Part. Nucl. Phys.*, 58:351–386, 2013.

[17] K. G. Wilson. Confinement of Quarks. *Phys.Rev.*, D10:2445–2459, 1974.

[18] H. Hamber and G. Parisi. Numerical Estimates of Hadronic Masses in a Pure SU(3) Gauge Theory. *Phys.Rev.Lett.*, 47:1792, 1981.

[19] D. Weingarten. Monte Carlo Evaluation of Hadron Masses in Lattice Gauge Theories with Fermions. *Phys.Lett.*, B109:57, 1982.

[20] A. Ali Khan et al. Light hadron spectroscopy with two flavors of dynamical quarks on the lattice. *Phys.Rev.*, D65:054505, 2002.

[21] S. Prelovsek, C. Dawson, T. Izubuchi, K. Orginos, and A. Soni. Scalar meson in dynamical and partially quenched two-flavor QCD: Lattice results and chiral loops. *Phys.Rev.*, D70:094503, 2004.

[22] S. Dürr, Z. Fodor, J. Frison, C. Hoelbling, R. Hoffmann, et al. Ab-Initio Determination of Light Hadron Masses. *Science*, 322:1224–1227, 2008.

[23] S. Aoki et al. 2+1 Flavor Lattice QCD toward the Physical Point. *Phys.Rev.*, D79:034503, 2009.

[24] S. Aoki et al. Physical Point Simulation in 2+1 Flavor Lattice QCD. *Phys.Rev.*, D81:074503, 2010.

[25] A. Walker-Loud, H.-W. Lin, D. Richards, R. Edwards, M. Engelhardt, et al. Light hadron spectroscopy using domain wall valence quarks on an Asqtad sea. *Phys.Rev.*, D79:054502, 2009.

[26] H.-W. Lin et al. First results from 2+1 dynamical quark flavors on an anisotropic lattice: Light-hadron spectroscopy and setting the strange-quark mass. *Phys.Rev.*, D79:034502, 2009.

[27] W. Bietenholz, V. Bornyakov, N. Cundy, M. Gockeler, R. Horsley, et al. Tuning the strange quark mass in lattice simulations. *Phys.Lett.*, B690:436–441, 2010.

[28] W. Bietenholz, V. Bornyakov, M. Gockeler, R. Horsley, W. Lockhart, et al. Flavour blindness and patterns of flavour symmetry breaking in lattice simulations of up, down and strange quarks. *Phys.Rev.*, D84:054509, 2011.

[29] S. Beane, E. Chang, W. Detmold, H. Lin, T. Luu, et al. High Statistics Analysis using Anisotropic Clover Lattices: (IV) Volume Dependence of Light Hadron Masses. *Phys.Rev.*, D84:014507, 2011.

[30] S. Durr, Z. Fodor, C. Hoelbling, S. Katz, S. Krieg, et al. Lattice QCD at the physical point: Simulation and analysis details. *JHEP*, 1108:148, 2011.

[31] A. Bazavov et al. Lattice QCD ensembles with four flavors of highly improved staggered quarks. *Phys.Rev.*, D87:054505, 2013.

[32] S. Weinberg. Phenomenological Lagrangians. *Physica*, A96:327, 1979.

[33] J. Gasser and H. Leutwyler. Chiral Perturbation Theory to One Loop. *Annals Phys.*, 158:142, 1984.

[34] J. Gasser and H. Leutwyler. Chiral Perturbation Theory: Expansions in the Mass of the Strange Quark. *Nucl.Phys.*, B250:465, 1985.

[35] J. Gasser, M. Sainio, and A. Svarc. Nucleons with Chiral Loops. *Nucl.Phys.*, B307:779, 1988.

[36] U. G. Meissner. Recent developments in chiral perturbation theory. *Rept. Prog. Phys.*, 56:903–996, 1993.

[37] H. Leutwyler. Principles of chiral perturbation theory. *arXiv:hep-ph/9406283*, pages 1–46, 1994.

[38] V. Bernard, N. Kaiser, and U.-G. Meissner. Chiral dynamics in nucleons and nuclei. *Int.J.Mod.Phys.*, E4:193–346, 1995.

[39] A. Pich. Chiral perturbation theory. *Rept.Prog.Phys.*, 58:563–610, 1995.

[40] G. Ecker. Chiral perturbation theory. *Prog.Part.Nucl.Phys.*, 35:1–80, 1995.

[41] A. Pich. Effective field theory: Course. *arXiv:hep-ph/9806303*, pages 949–1049, 1998.

[42] S. Scherer. Introduction to chiral perturbation theory. *Adv. Nucl. Phys.*, 27:277, 2003.

[43] V. Bernard and U.-G. Meissner. Chiral perturbation theory. *Ann.Rev.Nucl.Part.Sci.*, 57:33–60, 2007.

[44] J. Bijnens. Chiral perturbation theory beyond one loop. *Prog.Part.Nucl.Phys.*, 58:521–586, 2007.

[45] V. Bernard. Chiral Perturbation Theory and Baryon Properties. *Prog.Part.Nucl.Phys.*, 60:82–160, 2008.

[46] S. Scherer and M. R. Schindler. *A Primer for Chiral Perturbation Theory.* Spinger, Heidelberg Germany, 2012.

[47] E. E. Jenkins. Baryon masses in chiral perturbation theory. *Nucl.Phys.*, B368:190–203, 1992.

[48] V. Bernard, N. Kaiser, and U. G. Meissner. Critical analysis of baryon masses and sigma terms in heavy baryon chiral perturbation theory. *Z.Phys.*, C60:111–120, 1993.

[49] M. Banerjee and J. Milana. Baryon mass splittings in chiral perturbation theory. *Phys.Rev.*, D52:6451–6460, 1995.

[50] B. Borasoy and U.-G. Meissner. Chiral Expansion of Baryon Masses and σ-Terms. *Annals Phys.*, 254:192–232, 1997.

[51] A. Walker-Loud. Octet baryon masses in partially quenched chiral perturbation theory. *Nucl.Phys.*, A747:476–507, 2005.

[52] P. Ellis and K. Torikoshi. Baryon masses in chiral perturbation theory with infrared regularization. *Phys.Rev.*, C61:015205, 2000.

[53] M. Frink and U.-G. Meissner. Chiral extrapolations of baryon masses for unquenched three flavor lattice simulations. *JHEP*, 0407:028, 2004.

[54] M. Frink, U.-G. Meissner, and I. Scheller. Baryon masses, chiral extrapolations, and all that. *Eur.Phys.J.*, A24:395–409, 2005.

[55] B. Lehnhart, J. Gegelia, and S. Scherer. Baryon masses and nucleon sigma terms in manifestly Lorentz-invariant baryon chiral perturbation theory. *J.Phys.*, G31:89–104, 2005.

[56] J. Martin Camalich, L. Geng, and M. Vicente Vacas. The lowest-lying baryon masses in covariant SU(3)-flavor chiral perturbation theory. *Phys.Rev.*, D82:074504, 2010.

[57] L. S. Geng, X.-L. Ren, J. Martin-Camalich, and W. Weise. Finite-volume effects on octet-baryon masses in covariant baryon chiral perturbation theory. *Phys.Rev.*, D84:074024, 2011.

[58] R. Young and A. Thomas. Octet baryon masses and sigma terms from an SU(3) chiral extrapolation. *Phys.Rev.*, D81:014503, 2010.

[59] A. Semke and M. Lutz. Baryon self energies in the chiral loop expansion. *Nucl.Phys.*, A778:153–180, 2006.

[60] A. Semke and M. Lutz. On the possibility of a discontinuous quark-mass dependence of baryon octet and decuplet masses. *Nucl.Phys.*, A789:251–259, 2007.

[61] A. Semke and M. Lutz. On the quark-mass dependence of the baryon ground-state masses. *Phys.Rev.*, D85:034001, 2012.

[62] P. C. Bruns, L. Greil, and A. Schafer. Chiral extrapolation of baryon mass ratios. 2012.

[63] M. Lutz and A. Semke. On the consistency of recent QCD lattice data of the baryon ground-state masses. *Phys.Rev.*, D86:091502, 2012.

[64] X. L. Ren, L. S. Geng, J. Martin Camalich, J. Meng, and H. Toki. Octet baryon masses in next-to-next-to-next-to-leading order covariant baryon chiral perturbation theory. *JHEP*, 12:073, 2012.

[65] X.-L. Ren, L. S. Geng, J. Meng, and H. Toki. Virtual decuplet effects on octet baryon masses in covariant baryon chiral perturbation theory. *Phys.Rev.*, D87:074001, 2013.

[66] X.-L. Ren, L.-S. Geng, and J. Meng. Decuplet baryon masses in covariant baryon chiral perturbation theory. *Phys.Rev.*, D89:054034, 2014.

[67] X.-L. Ren, L.-S. Geng, and J. Meng. Baryon chiral perturbation theory with Wilson fermions up to $\mathcal{O}(a^2)$ and discretization effects of latest $n_f = 2 + 1$ LQCD octet baryon masses. *Eur.Phys.J.*, C74:2754, 2014.

[68] X.-L. Ren, L.-S. Geng, and J. Meng. Scalar strangeness content of the nucleon and baryon sigma terms. *Phys. Rev.*, D91:051502, 2015.

[69] E. E. Jenkins and A. V. Manohar. Baryon chiral perturbation theory using a heavy fermion Lagrangian. *Phys.Lett.*, B255:558–562, 1991.

[70] T. Becher and H. Leutwyler. Baryon chiral perturbation theory in manifestly Lorentz invariant form. *Eur.Phys.J.*, C9:643–671, 1999.

[71] J. Gegelia and G. Japaridze. Matching heavy particle approach to relativistic theory. *Phys.Rev.*, D60:114038, 1999.

[72] T. Fuchs, J. Gegelia, G. Japaridze, and S. Scherer. Renormalization of relativistic baryon chiral perturbation theory and power counting. *Phys.Rev.*, D68:056005, 2003.

[73] V. Bernard, T. R. Hemmert, and U.-G. Meissner. Cutoff schemes in chiral perturbation theory and the quark mass expansion of the nucleon mass. *Nucl.Phys.*, A732:149–170, 2004.

[74] R. D. Young, D. B. Leinweber, and A. W. Thomas. Convergence of chiral effective field theory. *Prog.Part.Nucl.Phys.*, 50:399–417, 2003.

[75] D. B. Leinweber, A. W. Thomas, and R. D. Young. Physical nucleon properties from lattice QCD. *Phys.Rev.Lett.*, 92:242002, 2004.

[76] K.-I. Ishikawa et al. SU(2) and SU(3) chiral perturbation theory analyses on baryon masses in 2+1 flavor lattice QCD. *Phys.Rev.*, D80:054502, 2009.

[77] J. Gasser and H. Leutwyler. Light Quarks at Low Temperatures. *Phys.Lett.*, B184:83, 1987.

[78] J. Gasser and H. Leutwyler. Spontaneously Broken Symmetries: Effective Lagrangians at Finite Volume. *Nucl.Phys.*, B307:763, 1988.

[79] M. Luscher. Volume Dependence of the Energy Spectrum in Massive Quantum Field Theories. 1. Stable Particle States. *Commun. Math. Phys.*, 104:177, 1986.

[80] A. Ali Khan et al. The Nucleon mass in $N_f = 2$ lattice QCD: Finite size effects from chiral perturbation theory. *Nucl.Phys.*, B689:175–194, 2004.

[81] M. Procura, B. Musch, T. Wollenweber, T. Hemmert, and W. Weise. Nucleon mass: From lattice QCD to the chiral limit. *Phys.Rev.*, D73:114510, 2006.

[82] K. Symanzik. Continuum Limit and Improved Action in Lattice Theories. 1. Principles and ϕ^4 Theory. *Nucl.Phys.*, B226:187, 1983.

[83] K. Symanzik. Continuum Limit and Improved Action in Lattice Theories. 2. $O(N)$ Nonlinear Sigma Model in Perturbation Theory. *Nucl.Phys.*, B226:205, 1983.

[84] B. Sheikholeslami and R. Wohlert. Improved Continuum Limit Lattice Action for QCD with Wilson Fermions. *Nucl.Phys.*, B259:572, 1985.

[85] M. Luscher, S. Sint, R. Sommer, and P. Weisz. Chiral symmetry and $O(a)$ improvement in lattice QCD. *Nucl.Phys.*, B478:365–400, 1996.

[86] G. Rupak and N. Shoresh. Chiral perturbation theory for the Wilson lattice action. *Phys.Rev.*, D66:054503, 2002.

[87] O. Bar, G. Rupak, and N. Shoresh. Simulations with different lattice Dirac operators for valence and sea quarks. *Phys.Rev.*, D67:114505, 2003.

[88] S. Aoki. Chiral perturbation theory with Wilson type fermions including a^2 effects: $N_f = 2$ degenerate case. *Phys.Rev.*, D68:054508, 2003.

[89] O. Bar, G. Rupak, and N. Shoresh. Chiral perturbation theory at $O(a^2)$ for lattice QCD. *Phys.Rev.*, D70:034508, 2004.

[90] S. R. Beane and M. J. Savage. Nucleon properties at finite lattice spacing in chiral perturbation theory. *Phys.Rev.*, D68:114502, 2003.

[91] B. C. Tiburzi. Baryon masses at $O(a^2)$ in chiral perturbation theory. *Nucl.Phys.*, A761:232–258, 2005.

[92] H. R. Grigoryan and A. W. Thomas. Vector meson mass corrections at $O(a^2)$ in PQChPT with Wilson and Ginsparg-Wilson quarks. *Phys.Lett.*, B632:657–662, 2006.

[93] D. Arndt and B. C. Tiburzi. Hadronic electromagnetic properties at finite lattice spacing. *Phys.Rev.*, D69:114503, 2004.

[94] P. F. Bedaque, M. I. Buchoff, and A. Walker-Loud. Effective Field Theory for the Anisotropic Wilson Lattice Action. *Phys.Rev.*, D77:074501, 2008.

[95] C. Aubin and C. Bernard. Pion and kaon masses in staggered chiral perturbation theory. *Phys.Rev.*, D68:034014, 2003.

[96] C. Aubin and C. Bernard. Pseudoscalar decay constants in staggered chiral perturbation theory. *Phys.Rev.*, D68:074011, 2003.

[97] S. R. Sharpe and R. S. Van de Water. Staggered chiral perturbation theory at next-to-leading order. *Phys.Rev.*, D71:114505, 2005.

[98] B. C. Tiburzi. Baryons with Ginsparg-Wilson quarks in a staggered sea. *Phys.Rev.*, D72:094501, 2005.

[99] C. Aubin and C. Bernard. Staggered chiral perturbation theory with heavy-light mesons. *Nucl.Phys.Proc.Suppl.*, 140:491–493, 2005.

[100] C. Aubin and C. Bernard. Staggered chiral perturbation theory for heavy-light mesons. *Phys.Rev.*, D73:014515, 2006.

[101] C. Aubin and C. Bernard. Heavy-light semileptonic decays in staggered chiral perturbation theory. *Phys.Rev.*, D76:014002, 2007.

[102] C. Bernard and J. Komijani. Chiral Perturbation Theory for All-Staggered Heavy-Light Mesons. *Phys.Rev.*, D88:094017, 2013.

[103] L. Scorzato. Pion mass splitting and phase structure in twisted mass QCD. *Eur.Phys.J.*, C37:445–455, 2004.

[104] S. R. Sharpe and J. M. Wu. The Phase diagram of twisted mass lattice QCD. *Phys.Rev.*, D70:094029, 2004.

[105] S. R. Sharpe and J. M. Wu. Twisted mass chiral perturbation theory at next-to-leading order. *Phys.Rev.*, D71:074501, 2005.

[106] A. Walker-Loud and J. M. Wu. Nucleon and Delta masses in twisted mass chiral perturbation theory. *Phys.Rev.*, D72:014506, 2005.

[107] S. R. Sharpe. Observations on discretization errors in twisted-mass lattice QCD. *Phys.Rev.*, D72:074510, 2005.

[108] M. I. Buchoff, J.-W. Chen, and A. Walker-Loud. pi-pi Scattering in Twisted Mass Chiral Perturbation Theory. *Phys.Rev.*, D79:074503, 2009.

[109] G. Munster and T. Sudmann. Twisted mass chiral perturbation theory for 2+1+1 quark flavours. *JHEP*, 1104:116, 2011.

[110] P. Damgaard, K. Splittorff, and J. Verbaarschot. Microscopic Spectrum of the Wilson Dirac Operator. *Phys.Rev.Lett.*, 105:162002, 2010.

[111] G. Akemann, P. Damgaard, K. Splittorff, and J. Verbaarschot. Spectrum of the Wilson Dirac Operator at Finite Lattice Spacings. *Phys.Rev.*, D83:085014, 2011.

[112] M. T. Hansen and S. R. Sharpe. Constraint on the Low Energy Constants of Wilson Chiral Perturbation Theory. *Phys.Rev.*, D85:014503, 2012.

[113] M. T. Hansen and S. R. Sharpe. Determining low-energy constants in partially quenched Wilson chiral perturbation theory. *Phys.Rev.*, D85:054504, 2012.

[114] G. Herdoiza, K. Jansen, C. Michael, K. Ottnad, and C. Urbach. Determination of Low-Energy Constants of Wilson Chiral Perturbation Theory. *JHEP*, 1305:038, 2013.

[115] S. Puglia, M. Ramsey-Musolf, and S.-L. Zhu. Octet baryon charge radii, chiral symmetry and decuplet intermediate states. *Phys.Rev.*, D63:034014, 2001.

[116] E. E. Jenkins and A. V. Manohar. Chiral corrections to the baryon axial currents. *Phys.Lett.*, B259:353–358, 1991.

[117] M. Luty and . White, Martin J. Decouplet contributions to hyperon axial vector form-factors. *Phys.Lett.*, B319:261–268, 1993.

[118] L. Geng, J. Martin Camalich, and M. Vicente Vacas. Leading-order decuplet contributions to the baryon magnetic moments in Chiral Perturbation Theory. *Phys.Lett.*, B676:63–68, 2009.

[119] J. Alarcon, L. Geng, J. Martin Camalich, and J. Oller. The strangeness content of the nucleon from effective field theory and phenomenology. *Phys.Lett.*, B730:342–346, 2014.

[120] I. Montvay and G. Munster. *Quantum fields on a lattice*, volume 2264 of *Cambridge monographs on mathematical physics*. Cambridge University Press, Cambridge, England, 1994.

[121] R. Gupta. Introduction to lattice QCD: Course. *arXiv:hep-lat/9807028*, pages 83–219, 1997.

[122] M. Di Pierro. From Monte Carlo integration to lattice quantum chromodynamics: An Introduction. In *GSA Summer School on Physics on the Frontier and in the Future Batavia, Illinois, July 31-August 7, 2000*, 2000.

[123] J. Smit. Introduction to quantum fields on a lattice: A robust mate. *Cambridge Lect.Notes Phys.*, 15:1–271, 2002.

[124] H. Rothe. Lattice gauge theories: An Introduction. *World Sci.Lect.Notes Phys.*, 43:1–381, 1992.

[125] T. DeGrand and C. E. Detar. *Lattice Methods for Quantum Chromodynamics.* World Scientific Publishing Co Pte Ltd, 2006.

[126] P. Hagler. Hadron structure from lattice quantum chromodynamics. *Phys. Rept.*, 490:49–175, 2010.

[127] C. Gattringer and C. B. Lang. *Quantum Chromodynamics on the Lattice - An Introductory Presentation.* Springer, Heidelberg Germany, 2010.

[128] Z. Fodor and C. Hoelbling. Light Hadron Masses from Lattice QCD. *Rev.Mod.Phys.*, 84:449, 2012.

[129] S. Aoki et al. Review of lattice results concerning low-energy particle physics. *Eur. Phys. J.*, C74:2890, 2014.

[130] P. A. Dirac. The Lagrangian in quantum mechanics. *Phys.Z.Sowjetunion*, 3:64–72, 1933.

[131] R. P. Feynman and A. R. Hibbs. *Quantum Mechanics and Path Integrals.* McGraw-Hill Companies; First Edition edition, 1965.

[132] G. P. Lepage. Lattice QCD for novices. In *Strong interactions at low and intermediate energies. Proceedings, 13th Annual Hampton University Graduate Studies, HUGS'98, Newport News, USA, May 26-June 12, 1998*, pages 49–90, 1998.

[133] A. Ukawa. Computational cost of full QCD simulations experienced by CP-PACS and JLQCD Collaborations. *Nucl. Phys. Proc. Suppl.*, 106:195–196, 2002. [,195(2002)].

[134] L. Del Debbio, L. Giusti, M. Luscher, R. Petronzio, and N. Tantalo. QCD with light Wilson quarks on fine lattices (I): First experiences and physics results. *JHEP*, 02:056, 2007.

[135] E. Witten. Global Aspects of Current Algebra. *Nucl. Phys.*, B223:422–432, 1983.

[136] D. B. Kaplan. Chiral Symmetry and Lattice Fermions. In *Modern perspectives in lattice QCD: Quantum field theory and high performance computing. Proceedings, International School, 93rd Session, Les Houches, France, August 3-28, 2009*, pages 223–272, 2009.

[137] J. B. Kogut and L. Susskind. Hamiltonian Formulation of Wilson's Lattice Gauge Theories. *Phys.Rev.*, D11:395–408, 1975.

[138] T. Banks, L. Susskind, and J. B. Kogut. Strong Coupling Calculations of Lattice Gauge Theories: (1+1)-Dimensional Exercises. *Phys.Rev.*, D13:1043, 1976.

[139] L. Susskind. Lattice Fermions. *Phys.Rev.*, D16:3031–3039, 1977.

[140] K. G. Wilson. *Proceedings of the First Half of the 1975 International School of Subnuclear Physics, Erice, Sicily, edited by A. Zichichi (Plenum Press, New York)*, page 69, 1975.

[141] R. Frezzotti, P. A. Grassi, S. Sint, and P. Weisz. A Local formulation of lattice QCD without unphysical fermion zero modes. *Nucl.Phys.Proc.Suppl.*, 83:941–946, 2000.

[142] R. Frezzotti, P. A. Grassi, S. Sint, and P. Weisz. Lattice QCD with a chirally twisted mass term. *JHEP*, 0108:058, 2001.

[143] P. H. Ginsparg and K. G. Wilson. A Remnant of Chiral Symmetry on the Lattice. *Phys.Rev.*, D25:2649, 1982.

[144] R. Narayanan and H. Neuberger. A Construction of lattice chiral gauge theories. *Nucl.Phys.*, B443:305–385, 1995.

[145] P. Hasenfratz, V. Laliena, and F. Niedermayer. The Index theorem in QCD with a finite cutoff. *Phys.Lett.*, B427:125–131, 1998.

[146] M. Luscher. Exact chiral symmetry on the lattice and the Ginsparg-Wilson relation. *Phys.Lett.*, B428:342–345, 1998.

[147] C. Michael. Adjoint Sources in Lattice Gauge Theory. *Nucl.Phys.*, B259:58, 1985.

[148] M. Luscher and U. Wolff. How to Calculate the Elastic Scattering Matrix in Two-dimensional Quantum Field Theories by Numerical Simulation. *Nucl.Phys.*, B339:222–252, 1990.

[149] C. N. Papanicolas and E. Stiliaris. A novel method of data analysis for hadronic physics. *arXiv:1205.6505*, 2012.

[150] C. Alexandrou, T. Leontiou, C. N. Papanicolas, and E. Stiliaris. Novel analysis method for excited states in lattice QCD: The nucleon case. *Phys. Rev.*, D91:014506, 2015.

[151] R. Sommer. Scale setting in lattice QCD. *PoS*, LATTICE2013:015, 2014.

[152] R. Sommer. A New way to set the energy scale in lattice gauge theories and its applications to the static force and alpha-s in SU(2) Yang-Mills theory. *Nucl.Phys.*, B411:839–854, 1994.

[153] M. Lüscher. Properties and uses of the Wilson flow in lattice QCD. *JHEP*, 08:071, 2010. [Erratum: JHEP03,092(2014)].

[154] S. Borsanyi et al. High-precision scale setting in lattice QCD. *JHEP*, 09:010, 2012.

[155] C. Morningstar, J. Bulava, B. Fahy, J. Foley, Y. C. Jhang, K. J. Juge, D. Lenkner, and C. H. Wong. Progress with excited states in lattice QCD. *AIP Conf. Proc.*, 1560:448–450, 2013.

[156] A. Abdel-Rehim et al. Nucleon and pion structure with lattice QCD simulations at physical value of the pion mass. *arXiv:1507.04936*, 2015.

[157] T. M. Doi, H. Suganuma, and T. Iritani. Lattice QCD analysis for relation between quark confinement and chiral symmetry breaking. In *11th Conference on Quark Confinement and the Hadron Spectrum (Confinement XI) St. Petersburg, Russia, September 8-12, 2014*, 2014.

[158] G. Aarts, F. Attanasio, B. Jäger, E. Seiler, D. Sexty, and I.-O. Stamatescu. QCD at nonzero chemical potential: recent progress on the lattice. In *11th Conference on Quark Confinement and the Hadron Spectrum (Confinement XI) St. Petersburg, Russia, September 8-12, 2014*, 2014.

[159] B. Blossier, P. Boucaud, M. Brinet, F. De Soto, V. Morenas, O. Pene, K. Petrov, and J. Rodriguez-Quintero. High statistics determination of the strong coupling constant in Taylor scheme and its OPE Wilson coefficient from lattice QCD with a dynamical charm. *Phys. Rev.*, D89:014507, 2014.

[160] C. Alexandrou, V. Drach, K. Jansen, C. Kallidonis, and G. Koutsou. Baryon spectrum with $N_f = 2 + 1 + 1$ twisted mass fermions. *Phys. Rev.*, D90(7):074501, 2014.

[161] J. Beringer et al. Review of Particle Physics (RPP). *Phys.Rev.*, D86:010001, 2012.

[162] L. D. Roper. Evidence for a P-11 Pion-Nucleon Resonance at 556 MeV. *Phys.Rev.Lett.*, 12:340–342, 1964.

[163] M. S. Mahbub, W. Kamleh, D. B. Leinweber, P. J. Moran, and A. G. Williams. Roper Resonance in 2+1 Flavor QCD. *Phys.Lett.*, B707:389–393, 2012.

[164] R. G. Edwards, J. J. Dudek, D. G. Richards, and S. J. Wallace. Excited state baryon spectroscopy from lattice QCD. *Phys.Rev.*, D84:074508, 2011.

[165] G. P. Engel, C. Lang, D. Mohler, and A. Schäfer. QCD with Two Light Dynamical Chirally Improved Quarks: Baryons. *Phys.Rev.*, D87:074504, 2013.

[166] C. Alexandrou, T. Korzec, G. Koutsou, and T. Leontiou. Nucleon Excited States in N_f=2 lattice QCD. *Phys.Rev.*, D89:034502, 2014.

[167] K.-F. Liu, Y. Chen, M. Gong, R. Sufian, M. Sun, et al. The Roper Puzzle. *PoS*, LATTICE2013:507, 2014.

[168] A. Manohar and H. Georgi. Chiral Quarks and the Nonrelativistic Quark Model. *Nucl. Phys.*, B234:189, 1984.

[169] H. Georgi. Effective field theory. *Ann.Rev.Nucl.Part.Sci.*, 43:209–252, 1993.

[170] D. B. Kaplan. Effective field theories. In *Beyond the standard model 5. Proceedings, 5th Conference, Balholm, Norway, April 29-May 4, 1997*, 1995.

[171] A. V. Manohar. Effective field theories. *Lect. Notes Phys.*, 479:311–362, 1997.

[172] P. F. Bedaque and U. van Kolck. Effective field theory for few nucleon systems. *Ann. Rev. Nucl. Part. Sci.*, 52:339–396, 2002.

[173] I. Z. Rothstein. TASI lectures on effective field theories. 2003.

[174] N. Brambilla, A. Pineda, J. Soto, and A. Vairo. Effective field theories for heavy quarkonium. *Rev. Mod. Phys.*, 77:1423, 2005.

[175] G. Ecker. Effective field theories. *arXiv:hep-ph/0507056*, 2005.

[176] C. P. Burgess. Introduction to Effective Field Theory. *Ann. Rev. Nucl. Part. Sci.*, 57:329–362, 2007.

[177] G. 't Hooft. A Planar Diagram Theory for Strong Interactions. *Nucl. Phys.*, B72:461, 1974.

[178] E. L. Hill. Hamilton's principle and the conservation theorems of mathematical physics. *Rev. Mod. Phys.*, 23:253–260, Jul 1951.

[179] E. Noether. Invariant Variation Problems. *Gott.Nachr.*, 1918:235–257, 1918.

[180] M. Gell-Mann and M. Levy. The axial vector current in beta decay. *Nuovo Cim.*, 16:705, 1960.

[181] J. Goldstone. Field Theories with Superconductor Solutions. *Nuovo Cim.*, 19:154–164, 1961.

[182] S. R. Coleman, J. Wess, and B. Zumino. Structure of phenomenological Lagrangians. 1. *Phys. Rev.*, 177:2239–2247, 1969.

[183] C. G. Callan, Jr., S. R. Coleman, J. Wess, and B. Zumino. Structure of phenomenological Lagrangians. 2. *Phys. Rev.*, 177:2247–2250, 1969.

[184] H. Georgi. *Weak Interactions and Modern Particle Theory.* 1984.

[185] M. Gell-Mann. The Eightfold Way: A Theory of strong interaction symmetry. 1961.

[186] S. Okubo. Note on Unitary Symmetry in Strong Interactions. *Progress of Theoretical Physics*, 27:949–966, May 1962.

[187] S. Okubo. Note on Unitary Symmetry in Strong Interaction. II: Excited States of Baryons. *Progress of Theoretical Physics*, 28:24–32, July 1962.

[188] A. Krause. Baryon Matrix Elements of the Vector Current in Chiral Perturbation Theory. *Helv. Phys. Acta*, 63:3–70, 1990.

[189] M. E. Luke and A. V. Manohar. Reparametrization invariance constraints on heavy particle effective field theories. *Phys. Lett.*, B286:348–354, 1992.

[190] G. Ecker and M. Mojzis. Low-energy expansion of the pion - nucleon Lagrangian. *Phys. Lett.*, B365:312–318, 1996.

[191] V. Bernard, N. Kaiser, and U.-G. Meissner. Nucleon electroweak form-factors: Analysis of their spectral functions. *Nucl. Phys.*, A611:429–441, 1996.

[192] N. Kaiser. Spectral functions of isoscalar scalar and isovector electromagnetic form-factors of the nucleon at two loop order. *Phys. Rev.*, C68:025202, 2003.

[193] H.-B. Tang. A New approach to chiral perturbation theory for matter fields. *arXiv:hep-ph/9607436*, 1996.

[194] P. J. Ellis and H.-B. Tang. Pion nucleon scattering in a new approach to chiral perturbation theory. *Phys. Rev.*, C57:3356–3375, 1998.

[195] V. Pascalutsa, B. R. Holstein, and M. Vanderhaeghen. A Derivative of the Gerasimov-Drell-Hearn sum rule. *Phys.Lett.*, B600:239–247, 2004.

[196] L. Geng, J. Martin Camalich, L. Alvarez-Ruso, and M. Vicente Vacas. Leading SU(3)-breaking corrections to the baryon magnetic moments in Chiral Perturbation Theory. *Phys.Rev.Lett.*, 101:222002, 2008.

[197] M. R. Schindler, J. Gegelia, and S. Scherer. Infrared regularization of baryon chiral perturbation theory reformulated. *Phys. Lett.*, B586:258–266, 2004.

[198] M. Dorati, T. A. Gail, and T. R. Hemmert. Chiral perturbation theory and the first moments of the generalized parton distributions in a nucleon. *Nucl. Phys.*, A798:96–131, 2008.

[199] L. Geng. Recent developments in SU(3) covariant baryon chiral perturbation theory. *Front.Phys.China.*, 8:328–348, 2013.

[200] A. Semke and M. Lutz. Strangeness in the baryon ground states. *Phys.Lett.*, B717:242–247, 2012.

[201] M. Lutz, R. Bavontaweepanya, C. Kobdaj, and K. Schwarz. On finite volume effects in the chiral extrapolation of baryon masses. *Phys.Rev.*, D90:054505, 2014.

[202] J. A. Oller, M. Verbeni, and J. Prades. Meson-baryon effective chiral lagrangians to $\mathcal{O}(q^3)$. *JHEP*, 0609:079, 2006.

[203] W. Rarita and J. Schwinger. On a theory of particles with half integral spin. *Phys. Rev.*, 60:61, 1941.

[204] L. M. Nath, B. Etemadi, and J. D. Kimel. Uniqueness of the interaction involving spin 3/2 particles. *Phys. Rev.*, D3:2153–2161, 1971.

[205] V. Pascalutsa. Quantization of an interacting spin-3/2 field and the Delta isobar. *Phys.Rev.*, D58:096002, 1998.

[206] V. Pascalutsa and R. Timmermans. Field theory of nucleon to higher spin baryon transitions. *Phys.Rev.*, C60:042201, 1999.

[207] L. Alvarez-Ruso, T. Ledwig, J. Martin Camalich, and M. Vicente-Vacas. Nucleon mass and pion-nucleon sigma term from a chiral analysis of lattice QCD data. *Phys.Rev.*, D88:054507, 2013.

[208] J. Bijnens and I. Jemos. A new global fit of the L_i^r at next-to-next-to-leading order in Chiral Perturbation Theory. *Nucl.Phys.*, B854:631–665, 2012.

[209] S. R. Beane. Nucleon masses and magnetic moments in a finite volume. *Phys.Rev.*, D70:034507, 2004.

[210] O. Bar. Chiral perturbation theory at non-zero lattice spacing. *Nucl.Phys.Proc.Suppl.*, 140:106–119, 2005.

[211] S. R. Sharpe and J. Singleton, Robert L. Spontaneous flavor and parity breaking with Wilson fermions. *Phys.Rev.*, D58:074501, 1998.

[212] W.-J. Lee and S. R. Sharpe. Partial flavor symmetry restoration for chiral staggered fermions. *Phys.Rev.*, D60:114503, 1999.

[213] G. Munster and C. Schmidt. Chiral perturbation theory for lattice QCD with a twisted mass term. *Europhys.Lett.*, 66:652–656, 2004.

[214] M. Luscher, S. Sint, R. Sommer, P. Weisz, and U. Wolff. Nonperturbative O(a) improvement of lattice QCD. *Nucl.Phys.*, B491:323–343, 1997.

[215] R. Frezzotti and G. Rossi. Chirally improving Wilson fermions-1: $O(a)$ improvement. *JHEP*, 0408:007, 2004.

[216] H.-H. Zhang, W.-B. Yan, and X.-S. Li. Trace Formulae of Characteristic Polynomial and Cayley-Hamilton's Theorem, and Applications to Chiral Perturbation Theory and General Relativity. *Commun.Theor.Phys.*, 49:801, 2008.

[217] G. Amoros, J. Bijnens, and P. Talavera. QCD isospin breaking in meson masses, decay constants and quark mass ratios. *Nucl.Phys.*, B602:87–108, 2001.

[218] M. Procura, T. R. Hemmert, and W. Weise. Nucleon mass, sigma term and lattice QCD. *Phys.Rev.*, D69:034505, 2004.

[219] P. Chen. Heavy quarks on anisotropic lattices: The Charmonium spectrum. *Phys.Rev.*, D64:034509, 2001.

[220] A. S. Kronfeld. Uses of effective field theory in lattice QCD: Chapter 39 in At the Frontiers of Particle Physics, Handbook of QCD. *arXiv:hep-lat/0205021*, 2002.

[221] S. Durr, Z. Fodor, C. Hoelbling, R. Hoffmann, S. Katz, et al. Scaling study of dynamical smeared-link clover fermions. *Phys.Rev.*, D79:014501, 2009.

[222] W.-C. Chang and J.-C. Peng. Flavor Structure of the Nucleon Sea. *Prog. Part. Nucl. Phys.*, 79:95–135, 2014.

[223] G. S. Bali et al. Strangeness Contribution to the Proton Spin from Lattice QCD. *Phys.Rev.Lett.*, 108:222001, 2012.

[224] Z. Ahmed et al. New Precision Limit on the Strange Vector Form Factors of the Proton. *Phys.Rev.Lett.*, 108:102001, 2012.

[225] T. Cheng. Chiral Symmetry and the Higgs Nucleon Coupling. *Phys.Rev.*, D38:2869, 1988.

[226] G. Aad et al. Expected Performance of the ATLAS Experiment - Detector, Trigger and Physics. *arXiv:0901.0512 [hep-ex]*, 2009.

[227] A. Bottino, F. Donato, N. Fornengo, and S. Scopel. Implications for relic neutralinos of the theoretical uncertainties in the neutralino nucleon cross-section. *Astropart.Phys.*, 13:215–225, 2000.

[228] J. Gasser, H. Leutwyler, and M. Sainio. Sigma term update. *Phys.Lett.*, B253:252–259, 1991.

[229] J. Alarcon, J. Martin Camalich, and J. Oller. The chiral representation of the πN scattering amplitude and the pion-nucleon sigma term. *Phys.Rev.*, D85:051503, 2012.

[230] K. Takeda et al. Nucleon strange quark content from two-flavor lattice QCD with exact chiral symmetry. *Phys.Rev.*, D83:114506, 2011.

[231] R. Babich, R. C. Brower, M. A. Clark, G. T. Fleming, J. C. Osborn, et al. Exploring strange nucleon form factors on the lattice. *Phys.Rev.*, D85:054510, 2012.

[232] G. S. Bali et al. The strange and light quark contributions to the nucleon mass from Lattice QCD. *Phys.Rev.*, D85:054502, 2012.

[233] S. Dinter et al. Sigma terms and strangeness content of the nucleon with $N_f = 2+1+1$ twisted mass fermions. *JHEP*, 1208:037, 2012.

[234] M. Engelhardt. Strange quark contributions to nucleon mass and spin from lattice QCD. *Phys.Rev.*, D86:114510, 2012.

[235] H. Ohki, K. Takeda, S. Aoki, S. Hashimoto, T. Kaneko, H. Matsufuru, J. Noaki, and T. Onogi. Nucleon strange quark content from $N_f = 2+1$ lattice QCD with exact chiral symmetry. *Phys. Rev.*, D87:034509, 2013.

[236] M. Gong, A. Alexandru, Y. Chen, T. Doi, S. Dong, et al. Strangeness and charmness content of nucleon from overlap fermions on 2+1-flavor domain-wall fermion configurations. *Phys.Rev.*, D88:014503, 2013.

[237] C. Alexandrou, M. Constantinou, S. Dinter, V. Drach, K. Hadjiyiannakou, K. Jansen, G. Koutsou, and A. Vaquero. Strangeness of the nucleon from lattice QCD. *Phys. Rev.*, D91:094503, 2015.

[238] S. Durr, Z. Fodor, T. Hemmert, C. Hoelbling, J. Frison, et al. Sigma term and strangeness content of octet baryons. *Phys.Rev.*, D85:014509, 2012.

[239] R. Horsley, Y. Nakamura, H. Perlt, D. Pleiter, P. Rakow, et al. Hyperon sigma terms for 2+1 quark flavours. *Phys.Rev.*, D85:034506, 2012.

[240] P. E. Shanahan, A. W. Thomas, and R. D. Young. Sigma terms from an SU(3) chiral extrapolation. *Phys. Rev.*, D87:074503, 2013.

[241] C. Jung. Nucleon mass and strange content from (2+1)-flavor Domain Wall Fermion. *PoS*, LATTICE2012:164, 2012.

[242] P. Junnarkar and A. Walker-Loud. The Scalar Strange Content of the Nucleon from Lattice QCD. *Phys.Rev.*, D87:114510, 2013.

[243] P. Shanahan, A. Thomas, and R. Young. Scale setting, sigma terms and the Feynman-Hellman theorem. *PoS*, LATTICE2012:165, 2012.

[244] R. Feynman. Forces in Molecules. *Phys.Rev.*, 56:340–343, 1939.

[245] N. Cabibbo, E. C. Swallow, and R. Winston. Semileptonic hyperon decays. *Ann. Rev. Nucl. Part. Sci.*, 53:39–75, 2003.

[246] A. Walker-Loud. Evidence for non-analytic light quark mass dependence in the baryon spectrum. *Phys.Rev.*, D86:074509, 2012.

[247] S. R. Beane, K. Orginos, and M. J. Savage. Strong-isospin violation in the neutron-proton mass difference from fully-dynamical lattice QCD and PQQCD. *Nucl.Phys.*, B768:38–50, 2007.

[248] S. Borsanyi, S. Dürr, Z. Fodor, J. Frison, C. Hoelbling, et al. Isospin splittings in the light baryon octet from lattice QCD and QED. *Phys.Rev.Lett.*, 111:252001, 2013.

[249] G. E. J. Bijnens and J. Gasser. *The Second DAPhNE Physics Handbook*. INFN-LNF, Frascati Publications, Frascati, Italy, 1995.

[250] P. Hasenfratz and H. Leutwyler. Goldstone Boson Related Finite Size Effects in Field Theory and Critical Phenomena With O(N) Symmetry. *Nucl.Phys.*, B343:241–284, 1990.

[251] C. Aubin, C. Bernard, C. DeTar, J. Osborn, S. Gottlieb, et al. Light hadrons with improved staggered quarks: Approaching the continuum limit. *Phys.Rev.*, D70:094505, 2004.

[252] S. Durr et al. Lattice computation of the nucleon scalar quark contents at the physical point. 2015.

[253] Y.-B. Yang, A. Alexandru, T. Draper, J. Liang, and K.-F. Liu. πN and strangeness sigma terms at the physical point with chiral fermions. 2015.

[254] W. Freeman and D. Toussaint. The intrinsic strangeness and charm of the nucleon using improved staggered fermions. *Phys.Rev.*, D88:054503, 2013.

[255] D. B. Leinweber, A. W. Thomas, K. Tsushima, and S. V. Wright. Baryon masses from lattice QCD: Beyond the perturbative chiral regime. *Phys.Rev.*, D61:074502, 2000.

[256] V. Bernard, T. R. Hemmert, and U.-G. Meissner. Chiral extrapolations and the covariant small scale expansion. *Phys.Lett.*, B622:141–150, 2005.

[257] C. Hacker, N. Wies, J. Gegelia, and S. Scherer. Including the Delta(1232) resonance in baryon chiral perturbation theory. *Phys.Rev.*, C72:055203, 2005.

[258] V. Pascalutsa and M. Vanderhaeghen. The Nucleon and delta-resonance masses in relativistic chiral effective-field theory. *Phys.Lett.*, B636:31–39, 2006.

[259] B. C. Tiburzi and A. Walker-Loud. Strong isospin breaking in the nucleon and Delta masses. *Nucl.Phys.*, A764:274–302, 2006.

[260] R. F. Lebed and M. A. Luty. Baryon masses at second order in chiral perturbation theory. *Phys.Lett.*, B329:479–485, 1994.

[261] M. Banerjee and J. Milana. The Decuplet revisited in χPT. *Phys.Rev.*, D54:5804–5811, 1996.

[262] B. C. Tiburzi and A. Walker-Loud. Hyperons in Two Flavor Chiral Perturbation Theory. *Phys.Lett.*, B669:246–253, 2008.

[263] B. C. Tiburzi and A. Walker-Loud. Decuplet baryon masses in partially quenched chiral perturbation theory. *Nucl.Phys.*, A748:513–536, 2005.

[264] B. C. Tiburzi. Baryon masses in partially quenched heavy hadron chiral perturbation theory. *Phys.Rev.*, D71:034501, 2005.

[265] P. F. Bedaque and M. A. Luty. Baryon masses at second order in large N chiral perturbation theory. *Phys.Rev.*, D54:2317–2327, 1996.

[266] A. C. Cordon and J. Goity. Baryon Masses and Axial Couplings in the Combined $1/N_c$ and Chiral Expansions. *Phys.Rev.*, D87:016019, 2013.

[267] M. Lutz and A. Semke. Large-N_c operator analysis of 2-body meson-baryon counterterms in the chiral Lagrangian. *Phys.Rev.*, D83:034008, 2011.

[268] V. Bernard, U.-G. Meissner, and A. Rusetsky. The Delta-resonance in a finite volume. *Nucl.Phys.*, B788:1–20, 2008.

[269] J. F. Donoghue, B. R. Holstein, and B. Borasoy. SU(3) baryon chiral perturbation theory and long distance regularization. *Phys.Rev.*, D59:036002, 1999.

[270] S. Descotes-Genon, N. H. Fuchs, L. Girlanda, and J. Stern. Resumming QCD vacuum fluctuations in three flavor chiral perturbation theory. *Eur. Phys. J.*, C34:201–227, 2004.

[271] V. Bernard, S. Descotes-Genon, and G. Toucas. Chiral dynamics with strange quarks in the light of recent lattice simulations. *JHEP*, 01:107, 2011.

[272] C. Alexandrou, K. Hadjiyiannakou, K. Jansen, and C. Kallidonis. Sigma-terms and axial charges for hyperons and charmed baryons. *PoS*, Lattice2013:279, 2014.

[273] T. Barnes and F. Close. Where Are Hermaphrodite Baryons? *Phys.Lett.*, B123:89, 1983.

[274] Z. Li. Photoproduction signatures of hybrid baryons: An Application of the quark model with gluonic degrees of freedom. *Phys.Rev.*, D44:2841–2850, 1991.

[275] O. Krehl, C. Hanhart, S. Krewald, and J. Speth. What is the structure of the Roper resonance? *Phys.Rev.*, C62:025207, 2000.

[276] P. A. Guichon. A Nonstatic Bag Model for the Roper Resonances. *Phys.Lett.*, B164:361, 1985.

[277] I. Aznauryan, A. Bashir, V. Braun, S. Brodsky, V. Burkert, et al. Studies of Nucleon Resonance Structure in Exclusive Meson Electroproduction. *Int.J.Mod.Phys.*, E22:1330015, 2013.

[278] V. Crede and W. Roberts. Progress towards understanding baryon resonances. *Rept.Prog.Phys.*, 76:076301, 2013.

[279] K. Olive et al. Review of Particle Physics. *Chin.Phys.*, C38:090001, 2014.

[280] G. P. Engel, C. Lang, M. Limmer, D. Mohler, and A. Schafer. Meson and baryon spectrum for QCD with two light dynamical quarks. *Phys.Rev.*, D82:034505, 2010.

[281] B. Long and U. van Kolck. The Role of the Roper in Chiral Perturbation Theory. *Nucl.Phys.*, A870-871:72–82, 2011.

[282] S. R. Beane and U. van Kolck. The Role of the Roper in QCD. *J.Phys.*, G31:921–934, 2005.

[283] V. Bernard, N. Kaiser, and U.-G. Meissner. The Reaction $\pi N \to \pi\pi N$ at threshold in chiral perturbation theory. *Nucl.Phys.*, B457:147–174, 1995.

[284] A. Datta and S. Pakvasa. Pion - nucleon phase shifts in heavy baryon chiral perturbation theory. *Phys.Rev.*, D56:4322–4327, 1997.

[285] B. Borasoy, P. Bruns, U.-G. Meissner, and R. Lewis. Chiral corrections to the Roper mass. *Phys.Lett.*, B641:294–300, 2006.

[286] D. Djukanovic, J. Gegelia, and S. Scherer. Chiral structure of the Roper resonance using complex-mass scheme. *Phys.Lett.*, B690:123–128, 2010.

[287] T. Bauer, J. Gegelia, and S. Scherer. Magnetic moment of the Roper resonance. *Phys.Lett.*, B715:234–240, 2012.

[288] B. Borasoy and B. R. Holstein. Resonances in radiative hyperon decays. *Phys.Rev.*, D59:054019, 1999.

[289] U.-G. Meissner and J. Oller. Chiral unitary meson baryon dynamics in the presence of resonances: Elastic pion nucleon scattering. *Nucl.Phys.*, A673:311–334, 2000.

[290] M. Mojzis. Elastic pi N scattering to $O(p^3)$ in heavy baryon chiral perturbation theory. *Eur. Phys. J.*, C2:181–195, 1998.

[291] N. Fettes, U.-G. Meissner, and S. Steininger. Pion - nucleon scattering in chiral perturbation theory. 1. Isospin symmetric case. *Nucl. Phys.*, A640:199–234, 1998.

[292] N. Fettes and U.-G. Meissner. Pion nucleon scattering in chiral perturbation theory. 2.: Fourth order calculation. *Nucl. Phys.*, A676:311, 2000.

[293] N. Fettes and U.-G. Meissner. Complete analysis of pion nucleon scattering in chiral perturbation theory to third order. *Nucl. Phys.*, A693:693–709, 2001.

[294] T. Becher and H. Leutwyler. Low energy analysis of $\pi N \to \pi N$. *JHEP*, 06:017, 2001.

[295] J. M. Alarcon, J. Martin Camalich, J. A. Oller, and L. Alvarez-Ruso. πN scattering in relativistic baryon chiral perturbation theory revisited. *Phys. Rev.*, C83:055205, 2011. [Erratum: Phys. Rev.C87,no.5,059901(2013)].

[296] N. Fettes and U. G. Meissner. Pion - nucleon scattering in an effective chiral field theory with explicit spin 3/2 fields. *Nucl.Phys.*, A679:629–670, 2001.

[297] K. Torikoshi and P. J. Ellis. Low-energy pion nucleon scattering in the heavy baryon and infrared schemes. *Phys. Rev.*, C67:015208, 2003.

[298] B. Long and U. van Kolck. pi N Scattering in the Delta(1232) Region in an Effective Field Theory. *Nucl. Phys.*, A840:39–75, 2010.

[299] C. Alexandrou et al. Light baryon masses with dynamical twisted mass fermions. *Phys.Rev.*, D78:014509, 2008.

[300] S. Weinberg. Effective chiral Lagrangians for nucleon - pion interactions and nuclear forces. *Nucl. Phys.*, B363:3–18, 1991.

[301] N. Fettes, U.-G. Meissner, M. Mojzis, and S. Steininger. The Chiral effective pion nucleon Lagrangian of order p^4. *Annals Phys.*, 283:273–302, 2000.

[302] L. Geng, J. Martin Camalich, L. Alvarez-Ruso, and M. Vicente Vacas. Nucleon-to-Delta axial transition form factors in relativistic baryon chiral perturbation theory. *Phys.Rev.*, D78:014011, 2008.

[303] B. Long and V. Lensky. Heavy-particle formalism with Foldy-Wouthuysen representation. *Phys.Rev.*, C83:045206, 2011.

[304] D. Siemens, V. Bernard, E. Epelbaum, H. Krebs, and U.-G. Meissner. The reaction $\pi N \to \pi\pi N$ in chiral effective field theory with explicit $\Delta(1232)$ degrees of freedom. *Phys.Rev.*, C89(6):065211, 2014.

[305] V. Bernard, D. Hoja, U.-G. Meissner, and A. Rusetsky. The Mass of the Delta resonance in a finite volume: fourth-order calculation. *JHEP*, 0906:061, 2009.

[306] C. Alexandrou et al. Low-lying baryon spectrum with two dynamical twisted mass fermions. *Phys.Rev.*, D80:114503, 2009.

[307] S. Capitani, M. Della Morte, G. von Hippel, B. Jager, A. Juttner, et al. The nucleon axial charge from lattice QCD with controlled errors. *Phys.Rev.*, D86:074502, 2012.

[308] G. Bali, P. Bruns, S. Collins, M. Deka, B. Glasle, et al. Nucleon mass and sigma term from lattice QCD with two light fermion flavors. *Nucl.Phys.*, B866:1–25, 2013.

[309] M. S. Mahbub, A. O. Cais, W. Kamleh, B. G. Lasscock, D. B. Leinweber, and A. G. Williams. Isolating Excited States of the Nucleon in Lattice QCD. *Phys. Rev.*, D80:054507, 2009.

[310] M. Mahbub, W. Kamleh, D. B. Leinweber, A. O Cais, and A. G. Williams. Ordering of Spin-1/2 Excitations of the Nucleon in Lattice QCD. *Phys.Lett.*, B693:351–357, 2010.

[311] B. J. Menadue, W. Kamleh, D. B. Leinweber, and M. S. Mahbub. Isolating the $\Lambda(1405)$ in Lattice QCD. *Phys. Rev. Lett.*, 108:112001, 2012.

[312] G. P. Engel, C. B. Lang, and A. Schäfer. Low-lying Λ baryons from the lattice. *Phys. Rev.*, D87(3):034502, 2013.

[313] J. Bulava, R. G. Edwards, E. Engelson, B. Joo, H.-W. Lin, C. Morningstar, D. G. Richards, and S. J. Wallace. Nucleon, Δ and Ω excited states in $N_f = 2+1$ lattice QCD. *Phys. Rev.*, D82:014507, 2010.

[314] L. Liu, G. Moir, M. Peardon, S. M. Ryan, C. E. Thomas, P. Vilaseca, J. J. Dudek, R. G. Edwards, B. Joo, and D. G. Richards. Excited and exotic charmonium spectroscopy from lattice QCD. *JHEP*, 07:126, 2012.

[315] M. González-Alonso and J. M. Camalich. Isospin breaking in the nucleon mass and the sensitivity of β decays to new physics. *Phys.Rev.Lett.*, 112(4):042501, 2014.

[316] T. Blum, R. Zhou, T. Doi, M. Hayakawa, T. Izubuchi, et al. Electromagnetic mass splittings of the low lying hadrons and quark masses from 2+1 flavor lattice QCD+QED. *Phys.Rev.*, D82:094508, 2010.

[317] R. Horsley et al. Isospin breaking in octet baryon mass splittings. *Phys.Rev.*, D86:114511, 2012.

[318] P. Shanahan, A. Thomas, and R. Young. Strong contribution to octet baryon mass splittings. *Phys.Lett.*, B718:1148–1153, 2013.

[319] G. de Divitiis et al. Leading isospin breaking effects on the lattice. *Phys.Rev.*, D87(11):114505, 2013.

[320] S. Borsanyi et al. Ab initio calculation of the neutron-proton mass difference. *Science*, 347:1452–1455, 2015.

[321] A. W. Thomas, X. G. Wang, and R. D. Young. Electromagnetic Contribution to the Proton-Neutron Mass Splitting. *Phys. Rev.*, C91(1):015209, 2015.

[322] F. Erben, P. Shanahan, A. Thomas, and R. Young. Dispersive estimate of the electromagnetic charge symmetry violation in the octet baryon masses. 2014.

[323] Z. Davoudi and M. J. Savage. Finite-Volume Electromagnetic Corrections to the Masses of Mesons, Baryons and Nuclei. *Phys.Rev.*, D90:054503, 2014.

[324] N. Kaiser, P. B. Siegel, and W. Weise. Chiral dynamics and the low-energy kaon - nucleon interaction. *Nucl. Phys.*, A594:325–345, 1995.

[325] J. A. Oller, E. Oset, and A. Ramos. Chiral unitary approach to meson meson and meson - baryon interactions and nuclear applications. *Prog. Part. Nucl. Phys.*, 45:157–242, 2000.

[326] X.-L. Ren, E. Oset, L. Alvarez-Ruso, and M. J. Vicente Vacas. Antineutrino induced $\Lambda(1405)$ production off the proton. *Phys. Rev.*, C91:045201, 2015.

[327] X.-L. Ren, L.-S. Geng, E. Oset, and J. Meng. Test of the $h_1(1830)$ made of $K^*\bar{K}^*$ with the $\eta_c \to \phi K^*\bar{K}^*$ decay. *Eur. Phys. J.*, A50:133, 2014.

[328] Y. Zhou, X.-L. Ren, H.-X. Chen, and L.-S. Geng. Pseudoscalar meson and vector meson interactions and dynamically generated axial-vector mesons. *Phys. Rev.*, D90:014020, 2014.

[329] L.-S. Geng, X.-L. Ren, Y. Zhou, H.-X. Chen, and E. Oset. S-wave KK^* interactions in a finite volume and the $f_1(1285)$. *Phys. Rev.*, D92:014029, 2015.

[330] M. Bayar, X.-L. Ren, and E. Oset. States of $\rho D^*\bar{D}^*$ with J $=3$ within the fixed center approximation to the Faddeev equations. *Eur. Phys. J.*, A51(5):61, 2015.

[331] R. Aaij et al. Observation of $J/\psi p$ Resonances Consistent with Pentaquark States in $\Lambda_b^0 \to J/\psi K^- p$ Decays. *Phys. Rev. Lett.*, 115:072001, 2015.

[332] J. Gasser and H. Leutwyler. Quark Masses. *Phys. Rept.*, 87:77–169, 1982.

Acknowledgments

After five years Ph.D. studies, I am becoming more professional, confident, courageous, and wise. These changes cannot be separated from the people who have ever given me guidance, assistance, and support.

First of all, I would like to express my heartfelt indebtedness to my supervisor Prof. Jie Meng. As a talented physicist, his enthusiasm, dedication, self-discipline, art of managing research group, way of thinking physics are truly inspiring me. He taught the basic principles and specifications of research when I was a novice. He always pushed and encouraged me to keep this work going well. Besides the physics, more important, I benefit a lot from his unique way of looking at the society and world.

I sincerely appreciate to my vice-supervisor Prof. Li-Sheng Geng, not only for teaching me the chiral perturbation theory and related numerical skills, but for the development of my views on these and related subjects. His efficient working style and good living habits have a great influence on me. He is a wonderful mentor, collaborator, and friend. I really treasure the time to get along with him.

With the help of Prof. Meng and Prof. Geng and the financial support from the Chinese Scholarship Council, I had the opportunity to visit the Institut de Physique Nucléaire Orsay, Université Paris-Sud, to be a joint-Ph.D. student under the supervision of Prof. Ubirajara van Kolck. I deeply indebted him for teaching me an amazing viewpoint of the physical world with effective field theories. It is enlightening and a rare pleasure to discuss with him. Under his encouragements, I began to learn the heavy baryon chiral perturbation theory. He is very patient and meticulous to modify my dissertation and prepare all matters of my defense from French side.

I am truly grateful to Prof. Véronique Bernard, who greatly helped me both in physics and in life when I was in France. With the help of her, I learnt the infrared baryon chiral perturbation theory, and several key problems appeared in this work were solved. She was deeply concerned about my dissertation and suggested many valuable improvements. I appreciate Dr. Manuel Pavon Valderrama for taking care of my routine affairs in IPNO. Thanks the members of theoretical physics group of IPNO, Prof. Elias Khan, Prof. Michael Urban, Prof. Marcella Grasso, Prof. Denis Lacroix, Prof. Nguyen van Giai, Prof. Bachir Moussallam, Prof. Shuck Peter, Dr. Jerry Yang, Mario Scanchez, Dr. Yusuke Tanimura, Noel Martin, Peng Yin, for hospitality and valuable discussions. I sincerely cherished the memory with my dear friends, Zi-Zhao Zong, Chao Meng, Bin Wang, Meng Wang, Ya-Qiong Wang, Yong-Hao Chen, Ying Wang, Wen-Long Zhang, Yan-Zhou Wang, Dan-Qiu Lin, in Paris.

With the financial support of Beihang University, I had the opportunity to visit IFIC, Valencia University for three months. I sincerely appreciate my collaborator Prof. Eulogio Oset, and his clear physical intuition and high efficiency are really impressive. Fruitful collaborations with Prof. Oset, Prof. Luis Alvarez-Ruso, Prof. Manuel Jose Vicente Vacas, Dr. Melahat Bayar, enlarged my research interests to the hadron structure. Thanks Prof. Juan Miguel Nieves Pamplona, Prof. Wei-Hong Liang, Dr. Tim Ledwig, Dr. Chu-Wen Xiao, Dr. En Wang, Dr. Toshikaka Uchino, Astrid Hiller Blin, Jorgivan Morais Dias, for their helpful discussions. I also thank my friends, Dr. En Wang, Dr. Chu-Wen Xiao, Dr. Jie Lu, Dan Zhou, Ying-Yi

Lou, for warmhearted help in my daily life when I was in Spain.

Thanks my undergraduate advisors, Prof. Shou-Yu Wang and Prof. Bin Qi. The initial scientific research triggered my interest in nuclear physics and laid a solid foundation for my Ph.D. studies. Thanks Dr. Hao-Zhao Liang and Dr. Peng-Wei Zhao for the valuable suggestions. Every time I felt inspired after chatting with them. Thanks Prof. Toki Hiroshi, Prof. Emiko Hiayam for the useful discussions when they visited Beihang University. Thanks Dr. Jorge Martin Camalich for nice collaboration.

For four years studying in Beijing, I would like to thank the members of the nuclear theory group of Beihang University, Dr. Hua-Xing Chen, Dr. Chun-Yan Song, Xiao-Dong Xu, Guang-Zhi Xu, Kai-Wen Li, Dan Zhou, Zhi Shi, Xue-Wei Xia, Jun-Xu Lu, Er-Liang Cui, Zhu-Li, Zhao-Xi Li, Bin-Zhao, Xiao-Ying Qu, and the members of JCNP group of Peking University, Prof. Shuang-Quan Zhang, Dr. Qi-Bo Chen, Ling-Shuang Song, Shi-Hang Shen, Zheng-Xue Ren, and the former members, Dr. Wei Zhang, Dr. Lu-Lu Li, Dr. Jin-Niu Hu, Dr. Ying Zhang, Dr. Lang Liu, Dr. Zhen-Hua Zhang, Dr. Jian Li, Dr. Zhong-Ming Niu, Dr. Yi-Fei Niu, Dr. Ting-Ting Sun, Dr. Ying Chen, Ling-Fei Yu, Ji-Xuan Wei, Yu Zhou, Tian-Tian Wang, Yu-Zhi Zhou, Ming Li, for their helpful discussions and kind help in my daily life.

I am grateful to my thesis committee members Prof. Bing-Song Zou, Prof. Constantia Alexandrou, Prof. Matthias Schindler, Prof. Jaume Carbonell, Prof. Li-Hua Zhu, and Prof. Bing-Wei Long, for their assistance and helpful discussions. Thanks Ling-Shuang Song, Kai-Wen Li, Dan Zhou, Jun-Xu Lu, Rong An, for their valuable suggestions to the dissertation. Thanks the financial support from the Innovation Foundation of Beihang University for Ph.D. Graduates.

Thanks my dear friends, Lin Yu who gives me many advices in life and witnesses my growth and changes in this five years, Fu-He Liang, Chang-Hai Shan, Guang Li, Kai Zhang, Yan-Lei Zhang, and Ting-Wei Niu for their helpful encouragements and hospitality in Jinan and Jiaxiang, especially for Yan-Lei Zhang who designed several wonderful figures in the dissertation; De-Jing Yu, Yong-Qiang Pan, Ji-Long Wu, and Mu Cao who, interesting guys, provided a warm dormitory in undergraduate and cherish our friendship after graduation. Thanks my roommates, Dian Zhang and Guo Nan for their tolerance to my shortcomings in daily life. Thanks Jing Lu and Ge Zhang who accompanied me some periods in my life and left many happiness memories. Wish you have a bright future.

Finally, I must express my deepest gratitude to my family and my parents for their love! Without their permanent support and encouragement, I could't go so far!

Xiu-Lei

Beijing, China
2015.10.22

Publication List

Peer-reviewed publications

1. Li-Sheng Geng, **Xiu-Lei Ren**, Yu Zhou, Hua-Xing Chen, and E. Oset, "S-wave KK^* interactions in a finite volume and the $f_1(1285)$, Phys. Rev. D91 (2015) 014029, arXiv:1503.06633.

2. M. Bayar, **Xiu-Lei Ren**, and E. Oset, States of $\rho D^* \bar{D}^*$ with $J = 3$ within the Fixed Center Approximation to the Faddeev equations, Eur. Phys. J. A51 (2015) 61, arXiv:1501.02962.

3. **Xiu-Lei Ren**, E. Oset, L. Alvarez-Ruso and M. J. Vicente Vacas, Antineutrino induced $\Lambda(1405)$ production off the proton, Phys. Rev. C91 (2015) 045201, arXiv:1501.04073

4. **Xiu-Lei Ren**, Li-Sheng Geng, and Jie Meng, Scalar strangeness content of the nucleon and baryon sigma terms, Phys. Rev. D91 (2015) 051502(R), arXiv:1404.4799

5. **Xiu-Lei Ren**, Li-Sheng Geng, Eulogio Oset, Jie Meng, Test of the $h1(1830)$ made of $K^* \bar{K}^*$ with the $\eta_c \to \phi K^* \bar{K}^*$ decay, Eur. Phys. J. A50 (2014) 133, arXiv:1405.0153

6. Yu Zhou, **Xiu-Lei Ren**, Hua-Xing Chen, Li-Sheng Geng, Pseudocalar meson and vector meson interactions and dynamically generated axial-vector mesons, Phys. Rev. D90 (2014) 014020, arXiv:1404.6847

7. **Xiu-Lei Ren**, Li-Sheng Geng, and Jie Meng, Decuplet baryon masses in covariant baryon chiral perturbation theory, Phys. Rev. D89 (2014) 054034, arXiv:1307.1896

8. **Xiu-Lei Ren**, Li-Sheng Geng, and Jie Meng, Baryon chiral perturbation theory with Wilson fermions up to $\mathcal{O}(a^2)$ and discretization effects of latest $n_f = 2 + 1$ LQCD octet baryon masses, Eur. Phys. J. C74 (2014) 2754, arXiv:1311.7234

9. **Xiu-Lei Ren**, Lisheng Geng, Jie Meng, and Hiroshi Toki, Virtual decuplet effects on octet baryon masses in covariant baryon chiral perturbation theory, Phys. Rev. D87 (2013) 074001, arXiv: 1302.1953

10. **X.-L. Ren**, L. S. Geng, J. Martin Camalich, J. Meng, and H. Toki, Octet baryon masses in next-to-next-to-next-to-leading order covariant baryon chiral perturbation theory, J. High Energy Phys. 12 (2012) 073, arXiv: 1209.3641

11. Lisheng Geng, **Xiu-Lei Ren**, J. Martin Camalich, and W. Weise, Finite-volume effects on octet-baryon masses in covariant baryon chiral perturbation theory, Phys. Rev. D84 (2011) 074024, arXiv: 1108.2231

12. S.Y. Wang, B. Qi, D.P. Sun, **X.L. Ren**, B.T. Duan, F. Chen, C. Liu, C.J. Xu, L. Liu, et al., Shape coexistence and strongly coupled bands in ^{118}Sb, Phys. Rev. C82 (2010) 057303

13. S.Y. Wang, D.P. Sun, B.T. Duan, **X.L. Ren**, B. Qi, et al., Coexistence of collective and noncollective structures in ^{118}Sn, Phys. Rev. C81 (2010) 017301

Conference proceedings

1. **Xiu-Lei Ren**, Li-Sheng Geng, Jie Meng, Ground-state octet baryon masses in covariant baryon chiral perturbation theory, Proceedings of the Seventh International Symposium on Chiral Symmetry in Hadrons and Nuclei (Chiral 2013)

2. **Xiu-Lei Ren**, Li-Sheng Geng, Jie Meng, Lowest-lying octet baryon masses up to $\mathcal{O}(p^4)$ in covariant baryon chiral perturbation theory, Int. J. Mod. Phys. Conf. Ser. 29 (2014) 1460215, Proceedings of Workshop on Hadron Nuclear Physics (HNP 2013)

3. **Xiu-Lei Ren**, Li-Sheng Geng, Jie Meng, Lowest-lying octet baryon masses in covariant baryon chiral perturbation theory, Int. J. Mod. Phys. Conf. Ser. 26 (2014) 1460068, Proceedings of the 9th International Workshop on the Physics of Excited Nucleons (NSTAR 2013)

4. **X.-L. Ren**, L.S. Geng, J. Martin Camalich, J. Meng, H. Toki, Quark mass dependence of the groundstate octet baryons in next-to-next-to-next-to-leading order covariant baryon chiral perturbation theory, Few Body Syst. 54 (2013) 1491, Proceedings of the 20th International IUPAP Conference on Few-Body Problems in Physics (FB20)

5. **Xiu-Lei Ren**, Li-Sheng Geng, Jie Meng, Octet baryon masses in finite space, Nuclear Structure in China 2012, Proceedings of the 14th National Conference on Nuclear Structure in China

To be published

1. **Xiu-Lei Ren**, V. Bernard, Li-Sheng Geng, Jie Meng, and U. van Kolck, Nucleon, Delta and Roper masses and widths in chiral perturbation theory, in preparation

2. **Xiu-Lei Ren**, Li-Sheng Geng, Jie Meng, Lowest-lying octet baryon masses in covariant baryon chiral perturbation theory up to $\mathcal{O}(p^4)$, Proceedings of The 8th International Workshop on Chiral Dynamics 2015 (CD2015), in preparation

3. **Xiu-Lei Ren**, Roper mass in chiral perturbation theory, Proceedings of The 8th International Workshop on Chiral Dynamics 2015 (CD2015), in preparation

Titre : Théorie effective des champs pour les masses des baryons

Mots clés : théorie effective des champs, Lagrangiens chiraux, QCD sur réseau, masses des baryons, termes sigma

Résumé : Comprendre QCD non perturbative pour produire les masses des baryons lumière est d'un intérêt fondamental. Aujourd'hui, interaction entre la CDQ sur réseau et de la théorie de perturbation chirale devient un outil puissant pour étudier la lumière masses des baryons. Utilisant des simulations récentes CDQ sur réseau et de la théorie de perturbation chirale, nous présentons une étude détaillée des masses de l'octet et décuplet baryons les plus basses masses ainsi que la masse et la largeur de la résonance Roper.

Nous étudions les les plus basses masses octet des baryons dans baryon covariante théorie de la perturbation chirale avec le schéma étendu-sur-masse coquille jusqu'à avant-avant-avant-ordre dominant. Afin d'examiner les artefacts de treillis, des corrections volumes finis et treillis fini effets espacement de discrétisation à treillis masses des baryons sont estimés. Nous effectuons une étude systématique de toutes les dernières n_f=2+1 données de treillis avec extrapolation chiral, corrections volumes finis, et le continuum extrapolation. Les artefacts de réseau sont bien comprises et discutées. Nous constatons également que les données du réseau de différentes collaborations sont compatibles les uns avec les autres. En utilisant les formules chiraux de masses octet de baryons, nous prédire avec précision les termes sigma octet de baryons via le théorème de Feynman-Hellmann. La valeur déterminée pour le nucléon étrangeté terme sigma est en accord avec les décisions de treillis.

Nous présentons également une analyse systématique des masses les plus basses décuplet des baryons dans baryon covariante théorie de la perturbation chirale en ajustant simultanément les données n_f = 2 + 1 en treillis.

Enfin, nous étudions également la masse Roper en théorie de perturbation chirale en incluant explicitement le nucléon / contributions Delta. Les contributions mixtes entre nucléons et Roper aux masses des baryons sont pris en compte pour la première fois. Une première analyse des treillis masses Roper est présenté.

Title : Effective Field Theory for Baryon Masses

Keywords : effective field theory, chiral Lagrangians, lattice QCD, baryon masses, sigma terms

Abstract : Understanding nonperturbative QCD to produce the light baryon masses is of fundamental interest. Nowadays, interplay between lattice QCD and chiral perturbation theory is becoming a powerful tool to study light baryon masses. Utilizing recent lattice QCD simulations and chiral perturbation theory, we present a detailed study of the masses of the lowest-lying octet and decuplet baryon masses as well as the mass and width of the Roper resonance.

We study the lowest-lying octet baryon masses in covariant baryon chiral perturbation theory with the extended-on-mass-shell scheme up to next-to-next-to-next-to-leading order. In order to consider lattice artifacts, finite-volume corrections and finite lattice spacing discretization effects to lattice baryon masses are estimated. We perform a systematic study of all the latest n_f = 2 + 1 lattice data with chiral extrapolation, finite-volume corrections, and continuum extrapolation. The lattice artifacts are well understood and discussed. We also find that the lattice data from different collaborations are consistent with each other. Using the chiral formulas of octet baryon masses, we accurately predict the octet baryon sigma terms via the Feynman-Hellmann theorem. The value determined for the nucleon strangeness sigma term is in agreement with lattice determinations.

We also present a systematic analysis of the lowest-lying decuplet baryon masses in covariant baryon chiral perturbation theory by simultaneously fitting n_f= 2+1 lattice data.

Finally, we also study the Roper mass in chiral perturbation theory by explicitly including the nucleon/Delta contributions. The mixed contributions between nucleon and Roper to the baryon masses are taken into account for the first time. A first analysis of lattice Roper masses is presented.

Université Paris-Saclay
Espace Technologique / Immeuble Discovery
Route de l'Orme aux Merisiers RD 128 / 91190 Saint-Aubin, France